



Developing Tools for the Remote Control of Genetic Circuits

John Hunter Allan

Submitted for the Qualification of Doctor of Philosophy

School of Natural and Environmental Sciences,

Faculty of Science Agriculture and Engineering

Newcastle University

January 2020

For Grampa, who taught me to make things

Contributions

Conference Presentations

Microbiology Society Annual General Meeting, 2017, Edinburgh, UK,

Poster presentation and flash talk, supported by Microbiology Society Conference Grant

Synthetic Biology UK 2017, Manchester University, UK

Poster presentation and flash talk, supported by Biochemical Society Student Bursary

SB7.0, 2018, National University of Singapore, Singapore

Poster presentation, supported by BioBricks Foundation travel grant

Synthetic Biology UK 2018, Bristol University, UK

Poster Presentation, Supported by Biochemical Society Student Bursary

6th Molecular Microbiology Meeting, 2018, Newcastle University, UK

Poster Presentation

Designer Biology, 2019, Newcastle University, UK

Oral Presentation

Abstract

With the advent of industrial biotechnology, we can use microbes to produce myriad valuable compounds with a range of useful applications. These may be drugs, flavourings preservatives or many others. With contemporary synthetic biology approaches we are able to bring together enzymes from a variety of different genomic contexts and build pathways that don't yet exist in nature. This naturally proposes an increase in complexity in pathway design and function, that will require more complex methods to regulate and control.

One way to achieve this regulation is using magnetic fields. Physical stimuli like this hold many advantages over the chemical induction methods used contemporarily. Every cell could be reached simultaneously using physical stimuli, promoting metabolic synchronicity. There is also no risk of some cells sequestering chemical inducers, leaving some cells experiencing greater levels of induction, and others none at all.

A magnetic stimulus could penetrate an entire culture and stimulate each cell simultaneously and repeatedly. Magnetic nanoparticles when placed in oscillating magnetic fields have their magnetic dipoles forcibly switched to align with oscillations. At high frequency magnetic oscillations, the MNP loses some energy as heat. By conjugating magnetic nanoparticles with temperature sensitive proteins it may be possible to produce stimulus of specific genetic elements with hitherto unseen precision.

To achieve this, microbes must be equipped with two things – a magnetic “aerial” module which can receive the magnetic stimulus, and genetically encoded heat-sensitive apparatus that responds to changes in temperature induced by the magnetic field.

This thesis has surveyed the potential for Pd nanoparticles to perform the role of a magnetic aerial, and heterologous gene expression with genes from magnetotactic bacterial genomes to produce magnetic material *de novo*. This strand of work illuminated the potential for a model contrary to how Pd-NPs are made in *E. coli*. This being that instead of microbial hydrogenases directly nucleating production of a nanoparticle in the active site of the enzyme, hydrogen produced by microbial hydrogenases reacts with soluble Pd(II) precipitating Pd nanoparticles.

Work performed in parallel has provided a novel mechanism to produce magnetic material *de novo* using heterologous expression of the *mms6* gene from *Magnetospirulum gryphiswaldense*.

This work has also used contemporary synthetic biology approaches to produce genetic programs that respond to temperature changes, using the genes *tplA*, *mogR* and *gmaR*, with *mogR* and *gmaR* being new

additions to the pantheon of genetic elements used in synthetic gene circuits. This thesis contains designs, characterisation and optimisation of functional novel genetic circuits which utilise *mogR* and *gmaR* in the pMOGMAR-20K plasmid.

Using genetic elements characterised in this work in concert, the apparatus to begin producing novel magnetoreceptive mechanisms in *E. coli* is now available.

Acknowledgements

In the preparation of this thesis, numerous people have contributed materials, time, effort and support.

To begin in purely pragmatic terms, Prof Nicola Stanley-Wall at the University of Dundee for supplying me with a few microliters of *Listeria monocytogenes* str. EGD-e genomic DNA for use as template in pMOGMAR construction.

Dr Alan Prescott at the University of Dundee and Dr Kathryn White at Newcastle University Electron Microscopy Research Services must also be thanked for preparing TEM grids and helping me image them.

My supervisor Prof Frank Sargent cannot be thanked enough for his support and guidance throughout my PhD. It's been something! Along with Prof Tracy Palmer, without both of whom I would not have made it this far. Dr Ciarán Kelly and Dr Magali Roger from FS lab have been and continue to be excellent mentors and role models which I must thank too.

I must also thank my friends Dr Chris "Birdman" Earl and Dr Connor "Connie" Bowen who were there the whole time. All of those in TP/FS labs and in MMB back in Dundee also provided a great environment to do science in.

My family have also endured me through my PhD and I'm grateful for their support, Mum, Dad, Kirsten. And Jessica, who never left my side.

Table of Contents

Developing Tools for the Remote Control of Genetic Circuits	i
Chapter 1: Introduction	2
1.1. The Invention and Development of Biotechnology.....	3
1.2. Engineering Microbial Metabolism	4
1.2.1. Implementing Entirely Novel Pathways.....	5
1.3. Synthetic Control of Metabolism	6
1.4. Synthetic Gene Circuits	8
1.4.1. Synthetic Gene Regulators	9
1.4.1.1. Protein-based Synthetic Regulation.....	9
1.4.1.2. RNA-based Synthetic Regulation	11
1.4.2. Oscillating Circuits	12
1.4.3. Toggle Switches	15
1.4.4. The Band Pass Filter	17
1.5. The Need for New Methods to Control Synthetic Physiology.....	19
1.5.1. Light-Controlled Synthetic Regulation	20
1.5.2. Magnetically Induced Regulation	21
1.5.2.1. Magnetism and Cellular Scale Magnets.....	22
1.5.2.2. Magnetism in Electrical Systems	24
1.5.2.3. Synthetic Magnetoreception	26
1.5.3. A Design for Synthetic Bacterial Magnetoreception	28
1.5.3.1. Thermoreception in Bacteria.....	28
1.6. Bacteria and Metal Nanoparticles	30
1.6.1. Diversity of Metal Nanoparticles	33
1.6.2. The Discovery of Magnetotactic Bacteria and Magnetotaxis.....	37
1.6.3. Diversity of Magnetotactic and Magnetosome Producing Organisms.....	39
1.6.4. The Magnetosome Assembly Island	40

1.6.5. Magnetosome Assembly	41
1.6.6. Magnetosome Membrane Invagination	41
1.6.7. Iron Transport into the Magnetosome.....	42
1.6.8. Magnetite Crystallisation	43
1.6.9. Magnetosome Alignment	45
1.6.10. Applied Biomagnetism.....	46
1.6.11. The Aims of This Project.....	48
Chapter 2: Production of Palladium Nanoparticles by <i>E. coli</i>	51
2.1. Introduction	52
2.1.1. Previous characterisation of Pd-NP formation in <i>E. coli</i>	52
2.1.2. Aims	53
2.2. Results.....	55
2.2.1. Characterising Pd-NP formation by <i>E. coli</i> Hydrogenases.....	55
2.2.2. Pd-NP production is correlated with a reduction in H ₂ evolution.....	60
2.2.3. Pd-NPs can be produced by H ₂ alone	62
2.3. Discussion.....	67
2.3.1. Direct Biological Contribution to Production of Pd-NPs by <i>E. coli</i>	67
2.3.2. The Atomic Constituents of the Pd-NP	71
2.3.3. Biotechnological Applications of Pd-NPs	74
2.3.4. Use of Pd-NPs as an “aerial” conduit module.....	75
Chapter 3: Engineering Magnetic Phenotypes in <i>E. coli</i>	76
3.1. Introduction	77
3.1.1. Aims	79
3.2. Results.....	80
3.2.1. Heterologous Expression of Genes from MTB.....	80
3.2.2. Production and Characterisation of Mms6 and MmsF in <i>E. coli</i>	82
3.2.3. Development of a Magnetic Retention Assay	88
3.2.4. Developing a Magnetite Pull Down Assay	100

3.2.5. Examination of Mms6 producing cells by TEM.....	104
3.2.6. Design and Characterisation of Magnetite Importers	108
3.3. Discussion.....	118
3.3.1. Mms6 production can produce magnetic phenotypes in <i>E. coli</i>	118
3.3.2. MmsF may interact with MNPs but does not produce magnetic material <i>de novo</i>	120
3.3.3. CWPM may import MNPs	122
3.3.4. but MNP import defeats the purpose of this project.....	123
3.3.5. Identification of Genes for Magnetic “Aerial” Production.....	125
Chapter 4: Development of Temperature Responsive Synthetic Gene Circuits	127
4.1. Introduction	128
4.1.1. The <i>Salmonella typhimurium</i> protein TlpA	129
4.1.2. The Transcriptional Repressor MogR and its Antirepressor GmaR	131
4.1.3. Aims	134
4.2. Results.....	135
4.2.1. Construction of a Synthetic Gene Circuit Using TlpA.....	135
4.2.2. Construction of a Synthetic Gene Circuit using MogR and GmaR	143
4.2.3. pMOGMAR responds to temperature and IPTG.....	145
4.2.4. Improving pMOGMAR characterisation	151
4.2.5. Translation of <i>gmaR</i> may be a limiting factor	157
4.2.6. The pMOGMAR-20K plasmid outperforms pMOGMAR as a sensor	162
4.2.7. The biochemical influence of temperature on MogR : GmaR interaction is still unclear	170
4.3. Discussion.....	182
4.3.1. The pC1R7 system needs improved characterisation and optimisation.....	182
4.3.2. The pMOGMAR-20K system is an improved version of pMOGMAR but requires additional optimisation.....	183
4.3.3. Flow Cytometry is an insightful tool for genetic circuit characterisation....	183
4.3.4. Improving the pMOGMAR-20K reporter	185

4.3.5. A model of the circuit encoded by pMOGMAR-20K	187
Chapter 5: Future Work	190
5.1. The Future of Remote Control of Gene Circuits (RC/GC)	191
5.1.1. A Prototype RC/GC model using pMOGMAR-20K and Mms6	191
5.1.2. RC/GC Applicable Apparatus from the Broader Field	193
5.1.3. The Glass Catfish and its Genetically-Encoded Electromagnetic Perception	194
5.2. New Projects Inspired by This Research	196
5.2.1. Development of a Pd-based reporter for H ₂ production	196
5.3. Concluding Remarks.....	198
Chapter 6: Materials and Methods	200
6.1. Microbiological Methods.....	201
6.1.1. Bacterial Culture Methods.....	201
6.1.2. Plasmid Extraction	204
6.1.3. Preparation of Competent <i>E. coli</i> cells and their Transformation	204
6.1.4. Reduction of Pd(II) to Pd(0)	205
6.1.5. Gas Chromatography	205
6.1.6. Characterisation of Pd(II) reduction by OD600	205
6.1.7. Spectral Scanning of PdNP production reactions	206
6.1.8. Magnetic Retention Assay	206
6.1.9. Platereader Characterisation of pMOGMAR and associated variants	206
6.1.10. Initial Characterisation of pMOGMAR and pC1R7	207
6.1.11. Flow Cytometry	207
6.2. Molecular Biology and Biochemistry Methods	208
6.2.1. Polymerase Chain Reaction	208
6.2.2. Colony PCR.....	213
6.2.3. Gibson Assembly	214
6.2.4. Site Directed Mutagenesis of Plasmids	214
6.2.5. Buffer Recipes and Solutions	215

6.2.6. Room Temperature Co-Precipitation of Magnetite.....	216
6.2.7. Magnetite washing experiment	216
6.2.8. Magnetite Pull Downs.....	216
6.2.9. GmaR degradation experiment	217
6.2.10. Co-purification of His-tagged MogR with GmaR	217
6.2.11. Fractionation of <i>E. coli</i> Cells	218
Chapter 7: Bibliography	219

Table of Figures

Figure 1.1 Diagrammatic representation of the repressilator circuit	13
Figure 1.2 Diagrammatic representation of the toggle switch circuit	15
Figure 1.3 Diagram of the band pass filter circuit	17
Figure 1.4 A magnetically susceptible material can be magnetised by an external field in opposing polarities in a hysteresis loop	25
Figure 1.5 Examination of magnetosomes within <i>Magnetospirulum gryphiswaldense</i>	37
Figure 1.6 Arrangement and function of genes in the MAI of <i>Magnetospirulum gryphiswaldense</i>	40
Figure 1.7 Cartoon of magnetosome membrane invagination and the proteins associated with it	42
Figure 1.8 Cartoon of a maturing magnetite crystal	45
Figure 1.9 Magnetosomes are aligned by MamK and MamJ	46
Figure 1.10 A platform for magnetically-stimulated control of bacterial physiology..	49
Figure 2.1 Pd-NPs are produced only in the presence of active Hyd-3	56
Figure 2.2 Pd-NPs can be observed by TEM	58
Figure 2.3 Pd-NP production correlates with decreased H ₂ production	61
Figure 2.4 Direct reduction of Pd(II) using chemical H ₂	63
Figure 2.5 Pd inhibits H ₂ evolution by FHL at an early stage	65
Figure 2.6 Palladium may permanently disrupt Hyd-3 activity	66
Figure 2.7 Model of Pd-NP production by E. coli.....	69
Figure 2.8 Pd-NPs may be elemental Pd(0) NPs or PdH _x NPs.....	73
Figure 3.1 Plasmid maps of clones harbouring optimised mms6 and mmsF	81
Figure 3.2 Mms6 and MmsF are located in the E. coli membrane fraction	83
Figure 3.3 MNPs produced by the RTCP method.....	85
Figure 3.4 Cells containing pQEmms6 interact with magnetite	87
Figure 3.5 Magnetic Retention Assay (MRA)	89
Figure 3.6 Initial Magnetic Retention Assays	91

Figure 3.7 Comparison of MRA column pre-treatments on pQEmms6 containing cells	93
Figure 3.8 Validation and vindication of the MRA protocol using MftN	95
Figure 3.9 <i>E. coli</i> producing Mms6 is retained on a magnetic column.	97
Figure 3.10 Growth in Chelex-treated LB medium affects retention of cells on the magnetic column	99
Figure 3.11 The MNP pull down experiment.....	101
Figure 3.12 Both Mms6 and MmsF can be isolated in a magnetite pull down assay ..	103
Figure 3.13 Cells producing Mms6 change shape and exhibit unusual intracellular structures.	105
Figure 3.14 Cells shape changes significantly upon production of Mms6	107
Figure 3.155 Designing a putative magnetite importer using the holin protein ChiW.	109
Figure 3.166 Cells producing native ChiW are poorly retained on a magnetic column	113
Figure 3.177 Identification of engineered ChiW variant proteins with increased magnetic retention behaviour	115
Figure 3.188 Extracellular magnetite nanoparticles are sparse in CWPM expressing cells	117
Figure 3.19 Proteins predicted to be direct contributors to MNP precipitation.	121
Figure 4.1 TlpA is a transcriptional repressor influenced by temperature	130
Figure 4.2 MogR is antirepressed by the product of the DegU activated gene gmaR	133
Figure 4.3 The pC1R7 plasmid encodes tlpA, and gfpmut3b under the control of the PtlpA promoter.....	136
Figure 4.4 GFP and TlpA proteins are produced by pC1R7	138
Figure 4.5 TlpA does not activate transcription with increasing temperature in small cultures.....	140

Figure 4.6 When cultured in 250 mL conical flasks at 44 oC, GFP expression is increased in pC1R7 containing cells.....	142
Figure 4.7 The pMOGMAR plasmid encodes a synthetic operon with mogR and gmaR, in parallel with a gfpmut3b MogR sensitive reporter	144
Figure 4.8 Evidence for temperature-dependent GFP production in E. coli using pMOGMAR.....	146
Figure 4.9 In pMOGMAR containing cells, GFP expression is inhibited as IPTG concentration increases.....	148
Figure 4.10 IPTG concentration and temperature influence GFP production by pMOGMAR	150
Figure 4.11 PflaA shows divergent activities at different temperatures.....	152
Figure 4.12 PflaA shows similar behaviours in exponential phase when grown using glucose or glycerol as a carbon source.	154
Figure 4.13 GFP is most fluorescent at 30 °C.....	156
Figure 4.14 pMOGMAR-20K shows enhanced promoter activity at 24-30 oC compared to pMOGMAR, pMOGMAR-700 and pMOGMAR-10K during exponential phase.	160
Figure 4.15 pMOGMAR activity is noisy at stationary phase, and promoter activity is minimal in most variants	161
Figure 4.16 pFLA-gfp containing cells have a growth defect, while pMOGMAR and pMOGMAR-20K containing cells have similar growth profiles to each other	163
Figure 4.17 GFP production by pMOGMAR-20K is repressed at 42 °C	165
Figure 4.18 Temperature influenced behaviours of pMOGMAR plasmids break down at stationary phase	167
Figure 4.19 At both exponential phase and stationary phase, pMOGMAR-20K cells are turned off at 42 oC.....	169
Figure 4.20 There are numerous rare codons in <i>mogR</i> and <i>gmaR</i>	171
Figure 4.21 Both MogR and GmaR can be detectably produced in E. coli.....	173

Figure 4.22 MogR and GmaR each contain putative domains for protein:protein interactions	175
Figure 4.23 GmaR can be co-purified with MogR	177
Figure 4.24 MogR interacts with GmaR at room temperature and 30 °C but not at 42 °C	179
Figure 4.25 GmaR is degraded by proteases.....	181
Figure 4.26 pMOGMAR-20K produces GFP at 30 °C and does not at 42 °C	189
Figure 5.1 An absorbance peak at 340 nm is diminished upon Pd-NP formation	197

Table of Tables

Table 1.1 Selected examples of successful synthetic biology enterprises.....	4
Table 1.2 Selected examples of metal nanoparticles produced by microbes.....	31
Table 3.1 Amino acid sequences implicated in protein interactions with magnetite	111
Table 4.1 Predicted TIRs of designated RBSs in pMOGMAR and its variants	158
Table 6.1 Media Recipes used for bacterial cultivation in this thesis	202
Table 6.2 List of bacterial strains utilised in this thesis	204
Table 6.3 showing standard PCR program conditions.....	208
Table 6.4 List of buffers used in this thesis and their recipes	215

Standard Abbreviations Used in this Thesis

Abbreviation	Expansion
KLD	Kinase Ligase Dpni
LB	Lysogeny Broth
MACS	Magnetically Activated Cell Separation (Reg. Trademark Of Miltenyi Biotec)
MAI	Magnetosome Assembly Island
MNP	Magnetic Nanoparticle
MOGMAR	A Portmanteau Of Mogr And Gmar
MOPS	3-Morpholinopropane-1-Sulfonic Acid
MTB	Magnetotactic Bacterium
NP	Nanoparticle
OD600	Optical Density At 600 Nm
PCR	Polymerase Chain Reaction
Pd-NP	Palladium Nanoparticle
QS	Quorum Sensing
RBS	Ribosome Binding Site
RC/GC	Remote Control Of Genetic Circuits
RTCP	Room Temperature Co-Precipitation
SDS	Sodium Dodecyl Sulphate
SDS-PAGE	Sodium Dodecyl Sulphate Polyacrylamide Gel Electrophoresis
SNP	Single Nucleotide Polymorphism
TEM	Transmission Electron Microscopy
UV	Ultraviolet
WT	Wild Type

Chapter 1
Introduction

1.1.The Invention and Development of Biotechnology

People of Shang Dynasty China (7000 BC) were the first humans we have evidence of to harness the abilities of microbes to synthesise valuable molecules and transform the nature of organic material¹. The oldest recipes for fermented alcoholic beverages date back to this period, and preparations of pottery found in archaeological digs was shown to give FT-IR and HPLC profiles similar to modern rice wines¹. It is thought that the method used was mostly the same as the traditional amylolysis, or mould saccharification, method used to this day in modern China to produce rice wine, where steamed rice or other cereals is used as a crude growth medium for *Aspergillus* or other fungi present in the environment. It could be argued thus that biotechnology dates back to this early period in human history.

Nine thousand years later mankind has upheld this tradition of using microbes to transform materials. Until recently humans have relied upon the latent properties of wild microbes in their immediate environment. The classical example in the Western hemisphere is baker's and brewer's yeast, *Saccharomyces cerevisiae* (alongside bacteria like *Lactobacilli* or other fungi like *Brettanomyces*), however Mexican Nahua people have used lactic acid bacteria such as *Lactobacillus lactis* found on fruit rinds to ferment drinks called Tepache² and Japanese cultures have used for centuries similar saccharification procedures using grains to produce a preparation of *Aspergillus oryzae* called *koji* to ferment sauces and drinks such as mirin and sake³.

Naturally, the emergence of recombinant DNA technologies and whole genome sequencing has allowed us to begin to engineer the properties in these microbes and many others. The emerging technology of synthetic biology theoretically allows us to bring together the entirety of Nature's molecular capabilities in order to produce entirely novel phenotypes and properties in cells, either natural or synthetic. With microbes possessing metabolic versatility in the realms of carbon polymer synthesis and catabolism, their engineering could relieve us of our dependence on fossil fuels, revolutionise medical strategies, and set forth a new era in materials science. Indeed, a number of significantly sized enterprises, described in Table 1.1, have blossomed using synthetic biology technologies as their foundations. These range from biofuel producers to the more bizarre "genetic preservation service" Viagen Pets, who were parodied in the 2006 Arnold Schwarzenegger classic "The 6th Day", and of whom the great Barbra Streisand is said to be a valued customer⁴.

Table 1.1 Selected examples of successful synthetic biology enterprises

Company	Year started	Description	Products	Website
Intrexon	1998	Massive conglomerate, ranging from biofuels to food and medical	Arctic Apple™, Butanol	www.dna.com
Oxitec	2002	Sterile male mosquitoes for disease transmission control	Friendly Aedes™ OX513A	www.oxitec.com
Viagen Pets	2002	Clone your beloved pets	Services including pet genetic preservation and cloning post mortem	www.viagenpets.com
Amyris	2003	Large company started by fraternity of academics and entrepreneurs	Artemisinin, biofuels, food additives and cosmetics	www.amyris.com
Bolt Threads	2009	Synthetic spider silk and mycological fibres	Mylo™, Microsilk™, hats, ties	www.boltthreads.com
Ginkgo Bioworks	2009	The Organism Company	Bespoke strains and organisms to ordered specification	www.ginkgobioworks.com
Mycoworks	2013	Mycologically synthesized leather producer	Myco leather™	www.mycoworks.com

1.2.Engineering Microbial Metabolism

Many strategies have been explored and invented for the microbial production of biofuels. The most successful may well be the nationwide implementation of bio-ethanol as fuel in Brazil. Here sugar cane is fermented by wild microbes that live on the sugar cane to ethanol, which is used as fuel for automobiles. Ethanol is however far less efficient as fuel than conventional gasoline and the development of strategies that use food crops as primary feedstock for fuel production could tether food prices with fuel prices, which could be problematic for economies that might grow to rely on a biofuel industry.

Even before the advent of fossil fuels and the petrochemical industry, microbes were used to produce acetone and butanol from a range of complex substrates. Discovered initially by Louis Pasteur and developed largely during the First World War by Charles Weizmann – more famously known as Chaim in his political spheres of activity – in to the “Weizmann Process”⁵⁶ where it was used to produce acetone for nitrocellulose solvents from mostly maize or molasses, arguably keeping the war effort afloat while conventional sources were cut off.

After the war this industry was sustained by the emerging demand for solvents used in automobile production. The issue with the microbial fermentation method of butanol production, however, was the slow anaerobic growth rate of the *Clostridial* species involved and the limiting toxicity of butanol at titres above 13 g l⁻¹. This limited production to only around 2% of the theoretical maximum given the feedstock added⁶. It is clear then that in this instance at least, engineering of metabolism is needed to improve yields and efficiencies.

One landmark work demonstrated that, by the introduction of two enzymes, *Escherichia coli* could be engineered to produce a range of higher alcohols⁷. Native *E. coli* metabolism permits the production of 2-keto-acids from aliphatic amino acids. By the introduction of heterologous 2-ketodecarboxylases and alcohol dehydrogenases this was extended to the decarboxylation of these 2-keto-acids and subsequent reduction of the intermediate to produce propanol; butanol; isobutanol; N-methyl-butanol; and phenylethanol. Further modifications involving deletions of native pathways to increase substrate pool, overexpression of the iso-valerate pathway enzymes and movement of the platform in to a strain engineered for threonine overproduction enhanced butanol production and selectivity in the engineered pathway.

Beyond this, the American synthetic biology giant Amyris, Inc. is making significant progress towards replacing the petrochemically-derived isoprenoids used in tyre production with that synthesised by an engineered *Saccharomyces cerevisiae* strain^{8,9}.

1.2.1. Implementing Entirely Novel Pathways

An entirely novel biosynthetic pathway introduced to *S. cerevisiae* was a synthetic opiate pathway that included enzymes from four different plant species, one mammalian enzyme and one bacterial protein, as well as modified genes from the host genome, totalling 21 different enzymes¹⁰. The resultant strain was able to produce the medically-relevant opiate hydrocodone using only ‘sugar’ as a starting point. Significant work was published prior to this and developed strategies to implement and optimise specific stretches of this pathway over the course of a decade¹¹⁻¹⁴.

Implementing such a long pathway using enzymes that have never worked together before brought numerous challenges, however a number of schemes were employed to overcome these. In one example a synthetic chimeric enzyme was found to be poorly trafficked to the cytoplasmic membrane resulting in poor activity and a build-up of (R)-reticuline, thus causing a bottle-neck in the pathway. To overcome this, the membrane helix coding region was replaced with that of a cytochrome P450 protein that had homologous sequence to the original one but was known to be trafficked correctly. This modification improved (R)-reticuline turnover almost five times¹⁰.

In another instance, the potential for neomorphine over morphine as an end product was made possible by virtue of employing a promiscuous enzyme with the capability to use either neopinone or codeinone as a substrate¹³. Action on codeinone is required in this pathway in order to produce the preferred product morphine, but neopinone spontaneously converts itself to codeinone. In order to give spatiotemporal separation between neopinone production and codeinone and conversion to codeine, the neopinone producing enzyme (T6ODM) was modified to have an endoplasmic reticulum targeting region forcing it to be retained in the membrane here and produce neopinone in the ER lumen where it would then diffuse the cytoplasm, where by which time it should have converted to codeinone and could be reduced by codeinone reductase (COR) to codeine. This improved selection of the platform for the morphine producing pathway to 86% morphine of the total opiate content from 44%.

1.3. Synthetic Control of Metabolism

Encountering unexpected obstacles and bottle-necks are common in the development of novel biosynthetic pathways, even with simple pathways native to the organism. A common strategy to overcome poor efficiencies is to uncouple growth of the culture from production of the desired metabolite. In this way biomass can be accumulated unhindered by any build-up of toxic intermediates. One of the earliest examples of this is in the production of antibiotics, which as secondary metabolites are usually produced during the non-growing stationary phase.

For production of useful proteins by recombinant production the classical method has been to exploit the properties of the *lac* operon. Genes required for lactose catabolism are encoded by the *lac* operon *lacAYZ*. Downstream of the *lac* promoter lies an operator region termed *lacO*, which is bound by the transcriptional repressor LacI. Under the influence of allolactose or isopyranosylthiogalactoside (IPTG) LacI changes conformation to a state where it cannot interact with *lacO*, permitting transcription of *lacAYZ*¹⁵¹⁶. The harnessing and development of this system was no small feat and thus Jacques Monod,

Andre Lwoff and Francois Jacob shared a Nobel prize for its characterisation and the discovery of the operator as a genetic element¹⁷.

The exploitation of the *lac* promoter and operator sequences have been engineered to remove interfering factors such as catabolite repression and to improve induction rates¹⁸¹⁹, and its use published and reviewed extensively^{19–26}. In one example the expression of human pro-insulin in *E. coli* was seen to increase almost ten times when cells were allowed to grow to stationary phase before addition of IPTG²⁵. Others though have found that IPTG induction can hinder production by causing metabolic burden²⁷, leading to the development of autoinduction strategies which induce expression of a target gene based on metabolic sensing²⁸. This platform utilises plasmids bearing the pBAD promoter which can be repressed by glucose and activated by arabinose. When glucose is added as the sole carbon source, glucose depletion tracks with biomass accumulation, thus cells are said to autoinduce when they reach stationary phase. This has been demonstrated in one instance to increase enzyme activity of a culture as much as three times compared to IPTG induction²⁶.

Molecules or culture conditions which cause stress to microbes have also been applied in the place of IPTG in two-stage fermentation procedures. In one example, production of 5-aminolevulinic acid in *Corynebacterium glutamicum* was quadrupled by applying a method where cells were cultured for 24 hours before being washed and added to a fermentation buffer that contained relatively few nutrients other than those required for the heterologous pathway²⁹. In another instance, *S. cerevisiae* was arrested in its growth by application of the alpha-pheromone, which instigates a mating phenotype³⁰. Cells treated like this were observed to maintain as active a central network as non-treated cells, but were able to produce greater amounts of acetate and glycerol using endogenous metabolic pathways, and had limited success with an engineered pathway for para-hydroxybenzoic acid.

Inexorable development of metabolic engineering technologies has led to the invention of so called “dynamic metabolic control” (DMC) strategies that are said to be more effective than two stage processes in some instances, offering unique strengths particularly to longer more complex engineered pathways³¹. In these strategies, levels of specific metabolites or enzymes are controlled dynamically by the integration of normally bespoke modules for each pathway. The major practical distinction of dynamic metabolic control strategies over two-stage methods is the linear increase in product regardless of biomass level in DMC *versus* biomass dependent production in other strategies.

Commonly, RNA silencing is deployed in this approach^{32–35}. This can be applied in different ways in different organisms and platforms. In *E. coli*, the translation inhibitor protein has been utilised³² where

the *micC* mRNA's Hfq interacting motif was applied to transcripts of genes that would otherwise downregulate tyrosine producing pathway genes or substrate recycling in this pathway in one experiment and in another tested a synthetic library of 130 sRNAs targeting genes encoding enzymes that could impinge on cadaverine synthesis. This revealed that knockdown of two essential genes (*murE* and *accA*) could improve cadaverine synthesis. Observations like this would likely be missed in less subtle screens that disrupted genes instead, indicating that sRNA knockdown strategies could reveal hitherto hidden properties of engineered pathways.

Another large screening experiment used 71 sRNAs that targeted central carbon metabolism with an added 38 nucleotide motif that formed a hairpin stabilising the sRNA to increase the pool of translation inhibitors in the cytoplasm³⁴. This demonstrated that, in a *cra* deletion strain, silencing of *accA* and *aceA* enabled fermentative build-up of pyruvate, likely by combined inhibition of pyruvate dehydrogenase and diversion of carbon flux towards fermentative conditions.

Degradation of competing enzymes can also enable flux of substrate away from endogenous pathways. Commonly, the *ssrA* tag is used³⁶. This is a motif placed at the C terminus of a protein and originally derived from the SsrA sRNA which adds this sequence to nascent stalled mRNAs³⁷. The motif allows the protein to interact with SspB³⁸, which directs the protein to the housekeeping protein degradation apparatus ClpXP³⁹. By adding the SsrA tag to the enzymes phosphoglucokinase, phosphoglycerol mutase and glucose-6-phosphate dehydrogenase (with SspB under the control of a *tetO* influenced promoter), inducible control of carbon flux towards the heterologous INO1 enzyme which converts glucose-6-phosphate to myo-inositol-1-phosphate was achieved to produce myo-inositol without any change in growth profile of the *E. coli* chassis organism⁴⁰. This has also been used to control essential phospholipid metabolism by adding degradation tags to the FabF enzyme, with once again inducible SspB expression, to allow on-demand limitation of phospholipid synthesis without toxicity and diversion of flux toward fatty acid elongation by mutant FabF that synthesises only shorter fatty acyl chains⁴¹. This resulted in a yield of free fatty acids of chain length only between four and 13 carbons that might be used in plastics production.

1.4. Synthetic Gene Circuits

Almost in parallel to the development of useful microbial biosynthetic production lines, highly complex gene circuits have been invented, however their implementation in the production of useful products has been limited. These circuits control the genetic makeup of common microbial laboratory denizens

leading to the recreation of principles and phenomena that were originally invented for electronic platforms in a biological context. The earliest example of this was the biological “repressilator” invented by Elowitz and Leibler⁴². A pair of transcriptional regulators that repress each other in turn, leading to an oscillation in repressive behaviours that could permit the emergence of predictable rhythms in transcription of designer operons.

1.4.1. Synthetic Gene Regulators

At their simplest, man-made genetic circuits like the repressilator depend on the deep understanding of transcriptional regulators and their porting into other genetic contexts. These transcription factors become synthetic by transplantation to foreign genetic backgrounds, and can be characterized by three features: 1) are they transcriptional activators or repressors?; 2) what is their molecular nature (protein, RNA or other?) and 3) how can they be controlled by the user? Below are described examples of these.

1.4.1.1. Protein-based Synthetic Regulation

As described in Section 1.3 IPTG and other lactose analogs can be used to control the transcription of genes under the control of a promoter with a *lacO* element upstream^{15–17}. Briefly, the *lac* transcriptional repressor, LacI, in its apo state binds to the *lacO* operator element to prevent access to the promoter downstream by RNA polymerase. When bound by lactose analogs like IPTG, LacI changes to a conformation that is no longer capable of interacting with *lacO*, thus permitting transcription from downstream promoters.

This has long been a staple of laboratory-based molecular biological methods, however a problem presented is the lack of linear dose responses, *i.e.* it is difficult at high concentrations of inducer to produce a sensible change in transcription. IPTG and *lac* based methods show an exponential dose response that, if the gene of interest is required to be transcribed and controlled at high cellular concentrations, predictable changes become difficult to control with altering inducer concentration alone⁴³. “Leakiness” is also often reported with *lac* based synthetic regulons, which is blamed on the repressive nature of LacI, it must be bound to DNA in order to repress so there are naturally occasions where it is neither bound DNA or IPTG⁴⁴.

Tight and precise control of specific promoters was achieved with the invention of the pBAD vector system. This exploits the native AraC transcriptional regulator in *E. coli* with Janus-like transcriptional activating and repressing ability⁴⁵. Glucose binding represses transcription from AraC-controlled promoters while arabinose binding activates transcription. This makes the pBAD platform and the AraC

repressor a technique for both transcriptional activation and repression through the use of different ligands.

Other small molecule regulators have emerged that have more linear dose response curves. An example is the *rhaBAD* system that uses transcription factors of the same family as AraC. This been engineered to greater utility by Kelly *et al*⁴⁶. Native rhamnose metabolism in *E. coli* is under the control of the RhaR regulator, which acts similarly to LacI, where rhamnose interaction relieves inhibition of transcription of the *rhaS* gene, whose product RhaS is then activated by rhamnose interaction. By decoupling RhaS transcription from RhaR repression, a transcriptional activating factor was developed with near linear dose response to rhamnose and rhamnose analogues, some of which could be used to produces sustained activation in *E. coli*. This transcription factor has been engineered also for use in synthetic circuits in cyanobacteria⁴⁷.

The Tet repressor, TetR, has been used extensively to regulate expression of heterologous genes. This was developed to respond to tetracycline analog anhydrotetracycline (aTc), which relieves inhibition of TetR controlled promoters^{48,49}. Thus this is a transcriptional repressor that can be inactivated by application of its ligand aTc.

Social microbial cues known as quorum sensing (QS) molecules can be used in sophisticated ways to affect transcription either by direct application of the signalling molecule by the user or by the integration of signal synthesis in to more complex designs. A commonly described system is the *lux* operon encoded by *Vibrio fischeri*, a marine proteobacterium that inhabits the body of bobtail squids, controlling expression of luciferase, a protein that produces bioluminescence. The unique feature of QS circuits is that they respond in a digital fashion after build up to a critical concentration of the signalling molecule, and never below it⁵⁰. The *lux* platform uses acyl homoserine lactone molecules synthesized by LuxI, which at a critical concentration stabilize the homodimer state of the LuxR regulator permitting its interaction with DNA to activate transcription^{51,52}. LuxR then can be used as a transcriptional activator that responds to specific concentrations of acyl homoserine lactone.

QS controlled elements have been altered through engineering of the promoter site recognized by QS molecule sensing transcriptional activator⁵³, as well as directed evolution of the sensor protein itself⁵⁴. The EsaR protein is an interesting QS sensor protein with LuxR type activating properties, as well as acting as a QS induced repressor at specific promoters. By placing additional EsaR binding sites in EsaR activated promoters, the strength of the promoter was altered⁵³. This was then combined with an EsaR variant which was sensitized to AHL by error prone PCR and reporter-based screening⁵⁴.

1.4.1.2. RNA-based Synthetic Regulation

Besides proteins, RNA can also be used as a transcriptional regulator. Many of the techniques developed in this medium use either antisense sequences to either nascent transcripts or coding DNA sequences, or sophisticated and ingenious structural properties of RNA.

RNA with a complementary sequence to the coding region of a target RNA can be applied to specifically knockdown translation of specific genes. Na *et al*³² have applied this in an interesting tool which utilises the endogenous RNA housekeeping mechanisms of *E. coli*. By designing sRNAs with a 5' Hfq binding site with a downstream antisense targeting region, specific mRNAs can be destroyed rapidly and precisely. Dynamic remodelling of *E. coli* metabolism has been produced with this strategy without disrupting chromosomal coding structures.

While this strategy destabilizes a target mRNA, another tool can improve their stability³⁴. Nakashima *et al*, in their vector library for central carbon metabolism RNA silencing described in Section 1.2, added 38 nucleotide hairpin sequences at the 3' end of their sRNAs³⁴. This improved stability by preventing their recognition by housekeeping RNases.

Sophisticated strategies have been invented using RNA structural elements. The ribosome binding site (RBS) is an essential mRNA feature for translation of the transcript. By encoding a “*cis*-repressing” antisense sequence (called *cr*) immediately upstream of an RBS, Isaacs *et al*⁵⁵ repressed translation of a transcript, where the *cr* region folded over the RBS, precluding ribosome access. This could only be relieved by the binding of an additional RNA with sequence complementary to *cr* at its extreme 3' end, which peeled *cr* off the RBS.

Terminators are naturally occurring RNA structures that are found at the 3' end of mRNAs. They are looped structures that stall the RNA polymerase machinery and signal its departure from the coding region^{56,57}. Synthetic introduction of a terminator to the 5' untranslated region of a nascent transcript was used to attenuate transcription⁵⁸ before the coding sequence could be transcribed. The presence of RNA antisense to part of the terminator sequence was used to relieve this attenuation.

Ingeniously, active transcription has been employed as a repressor of a targeted transcript³³. In this tool, a composite terminator and antisense promoter part was designed. Transcription can be prevented doubly by the presence of a terminator, but also the action of an RNA polymerase acting in the opposite direction. When the two nascent transcripts collide, transcription of each is ended³³. An issue with this

tool, however, is the wastage of ribonucleotide incorporated in to the opposition transcript and the diversion of the RNA polymerase complex.

Riboswitches are RNA elements that can alter their structure in response to environmental signals. Normally, the change in conformation results in the facilitation of translation, or the continuation of transcription. The sensitivity of the riboswitch is dependent on a region of the sequence called the aptamer. The aptamer may be sensitive to temperature, pH or specific small molecules, thus changing conformation⁵⁹. Their modular nature readily produces the potential for engineering. Many studies have developed novel aptamer sequences that bind to small molecules, either through affinity screening from libraries of naturally occurring RNA, or by random mutagenesis to produce entirely synthetic riboswitches^{12,60,61}. One ambitious study invented an *in silico* method for designing functional small molecule binding riboswitches⁶².

1.4.2. Oscillating Circuits

By combining transcriptional and translational regulators from divergent backgrounds, more complex circuitry can emerge. A seminal work by Elowitz and Liebler combined a GFP reporter influenced by a synthetic network of three transcriptional repressors⁴² giving rise to an oscillating cycle of repression. GFP expression is directly repressed by TetR, however *tetR* is under the transcriptional control of LacI. This means that *gfp* can only be transcribed in the absence of LacI. LacI dependent repression of *tetR* transcription is relieved by lambda phage repressor cI which inhibits *lacI* repression. This layered repressive circuit topology generates three “phases” of transcriptional inhibition that foment GFP production only in the cI dominant phase, which subsides once TetR has accumulated to sufficiently repress the GFP reporter’s transcription and *cI* transcription.

This oscillation can be measured where the GFP reporter would only be detectable under conditions where LacI was present in great enough quantity to repress *tetR* transcription, thus under conditions where *cI* was not yet repressed by TetR, a juxtaposition that foments the oscillatory behaviour.

Repressilator

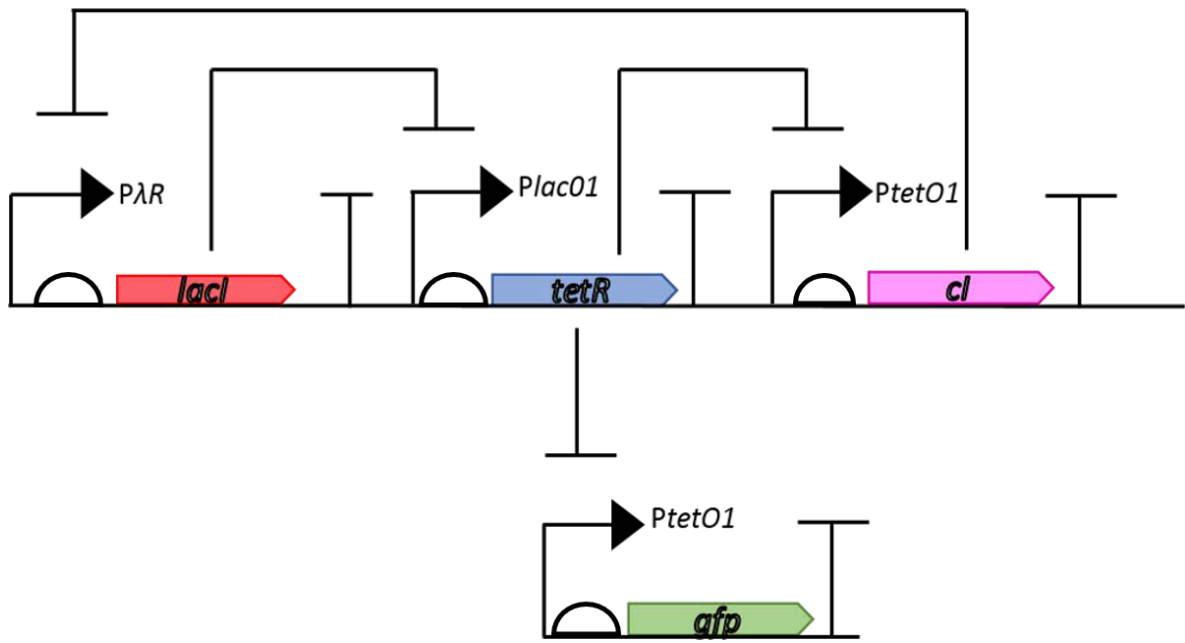


Figure 0.1 Diagrammatic representation of the repressilator circuit

In both Elowitz and Liebler's original design and the refined version by Potvin-Trotter et al, a GFP reporter is placed under the control of the TetR repressor, inhibition of tetR transcription by LacI will produce a period of GFP expression and permission of cI transcription, until the cI repressor accumulates to inhibit lacI transcription to sufficiently permit tetR transcription and renew the oscillatory cycle.

Oscillatory breakdown occurs after extended time periods in these circuits. Modelling and demonstrations in similar circuits led to an improved version of the repressilator with extended lifespan of oscillation and a reduction in the periodicity of oscillation⁶³. Three major changes were made to the repressilator circuit. First, the plasmid containing the GFP reporter part of the circuit was a high copy replicon with poor regulation of its replication, resulting in slow fluctuations in practical copy number within cells that can alter the GFP signal measured. This was changed to a lower copy plasmid. Observation that the TetR repressive phase of the oscillatory cycle was the noisiest prompted *in silico* prediction that this was due to a very low TetR concentration threshold for repression, leading to background from historical cycles causing premature repression with increased oscillation number. Adding in increased TetR binding sites outwith relevant operonic regions to act as sinks reduced this artefact. Last, protease targeting tags used to turnover the transcriptional repressors by ClpXP were removed after observations that in larger scale synthetic circuits, high affinity *ssrA* tags lead to competition for ClpXP and proposed machinery overloading and stalling of proteolysis⁶⁴.

More complex circuits using the repressilator by integrating in other divergent transcription factors have been proposed^{65–67}. One of these uses the integration of the *V. fischeri lux* circuit, where *luxI* transcription is promoted by a transcription factor “X”, which also promotes its own transcription along with a protease “Y”, which degrades it. LuxR responsive transcription of transcription factor *x* leads to a fully integrated repressilator in a QS program⁶⁵. Models^{65,66} indicated this could be a way to synchronise gene expression throughout an oscillating culture, a proposition vindicated experimentally in subsequent studies^{68,69}.

Fine tuning of oscillatory period has been achieved by altering the intron length of the operon encoding transcriptional repressors⁷⁰. Theoretically, increasing intron length increases the time taken to transcribe the gene, resulting in extended period between repressive phases.

Metabolic modes have been controlled using an oscillator circuit by Fung et al⁷¹. A metabolic circuit where metabolite flux in one direction ultimately results in flux back in the opposite direction was constructed by encoding repression of enzymes driving flux in one direction and promoting expression of enzymes in the other. Depletion of the metabolite produced by the first pathway leads to relief of repression of the enzymes that produce it, allowing the cycle to renew, hence oscillation. The authors used acetyl-coA metabolism to acetyl phosphate and acetate in their design and an acetate responsive reporter circuit to characterize their model in a designed called the “Metabolator”. The metabolic pathway selected relies upon glycolysis under most conditions, as such the application of different

carbon sources resulted in different oscillatory periods. Acetyl-coA metabolism engineered in this way also could also drive oscillation in metabolic modes between anabolic and catabolic periods, or at least balance on average substrate supplied to each mode in large scale synthetic pathways.

1.4.3. Toggle Switches

The repressilator arguably kick started the modern academic movement in synthetic biology by applying purely engineering principles to biological contexts, leading to the construction of a canon of synthetic gene circuits. Toggle switches quickly joined this group when Gardner, Cantor and Collins produced the first one⁷² by combining a TetR repressed *lacI* regulon that controls represses the *tetR* encoding operon in turn. This circuit can behave in a bimodal fashion where application of IPTG triggers a TetR dominant mode, and aTc a LacI dominant mode.

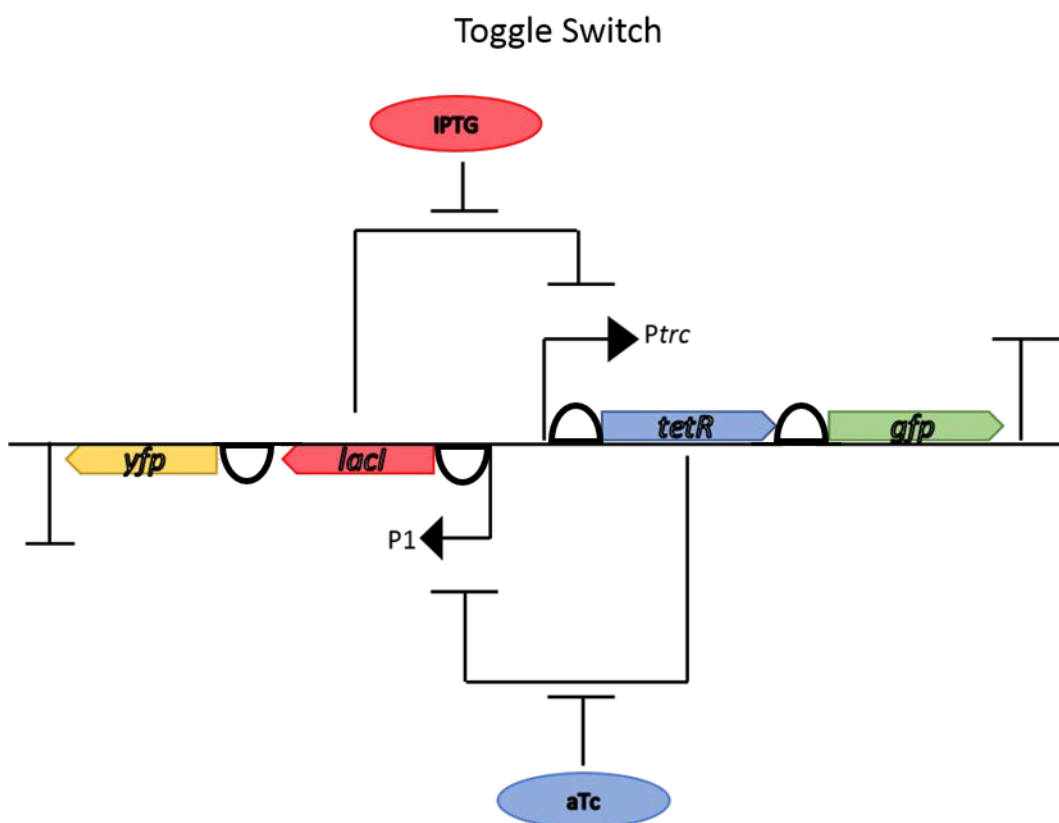


Figure 0.2 Diagrammatic representation of the toggle switch circuit

Complimentary transcription of *tetR* and *lacI* transcriptional repressors leads to a switching in to a TetR or LacI dominant mode upon application of aTc or IPTG respectively.

Wu *et al* made an interesting application of this circuit where its use in *S. cerevisiae* could produce evenly heterogeneous populations from an entirely homogenous starter culture where all cells were exposed to the same stimulus⁷³. By encoding a toggle switch with LacI and TetR as in Gardner *et al*⁷² and placing the circuit under a glucose repressive regime, the action of the toggle switch could be prevented during a pre-growth stage in glucose. Washing and inoculating the culture in galactose and an intermediate concentration of aTc lead to the emergence of two distinct populations, a TetR dominant one, and a LacI dominant one. Adding more aTc would lead to an entirely LacI dominant culture, and none at all to a TetR dominant one.

Integration in to additional circuits has lead to more complex toggle switch behaviours. The physical signal of UV radiation was used to trigger RecA cleavage and inactivation of the LexA transcriptional repressor, which converged on an engineered promoter with LacI which acted as a NOR gate controlling *gfp* transcription. Functional logic in this context then instigates GFP detection only in the presence of both IPTG and UV radiation. Integrating this further so that a cI / cI434 phage repressor based toggle switch acted as a memory module, UV stimulus could be used to throw the dominant state of the toggle, where the NOR gate promoter indirectly controlled *lacI* encoded on the cI controlled part of the toggle switch. This results in UV-inducible state switching⁷⁴.

Applications of toggle switch circuits have been explored in some detail. One study used a toggle switch to build predictable timer circuits, where application of stimulus would lead to a change in phenotype in a reliable time period⁷⁵. Their model was *S. cerevisiae* expressing a LacI/TetR toggle switch with a divergent LacI controlled GFP reporter. Using a library of randomly generated promoters generated from *lacO* and *tetO* promoters and quantifying promoter strength, they built a mathematical model that accurately predicted the time taken for the cell to return to a resting basal state determined by combination of promoters used. Interestingly, modelling indicated less predictable hysteresis using strong *lacO* promoters regardless of accompanying *tetO* promoter. By replacing *gfp* in the toggle's reporter with the *S cerevisiae* gene *FLO1*, which controls yeast sedimentation, it was possible to produce forecastable timing of culture sedimentation over a period of days. This property could be useful in the brewing industry where sedimentation is necessary for separation of the yeast from the fermentation broth.

1.4.4.The Band Pass Filter

A band pass filter is an electronics derived concept, where in a system receiving a multitude of signals a defined range can be selected and all others filtered out. This has been recreated biologically in a couple of examples.

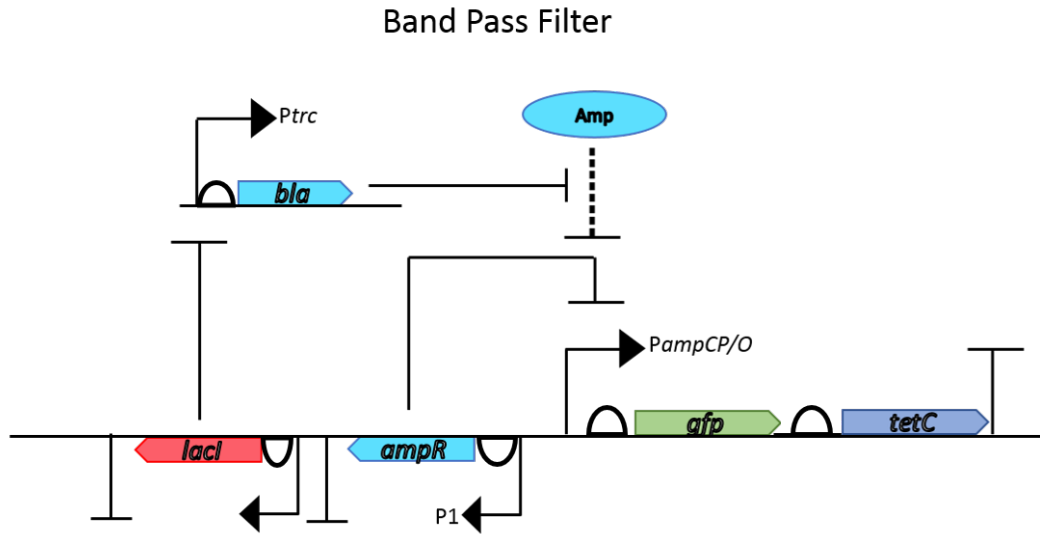


Figure 0.3 Diagram of the band pass filter circuit

AmpR represses tetracycline resistance gene $tetC$ transcription, which is relieved indirectly through cell wall breakdown by ampicillin, meaning cells will only grow on both ampicillin and tetracycline if an intermediate level of beta lactamase activity is displayed.

The first biological band pass filter utilised antibiotic resistance enzyme activity as the signal to filter, where only an intermediate level of activity in the enzyme conferring resistance would permit cell survival in an environment with two antibiotics⁷⁶. A circuit was assembled where an ampicillin activity sensitivity promoter *ampC* controlled tetracycline resistance gene *tetC*, and LacI controlled Bla expression. If Bla activity is too great, ampicillin activity will inhibit TetC expression, preventing growth on tetracycline, however if Bla activity is too low, growth on ampicillin will be impossible. The end result is a strain which is only capable of growth on both ampicillin and tetracycline at intermediate Bla activity. The band filtered was tuned, *i.e.* the concentration of ampicillin or activity of Bla at which cell growth was permitted, by altering Bla expression with IPTG and controlling media ampicillin concentrations. Further development of this circuit, building in additional transcriptional stimuli and small molecule inhibitors of Bla produced designer biogeography with multiple fluorophores, a phenomenon hitherto only fully described in more complex animal contexts^{76,77}.

Analogous designs have expanded on this production of synthetic biogeography using band pass filters by encoding a band pass filter responsive to the antibiotic nisin. A nisin reporter was built using a nisin sensitive two component system activating GFP expression, however cell death would result in abrogation of this. By building additional strains and circuits where nisin resistance and production could be tuned externally, genetically heterogeneous populations could be physically separated in to predefined patterns⁷⁸.

Recombination of the genetic elements within an encoded band pass filter has produced some clever circuit designs. By using the H₂O₂ sensitive transcriptional activated OxyR to control layers of recombinases and recombination sites, an array of band pass filters was built. Application of comparatively high and low sensitivity RBS and promoters controlled by OxyR lead to recombination of divergent loci encoding fluorescent reporters⁷⁹. Activation of a recombinase under the control of a low sensitivity promoter would flip a region encoding reporter gene in to the control of a divergent promoter. Activation of the higher sensitivity one could recombine the promoter to remove it from the control of this operon and in to another controlling a different reporter. Layering of this with additional recombinases lead to finally a triphasic band pass filter⁷⁹.

All of these synthetic circuit designs are suspect to flaws and disturbances during operation. These may arise from random physiological disturbances within the cell or artefacts during extended performance. If any of these devices are to be useful in practical applications, these disturbances might be more frequent and provide a larger perturbation than those experienced in the laboratory. Control and

recovery from these disturbances can be achieved using recently developed disturbance rejection circuits, so-called “antithetical integral feedback control”⁸⁰. These depend on regulatory factors which are said to “annihilate”, which in molecular biology terms relates to the interaction and sequestering of transcription factors acting in opposition to each other. This produces a “closed-loop” feedback circuit, while those which lack this are referred to as being “open-loop”. In closed-loop circuits, the annihilation phenomenon leads to recovery of circuit activity to normal within hours, while an open loop circuit will return to a baseline at a lower level.

Continued development of these programs and their integration into synthetic devices utilised in the real world should lead to more robust and effective synthetic gene circuits.

1.5. The Need for New Methods to Control Synthetic Physiology

Contemporarily used induction mechanisms rely on the application of small molecules and genetically integrated platforms, as discussed in Section 1.2. The use of small molecules to induce changes in physiology has many limitations for biotechnological applications. There is a continuous cost associated with purchase and repurchase of the chemical from a purely economic perspective. Beyond this rate of uptake of and response to the inducer is limited by its diffusion through the culture and its uptake by the cell. This could lead to metabolic asynchrony throughout the culture that may affect yields or at least contribute to the timescale of the production period. Physical stimuli may be able to overcome this. Phenomena such as light, sound or radiation is not hampered by the permeability of cell envelopes, and things like sound or electromagnetic waves could penetrate every cell in a culture simultaneously. Chemical inducers may also affect physiology long after they are required. A physical stimulus can be applied and removed in fractions of seconds, giving precision not afforded by chemical alternatives. Beyond this, more effective and instantaneous induction methods could allow investigators to interrogate complex systems with hitherto unseen precision. Methods like these have been explored but are not yet readily applicable at an industrial scale.

Additionally, the integration of more complex circuits like oscillators and toggle switches at an industrial scale combined with more effective exogenous controls could realise the precision bioengineering that synthetic biology promised.

1.5.1. Light-Controlled Synthetic Regulation

Light is a natural choice for engineering genetic responses to, given there are myriad platforms developed by Nature for its sensation and harvest. In a practical sense, the technology to transmit light with great efficiency can be deployed with something as simple as an array of cheap LEDs, making it an appealing strategy.

At its most simplistic, a form of IPTG that had been “photocaged” with a 6-nitropiperonal group has been used to build a light-inducible *lac* platform^{81,82}. Under stimulation with UV-A light, the 6-nitropiperonal group on the photocaged IPTG is destabilised and the resultant ‘naked’ IPTG can then activate *lacI*-repressed promoters. This is clearly a variation on the theme, however, of existing small molecule induction platforms.

Phototrophic bacteria are natural bearers of light-sensing genes that may be used in synthetic light controlled applications. In *Rhodobacter* species, the blue light sensing AppA protein agonizes the transcriptional repressor PpsR, leading to a relief on repression on photosynthetic genes. Light sensation in this example uses a flavin molecule bound to AppA⁸³.

A red and far-red sensing protein from *Synechocystis* PC6803 called Cph1 has been engineered and used in the eternal proof-of-concept organism *E. coli*⁸⁴ as a red light triggered transcriptional activator. Cph1 depends on the pigment cyanobilin for light reception. To engineer light reception using Cph1 the cyanobilin domain was fused with the signal transducing domain of the *E. coli* two component sensor EnvZ. Two component sensors like EnvZ have signal reception functions alongside kinase and phosphatases that autophosphorylates the protein and transduces this phosphate to a cognate response regulator protein that controls a phosphorylation influenced transcriptional program. A functional fusion produced was called Cph8⁸⁴ and effectively transduced signal to EnvZ’s partner response regulator OmpR as evidenced through genetic reporter systems. This was integrated into a more complex quorum sensing circuit that allowed genetically embedded “edge detection”, where QS controlled cells left in the dark gave rise to defined edges around areas of a colony where Cph8 mediated light sensation overrode the QS controlled circuit⁸⁴.

Blue light can be sensed using proteins with the LOV domain⁸⁵. This domain depends on flavin binding allowing conformational changes, which are not influenced directly by redox changes in the flavin, upon blue light excitation. By fusing the LOV domain from YtvA to a histidine kinase domain from the *Bradyrhizobium japonicum* protein FixL, Moglich *et al* were able to generate a blue light repressible regulon⁸⁶. FixL is a cytoplasmic histidine kinase that senses oxygen, under unaerobic conditions FixL

exhibits kinase activity upon its response regulator FixJ to activate it, and possibly phosphatase in anaerobic conditions^{82,87}. By fusing these, a recombinant protein called YF1 was generated that stimulated a FixJ controlled regulon in *E. coli* in the dark and repressed it under a light conditions⁸⁶.

By combining the Cph8 red light sensor with a cyanobacterial green light sensor CcaS, a strain that was able to distinguish red from green light was developed⁸⁸. CcaS is a two component histidine kinase that is stimulated by green light and phosphorylates CcaR to induce transcription of photosynthesis genes, and is repressed by red light. Expression of each of the synthetic Cph8 two component systems with the CcaSR system allowed the production of monochromatic bacterial “photographs” by spatial stimulation to two-tone (red-green) spatial stimuli.

Taking this to a natural conclusion, this platform was elevated to sense all three physical primary colours distinctly through the addition of the YF1 blue light sensor⁸⁹. By integrating genetic NOT gates in the form of repressive intermediate steps in between YF1 and Cph8 mediated sensation, excitation by specific wavelengths of light encompassing red, green and blue spectra was applied to produce impressive RGB images⁸⁹.

These studies comprise the most sophisticated invention to date of synthetic light sensation and response, however they are yet to find substantial practical application. Practical limitations on the technique of light induction may be important here, where light may not penetrate perfectly here or the volume of extra genetic information required to encode the more sophisticated RGB system.

1.5.2. Magnetically Induced Regulation

The use of magnetic fields to control synthetic biological processes is attractive as magnets are facile to produce in a range of different forms, and the signal of a magnetic field is not limited by the media of a growing culture, as light may be. A number of organisms have been reported to capable of magnetoreception, including birds⁹⁰, various social insects^{91,92} and magnetotactic bacteria^{93,94}, proposedly using this for navigation. Magnetotaxis in prokaryotes is the best characterised of these phenotypes but requires large amounts of genetic information and is yet to be effectively reconstituted heterologous in an industrially-relevant chassis organism. Cranial examinations of birds and social insects that display magnetoreception have found magnetite within supposedly specifically developed areas of the skull or cranium for magnetoreception⁹⁵, however deeper understanding of the mechanism of this phenotype is missing. Some work has proposed a new area of “quantum biology” to explain this phenotype in avian examples⁹⁶, where quantum entanglement between electrons in a cryptochrome protein in the birds eyes can effect light regulated signalling between the retina and the brain⁹⁷. This is

a sophisticated and remarkable mechanism, which has never been reproduced by experimenters or engineers *in vivo*, and efforts to produce magnetoreception synthetically to date have relied on bottom-up approaches.

1.5.2.1. Magnetism and Cellular Scale Magnets

Magnetism was first discovered in ancient Greece in the form of the magnetic mineral magnetite. Magnetism and magnetite take their names from either the Greek island where it was discovered, Magnesia, or in other accounts, from the hapless shepherd Magne who was surprised when the iron nails of his shoes were stuck to the ground as he led his sheep over a plain of magnetic rock⁹⁸.

Electrons are intrinsic to the physical model of magnetism. Practically all substances are full of electrons being building blocks of atoms and intrinsic to atomic interactions. The charge in motion produced by the electronic orbit around the atomic nucleus produces a constituent of the total magnetic moment called the orbital magnetic moment through a concept called Larmor precession. Larmor precession occurs when the spin axis of the electron is altered as a result of the charged electron moving around the nucleus. It can be expressed in Newtons as the Lorentz force which acts perpendicular to the vector the electron moves through. Larmor frequency refers to the rate of this precession around the central axis of the electron⁹⁹.

The other part of the atoms magnetic moment consists of the spin magnetic moment. This is produced by the spin state of the electron around its own axis. The entire magnetic moment of an atom or a magnetic material is expressed as the vector sum of the spin magnetic moment and the orbital magnetic moment.

All materials that contain electrons then can be said to have magnetic properties at some scale. At scales larger than individual atoms however, different materials take divergent magnetic states. These fall in to the categories of diamagnetism, paramagnetism, ferromagnetism and ferrimagnetism.

Diamagnetism occurs in materials where the atoms contain no unpaired electrons. The strength of a diamagnet is thus practically negligible compared to other stronger magnets as it is produced only by the orbital magnetic moment as the spin magnetic moment is cancelled by out by partner electrons in each shell.

Paramagnetism occurs through the presence of unpaired electrons where there is the combined effect of spin magnetic moment of the unpaired electron with the orbital magnetic moment of all others. The

magnetic field produced by this unpaired electron may align with an external magnetic field however thermal energy makes it impossible for perfect alignment.

Ferromagnetism is produced by its namesake Fe and other metals like Ni and Co. First considering a Bohr model Fe atom, it contains 26 electrons that can all be paired, however the spin states of all electrons here are not balanced. Filling the 4s electron shell takes less energy than filling the 3d electron shell and thus occurs before it. This leaves six electrons in the 3d shell, five in one spin state and two in the other. The magnetic moment of a single electron is given the fundamental quantity of the Bohr magneton, thus a single Fe atom produces a net magnetic moment of four Bohr magnetons, since there is a deficit of four electrons in unpaired spin states.

In the crystal lattice of a ferromagnetic material, electron orbitals can overlap and amplify this effect in what is called exchange coupling. Exchange coupling aligns these unbalanced spin states producing a magnetic moment that is hundreds of thousands times stronger than that of a diamagnet.

Materials containing ferromagnetic elements however might still not convey a net magnetic moment. This is controlled by crystal lattice architectures that might force antiparallel alignments of equal magnetic moments. This concept is called antiferromagnetism.

Ferrimagnetism occurs when what would be an antiferromagnetic lattice has unequal opposing magnetic moments. Magnetite is a ferrimagnetic Fe oxide with the formula $\text{Fe(II)}\text{Fe(III)}_2\text{O}_4$. The magnetic moments of Fe(II) atoms in the lattice structure of magnetite are antiparallel with the Fe(III) atoms. If they were equal in molar quantity, this would form an antiferromagnet, however there are twice as many Fe(III) atoms as Fe(II), producing a strong magnetic moment.

The alignment of magnetic moments within a magnetic crystal lattice of ferromagnets and ferrimagnets are usually not aligned uniformly throughout, instead aligned only in smaller regions called domains. This disordered alignment of domains can determine the strength of the magnetic moment by the material overall. Chunks of magnetite in the Earth that have had their domains aligned by lightning strikes have been studied historically as “lodestones” by pioneering students of magnetism Descartes, Porta, Gilbert. This is likely how Magnes lost his shoes. Since it takes great amounts of energy, as in a lightning strike, to align magnetic domains in a sample, the disordered state is more often adopted.

Particles of magnetite that are on the order of up to 50 nm in diameter are generally found as single domain nanoparticles. Larger particles than this likely to be multidomain particles due to the physical limitation of the domain walls. Domain walls are the regions between domains where the alignment of

the magnetic moment between adjacent domains gradually is changed. Since it costs energy per unit space of domain wall between domains, smaller particles are physically limited in how much space might become a domain wall. The surface of a magnetic nanoparticles has a so called magnetostatic energy by virtue of the poles of the particle. The larger the particle, the greater the magnetostatic energy. If the particle is split in to two domains the magnetostatic energy is halved, thus it becomes more stable at larger sizes to convert this energy to domain walls and contain multiple domains to diminish this magnetostatic energy.

1.5.2.2.Magnetism in Electrical Systems

As orbiting an atom, electrons moving through an electric wire are subject to Larmor precession through Lorentz forces due to the charge in motion. This means that electric wires also produce a magnetic field. By applying the canonical “right hand rule”, the Lorentz force is applied perpendicular to the direction of electron flow and the magnetic field thus produced perpendicular in the other dimension. The magnetic field can then be considered as a tube encasing the exterior of the wire, with no polarity, but movement around the circumference clockwise normal to the direction of current flow. As the current in Amperes moving through a wire is increased, so too is the strength of the magnetic field.

Polarity as is seen in bar magnets can be produced electrically by coiling wire in to a solenoid. In this conformation, the magnetic field propagates straight through the length of the centre of the solenoid and antiparallel along the exterior face. Again, increasing the current can increase the strength of the field, as well as can increasing the number of turns of wire in the solenoid.

Using an electromagnet like a solenoid can align the domains of ferromagnets and ferrimagnets. A magnetic influence called the coercive force aligns the magnetic domains in the crystal lattice with that of the electromagnet if it is strong enough. If a strong enough field is applied, all domains in the ferromagnet will be aligned by what is called the magnet’s coercive force, and it is said to be magnetically saturated. If the magnetic field is removed, the ferromagnetic can retain what is called remanent magnetism. This can be reversed by remanent coercion, which is exerted by applying a magnetic field of the opposite polarity.

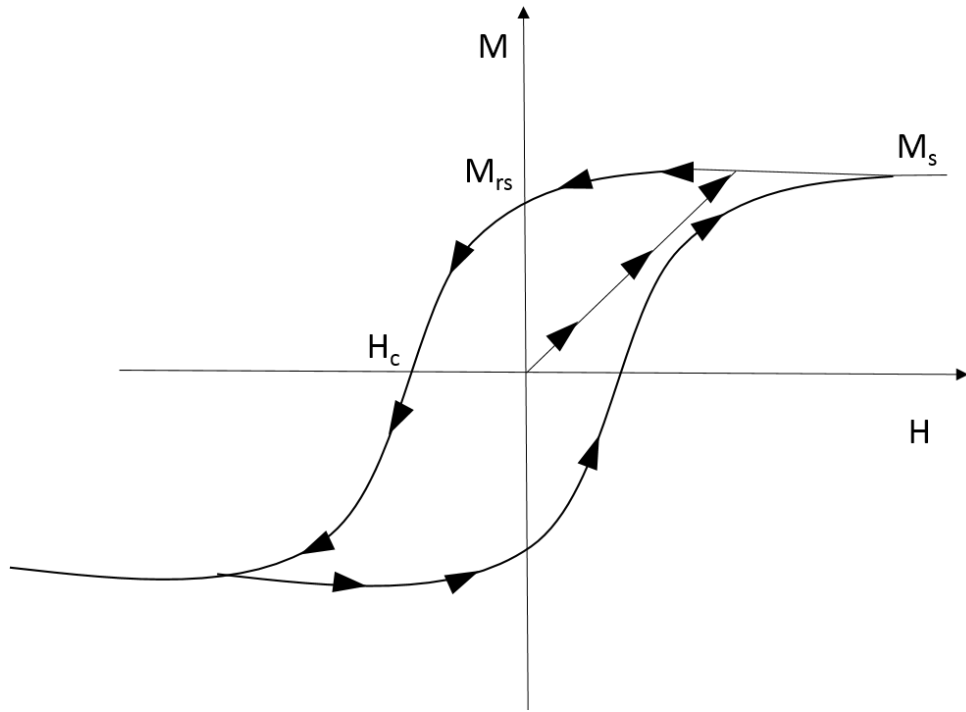


Figure 0.4 A magnetically susceptible material can be magnetised by an external field in opposing polarities in a hysteresis loop

The degree of magnetism imbued is denoted as M on the Y axis and the strength of the external field as H on the X axis. The magnetisation from the ground state of the ferromagnet with no net magnetic moment leads to, M_s indicating the saturation magnetism. M_{rs} denotes the remanent magnetism that is retained upon removal of the external field. As a field is applied with the opposite polarity to the original field, H_c denotes the coercive force required to remove all remanent magnetism.

Figure 1.4 shows a magnetic hysteresis loop, where a magnetic material is magnetised by coercive force, then demagnetised and remagnetised in the opposite polarity by coercive remanence. The space between the application of coercive forces and coercive remanence displays that there is energy required to perform multiple hysteresis loops. Through one hysteresis loop, in order to return the material towards a non-magnetic state energy is lost by the material as poles are reoriented and magnetic domain walls are morphed, and subsequently gained again as its magnetism is raised again. This energy is lost in the form of heat, and input again from the magnetic fields coercive force

If an alternating current is applied to a solenoid with a magnetic material within it, one hysteresis loop will be performed for every 2 Hz of the frequency of the alternating current, *i.e.* a 50 Hz AC solenoid would force 25 hysteresis loops per second. With alternating currents on the order of kHz and MHz, the heat produced in each phase of hysteresis can build up significantly. This is called magnetic hyperthermia.

1.5.2.3.Synthetic Magnetoreception

A few attempts have been made to instigate magnetoreception in mammalian systems. Largely these depend on the TRPV1 Ca^{2+} channel. TRPV1 is found throughout the human nervous system however it is popularly known as the receptor for capsaicin, giving spicy foods their “hot” sensation on the tongue. TRPV1 is temperature sensitive and conducts Ca^{2+} at temperatures from around 40 °C and above¹⁰⁰.

By coupling TRPV1 with a magnetically responsive “aerial”, the principle of magnetic hyperthermia has been applied to control membrane depolarization in neural circuits and other Ca^{2+} responsive behaviours in divergent tissues.

Blood glucose levels in mice has been controlled using oscillating magnetic fields by Stanley *et al.* Superparamagnetic iron oxide nanoparticles were antibody conjugated such that they would interact with TRPV1 in one example¹⁰¹. The Ca^{2+} activated kinase then phosphorylated the NFAT transcription factor to promote proinsulin gene transcription. Exposure to oscillating magnetic fields then lead to activation of this engineered pathway and reduced blood glucose over a period of approximately 1.5 hours.

In another example, ferritin was attached to TRPV1 to act as the aerial module and activate proinsulin release using the same pathway¹⁰². Ferritin attachment was achieved using a nanobody conjugation with a GFP-nanobody interaction between the proteins, and a myristolate tagged variant of ferritin that

would traffic the protein to the plasma membrane. The analogous methods showed that under oscillating magnetic fields the myristolated ferritin elicited the best response.

Mechanical forces exerted by a magnetic field have been explored as a method for synthetic control also by Wheeler et al¹⁰³. by fusing ferritin as an aerial to an actuator module using TRPV4, which is a mechanosensitive relative of TRPV1. Their data indicated that stimulation with static magnetic fields could trigger influx of Ca^{2+} to zebrafish neurons, imaged using a CgAMP6 reporter, and influence their larval coiling behaviour.

Exciting as these observations are, controversy has shrouded these results¹⁰⁴. Meister has posited that these models for genetically encoded magnetic remote control do not obey the laws of physics. The major problem with the strategies used by Stanley *et al*¹⁰² and Wheeler *et al*¹⁰⁵ is the use of ferritin as an aerial. Even if the entirety of the diameter of a ferritin cage was made of the ferric hydroxide mineral it stores, its size would comprise only 5 nm, which is considered far too small to convey any permanent magnetic moment critical to responding to the magnetic fields used in these experiments above temperatures of 40 K¹⁰⁶. Even if the ferritin-caged particle could sustain a permanent magnetic moment, Meister calculated that the temperature change would only be in the order of tens of nK, falling far short of the 5 K temperature difference required to open the TRPV1 channel. Modest temperature increases of this order were produced however by doping the ferric hydroxide core of ferritin with the magnetic metal cobalt by other investigators¹⁰⁷.

Meister permitted the cooperation of individual adjacent ferritin cages in a physical model of Wheeler et al's¹⁰⁵ platform and calculated that the even if this was controlling the phenotype observed, the strength of the force generated by ferritins collectively tugging on a single TRPV4 is 10^5 times too short an order to pull it open, based on physical measurements of similar channels^{104,108}.

Chen *et al*¹⁰⁹ have produced the most convincing platform for engineered magnetoreception in mammalian tissues. By injecting rat brains and mammalian tissue cultures with PEG coated magnetite nanoparticles (MNPs) they deployed oscillating magnetic fields to heat these MNPs, which were found extracellularly, which would raise local temperature enough to heat TRPV1 channels to open and trigger Ca^{2+} influx to surrounding cells. This was measured using a CgAMP6 reporter, a calcium responsive GFP variant that only fluoresces under Ca^{2+} ligation.

More recently, a gene was discovered in the glass catfish *Kryptopterus bicirrhos* that conveyed a magnetoreceptive phenotype to the fish that could be reconstituted in human epithelial tissue culture

models¹¹⁰. This did not rely on oscillating magnets; glass catfish were repulsed by the presence of a static magnetic field in their tank and would swim away from it. The gene proposed to be responsible for this phenotype, named EPG, was transfected into HEK cells and was found to depolarise the membrane by influx of Ca^{2+} as measured using a CGamP6 reporter. The exact mechanism by which EPG conveys this magnetoreception is not yet unravelled, however bioinformatic examination of the gene does not indicate it can function as a Ca^{2+} channel. Krishnan *et al* propose it interacts with Ca^{2+} channels present in the membrane and influences their conductance in a magnetically dependent fashion¹¹⁰.

Given our understanding of the response to magnetic stimuli at the cellular scale, it appears that a strategy that uses single domain magnetic nanoparticles as in Chen *et al*¹⁰⁹ is the best practical option at present for producing a synthetic magnetoreceptive phenotype.

1.5.3.A Design for Synthetic Bacterial Magnetoreception

Bacteria have been observed to synthesise an array of different metal nanoparticles, and magnetotactic bacteria have a sophisticated system for precipitating single magnetic domain magnetite crystals. Thus it may be possible to reconstitute a version of this phenotype heterologously to act as an “aerial” in a synthetic magnetoreceptive design in bacteria.

In this design a genetically encoded mechanism for magnetite synthesis and/or uptake would allow magnetic hyperthermia to be instigated within the cell, influencing a target thermoresponsive circuit.

1.5.3.1.Thermoreception in Bacteria

Response to temperature is essential for bacterial survival, without this bacteria may find themselves in the equivalent scenario of Scott of the Antarctic in a pair of Speedos, or Marco Polo in a fleece lined jumpsuit. Divergent bacterial species have evolved to thrive in relatively narrow temperature ranges, ranging from psychrophiles that can be isolated from Antarctic icebergs, to thermophiles that have evolved to succeed in deep ocean hydrothermal vents under extreme pressure and temperature. In the middle of all this lies mesophiles that may be found at a range of temperatures from 15 degrees centigrade to 45¹¹¹.

Pathogenic bacteria fall within this range also, and many of them sense temperature as a host indicative factor, making temperature response mechanisms intrinsic to pathogenesis.

As such mechanisms have evolved to control bacterial life cycles, from influencing and inducing specific behaviours, to homeostatic machinery that define the optimal range of temperatures for each organism.

When placed in an environment that exceeds the optimum temperature for the bacterium, a “heat shock” is experienced, and with this a specific program is induced mediated by the sensation of the temperature. A number of heat shock proteins (Hsp) were initially discovered in *E. coli* as being associated with this. Hsp32 is a member of this group intrinsic to transducing this signal. It is a sigma factor that guides RNA polymerase to a range of promoters of genes that allow the cell to survive the heat shock. As a sigma factor it has the alternate name RpoH, with the “H” indicating its involvement in Heat shock.

RpoH is an intrinsically unstable protein. It is routinely turned over in the cell by the ClpXP housekeeping apparatus with a half-life of only around one minute. This is promoted by the chaperone proteins DnaJ and DnaK. These bind to two distinct sites on RpoH that cooperatively enhance its turnover by ClpXP. Under heat shock conditions, DNA is negatively supercoiled and DnaJ and DnaK are employed as DNA chaperones instead, stabilising genomic structure in this period. This partially stabilises RpoH allowing it to control the specificity of RNA polymerase complexes and turn on the heat shock response.

Even more subtle than this however is RpoH translation control influenced by temperature. The RpoH mRNA contains a region which at cooler temperatures (30 °C), folds such that the ribosome binding site is occluded. This structure is unstable at higher temperatures representing heat shock conditions, thus *rpoH* is only translated under these conditions. By bypassing a transcriptional step, this represents a mechanism that, in a dynamic environment, cell physiology can be altered rapidly.

Virulence in the diarrhoeal pathogen *Shigella flexneri* is influenced strongly by temperature. The global virulence regulator VirF is transcriptionally repressed in conditions far cooler than host body temperature by DNA structures maintained by H-NS proteins^{112–114}. H-NS binds to DNA with a selectivity for regions which are curved and contain A tracts, including regions like this that occur at 5' and 3' ends of the *virF* promoter¹¹⁵ forming a structure impenetrable to RNA polymerases. Using *in vitro* experiments it was observed that at greater than 32 °C this structure is removed due to changes in DNA conformation¹¹⁶, permitting transcription from the *virF* promoter. This leads to the activation of a regulatory cascade that instigates the virulent phenotype¹¹³.

Listeria monocytogenes is another intracellular pathogen. This means it is found within host cells during infection. When it invades a cell, it loses its flagella and subsequent intracellular generations are also non-motile. This is controlled by a transcriptional repressor MogR^{117,118} which is antirepressed by the temperature sensitive GmaR^{119,120}. At 30 °C MogR is found only in association with GmaR. As

temperature increases GmaR levels decrease and MogR is then free to interact with and repress specific promoters¹¹⁹. The *flaA* gene controlling flagellar assembly bears the promoter with the predicted strongest affinity for MogR¹¹⁸, leading to strong repression of flagellar synthesis, and thus motility.

Bacteria then have evolved a range of mechanisms at the level of DNA, RNA and protein to control the expression of specific genes in accordance with changes in temperature. By combining some of these strategies with magnetically induced hyperthermia, precise control of gene expression and bacterial behaviour may be achieved.

1.6.Bacteria and Metal Nanoparticles

All of life is dependent on metals for the atomic wiring in the evolutionary ancient respiratory complexes. In addition, many organisms have evolved the capability to synthesise much more complex, and even perfectly crystalline, metallic materials. These range from the calcium carbonate shells of radiolarians and diatoms to other nanometer scale metal crystals that are used for a range of functions. The diversity of metal nanoparticles produced by microbes is displayed in Table 1.2. This transformation of soluble metals in the environment to solid types represents one of the ways microbes can influence and create geological and ecological phenomena over aeons.

Table 1.2 Selected examples of metal nanoparticles produced by microbes.

Metal NP	Organism(s)	Mechanism	Function	Reference
TiO ₂	<i>Halomonas elongata</i> <i>Aspergillus ochraceus</i>	Undescribed	Unknown	¹²¹ ¹²²
Au	<i>Cupriavadus metallireducins</i> , <i>Delftia acidovorans</i>	NRPS synthesised siderophores	Detoxification	^{123,124}
Au	<i>Leptothrix cholodnii</i>	Proposed RNA mediated reduction	Detoxification	^{125,126}
BiO	<i>Delftia acidovorans</i>	Likely nitrate reductase	Unknown, possible detoxification	¹²⁷
Bi ₂ S ₃	<i>Clostridium acetobutylicum</i>	Soluble Bi ²⁺ reduced by biogenic H ₂ S	Unknown, possibly contrived	¹²⁸
Ag	<i>Morganella</i> sp.	Genetically encoded Ag resistance mechanism	Detoxification	^{129,130} ¹³¹
AgNO ₃	<i>Fusarium oxysporum</i>	Nitrate reductase	Unknown	¹³²
Ag	<i>Aspergillus flavus</i>	Proposed secreted Ag reductase	Unknown, possibly contrived	¹³³
Ag	<i>Bacillus brevis</i>	Undescribed	Contrived	¹³⁴
Ag	<i>Pseudomonas stutzeri</i>	Undescribed	Unknown	¹³⁵
Pd	<i>Klebsiella oxytoca</i>	Biogenic H ₂ mediated reduction	Unknown	¹³⁶
Pd	<i>Shewanella oenidensis</i>	Likely hydrogenase dependent, pyruvate/formate metabolism dependent	Unknown	¹³⁷
Pd	<i>Bacillus benzeovorans</i> ,	Undescribed	Unknown	¹³⁸
Pd	<i>Desulfovibrio desulfuricans</i>	Likely hydrogenase	Detoxification	¹³⁹
Pd	<i>Escherichia coli</i>	Hydrogenase	Unknown, possibly contrived	^{140–142}
Pd	<i>Cupriavadus necator</i>	Probed but not defined	Unknown	¹⁴³
Pd	<i>Desulfovibrio vulgaris</i>	Cytochrome c3 and hydrogenase dependent	Unknown, possibly contrived	¹⁴⁴

Cu	<i>Morganella psychrotolerans</i>	Anaerobic metabolic process, details unknown	Detoxification	¹³¹
Cu	<i>Morganella morganii</i>	Proposed intracellular synthesis followed by export	Detoxification	¹⁴⁵
Cu, CuO	<i>Serratia</i>	Undescribed	Unknown, possibly contrived	¹⁴⁶
Cu	<i>Pseudomonas stutzeri</i>	Organic coat stabilisation	Proposed detoxification, possibly contrived	^{147,148}

1.6.1.Diversity of Metal Nanoparticles

Synthesis of metal nanoparticles has been described in a wealth of bacteria. It is often hypothesized that the complete reduction of metal anions in solution to stable nanoparticle states is a property that has evolved to combat metal stress and toxicity^{123,126,129,149}. Commonly this is used to isolate these organisms by direct selection from their environment. Typically following this, studies observe the visible effects of addition of soluble metal salts to culture media (*i.e.* colour changes and the appearances of precipitate); observe the nanoparticles under an electron microscope; and perform small angle electron diffraction (SAED) or similar techniques to observe crystallinity. Beyond these observations, the genetic bases of the phenotypes are sometimes probed but rarely fully elucidated.

Many bacteria have been isolated that are capable of silver nanoparticle (Ag-NP) synthesis. The earliest example is seen in *Pseudomonas stutzeri*¹³, a species isolated from a silver mine¹⁵⁰. These were observed under TEM to be large (up to 200 nm in diameter) crystals with pyramidal and hexagonal shapes found in the periplasm¹³⁵. The original study that isolated this strain demonstrated that the phenotype was dependent on a plasmid¹⁵⁰.

Peiris *et al*¹⁵¹ compared the properties of Ag-NPs produced by *Pseudomonas aeruginosa*, *Acinetobacter baumanii*, *Staphylococcus aureus* and *E. coli*. They found that all of these organisms were capable of producing Ag-NPs that had antimicrobial properties. The size of the Ag-NPs varied with the bacterium interestingly, however the authors proposed the same hypothesis for their synthesis across the board.

Another study found the capability of *Bacillus brevis* to produce Ag-NPs¹³⁴, these were very small (8 nm) compared to *Morganella* Ag-NPs on the order of around 50 nm.

Interestingly, extracellularly produced Ag-NPs from *Aspergillus flavus* were found to be coated in protein, where purified Ag-NPs after boiling in SDS still retain two protein bands observable in SDS-PAGE¹³³. It was proposed that these proteins were responsible for the synthesis of the Ag-NPs, one of them acting like an enzyme to synthesise the particle and the other acting to stabilize it. This hypothesis of enzymatic Ag-NP production was strengthened by the demonstration that purified nitrate reductase from the prolific NP producer *Fusarium oxysporum* was capable of crystalline Ag-NP synthesis¹³².

Morganella species have been touted as a useful organism for industrial production of Ag-NPs given its similarity to *E. coli* phylogenetically as well as in its culture conditions and genetic tractability. Originally, a *Morganella* isolated from an insect gut was observed to have greater resistance to Ag salts¹³⁰, and further work demonstrated the capability across the genus¹²⁹. Genomic inspection of the original

isolate found a number of genes encoding predicted silver binding proteins with up to 99% homology with characterized silver binding protein¹³⁰, PCR based methods showed that at least one of these genes, *silE*, was present across all other *Morganella* species studied¹²⁹. TEM indicated the Ag-NPs were found outside the cell.

Pulling together selected works that have investigated Ag-NP^{129,130,132,133}, there appear to be at least two mechanisms evolved for Ag-NP production. The first of that seen in *Morganella* species would appear to be dependent on the *sil* locus that is characterized in *Salmonella* species to control Ag efflux without Ag-NP production¹⁵². Further investigation into the *sil* homologs and surrounding genes in *Morganella* could be key to understanding Ag-NP synthesis by this method. Other candidate genes could be found under the control of a *Morganella* homolog *silR* regulator found in this loci in *Salmonella*¹⁵². The other uses nitrate reductase to enzymatically reduce Ag. This mechanism may be found in other organisms that reside in silver nitrate containing environments.

Thermotoga maritima encapsulin has been engineered to precipitate Ag-NPs in a heterologous *E. coli* background, producing an intracellular Ag-NP nanofactory¹⁵³. This used a modified version of the encapsulin gene, where the N-terminus was modified to include a silver binding peptide developed by phage display¹⁵⁴.

Palladium nanoparticle (Pd-NP) biominerization has been investigated in *Desulfovibrio desulfuricans*^{139,140,142} and *Desulfovibrio alaskensis*¹⁵⁵. It is proposed¹⁵⁵ that Pd, in *D. alaskensis* at least, is used as a respiratory electron acceptor and herein becomes reduced from soluble Pd(II) to fully reduced Pd(0) in the periplasm, atoms of which are then transported through the outer membrane and deposited where Pd(0) acts to nucleate and grow a crystalline Pd-NP. In vindication of this hypothesis *Desulfovibrio* also appear to be capable of producing this phenotype with the other platinum group metals Ni and Pt^{140,155}. Boring old *E. coli* has also been demonstrated to have the capability of Pd-NP generation^{141,156} in a mechanism that is thought to be dependent on its hydrogenases¹⁴¹. Using strains that encode only one out of three of the functional hydrogenases, Pd-NP reduction from the media was diminished compared to wild type *E. coli* and was abrogated entirely by deletion of all three. Interestingly however, large nanoparticles were observed on the outer membrane of cells of this strain when treated with Pd compared to hydrogenase active strains¹⁴¹. The lack of Pd reduction observed here but the presence of these enormous NPs could indicate the activity another non-hydrogenase dependent mechanism that produces Pd(II) containing alloy NPs. Metabolic engineering was performed to try to amplify hydrogenase activity by diverting the upstream metabolite pyruvate towards hydrogenase utilizing

pathways by deletion of *IdhA* and the Pd-NPs used as a catalyst in the proton electrolyte membrane of a hydrogen fuel cell¹⁵⁶. The activity of hydrogenases in the *E. coli* Pd-NP production system could indicate that homologous enzymes are responsible for the respiratory Pd reduction performed by *Desulfovibrio*. Further experimentation with analogous experiments to Deplanche et al in *Desulfovibrio* could vindicate this hypothesis.

Considering all of these examples of Pd-NP synthesis by bacteria, it is likely that their production is reliant upon hydrogenases, however concrete vindication of this hypothesis is required. Deplanche *et al*¹⁴¹ produced the most comprehensive study of hydrogenase mediated Pd-NP production in *E. coli*, however specific data in this study indicated additional mechanisms and overall failed to pin point an individual mechanism that could explain their production. Pd-NPs differ from biological Ag-NPs in this respect where distinct mechanisms appear to have evolved with this function. Pd-NPs also appear in most TEM observations to remain attached to the cell, in this way they differ from most other biologically produced metal NPs, which are normally synthesized extracellularly.

There are three good examples of bacteria that are able to biominerlize Au. *Cupriavidus metallidurans* is found cohabiting with *Delftia acidovorans* on naturally occurring gold nuggets^{124,157}, and each of these has developed unique mechanisms to biominerlize and detoxify the soluble Au(III) that they encounter in this environment. It is hypothesised that these bacteria are detoxifying the environment around Au deposits found in Arctic soils permitting the development of more complex microbial communities¹²⁴. *C. metallidurans* was observed to contain Au-NPs in its cytoplasm as shown by SEM and XRF studies. The metal stress responsive loci *cup* and *cip* were upregulated during Au biominerlization, as well as those genes induced by oxidative stress, indicating that the phenotype is produced by a response to Au stress¹⁵⁷. *D. acidovorans* in this environment was found to be able to efflux Au-NPs, while *C. metallidurans* was not¹²³. This was likely due to a putative metal efflux protein encoded alongside predicted secondary metabolite non-ribosomal peptide synthase (NRPS) genes. One of these genes annotated in this study¹²³, *delG*, was demonstrated to be responsible for Au biominerlization where its deletion triggered a non-mineralising phenotype along with Au(III) salt sensitivity. The DelG protein is predicted to encode a NRPS which synthesizes the Au specific siderophore delfibactin which was purified in association with AuNPs secreted by *D. acidovorans*¹²³.

D. acidovorans has also been demonstrated to be able to reduce Bi³⁺ to B⁰ NPs in a screen of wild organisms from an Iranian lake¹⁵⁸. It is unclear at this stage however what mechanisms are used to fulfill this activity and how related it is to delfibactin and the genomic island seen by¹²³ containing *delG*.

Outside of this ecosystem, *Leptothrix cholohnii* was demonstrated to be able to bind to¹²⁵ and precipitate AuNPs¹²⁶. *Leptothrix* sp. are coated with a shell made of protein, polysaccharide and embedded inorganic materials. The protein/polysaccharide mixture here was shown to adsorb a range of different metals including Au¹²⁵. Subsequently, it was hypothesized that RNA found in this sheath¹²⁶ and secreted into the culture medium might be responsible for the biominerilization where free guanosine was found¹⁴⁶ to quickly precipitate AuNPs. A specific sequence for this RNA is yet to be elucidated.

Copper nanoparticles (CuNPs) are produced by a number of different organisms. The AgNP producers *Morganella morganii* and *M. psychrotolerans* also synthesise CuNPs^{131,145}. A mechanism is proposed for this biosynthetic mechanism by Ramanathan *et al*¹⁴⁵ that involves Cu(II) influx followed by periplasmic reduction and efflux by a specific protein. This appears unlikely given the size of the CuNPs (up to 100nm in diameter^{131,145}).

Similar activities have been observed in organisms screened from Cu waste containing environments. Hasan *et al*¹⁴⁶ isolated a *Serratia* strain from the gut microbiota of Indian Stibara beetles¹⁴⁶ and Cu electroplating waste was shown to harbour a *Pseudomonas stutzeri* strain capable of making Cu-NPs^{147,148}. This raises again the possibility that CuNP biominerilization is a mechanism of Cu detoxification in these organisms. It is unclear if *Morganella* CuNP production is an analogous strategy.

Microbial precipitation is thus seen as a commonly identified feature. In many cases it is likely a strategy to reduce toxicity of heavy metal ions or other oxidising species, in others the properties studied are potentially artefacts of contrived experimental environments, as indicated in Table 1.2 where mechanisms are undescribed. Nonetheless the production of metal nanoparticles by microbes could become an industry standard “green” method of the future for the production of metal nanoparticles for myriad applications.

1.6.2. The Discovery of Magnetotactic Bacteria and Magnetotaxis

While searching for *Spirocheates* in the Cedar Swamp around the illustrious marine biology laboratory Woods Hole in Massachusetts USA, Richard Blakemore happened upon microbes that refused to stay at the centre of his microscope slide. After first investigating his hunch that these were extremely photosensitive organisms, he determined by application of magnets to his slides that their tactic influence was a magnetic field⁹³, thus these cells were “magnetotactic”.

Blakemore isolated this organism from stratified samples taken from the swamp and found it in an aerobic transition zone between layers of oxidized and reduced iron¹⁵⁹. TEM images of these bacteria revealed a strong helical morphology and chains of up to 22 magnetite crystals^{93,159,160} as displayed in Figure 1.4A, and a total iron content in the cells up to ten times that of other similar bacteria from this environment¹⁵⁹. Later it was found that the magnetite crystals were enveloped in what appeared to be inclusions of the plasma membrane^{161,162}, shown in Figure 1.4B. Henceforth this earned them the term “magnetosome”.

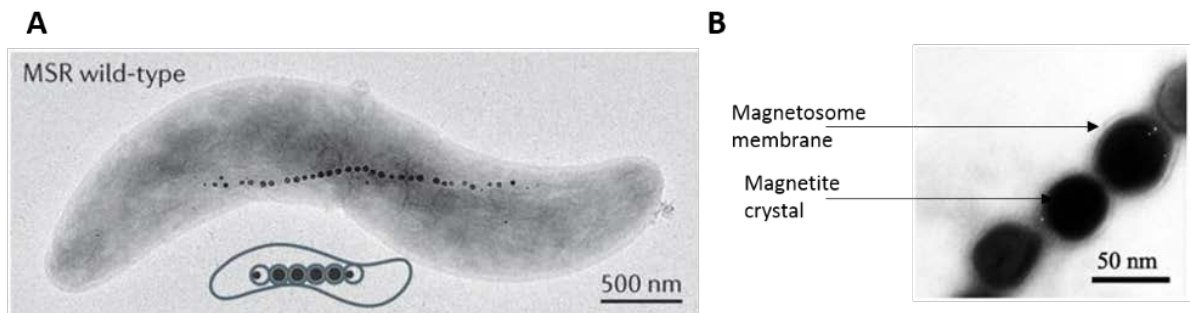


Figure 0.5 Examination of magnetosomes within *Magnetospirulum gryphiswaldense*

A, *M. gryphiswaldense* viewed with TEM, note the chain of magnetosomes along the mid cell. Taken from Uebe and Schuler¹⁶³ and reproduced with permission from Springer-Nature (License no. 4731470851386). B, Magnetosomes isolated from *M. gryphiswaldense* from Arakaki *et al*¹⁶⁴. Magnetosome membrane and magnetosome crystal are indicated.

The movement of magnetotactic cells in the absence of any external magnetic field indicated the cells were moving towards geomagnetic North. Oxygen sensitivity of these organisms and the oxic zone they were observed in swamp mud samples¹⁵⁹ led Blakemore to theorise that magnetotaxis was a strategy evolved to allow cells to migrate deeper in to soil towards micro- and anaerobic environments

when their habitat here is disrupted by the movement of water currents, movement of animals through the swamp or other naturally occurring phenomena.

Over multiple culture passages, MS-1 cells were observed to lose their magnetotactic ability. When these cells were selected and cultured alone, they were observed to have changed colour from dark brown to greyish white, reflected in the lack of defined magnetite crystals in these cells, however they still contained iron¹⁵⁹. Later Komeili 2012 indicates that this is through loss of the MAI. It was concluded thus that the production of magnetite crystals was required for the magnetotaxis phenotype.

This was a significant discovery, given magnetite had been discovered in the guts of bees, the skulls of pigeons and the shells of marine organisms called chitons, however a defined function had never been assigned to biologically occurring magnetite.

An interesting addition to the magnetotaxis phenomenon was the subtle variation in phenotype between MTB isolated in the Northern and Southern hemispheres¹⁶⁵. Blakemore led an excursion from Massachusetts to New Zealand to isolate MTB from similar environments to the Cedar Swamp, but in the Southern hemisphere. Here it was observed that MTB would migrate towards geomagnetic South¹⁶⁵. This built upon the theory that magnetosomes influenced migration of cells towards Earth's magnetic core. This was not demonstrated to be hard wired in to the magnetotactic mechanism, however. Demagnetisation of magnetite crystals inside both North or South seeking isolates would immediately result in a stochastic migration to both poles. After the cells had settled however they would migrate towards whatever pole signified "down" relative to Earth's surface. Application of a permanent magnet that opposed Earth's magnetic field but retaining an environmentally relevant oxygen gradient in North seeking isolates resulted in cells initially following the applied magnetic field, but upon weeks of culture, they would reorient to move down the oxygen gradient.

Physical characteristics of the magnetite crystals themselves are revealed by this experiment too. This ability of demagnetized magnetosomes to reorient with an applied magnetic field indicates that each crystal is formed as a single independent magnetic domain. This brings upon certain physical limits to the scale of magnetite crystal that might be found among MTB, otherwise incredibly sophisticated mechanisms would be required to form a larger crystal with a single magnetic domain.

Oxygen gradients were later added to the Blakemoreian model of magnetotaxis when an isolate similar to *M. magnetoacticum* was demonstrated to form "bands" of bacteria in liquid media drops in microscope slides containing air bubbles¹⁶⁶. Inversion of the magnetic field in these microscope observations showed

cells first begin to move again to the North pole of the magnet, but would then reorient towards their original position, all without the conventional “tumble” mechanism used in flagellar motility. This lack of tumbling led to the development of a model of *Magnetospirulum* magneto- and aerotaxis where the magnetic moment applied to the cell by Earth’s magnetic field influences direction of movement and oxygen stimulation would determine the “on” or “off” state of the flagellar motor. This would result in movement of cells far removed from the microaerobic zone towards Earth’s core, thus down the oxygen gradient, and when they reach this environment turn off their flagellar motor and cease taxis. This tactic cessation likely influenced by oxygen sensitive depletion of the proton motive force powering the flagellar motor as observed in other aerotactic organisms¹⁶⁷.

1.6.3.Diversity of Magnetotactic and Magnetosome Producing Organisms

Beyond the canonical Gram negative helical shaped *Magnetospirula*, a number of other magnetosome containing organisms have been discovered. Magnetotaxis is not a phenotype common to all of these organisms however and often there is no genome sequence or molecular investigations of their magnetosomes. The widespread isolation of these organisms indicates that the magnetosome phenotype is found throughout all aquatic ecosystems. This is an opportunity to discover hidden functions of magnetosomes.

One of these, referred to as the strain MC-1 for “magnetic coccus number one”, displayed magnetotaxis but with variations in its aerotactic phenotype.

The alkalinophilic environment found in soda lakes of Death Valley Junction, USA, harbour a magnetotactic isolate. These were helical rods like *Magnetospirula*, however its magnetosomes contained bullet shaped crystals. It was proposed that the naturally alkaline buffered environment found in these lakes could be the evolutionary origin of MTB, given the oxidizing environment could retain Fe in a form more favourable for crystallization¹⁶⁸.

Multicellular prokaryotes were isolated from the sediment ecosystems in a Brazilian lagoon that contained magnetosomes. These were balls of pyramidal cells that contained magnetosomes at their cell poles¹⁶⁹. Unlike most prokaryotes, this organism had an entirely multicellular life cycle, where cells proliferated within a ball like a tiny magnetic blastocyst then divided by separation into two balls of cells. It was originally proposed that the magnetosome aided the cohesion of cells in these balls however subsequent isolation of a strain identical to this one in all but magnetosome production has shed doubt on this¹⁷⁰.

Magnetic mineral diversity also exists among magnetotactic bacteria. Magnetite biomineralling organisms have become the archetypal model due to the ease of culture and genetic tractability of *Magnetospirula*. Nonetheless, organisms with the capability to produce other iron oxide magnetic nanoparticles such as maghemite and hematite, as well as the iron sulphide magnetic mineral greigite have been observed.

1.6.4.The Magnetosome Assembly Island

Reverse genetic techniques in *Magnetospirulum gryphiswaldense* has led to the discovery of a Magnetosome Assembly Island (MAI). This is a roughly 120 kb region on the chromosome that encodes the majority of genes identified to be unique to the magnetotactic phenotype. Around 20% of the coding sequence of the MAI belong to transposases and the entire region contains a number of insertion sites. This characterizes the MAI as a mobile genetic element, perhaps responsible for producing what is becoming recognised as near ubiquitous occurrence of magnetosomes across diverse genera¹⁷¹.

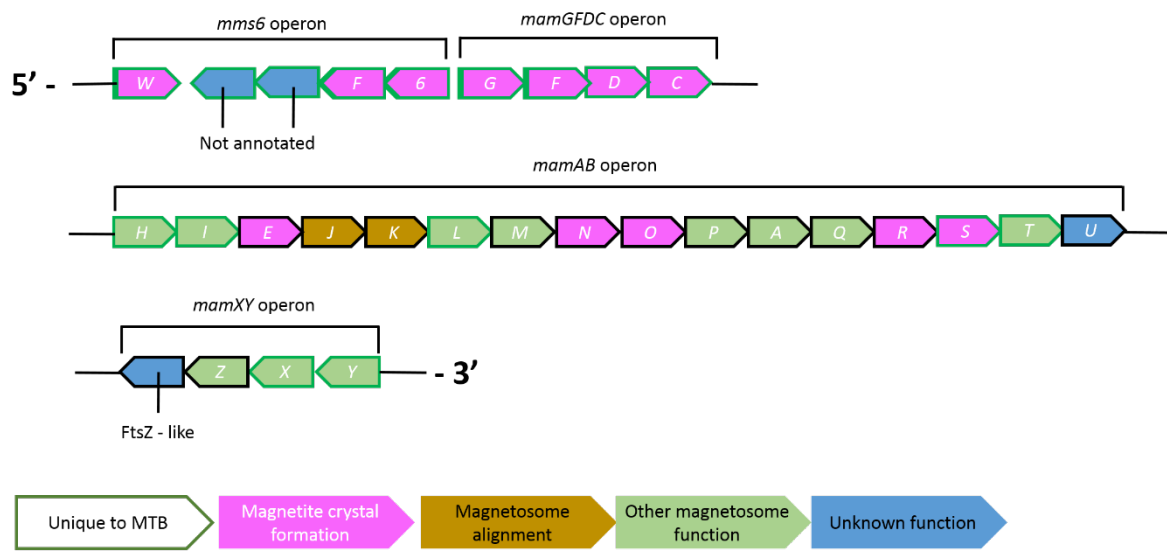


Figure 0.6 Arrangement and function of genes in the MAI of *Magnetospirulum gryphiswaldense*

Gene function indicated by colour as according to legend at bottom panel, genes are not shown to any scale. Function predictions are as Uebe *et al*¹⁶³

Other studies however have good evidence that, at least among *Nitrospiraceae*, the MAI was inherited vertically where codon bias within the MAI is identical to housekeeping regions of the genome. This suggests whether that *Nitrospiraceae* are direct descendants of the original MTB or they inherited the

MAI horizontally very recently after its genetic inception. The bullet shaped morphology of the magnetite crystals produced by these bacteria has provoked the hypothesis that this is the ancestral morphology¹⁷².

1.6.5. Magnetosome Assembly

In order for complete maturation of magnetite crystal loaded membrane vesicles there are four distinct processes that must be concerted. These are 1) membrane invagination; 2) iron transport in to magnetosome; 3) magnetite precipitation; and 4) magnetosome alignment. Modern genetic techniques are beginning to unravel how genetic elements encoded on the MAI relate to specific functions in magnetosome formation, however a comprehensive model with genetic elements assigned to each of these stages is yet to be fully vindicated.

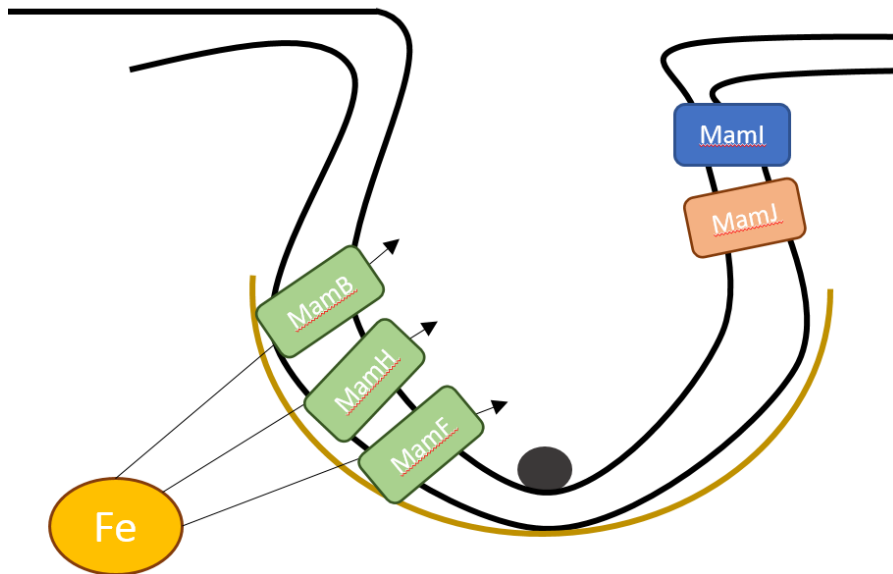
1.6.6. Magnetosome Membrane Invagination

Magnetosome biogenesis is probably the closest phenomenon observed in prokaryotes to endocytosis in eukaryotes. The complexity of this process is demonstrated by our lack of a proper understanding despite years of research⁹⁴. We do know that, in opposition to prokaryotic descriptions, magnetosome membrane biogenesis and invagination is not specifically regulated and seems to occur somewhat randomly across the cytoplasmic membrane.

Murat *et al* have assigned putative functions to a vast set of genes found on the MAI by deletion of predicted operons and phenotypic characterization¹⁷³. This proposed that MamI may be one of the proteins that initiates the process of magnetosome formation. Deletion of the locus this gene is found in was the only deletion made that entirely abrogated magnetosome formation. Other genetic deletions lead to formation of empty magnetosomes, or morphological defects in crystal. This tells us that this region is both essential for magnetosome biogenesis and that invagination is necessary for crystallization of magnetite. GFP-tagged MamI was localized to the cytoplasmic membrane in the strain lacking the genomic region encoding it, while its genomic neighbours were found spread diffusely around the cytoplasm. It was concluded that MamI may be the instigator of assembly of the magnetosome, acting as a hub for magnetosome invagination proteins.

Using atomic force microscopy, the ultrastructure of the mature magnetosome was found to contain an organic layer around the magnetite crystal that seemed larger than a lipid bilayer could be. The “wrinkly” surface of this when observed in phase contrasted images indicated a proteinaceous coat¹⁷⁴.

Further probing of this structure found that this was likely made of the MamA protein, whose structure was found to contain TPR motifs that would allow homo-oligomerisation in one domain and proposed interaction with other proteins of the magnetosome membrane in another¹⁷⁵. Figure 1.7 represents this hypothetical MamA layer as a gold sheath around the nascent magnetosome membrane.



Invagination and Fe transport

Figure 0.7 Cartoon of magnetosome membrane invagination and the proteins associated with it

Magnetosome initially invaginates, MamI is likely one of the early proteins involved in this, recruiting other proteins like MamJ. Fe is transported in to the magnetosome lumen by MamB, MamH and MamF.

A model could be proposed where MamI initiates magnetosome invagination at random points in the cytoplasmic membrane and, using a clathrin-like action in cooperation with the recruitment of other proteins by MamI, MamA oligomerisation then invaginates the magnetosomal membrane.

1.6.7.Iron Transport into the Magnetosome

Iron transport into the magnetosome could be considered possibly the best and worst understood part of magnetosome maturation. There are myriad studies characterizing Fe presence in the magnetosome and the magnetosome membrane; timing of Fe uptake during crystal formation; and the genes

responsible. A key question surrounds the direction of transport of Fe into the magnetosomal lumen; does it come from the cytoplasm or the periplasm? And then in which oxidation state would this be? A comprehensive study of magnetosomal Fe by Mossbauer spectroscopy¹⁷⁶ indicated that the magnetite fraction contained either magnetite or ferrihydrite, while membrane fractions contained Fe(II) and Fe-loaded ferritin. They used the observation of ferrihydrite and the presence of both Fe(II) and Fe(III) (in the form of ferritin) alongside ferrihydrite in the magnetosomal lumen to build a model of crystal precipitation that required Fe(II), leading them to propose that Fe(II) transport must transfer from the periplasm to the magnetosomal lumen, as cytoplasmic transport would quickly lead to oxidation of Fe(II) to Fe(III). However, specific proteins in the magnetosome membrane may be capable of reducing this again. Initially a candidate Fe transporter encoded uniquely in MTB termed MagA was tied to this function¹⁷⁷, where a spontaneous mutant that had lost this gene lost its magnetosomes along with it. However, later studies with *Magnetospirula* strains deleted for *magA* produced native magnetosomes. Either the function of MagA is redundant or additional suppressor mutations were selected for in the strain initially described. The most recent reviews on magnetosome formation predict MamA and MamB fulfill the role of Fe transport, along with specific Fe(II) and Fe(III) transporters predicted in MamH and MamF.

It is likely that some Fe is able to enter the magnetosome while it is still continuous with the periplasm, given the rapidity of Fe uptake proposed to be dedicated solely to magnetite crystallization (Schuler and Baeuerlein 1998), however the identification of cytoplasm directed Fe transporters found to be essential for magnetite production make it unfeasible that this is the only route of Fe uptake in to the magnetosome.

1.6.8. Magnetite Crystallisation

Reviews from the Schuler group^{94,178} propose MamE, MamO and MamM control magnetite nucleation, however there is potential overlap in the annotation of genes that control crystal nucleation and crystal maturation.

MamO is a catalytically-dead serine protease¹⁷⁹. Substitution of the amino acids of the predicted catalytic triad in MamO produced no change in phenotype, however its presence is required for the cleavage of other magnetosomal proteins. Crystallisation studies of MamO revealed that it had a metal binding site, further evidenced by FRET experiments¹⁷⁹, and substitution of the histidine residues that are proposed

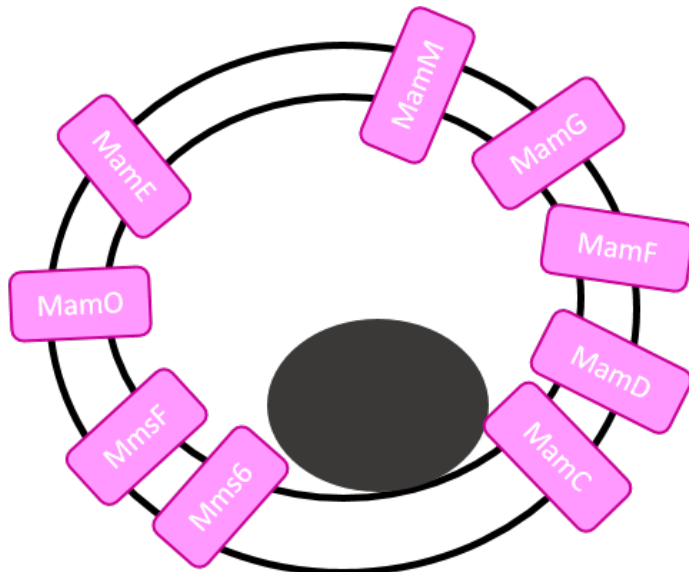
to ligate metals lead to abrogation of magnetite crystallization. This observation is a strong indication that MamO is required for crystal nucleation.

Proteolysis by MamE however is likely to be essential for proper biominerallisation¹⁸⁰. Catalytic inactivation of MamE produces significant reduction in magnetic activity in MSR-1 cells, and its catalytic activity was shown to be dependent on the presence of MamO *in vitro*. There is no experimental evidence, however, for MamE having a role in anything but magnetosome protein processing.

The entire process of magnetite precipitation within the magnetosome is not yet fully understood, however the Magnetosome Membrane Specific protein Mms6 is strongly associated with this step given *in vitro* characterization of the protein. Mms6 was first designated as Magnetosome Membrane Specific protein of Six kilodaltons by Arakaki *et al*¹⁶⁴ who purified the most closely associated proteins of the magnetite crystal contained in the magnetosome by magnetic purification of the crystal and subsequent iterative washes to leave what was indicated as the most high affinity interactors of the magnetosome proteome. This study and others^{181,182} have demonstrated the ability of purified recombinant Mms6 to produce morphologically homogenous magnetite crystals in a chemical magnetite synthesis method, while another study used purified Mms6 *in vitro* to produce magnetite crystals *de novo*.¹⁸³ This might indicate that Mms6 has a remarkable ability to nucleate and effectively catalyse magnetite crystal formation, however deletion of *mms6* resulted in a strain that still produced magnetite crystals, revealing either a redundant function, or a specific function in maturation of the crystal.

This redundant function was revealed by mutation of *mmsF*¹⁸⁴. The phenotype of an *mmsF* deletion mutant is identical to a mutant of the entire *mms6* operon, in fact *mms6* operon deletion can be almost entirely complemented *in trans* by expression of *mmsF* alone. *In vitro* experiments demonstrated that MmsF can also affect magnetite precipitation in chemical synthesis reactions, as well as is propensity to homo-oligomerise¹⁸⁵.

Current methods and understanding do not yet permit a detailed model of the exact process of the magnetite crystal's precipitation. The large number of genes involved in magntetite precipitation and control of crystal homogeneity shown in Figure 1.8 indicates the potential for either redundancy in functions or hitherto misunderstood diversity of specific functions.



Crystal maturation

Figure 0.8 Cartoon of a maturing magnetite crystal

Magnetite crystal growth is nucleated and mediated by MamM, MamE, MamO, MamG, MamD, MamF, MamC, Mms6 and MmsF. Knockouts of these genes indicates that there is a lot of functional redundancy based on mostly phenotypic analyses. Specific roles proposed include nucleation and stabilisation of the nascent crystal (Mms6, MmsF, MamGFDC, MamD, MamE, MamO, MamD), or proteolytic processing of other related proteins (MamE).

1.6.9. Magnetosome Alignment

Alignment of magnetosomes into chains along the mid cell is essential for maximizing the magnetic moment effect observed for individual MTB cells. Electron microscopy techniques produced high resolution 3D images of entire *M. gryphiswaldense* cells, revealing a proteinaceous filament associated with magnetosomes running down the mid-cell axis¹⁸⁶ shown by Figure 1.7A. This is likely to be the MamK protein encoded on the MAI, which is an actin homolog demonstrated to spontaneously form straight filaments by heterologous expression *in vivo*¹⁸⁷ and *in vitro*¹⁸⁸. *In vitro* studies also showed ATP induced depolymerization of the chain. This could implicate MamK filament breakage as a key event in magnetosome chain segregation during cell division.

MamK deletion mutants still produce magnetosomes, however they are found in shortchains or clusters¹⁸⁹, raising the potential of an additional protein being required for stringing together magnetosomes. MamJ is likely to fulfill this role, where an interaction between MamJ and MAmK has

been demonstrated by bacterial-two-hybrid experiments¹⁹⁰, and deletion of MamJ produces unaligned, free floating groups of well-defined magnetosomes in the cytoplasm.

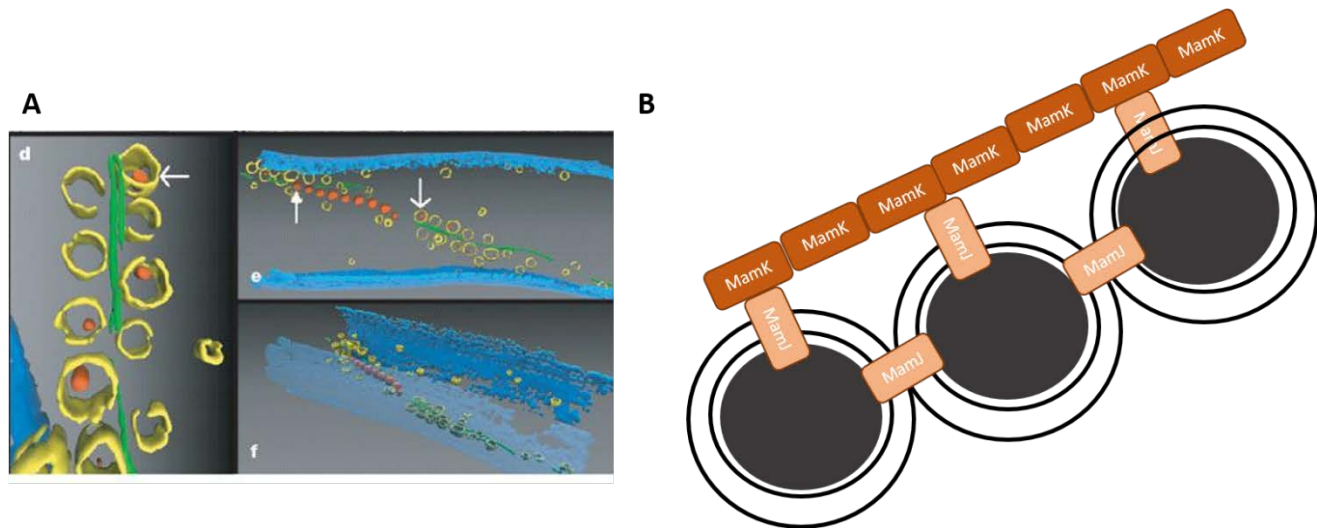


Figure 0.9 Magnetosomes are aligned by MamK and MamJ

A, cryo electron tomograph of the interior of *M. gryphiswaldense* produced by Scheffel *et al*¹⁸⁶ and reproduced with permission from ASBMB. Blue represents the cytoplasmic membrane, green the magnetosome filament, yellow the magnetosome membrane and orange magnetite crystals. B, cartoon of magnetosome alignment. MamJ connects individual magnetosomes in to chains that are aligned by the magnetosome filament made of MamK.

1.6.10. Applied Biomagnetism

The biological synthesis of magnetic nanoparticles as observed in MTBs is attractive for a number of practical applications, principally medical to date.

Magnetic Resonance Imaging (MRI) is a medical technique that allows imaging of biological samples by exciting specific nuclei using high frequency oscillating electromagnetic fields at their resonant Larmor frequency. Magnetosomes extracted directly from magnetotactic bacteria have been explored for use as contrast agents for this¹⁹¹⁻¹⁹³. In one case mice were injected with magnetosomes obtained from *M. gryphiswaldense* which were taken up by macrophages. This allowed macrophages to be monitored during induced peritonitis¹⁹¹.

Genes from MTB have been explored to produce genetically encoded MRI contrast agents. Namely MagA and Mms6 have produced interesting results to date. MagA expression in tumour cells allowed

them to be visualized by MRI once injected in to a mouse¹⁹⁴. Mms6 expression also produced similar phenotypes in tissue culture models¹⁹².

Another study overexpressed *mms6* in human mesenchymal stem cells and was observed to produce Fe containing magnetic deposits by atomic force microscopy¹⁹⁵. The type of magnetic mineral produced here was not effectively defined however. The propensity of Mms6 to produce these NPs has been noted as a limiting factor for use in clinical applications as it may divert Fe away from essential host physiology and have toxic effects¹⁹².

This property of Mms6 however has proved to be useful for other synthetic biology projects. The C terminus of Mms6 has a region that has been demonstrated to be essential for, or even necessarily responsible for, magnetic NP production and interaction by Mms6. This domain has been attached to other proteins to produce a colloidal magnetite solution^{196,197}, or added to the C terminus of a ferroxidase from *Rhodospirillum rubrum* in efforts to produce an enzyme catalyzing production of magnetic NPs. *E. coli* cells expressing the resultant protein were described as “ultraparamagnetic”¹⁹⁷, a term the authors coined to describe the magnetic phenotype they observed. Cells were attracted to a bar magnet and upon injection to mouse limb they were visible by MRI. The cells were determined to contain paramagnetic iron in a state consistent with ferrihydrite.

Nima *et al* have also investigated the use of magnetite NPs from MTBs for use as photoacoustic and photothermal inductive agents¹⁹⁸. The uniform size and morphology of magnetite NPs allows them to be excited by laser pulses to either produce acoustic waves or vibrate to produce heat. Photothermal induction of these NPs produced enough heat to produce nanobubbles that explode and caused destruction of cancer tissue *in vitro*.

Additionally, magnetotactic bacteria have even been put to use as antibacterial agents also using magnetic hyperthermia¹⁹⁹. In this study *Staphylococcus aureus* were coated with antibody raised against MTBs and then treated with MTBs to stick the cells together. A high frequency oscillating magnetic field was then applied to cause magnetic hyperthermia in the magnetosomes of the MTBs. The heat produced was then judged to have had inhibitory effects on *S. aureus* growth.

1.6.11.The Aims of This Project

In this body of work, the aim was to produce a platform to produce a platform for magnetically stimulated remote control of genetic circuits. In this way, the physiology of bacterial containing MNPs can be controlled using oscillating magnetic fields. In an industrial context, this could provide a novel method to control the metabolic activity of cells in fermenters producing high value products, providing unparalleled precision and obviating the requirement for continual repurchase of inducer chemicals.

This could be achieved using genetically encoded mechanisms to produce or take up MNPs and conjugating these to temperature sensitive proteins. By then placing these cells in a radio frequency oscillating magnetic field, the MNP would heat up and influence the behaviour of its partner protein specifically. The MNP in this case would function as an “aerial”, acting as a conduit for the magnetic stimulation, and transferring this signal in to heat which a temperature sensitive protein would be influenced by.

This protein might behave as a transcriptional regulator, acting to promote or inhibit transcription of specific genes in response to this stimuli, or as an enzyme, affecting the rate of its reaction, or change how it interacts with other proteins, as in figure 1.10.

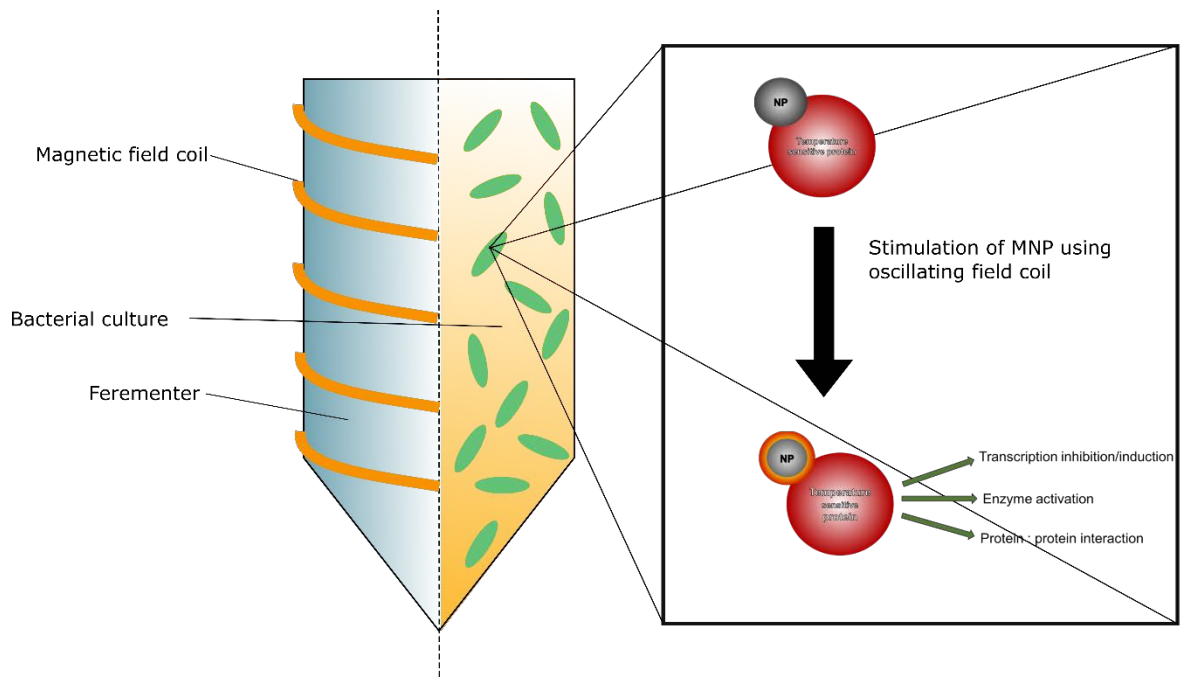


Figure 0.10 A platform for magnetically-stimulated control of bacterial physiology

In a fermenter of industrial scale, where microbes are cultivated for production and extraction of a useful product, a magnetic field may be produced using a conductive coil wrapped around the fermenter. Within the fermenter, microbes engineered to produce or take up MNPs and expressing a synthetic temperature responsive gene circuit can be stimulated by high frequency oscillations in the magnetic field produced by the coil. This would then lead to a change in physiological behaviours promoting yield of the desired product, instigated via magnetic stimulation of MNPs within cells, conjugated to elements of this temperature sensitive gene circuit.

By studying how genetically encoded magnetic phenotypes might be produced in *E. coli*, insights in to how this can be produced in an array of other industrially useful organisms could be produced. There are a range of temperature sensitive proteins that have been characterised in many organisms. By reproducing the behaviour of these proteins in *E. coli*, standard tools can be developed that will respond to MNPs produced by these mechanisms.

This project then can be broken down in to three more specific objectives:

- To engineer magnetic nanoparticle uptake and production in *E. coli*
- To design and characterise an effective temperature responsive synthetic gene circuit
- To embed the engineered MNP properties with the synthetic temperature responsive circuits to produce wireless magnetothermal stimulation of bacterial physiology.

Chapter 2:
Production of Palladium Nanoparticles by *E. coli*

2.1.Introduction

The first step in producing a magnetically stimulated transcriptional program in *E. coli* is introducing an “aerial” nanoparticle. It was proposed that investigating metal nanoparticle synthesis would be a good starting point, as some previous work suggests that *E. coli* is capable of Pt and Pd nanoparticle production under certain circumstances. Utilising the literature on this phenomenon in *E. coli*, it was deemed possible to replicate and possibly begin to use the nanoparticles produced or modify them to be used as “aerial” modules described in the wider aims of section 1.6.11.

2.1.1.Previous characterisation of Pd-NP formation in *E. coli*

A number of organisms have been identified that are capable of generating Palladium nanoparticles (Pd-NP) when exposed to palladium salts^{139,143,155,156,200–202}, including *Escherichia coli*^{141,156,203}, *Desulfovibrio sp.*^{138,144,204}, *Geobacter sulfurreducens*²⁰⁰, *Shewanella oneidensis*¹³⁷, *Klebsiella oxytoca*¹³⁶, *Bacillus benzevorans*¹³⁸ and *Cupriavidus necator*¹⁴³.

The experimental approach to producing Pd-NP in the biological systems studied generally involved the addition of a Pd(II) salt to a buffered suspension of bacteria. The available evidence suggests that soluble Pd(II) is reduced to insoluble elemental Pd(0) in the form of metal nanoparticles through direct interaction with the bacteria. The resultant nanoparticles were observed as black precipitate in samples, and have been visualised as nanoparticles using electron microscopy^{138,140–142,144,204}

Research based on using *E. coli* to catalyse Pd-NP formation suggests the [NiFe]-hydrogenases have key roles in the reduction of Pd(II)^{140–142}. *E. coli* produces three active [NiFe]-hydrogenases and individually these are termed Hyd-1, Hyd-2 and Hyd-3²⁰⁵. Hyd-1 is a H₂ oxidising enzyme located on the inner membrane with a periplasmic catalytic domain that is unusually oxygen tolerant. Hyd-2 is a hydrogenase that has been analogised as a ‘redox valve’²⁰⁵, which can both reduce protons using electrons from the quinone pool to evolve H₂²⁰⁶ or oxidise H₂²⁰⁷. The Hyd-2 catalytic subunit is, like Hyd-1, exposed to the periplasmic side of the inner membrane²⁰⁸. Hyd-3 is a component of the formate hydrogenlyase (FHL) complex, which also comprises a formate dehydrogenase subunit. FHL is membrane bound, but this time the catalytic subunits are located at the cytoplasmic side of the inner membrane. The model for Hyd-3 activity under physiological conditions describes glucose utilisation leading to formate secretion through a dedicated channel FocA, which in-turn acidifies the extracellular environment. At a critical extracellular pH (≤ 6.8), FocA changes from being formate exporter to a formate importer²⁰⁹, the formate is re-absorbed by the cell and FHL disproportionates formate to CO₂ and H₂^{210–212}. Overall,

this is a pH homeostasis system that acts to de-acidify the cell's environment under fermentative growth conditions.

By using strains deficient for activity of individual [Ni-Fe] hydrogenases it was demonstrated that any of these enzymes could contribute to reduction of Pd(II), when measuring Pd(II) reduction in a spectrophotometric assay¹⁴¹. In these experiments, hydrogenase strains producing only one active hydrogenase were examined. Specifically, the Pd(II) concentration was seen to decrease at a slightly slower rate when only Hyd-1 or Hyd-2 were present compared to the parental strain, and at quite a significantly slower rate when only Hyd-3 was present, however in transmission electron micrographs all strains were seen to make Pd-NPs of similar size and morphologies.

Other studies have indicated that the Pd-NPs produced by a strain engineered for amplified Hyd-3 activity produces more a more effective biocatalyst for hydrogen fuel cells (following processing of the resultant nanoparticles) than a parental strain¹⁵⁶. Together this points towards a correlation between hydrogen metabolism and Pd-NP formation.

Other studies however have suggested that the direct action of enzymes or other inherently biological properties upon Pd(II) salts to produce Pd-NPs are non-existent^{143,202}. Bunge *et al* demonstrated that *Cupriavidus necator* can produce Pd-NPs even after a Pasteurisation treatment that destroyed hydrogenase activity¹⁴³, and Rotaru *et al* showed that autoclaved *Pseudomonas putida*, *Shewanella oneidensis* and *E. coli* (strain MC4100) cells are also capable of Pd(II) reduction when supplied with formic acid as an electron donor²⁰². These works argue that it is the interaction of Pd(II) ions with functional groups on the surface of bacterial cells produces NPs¹⁴³. It could be argued that this fits the definition of enzyme activity at the cell surface, however the lack of biological intent is demonstrated by the use of functionalised PEG beads of comparable size to bacterial cells that are also able to nucleate production of Pd-NPs²⁰².

2.1.2.Aims

Biologically produced Pd-NP could form an “aerial” module of a genetic remote control platform. Given the involvement of *E. coli* hydrogenases in the synthesis of Pd-NP, it was hypothesised that Pd-NPs may be nucleated at the active sites of the enzymes and remain closely associated with the proteins as they grow. The resultant hydrogenase:Pd-NP complexes would in-turn then serve as important defined anchoring points for the aerial on the cell surface, and perhaps also act as conduits for

transduction of the “heat” signals generated upon stimulation. However, there is clearly a lack of consensus on the mechanism of biological Pd-NP production.

The aims of this Chapter were to take molecular genetic and biochemical approaches to investigate further the mechanism of Pd-NP formation by *E. coli* hydrogenases.

2.2. Results

2.2.1. Characterising Pd-NP formation by *E. coli* Hydrogenases

In order to study Pd-NP production by the [NiFe]- hydrogenases of *E. coli*, cells were grown in M9 medium with 0.2% (w/v) glucose overnight at 37 °C, diluted to an OD₆₀₀ of 0.3 in 40 mM MOPS buffer (pH 7) and then incubated anaerobically in Hungate tubes while the formation of Pd(0) was observed through the appearance of a black precipitate, shown in Figure 2.1A. It was considered that the level of “blackness”, and its rate of formation, could be semi-quantified by following OD₆₀₀ as a qualitative proxy of Pd-NP production. To test this, *E. coli* cells of the strains MC4100 (Hyd⁺), IC009($\Delta hycE \Delta hybC$), IC010 ($\Delta hycE \Delta hya4$), FTD89 ($\Delta hyaB \Delta hybC$) and FTD150 ($\Delta hyaB \Delta hycE \Delta hybC$) were grown anaerobically in M9 medium with 0.2 % (w/v) glucose, adjusted to an OD₆₀₀ of 0.3 in 40 mM MOPS and then aliquoted in to 250 µL volumes in a 96 well plate. Different treatments were prepared by adding 0.75 mM Na₂PdCl₄, 0.2 % (w/v) formate or both, as well as buffer-only controls, with three biological replicates of each. This plate was then monitored for 16 hours with no shaking at 37 °C in a Biotek Synergy HT platereader measuring OD₆₀₀ of each well every 20 minutes. Figure 2.1B shows that live *E. coli* MC4100 cells (which contain active hydrogenases) will produce black Pd(0) *in vitro* only under conditions where formate and Pd(II) are added in combination. This activity is abolished in when cells are killed by heat treatment prior to addition of Pd(II) or formate (Figure 2.1C).

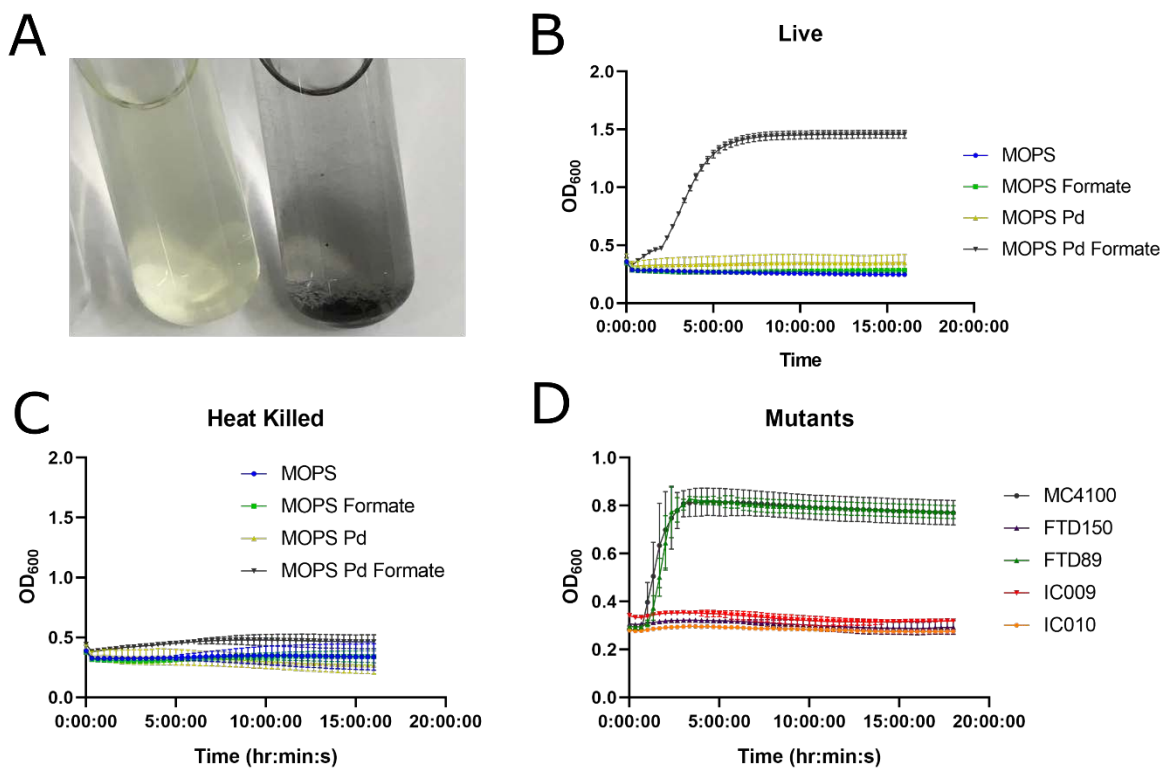


Figure 2.1 Pd-NPs are produced only in the presence of active Hyd-3

A) *E. coli* strain MC4100 was grown anaerobically in M9 medium with 0.2 % (w/v) glucose before being washed and diluted to an OD₆₀₀ of 0.3 in MOPS buffer (40 mM, pH 7). To one tube (left) 0.75 mM Na₂PdCl₄ was added and to the other this was added alongside 0.2 % (w/v) formate. Each were then incubated statically for 16 hours at 37 °C.

B) *E. coli* MC4100 cells were grown and prepared in MOPS buffer as in (A). 250 µL of the suspension was then added to individual wells of a 96 well plate, with the addition of 0.2 % (w/v) formate and 0.75 mM Na₂PdCl₄ where indicated and incubated statically at 37 °C in a Bioteck Synergy HT platereader statically with OD₆₀₀ measured every 20 minutes for 16 hours. Error bars represent standard deviation of three biological replicates.

C) Cells were grown as in B then washed and resuspended in MOPS buffer (40 mM, pH 7) at OD₆₀₀ of 0.3. This suspension was then incubated at 95 °C for 15 minutes before being added in 250 µL aliquots to wells of a 96 well plate with the addition of 0.2 % (w/v) formate and 0.75 mM Na₂PdCl₄ where noted, and incubated statically at 37 °C for 16 hours while in a Bioteck Synergy HT platereader with OD₆₀₀ measured every 20 minutes. Error bars represent the standard deviation of three biological replicates

D) *E. coli* cells of strains MC4100, IC009, IC010, FTD89 and FTD150 were grown as in (B) and (C) and monitored using a platereader with treatments as in (B) and (C). Error bars represent the standard deviation of three biological replicates.

To explore further the cellular process responsible for Pd(0) generation, a genetic dissection was performed next (Figure 2.1D). A strain of *E. coli* devoid of any hydrogenase active site subunits, FTD150 (Table 6.1, as MC4100, $\Delta hyaB$, $\Delta hybC$, $\Delta hycE$, $\Delta hyfA-R$) showed no increase in OD₆₀₀ when incubated with formate and Pd(II) (Figure 2.1D), demonstrating that hydrogenase activity was essential for black Pd(0) formation. In addition, strains IC009 (Table 6.1, as MC4100, $\Delta hybC$, $\Delta hycE$) and IC010 (Table 6.1, as MC4100, $\Delta hyaB$, $\Delta hycE$), which only bear an active Hyd-1 or Hyd-2, respectively, could not generate Pd(0) under the conditions tested (Figure 2.1D). However, the *E. coli* strain FTD89 (Table 6.1, as MC4100, $\Delta hyaB$, $\Delta hybC$), which retains an intact Hyd-3 alone, phenocopies the parental MC4100 strain and generates Pd(0) at the same rate (Figure 2.1D). These data, combined with the requirement of formate for Pd(0) production (Figure 2.1B), indicates that the formation of Pd-NPs observed in this model is dependent on an active Hyd-3.

If the Pd(0) generated by *E. coli* is in the form of Pd-NP they should be visible by transmission electron microscopy (TEM). To test this hypothesis, microscopic analysis of *E. coli* MC4100 cells previously incubated with Pd(II) and formate in MOPS buffer (40 mM, pH 7) was performed. Figure 2.2 shows the resultant images. Numerous Pd-NPs can be observed in clumps and tower-like structures attached to the surface of cells. In a few cases these might be judged to be intracellular, as in Figure 2.2A, however most are either attached to the surface or found free-floating in the extracellular milieu. Pd-NPs were further analysed using imageJ^{213,214} and were calculated to be around 20 nm in diameter with the mode particle size being 19.8 nm.

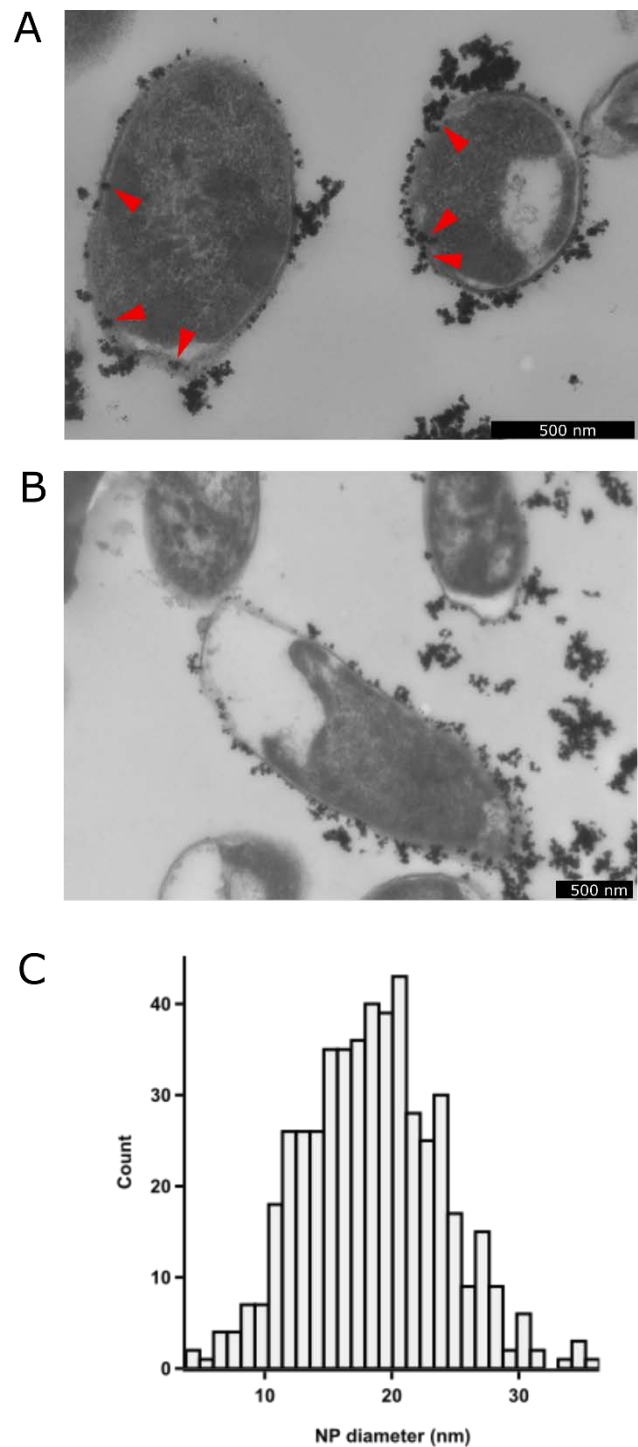


Figure 2.2 Pd-NPs can be observed by TEM

A),B), *E. coli* MC4100 cells were grown in M9 medium with 0.2% (w/v) glucose then washed and suspended to an OD₆₀₀ of 0.3 with the addition of 0.75 mM Na₂PdCl₄ and 0.2 % (w/v) formate and incubated statically at 37 °C for 16 hours and then fixed in glutaraldehyde buffer for TEM. After staining with OsO₄ and dehydration using graded EtOH solutions, the cell sample was embedded in resin and sectioned in to 70 µm thin sections and imaged using a JEOL 1200 EX transmission electron microscope. Red arrows point to what could be intracellular Pd-NPs.

C) 498 individual Pd-NPs were measured using imageJ and their diameters plotted as a histogram.

2.2.2.Pd-NP production is correlated with a reduction in H₂ evolution

The emerging hypothesis of *E. coli* hydrogenase-mediated Pd-NP production is that the Hyd-3 component of FHL is itself a direct participant in the production of the Pd-NP. If this is the case, then it should be considered that Pd(II) first occupies the active site of the Hyd-3 enzyme where it is directly reduced to Pd(0). It could then be hypothesised that electrons are diverted to reduce Pd(II) to produce Pd-NPs rather than to protons to produce H₂. This would then lead to diminished H₂ production by Hyd-3.

To test this hypothesis, the levels of H₂ evolution activity during Pd-NP formation were examined using gas chromatography (Figure 2.3). *E. coli* strains MC4100 (Hyd⁺), IC009 ($\Delta hybC, \Delta hycE$), IC010 ($\Delta hyaB, \Delta hycE$), FTD89 ($\Delta hyaB \Delta hybC$) were grown overnight in M9 medium with 0.2% glucose (w/v), washed in MOPS buffer (40 mM, pH 7) and the suspended to an adjusted OD₆₀₀ of 0.3. Next, 5 mL of each suspension was incubated in sealed Hungate tubes in MOPS buffer (40 mM, pH 7) supplemented either with 0.2 % (w/v) formate, 0.75 mM Na₂PdCl₄, neither or both, where indicated in Figure 2.3. Following static overnight incubation at 37°C, 1.5 mL of gas was removed from the headspace and any H₂ present quantified using a gas chromatograph (Figure 2.3).

The experiments revealed that Pd-NP formation is correlated with reduced H₂ production (Figure 2.3). Both MC4100 (Hyd⁺) cells and FTD89 (Hyd-3 only) cells produced in excess of 40 µmol H₂ per OD₆₀₀ per mL when supplied with 0.2% (w/v) formate under these conditions, however the addition of Pd(II) alongside formate almost entirely abrogates the H₂ evolution (Figure 2.3B). Note that, in both cases, the reduction in H₂ evolution was accompanied by the accumulation of the characteristic dark precipitate of Pd-NPs developing (Figure 2.3A). This fits with a hypothesis that Pd-NPs are generated at the active site of the enzyme and electrons are transferred directly to Pd(II).

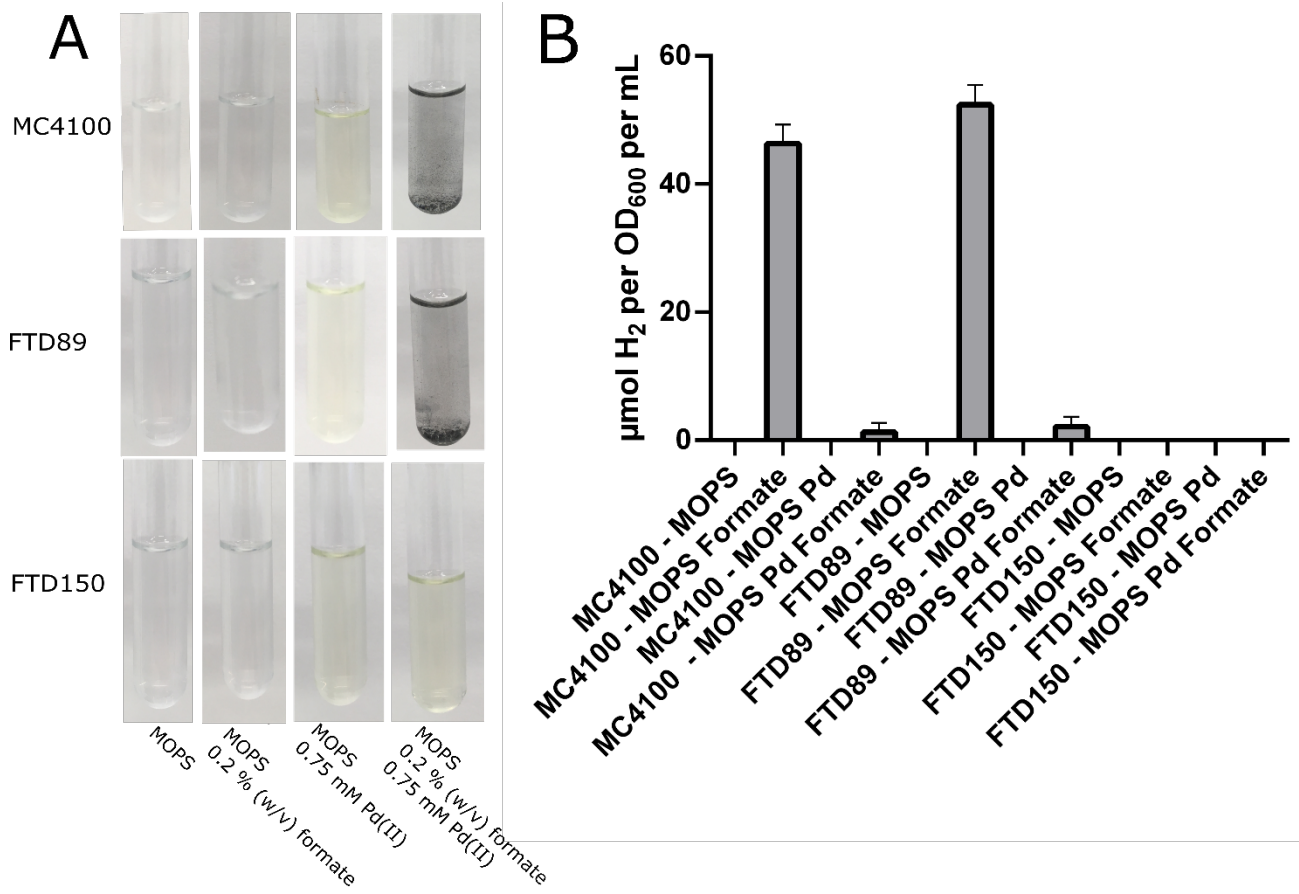


Figure 2.3 Pd-NP production correlates with decreased H₂ production

A) Cells of *E. coli* strains MC4100, FTD89, and FTD150 were grown in M9 with 0.2 % glucose (w/v) and then washed and resuspended at an OD_{600} of 0.3. Five mL of each suspension was then sealed in a Hungate tube with the addition of 0.2 % (w/v) formate or 0.75 mM Na_2PdCl_4 where indicated and incubated at 37 °C statically for 16 hours before being photographed, where photographs shown are representative of three biological replicates.

B) 1.5 mL of the headspace gas from each of the tubes represented in (A) was removed and H_2 quantified using a Shimadzu GC-2014. Three biological replicates were performed. Error bars represent standard deviation of three biological replicates.

2.2.3.Pd-NPs can be produced by H₂ alone

One interpretation of the data so far is that Pd(II) is reduced by Hyd-3/FHL to produce Pd-NPs rather than H₂. There is a counter hypothesis, which is that H₂ may be still be produced biologically initially, but then that H₂ is eventually consumed in a purely chemical, abiotic reaction that produces Pd-NPs. To probe the possibility of chemical reduction of Pd(II) by H₂ *in vitro*, experiments were designed whereby H₂ gas was injected in to sterile buffers containing Pd(II), as well as injected in to suspensions containing heat-killed *E. coli* FTD150 cells (Figure 2.4).

First, Hungate tubes containing either sterile MOPS buffer (40 mM, pH 7) with 0.2% (w/v) formate and 0.75 mM Pd(II), or an identical buffer with FTD150 cells normalised to an OD₆₀₀ of 0.3, were injected with H₂ straight out of the gas canister using a syringe for approximately thirty minutes. In each case, as imaged in Figure 2.4, a dark black precipitate was formed indicating Pd(0) production.

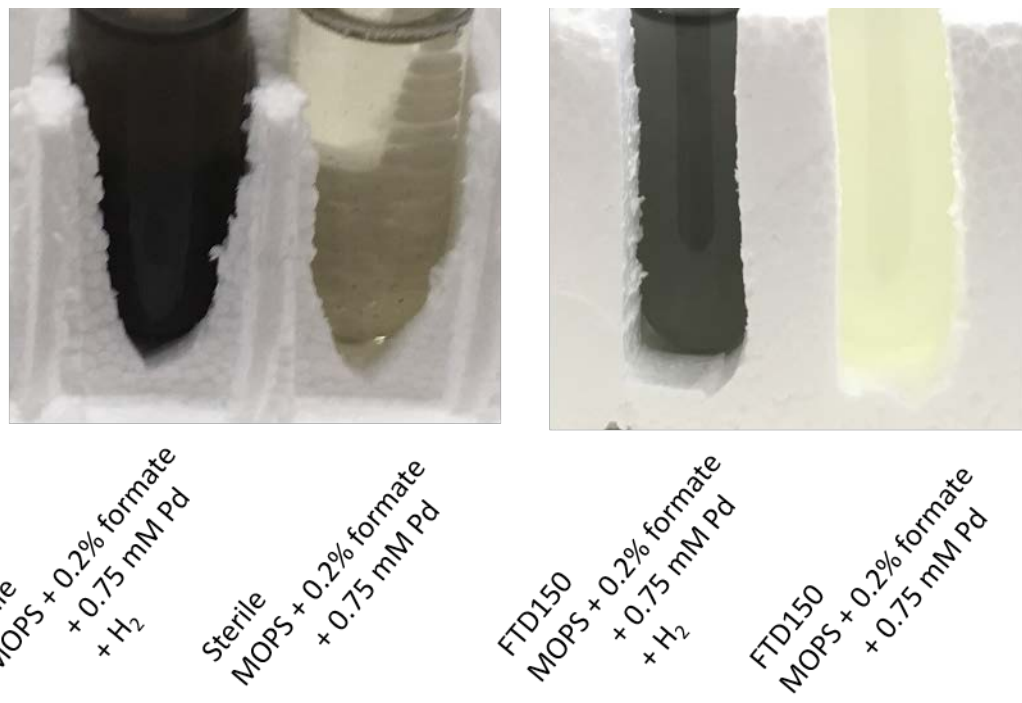


Figure 2.4 Direct reduction of Pd(II) using chemical H₂

A) 5 mL of MOPS buffer (40 mM, pH 7) with the addition of 0.2 % (w/v) formate and 0.75 mM Na₂PdCl₄ was sealed in a Hungate tube. Using a syringe connected to a canister of H₂, H₂ was gently bubbled through the solution for approximately 30 minutes.

B) *E. coli* FTD150 cells were grown in M9 with 0.2 % (w/v) glucose then washed in MOPS buffer (40 mM, pH 7) and adjusted to an OD₆₀₀ of 0.3 with added formate at 0.2 % (w/v) and 0.75 mM Na₂PdCl₄ in a sealed Hungate tube. H₂ was then added as in (A) before the tube was photographed.

In light of this result (Figure 2.4) it was necessary to probe if there was any evidence of an early spike in H₂ production that may then be consumed again and contribute to Pd-NP formation. Gas chromatography was therefore performed on cell suspensions at a timepoint prior to the visible production of Pd-NPs. This was taken as 6 hours post inoculation. In Figure 2.5, it can be seen in that six hours post inoculation, there is no black precipitate indicating Pd-NP synthesis in tubes containing Pd(II), importantly, however, H₂ production is not detectable in these tubes either. This suggests that Hyd-3 activity is blocked by the presence of Pd(II) or by Pd-NP production. In order to explore this further, it was tested whether recovery of hydrogen production activity was possible after Pd-NP production was complete. In this experiment, cells were challenged with Pd(II) and formate (where indicated in Figure 2.6) for approximately 16 hours with incubation at 37 °C in MOPS buffer (40 mM pH 7), then an additional dose of formate was added to bring the final amount added to the tube equivalent to 0.4 % (w/v). However, it is clear that even after a further 24 hours incubation no H₂ gas could be detected in any of the samples that has been exposed to Pd(II) (Figure 2.6).

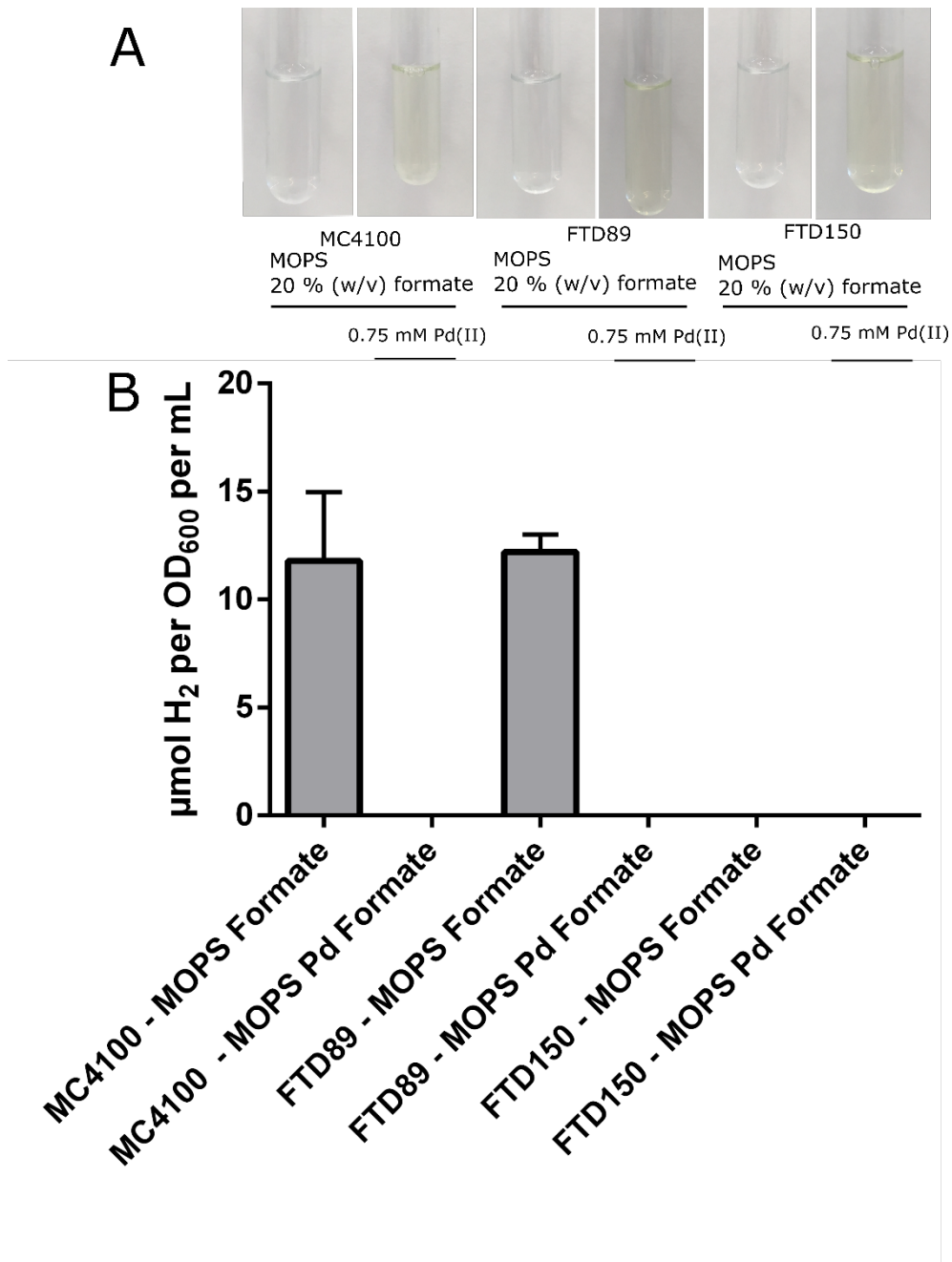


Figure 2.5 Pd inhibits H₂ evolution by FHL at an early stage

A) Cells of *E. coli* strain MC4100, FTD89 and FTD150 were grown in M9 medium with 0.2 % (w/v) glucose, then washed and suspended to an OD₆₀₀ of 0.3 in MOPS buffer (40 mM, pH 7) with 0.2 % (w/v) formate. Na₂PdCl₄ at 0.75 mM was added where indicated, and 5 mL of each suspension was sealed in Hungate tube and incubated at 37 °C for six hours and then photographed.

B) 1.5 mL of gas from the headspace of the Hungate tubes prepared in (A) was analysed by gas chromatography with a Shimadzu GC-2014 gas chromatograph and H₂ concentrations therein calculated. Error bars represent standard deviation of the mean of three biological replicates.

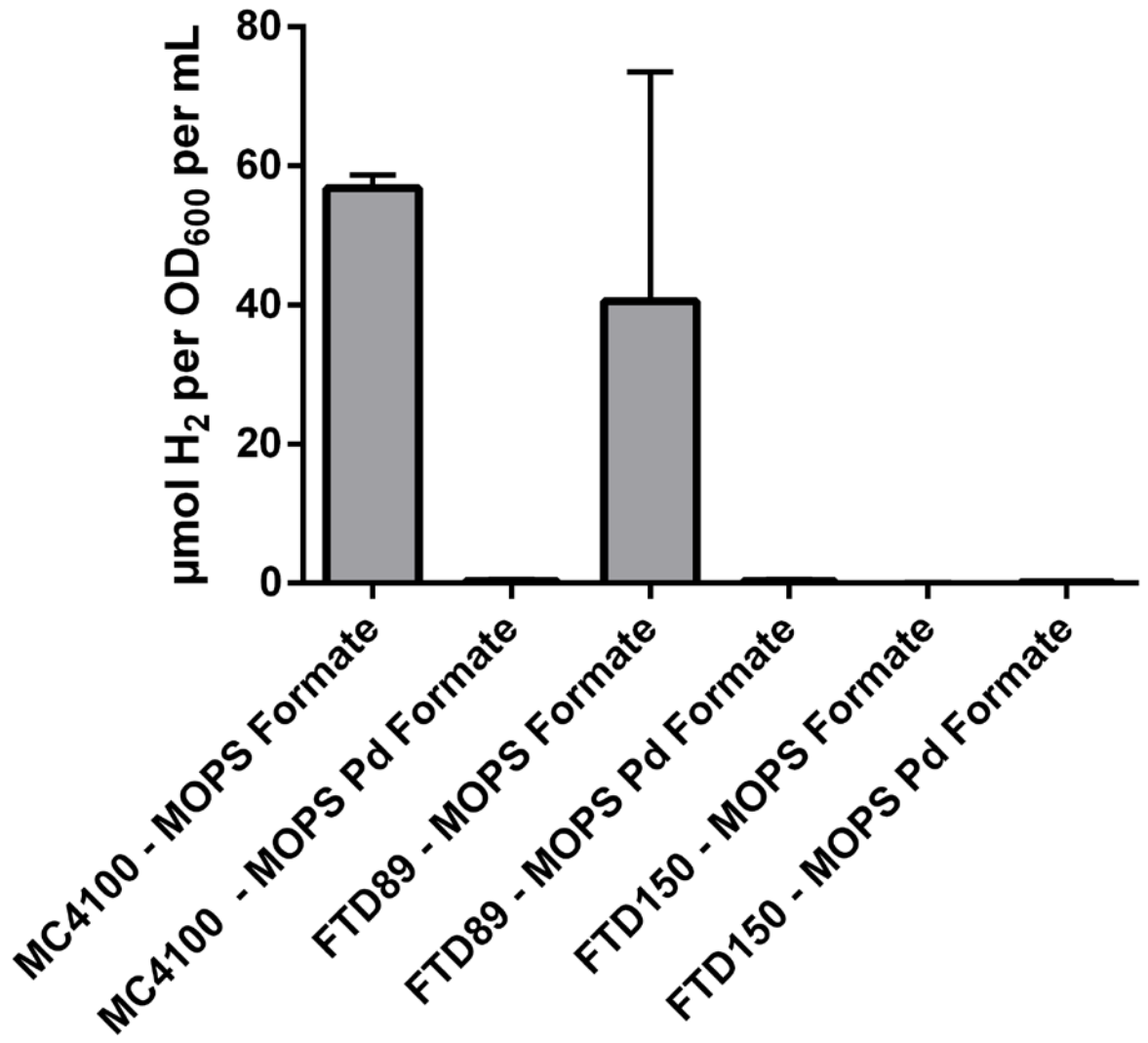


Figure 2.6 Palladium may permanently disrupt Hyd-3 activity

E. coli strains MC4100, FTD150 and FTD89 were cultivated in M9 media with 0.2 % glucose then washed and resuspended in MOPS buffer (40 mM, pH 7) to an OD_{600} of 0.3 with the addition of 0.2 % (w/v) formate. 0.75 mM Na_2PdCl_4 was added where indicated. Next, 5 mL of the resultant suspension was sealed in a Hungate tube and incubated at 37 °C statically for 16 hours. Following this, an extra dose of formate was added such that the final concentration of formate added was 0.4 % (w/v) and the tubes were incubated for a further 24 hours before 1.5 mL gas removed from the headspace and this measured using a Shimadzu GC-2014 gas chromatograph to determine H_2 concentration. Error bars represent the standard deviation of three biological replicates.

2.3.Discussion

2.3.1.Direct Biological Contribution to Production of Pd-NPs by *E. coli*

In this work, the production of Pd-NPs by *E. coli* was demonstrated to be directly influenced by biological activity, however it was not possible to conclude definitively that Pd-NPs are the product of a specific enzymatic reaction. Thus the hypothesis that any individual hydrogenase can directly catalyse Pd-NP production has not been satisfied. In this project, the method of Pd-NP production comprised Hungate tubes containing a bacterial cell suspension in conditions for H₂ production and measurement. When Pd(II) is added to H₂-producing *E. coli* cells the black precipitate that characterises Pd-NP production was consistently observed to form. This was abolished when the substrate of the H₂ evolving enzyme Hyd-3, formate, is absent. Thus it can be said that, in these experiments, Hyd-3 is the only hydrogenase capable of contributing to Pd-NP production.

It may be necessary to improve on OD₆₀₀ related measurements for Pd-NP formation. The current method provides a form of semi-quantitative data that could be used to calculate rate of Pd-NP production, however it provides no information about molar quantities of Pd(II) reduced as has been performed in previous work^{141,149,204}. Making this improvement would fully vindicate the observation of Pd-NPs in line with previous work.

FHL oxidises formate to produce CO₂ and donates the electrons to protons to produce molecular hydrogen. By measuring H₂ produced in this model system it was demonstrated that Pd-NP production is correlated with reduced H₂ accumulation in the headspace of the tube. There are two hypotheses that can be drawn from this observation: Hypothesis 1) instead of reducing protons, electrons are transferred enzymatically to Pd(II) thus nucleating a Pd-NP in the active site of Hyd-3; or Hypothesis 2) that Pd(II) is chemically reduced by molecular hydrogen to produce Pd-NPs.

Sterile controls and controls using the hydrogenase deficient strain FTD150 demonstrate that Pd-NPs can be produced by addition of H₂ alone, devoid of any influence by a hydrogenase. This supports Hypothesis 2, such that Pd-NPs are produced by a non-biological interaction with molecular H₂ and the involvement of Hyd-3 is indirect, but necessary in this model system, to produce Pd-NPs. In experiments using TEM, Pd-NPs can be seen in some cases inside cells, as well as stuck to the outside of cells in large groups. The observation of intracellular Pd-NPs supports the hypothesis that Pd-NPs are synthesised by the cytoplasmic Hyd-3 enzyme. While those that appear associated with the outer

membrane may have been produced by reaction with H₂ immediately as it diffused out of the cell. Hyd-3 may be imagined in this case as an exhaust billowing out a steady stream of H₂, and as it leaves the cell Pd(II) reacts with it to become reduced and nucleate the production of a Pd-NP. As this particular Pd-NP is formed by a notional stream of H₂, it will saturate in its size and begin to be able to pass electrons to other Pd(II) ions in solution and so nucleate the production of more Pd-NPs.

Figures 2.5 and 2.6 demonstrated that Pd(II) addition prevented H₂ evolution quickly and permanently in these experiments. This presents the hypothesis that Pd(II) might oxidise the Ni-Fe cofactor in the Hyd-3 active site, poisoning it so preventing its activity, however this remains to be completely explored experimentally. There are other explanations for this observation. For example, there may still have been excess Pd(II) remaining in solution that could have been reduced by any hydrogen produced by the second addition of formate. However, it may be estimated that 1 mol of H₂ can react to produce 1 mol of Pd(0) by donating each of its two available electrons, and that 1 mol of formate added can only contribute 1 mol of H₂. In this case, the quantity of H₂ produced by either MC4100 or FTD89 is far in excess of this in each tube, so this hypothesis could be rejected. This leaves the explanation that the cells were simply dead, unable to take up formate. They had been incubated at this point for in excess of 24 hours in buffer with no anabolic carbon source or other nutrients, most probably starving the cells. This could be tested by removing the cells from the tube at the beginning and end of the experiment and taking viable counts by serial dilutions and spotting on agar plates to count colony forming units.

An alternative way to test the hypothesis that Pd(II) permanently disrupts Hyd-3 activity would be to perform additional experiments where cells are grown in M9 medium with 0.2 % (w/v) glucose and washed and adjusted in MOPS buffer (40 mM, pH 7) to an OD₆₀₀ of 0.3 and sealed in Hungate tubes with the addition of 0.75 mM Na₂PdCl₄ and increasing concentrations of formate to find a concentration where Pd-NP formation was observed alongside H₂ production.

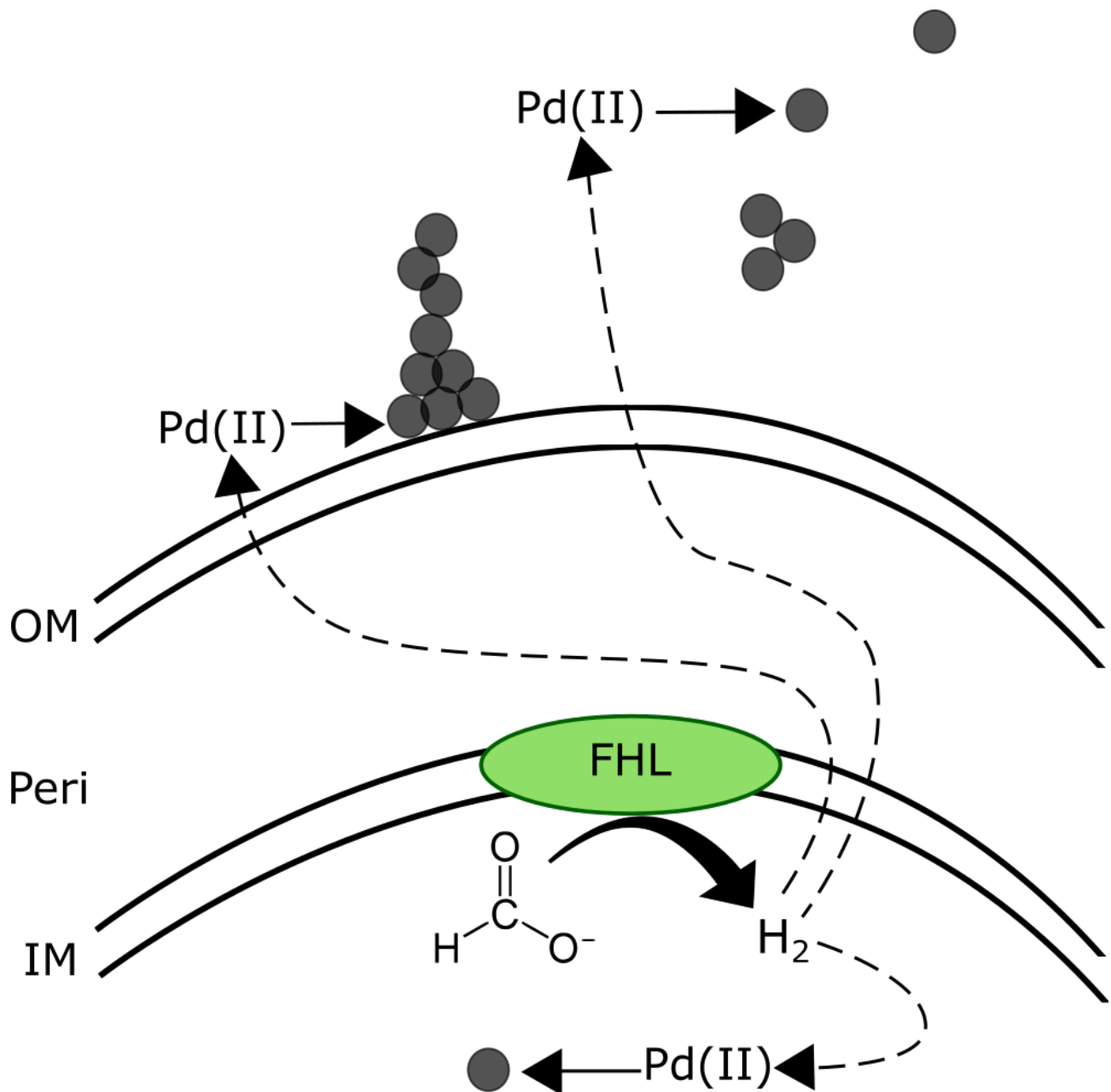


Figure 2.7 Model of Pd-NP production by *E. coli*

Cartoon of an *E. coli* cell envelope and its relationship to Pd-NP production. FHL is situated on the inner membrane (IM), which catalyses the oxidation of formate to produce molecular hydrogen at a cytoplasmic level. This H_2 diffuses through the periplasm (peri) and outer membrane (OM), reducing Pd(II) where it meets it, leading to the production of Pd-NPs (grey circles). This occurs at intracellular locations as well as at the cell surface leading to deposition of clumps and towers, as well as more distantly from cells.

Hypothesis 2 is concomitant with observations from work from the Meyer group^{143,202} where the direct contribution of biological processes in Pd-NP production is minimal. Bunge *et al*¹⁴³ demonstrated that autoclaved samples of *Pseudomonas putida*, *Cupriavadus necator*, and *Paracoccus denitrificans* still produced Pd-NPs, while Rotaru *et al*²⁰² saw that functionalised PEG beads decorated with acetyl groups or carboxyl functionalised polystyrene could also precipitate Pd-NPs, drawing conclusions that Pd-NPs are not produced by through any truly biological intervention. Experiments presented here however do not wholly agree with these conclusions. In the model system studied here, Pd-NPs were not produced by heat killed cells and required activity of an enzyme. A compromise can be made that biological activity contributes indirectly to Pd-NP production by *E. coli* specifically, but in other organisms, such as those considered in the Meyer group's experiments, it is an artefact of the chemical moieties at the cell surface.

The Macaskie group have produced a wealth of data about hydrogenase-influenced Pd-NP production^{138,141,149,156,204}. Their work lends itself to a theory where the Pd-NP is produced directly by the hydrogenase in *E. coli* and *Desulfovibrio desulfuricans*. This theory proposes that initial reduction of Pd(II) and nucleation of the Pd-NP is dependent on hydrogenases, however there have been no direct interrogations of the interaction of a hydrogenase and Pd(II) ions or Pd-NPs, only inferences from altered phenotypes in different genetic backgrounds. These experiments also concluded using heat killed *E. coli* that Pd(II) reduction was dependent on biological activity. TEM in these studies also showed Pd-NPs accumulating at the edges of the cell envelope in *E. coli* MC4100, IC009, IC010 and FTD89 at a similar size to those observed in this study¹⁴¹.

It may be possible to draw together a theory for biologically influenced Pd-NP production using data from this project that unifies these contrasting lines of thought. This project has demonstrated that Pd-NP production can be dependent on biological activity, however it has also suggested that this is likely an indirect effect of biotic factors that influence the chemical environment and not a directly biological phenomenon. This goes some way towards explaining some of the disparity in the literature on bio-Pd-NPs.

This Chapter also disagrees with work that indicates Hyd-1 and Hyd-2 can also contribute to Pd(II) reduction to produce Pd-NPs¹⁴¹, in fact more significantly apparently than Hyd-3. In this work, cells of the MC4100 background were grown in parallel conditions to trigger expression of individual hydrogenases. They were then incubated with Pd(II), and its reduction apparently driven by formate addition to the sample in each case. This is confusing as formate should only serve as a direct substrate

of FHL and thus only supply electrons to Hyd-3. The slower rate of Pd(II) reduction observed in FTD89 (Hyd-3 only) compared with the other strains used in these experiments may be explained by the change in the growth conditions¹⁴¹. FTD89 (Hyd-3 only) was grown in nutrient broth with the addition of formate while IC009 (Hyd-1 only), IC010 (Hyd-2 only) were grown in nutrient broth with the addition of fumarate and glycerol¹⁴¹. MC4100 (the parent strain) was grown for separate experiments in as FTD89 and IC009 and IC010, however only one dataset for MC4100 was shown in the publication and so it is not possible to compare the MC4100 Pd(II) reduction rate to that FTD89, or indeed to IC009 or IC010¹⁴¹. It may be stated then that Deplanche *et al*¹⁴¹ have not effectively elucidated the contribution of individual hydrogenases to Pd-NP formation.

2.3.2.The Atomic Constituents of the Pd-NP

The reaction with H₂ to produce Pd-NPs presents the question of the atomic nature of the Pd-NP. Indeed, the atomic nature of biologically synthesised Pd-NPs does not appear to have been studied previously. If H₂ donates electrons to Pd(II) to produce Pd-NPs and molecular H₂ is not detectable in this condition by gas chromatography, it is possible that either the hydrogen has been consumed and incorporated to form a Pd hydride NP, or that protons have simply dissolved back in to the aqueous phase.

Investigation in to metal hydride nanoparticle formation has mostly focussed on how elemental metal NPs become loaded with H₂. This study has demonstrated that direct exposure of soluble Pd(II) to H₂ can lead to precipitation of Pd-NPs. This may present a new way to produce Pd hydride NPs if that is their composition.

We can make weak predictions about the composition of the NPs produced in these experiments by considering the chemical reactions that could be taking place. Fully saturated Pd hydride NPs are characterised as having a ratio of roughly five Pd atoms to three H atoms in a H saturated state (PdH_{0.6}). In the formation of these NPs, Pd atoms form a crystal lattice with face-centred-cubic (fcc) geometry, with hydrogen atoms intercalated in to the interstitial spaces between these. At low concentrations of hydrogen, this is called the α -phase, which is structurally distinct from the saturated β -phase Pd hydride crystal structure with composition of PdH_{0.6}, meaning that 60% of the available interstitial sites have been occupied²¹⁵. The current model of Pd hydride NP composition requires that H⁻ ions interact with the Pd atom, in an alloy type interaction.

There are then two possible states for these Pd-NPs, either as elemental Pd(0) NPs, or as PdH_x NPs, shown in Figure 2.8. In the case of an elemental Pd(0) NP, there are only Pd atoms in a f-c-c crystal

lattice structure. Meanwhile a PdH_x NP would contain H^- ions in the interstitial sites between Pd atoms.

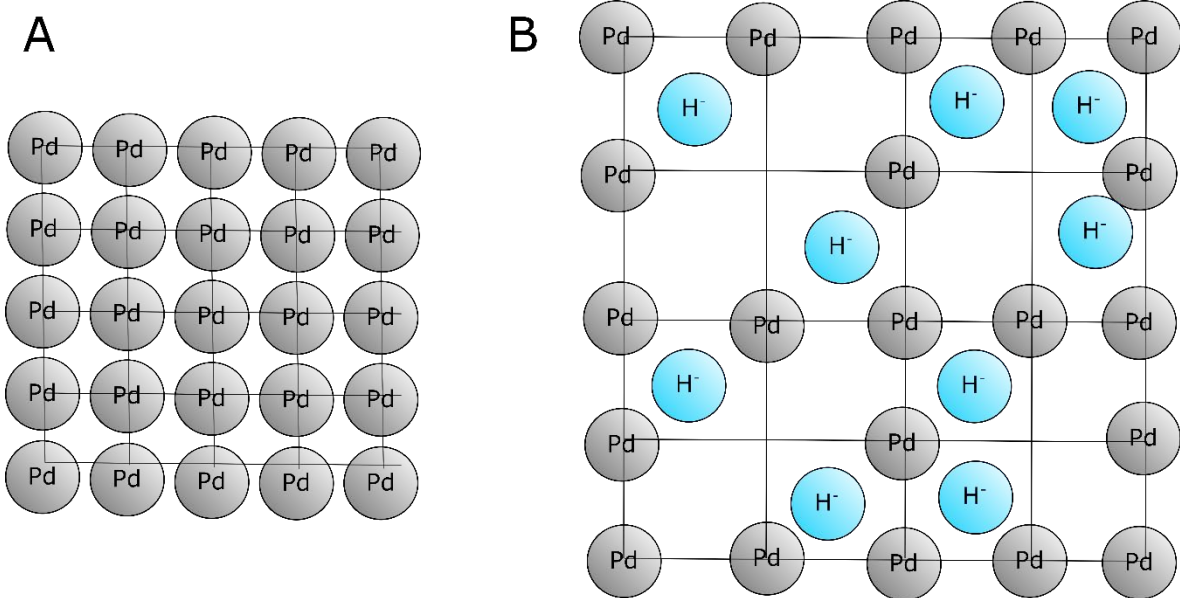


Figure 2.8 Pd-NPs may be elemental Pd(0) NPs or PdH_x NPs

A, In the crystal lattice structure of elemental Pd(0) NPs, there are no other atoms present other than Pd, and there is a small interstitial space between the Pd atoms in a forward-centred-crystal lattice structure.

B, In PdH_x nanoparticles, there is a much larger interstitial space between Pd atoms, but the f-c-c structure is retained. Hydrogen is also present, occupying the enlarged intersitria, in the form of hydride. A maximum of 60% of these interstitia can be occupied at any time, and hydrides may move freely between occupied and unoccupied spaces.

Pd-NPs produced in the model system studied in this Chapter could be further characterised using X-ray crystallography. This may not illuminate individual protons/hydrides in the lattice of a proposed Pd hydride NP but the size of the interstitial places in the structure would be indicative of this.

Monitoring pH change would provide useful information about the mechanism of Pd-NP formation that might contribute to understanding their atomic composition. If pH remains stable, this would indicate rapid incorporation of hydrogen in to Pd-NPs and the production of a PdH_x NP. Reduction in pH throughout this reaction would not obviate the hypothesis of a Pd-NP, and calculations would have to be performed to estimate moles of potential hydride incorporated in to PdH_x NPs, relative to the moles of formate oxidised to produce the H_2 precursor.

2.3.3. Biotechnological Applications of Pd-NPs

Metal hydride NPs such as Pd hydride NPs have been explored as a carrier of hydrogen fuel^{216,217}. To date their synthesis has been explored mostly as a two-step process involving H_2 production and NP production occurring in parallel with hydrogen loaded on to NPs^{218,219}. If the system studied in this Chapter using *E. coli* hydrogenases is producing Pd hydride NPs, it could present a cheap and eco-friendly new way to produce hydrogen fuel and store it in a safe to handle format in a single step.

The palladium reduction system studied here could be harnessed as biosensor for H_2 . There is a lack of a facile high-throughput reporter for biological H_2 production. Given the anticipation of developing clean and sustainable hydrogen fuel, a tool of this nature would greatly aid fundamental research and identification of novel H_2 producing enzymes, pathways and microbes. The colour change observed in Figures 2.1, 2.3, and 2.5 from yellow to black upon hydrogen:Pd(II) interactions provide an opportunity to develop a qualitative Pd based H_2 reporter assay for screening large collections of samples.

Direct interspecies electron transfer (DIET) is a rapidly growing area of microbial research with biotechnological applications. This is the phenomenon where lithotrophic microbes have been observed to transfer electrons to partner cells using nanowires²²⁰. This naturally proposes the possibility of consortia of cells consisting of lithotrophs receiving electrons from an electrode and sharing them with another strain engineered to generate a useful product. *E. coli* has not been explored for use in any DIET applications, but the production of Pd-NPs like those seen in these TEM images may prove useful for its introduction in to a synthetic DIET system.

Various NPs of divergent chemical makeups have been explored for sonodynamic therapy (SDT) applications²²¹. SDT is an emerging cancer treatment strategy where NPs are allowed to accumulate in or around solid tumours and radio frequency ultrasound is used to induce cavitation of the NPs which causes destruction of tumour tissue²²¹. Si-NPs of similar size ranges have been used before for ablation of tumours in a murine model of melanoma²²².

2.3.4. Use of Pd-NPs as an “aerial” conduit module

While Pd is a good model for understanding metal NP formation, Pd is a paramagnetic metal. Paramagnets are only weakly affected by magnetic fields and as such may not be effectively subjected to magnetic hyperthermia as in the original aims of this project. Clearly, this research has identified other limitations of these nanoparticles. The Pd-NPs were primarily found at the outer cell surface, which is not optimal for signal transduction should they be excited enough to produce heat. Moreover, a great number of them appeared free-floating in the extracellular milieu, indicating that they do not remain closely associated with the cell. For these reasons, Pd-NPs were rejected and alternative magnetic nanoparticles were explored next as suitable candidates for the “aerial” module of the system.

Chapter 3:
Engineering Magnetic Phenotypes in *E. coli*

3.1. Introduction

Since Pd-NPs were deemed to be not suitable for use as ‘aerial’ modules in the planned device (Chapter 2), magnetite nanoparticles (MNPs) were explored instead.

Magnetism is one of the four fundamental physical forces²²³. It is governed by the sub-atomic scale momentum imparted by electrons within a material and their interactions therein. Many organisms have been identified that are seemingly able to sense Earth’s magnetic fields and utilise this for navigation²²⁴, for example honey bees^{225,226}, termites^{227,228}, fish and birds²²⁹. However there are very few examples that are satisfactorily described mechanistically at the level of genes, proteins and molecular interactions¹⁰⁴. The best described case of biological magnetism and magnetoreception is that of magnetotactic bacteria⁹⁴. These organisms, described more detail in Chapter 1, produce magnetic nanoparticles (composed of the minerals, magnetite, maghemite or greigite²³⁰) in membrane-enclosed organelles called magnetosomes in a sophisticated program governed by genes located on a mobile genetic element called the magnetosome assembly island (MAI)^{94,178,231}. This is naturally an attractive source of genes for synthetic biology applications that require, or would be aided by, biologically produced magnetism.

The MAI comprises >120 kb of genetic information^{231,232} across multiple operons and the investigation of the role of each individual gene is still in progress. However, specific operons and genes have been identified and characterised that are proposed to contribute directly to MNP nucleation and growth via interactions with Fe or MNPs themselves. Given the nature of magnetosome biogenesis as a cooperative process between inclusion of the inner membrane and MNP precipitation, almost all characterised proteins encoded by the MAI are integral membrane proteins, with the notable exception of MamK, which helps to align mature magnetosomes in the cell with the assistance of the magnetosome membrane protein MamJ.

Production of the Mms6 protein in mammalian systems has produced Fe aggregates visible by TEM¹⁹² that produce a magnetic signature seen by MFM and SQUID¹⁹⁵. The Mms6 protein was first described as a magnetosome membrane specific protein of six kDa, where a proteolytically processed version of it was identified in a proteomic analysis of the proteins more closely associated with the MNP in *Magnetospirillum gryphiswaldense*¹⁶⁴. It has since been mapped in the MAI and is naturally a larger peptide of ~12 kDa that is encoded by an operon of five genes called the *mms6* operon. Deletion of either *mms6*

alone or the entire *mms6* operon produces defects in MNP synthesis and the magnetotactic phenotype^{182,184,233,234}.

Numerous *in vitro* experiments have demonstrated that Mms6 contributes to control of the size and morphology of the MNP^{164,234,235}, while other experiments have demonstrated the remarkable capability of small defined regions of this protein to nucleate MNPs¹⁸¹. This region of the protein is at the C terminus, predicted to be exposed to the periplasm²³⁶, and bears the amino acid sequence SDEEVE²³⁵. This makes a natural fit for it to contribute to MNP nucleation and growth as the inclusion of the periplasm produces the mature magnetosome. Mms6 also has the potential to produce MNPs in a variety of foreign biological backgrounds^{181,195}.

Another gene from the *mms6* operon whose deletion alone produces defects in MNP synthesis and magnetotaxis is *mmsF*. MmsF is another small protein of 14 kDa that resides on the inner membrane and the mature magnetosome membrane. MmsF has been shown to contribute to MNP size and morphology control as well as magnetotaxis in deletion studies, and *in vitro* contributes to MNP morphology regulation in a similar way to Mms6¹⁸⁵.

Deletion of the gene encoding the MamI protein has indicated that it is indispensable for magnetotaxis and, unlike Mms6 or MmsF, MamI is also indispensable for MNP production^{94,173,237}. A role was originally proposed in magnetosome membrane invagination for MamI since deletion of the region encoding it produced no magnetosomes at all, and in parallel with deletion of other regions of the locus it was surmised that this was its role¹⁷³. A later study using X-ray cryo tomography to explore the intracellular landscape of MTBs showed that deletion of *mamI* specifically produced no defect in magnetosome membrane biogenesis, but noted instead a lack of maturation of MNPs, where these compartments were filled with small hematite NPs instead of the larger mature MNPs²³⁷.

A specific region of MamI has been postulated to be responsible for its interaction with the MNP and has been successfully used to make a modified version of flagellin²³⁸. This MamI sequence was added to a loop region of the FliC protein, which makes up the repeating unit of the flagellum, that points away from the central axis of the structure. Cells were then incubated with MNPs and imaged by EM showing that the flagella of cells expressing the modified *fliC* allele were decorated with magnetite²³⁸.

Other attempts to produce magnetic phenotypes in non-magnetic microbes have focussed on directed evolution approaches rather than rational engineering using existing proteins. The Silver laboratory have used directed evolution to produce a ferritin allele with a magnetic screening tool with MACS®

columns²³⁹. Plasmids containing *ftnA* were subjected to rounds of mutagenesis followed by screening with MACS columns where magnetic cells were retained, recovered and then subjected to further rounds of mutagenesis. Two non-synonymous SNPs were observed to improve retention of *E. coli* on the magnetic column, which were also found together on the same allele in subsequent rounds of mutagenesis. This group have also produced magnetic phenotypes in yeast strains by expression of human ferritin alleles combined with alteration of cellular redox potential through copy number alteration of the genes *ccc1* and *tco89*²⁴⁰.

Heterologous expression of gene clusters straight from MTB genomes has not been reported, beyond introduction of slightly minimised version of the MAI in *Rhodospirulum rubrum*²⁴¹.

3.1.1.Aims

The aims of the work presented in this Chapter are to investigate the phenotypes produced by expression of genes from magnetotactic bacteria in *E. coli*. The ultimate aim is to identify and harness properties that enable nucleation of magnetic nanoparticles. In addition, strategies to produce magnetite-importing proteins by protein engineering will be investigated.

3.2. Results

3.2.1. Heterologous Expression of Genes from MTB

Work by the Staniland group has studied the properties of *Magnetospirulum gryphiswaldense* homologs of Mms6 and MmsF and have demonstrated interactions with magnetite nanoparticles and proposed nucleation thereof. For these reasons, these specific alleles were selected for study heterologously. The predicted primary sequences of the proteins Mms6 and MmsF from the MTB *Magnetospirulum gryphiswaldense* were obtained from the Kyoto Encyclopedia of Genes and Genomes database (KEGG²⁴²) and back-translated (codon optimised for *E. coli* preferences) using on-line tools operated by Integrated DNA Technologies (IDT). The synthetic genes were then ordered as gBlocks from IDT. These were cloned individually by the Gibson assembly method in to the pQE80L vector, which was linearised by digestion with the restriction enzymes BamHI and HindIII, resulting in the plasmids pQEmms6 and pQEmmsF (Figure 3.1).

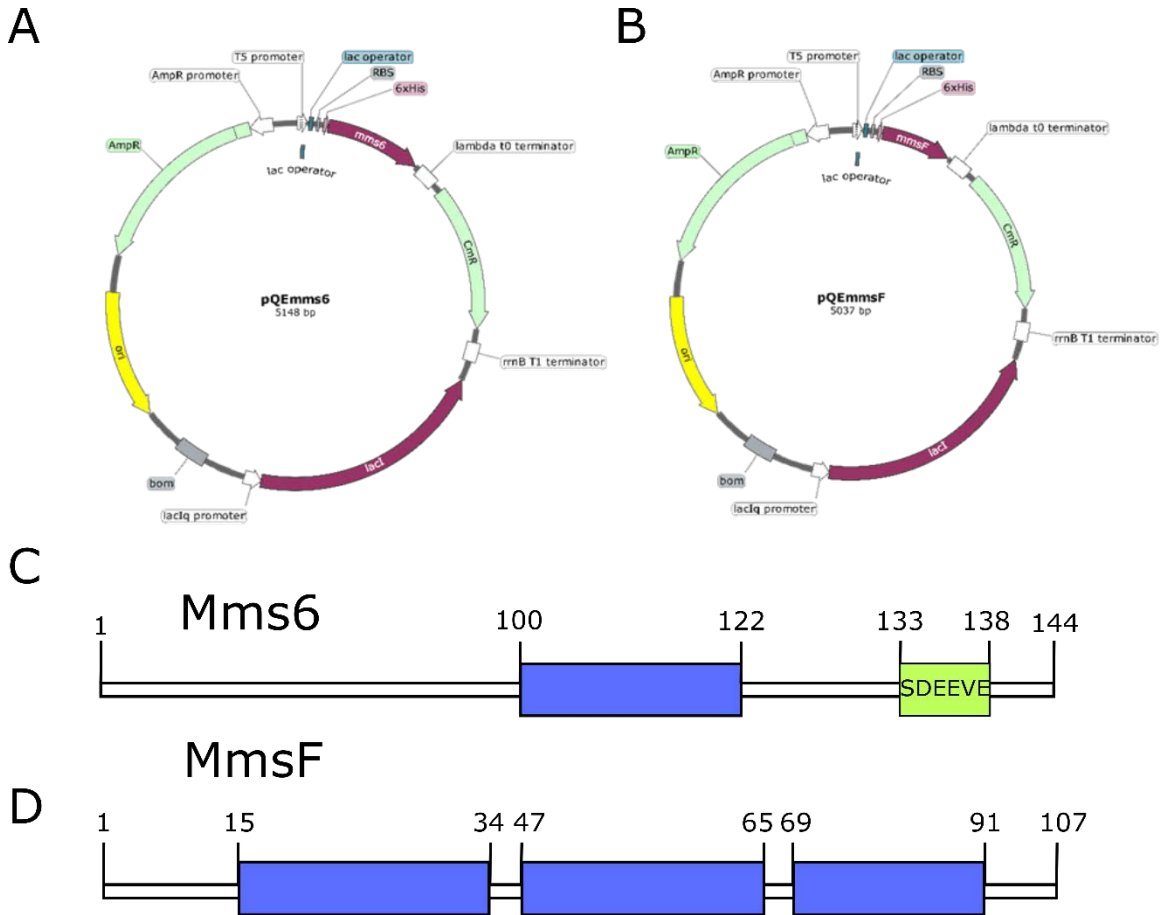


Figure 3.1 Plasmid maps of clones harbourin goptimised *mms6* and *mmsF*, which encode proteins with transmembrane domains

A,B, The vector pQE80L was linearised by digestion with BamHI and HindIII and used in a Gibson assembly reaction alongside PCR products of codon-optimised *mms6* or *mmsF*. Primers utilised added 20-25 nt of overlap suitable for Gibson assembly. Clones were verified by Sanger sequencing.

C,D, The amino acid sequences encoded by these genes were analysed using the TMHMM algorithm which uses the Kyte-Doolittle rules to predict transmembrane helices. Transmembrane helices are highlighted in blue and residue numbers noted above. In C, the SDEEVE region of Mms6 is highlighted also in green.

3.2.2.Production and Characterisation of Mms6 and MmsF in *E. coli*

This cloning design of synthetic *mms6* and *mmsF* in pQE80L facilitated addition of a hexahistidine tag at the N terminus of the protein products. Production of these proteins in *E. coli* was examined by Western immunoblotting, using both whole cell samples and cells fractionated into total membranes, periplasm and cytoplasmic proteins. Figure 3.2 indicates that both Mms6 and MmsF were translated and targeted to the membrane.

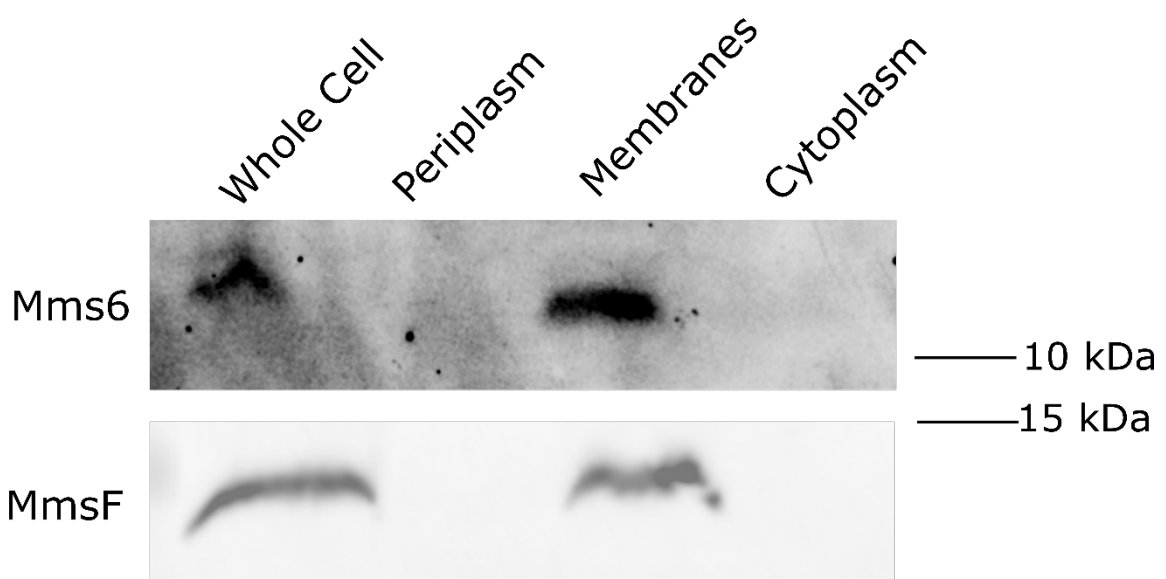


Figure 3.2 Mms6 and MmsF are located in the *E. coli* membrane fraction

E. coli MG1655 cells were transformed with pQEmms6 and pQEmmsF, and cultured in 25 mL LB with ampicillin and 1 mM IPTG at 37 °C overnight. Whole cell samples were taken straight from the culture, while others were prepared upon controlled lysis that separated periplasmic, total membranes and cytoplasmic samples. These were analysed on an 18 % (w/v) SDS-PAGE gel then transferred to a nitrocellulose membrane by semi-dry electroblotting and probed with an anti-His antibody from mouse serum and a secondary anti-mouse IgG antibody with conjugated horse radish peroxidase activity. This was then developed with addition of ECL and imaged using a GeneGnome.

Next, the proposition that the Mms6 and MmsF proteins may interact with magnetite was challenged. For this purpose, magnetite (or Fe_3O_4) was prepared by the Room Temperature Co-Precipitation (RTCP) method. Briefly, in this protocol 0.01 moles of ferrous sulfate were mixed in a solution with 0.02 moles of ferric citrate. Next, 0.08 moles NaOH was added and the reaction was mixed continuously since MNPs precipitate out of the solution. The resultant MNPs were cleaned with distilled water and then sonicated to prevent clumping. The MNPs were examined by electron microscopy. Figure 3.3 shows that the nanoparticles were at the nano scale and were approximately 6 nm in diameter (median = 5.5 nm, average = 5.81 nm, range= 2.88 – 10.25 nm).

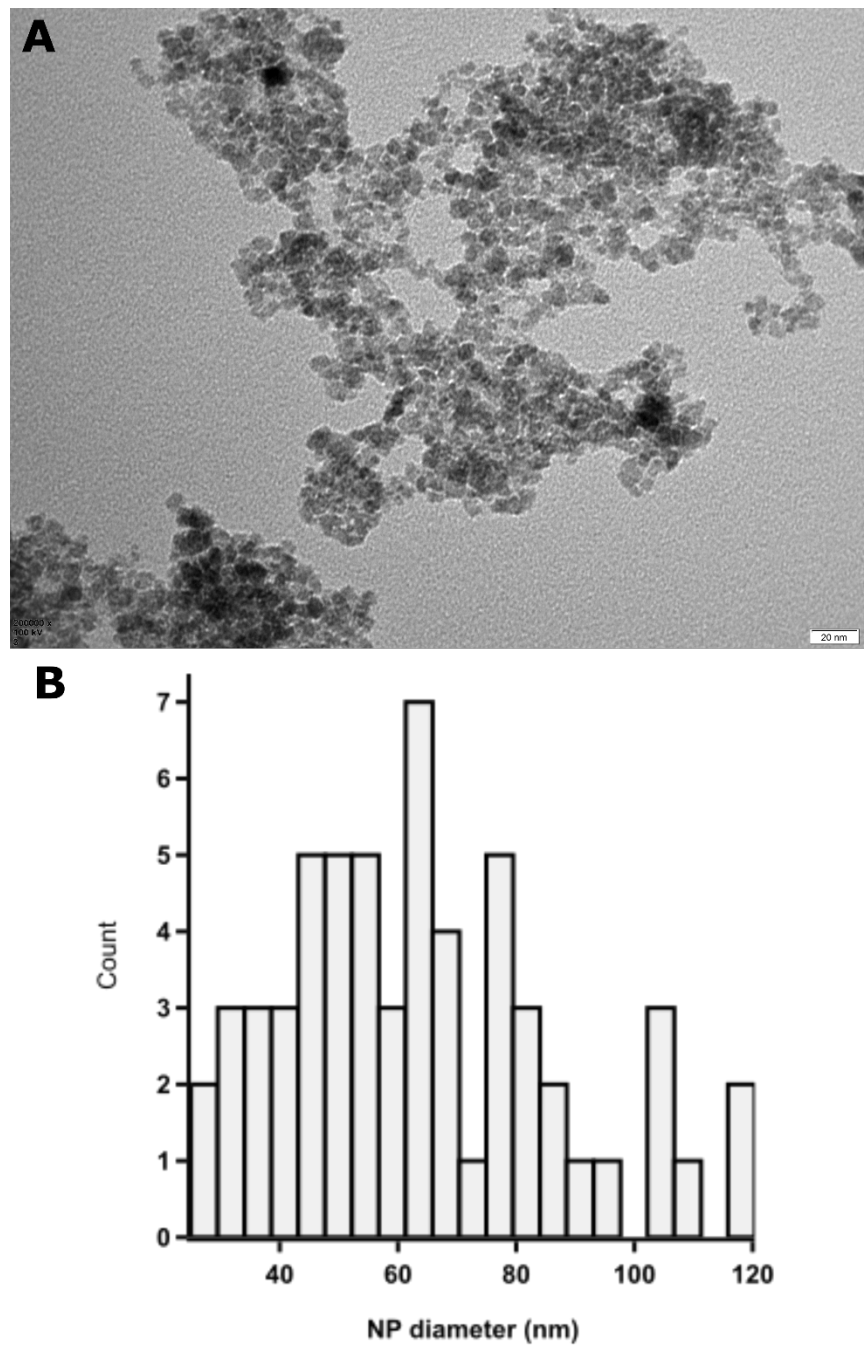


Figure 3.3 MNPs produced by the RTCP method are between 3 nm and 10 nm in diameter

A) MNPs were produced by the RTCP method and examined by electron microscopy. First, 0.01 mols ferrous sulfate were combined with 0.02 mols ferric citrate in 100 mL deionised water, followed by addition of 0.08 mols NaOH, at which point MNPs precipitated as a black sludge. This was washed by magnetic decantation with deionised water three times and sonicated for one minute. The solution was diluted to 0.01 mM and applied straight to an EM grid and dried under a lamp before being imaged on a Hitachi HT7800 transmission electron microscope at 100 kV. B) A total of 66 MNPs whose edges were easily distinguishable in EM images were measured using the “Measure” tool in imageJ. These data were then plotted in a histogram.

In order to assess potential magnetite binding or uptake properties imparted by MmsF or Mms6 production, magnetite was added at a concentration of 2 mM to cultures of *E. coli* MG1655 cells previously transformed with either pQE80L, pQEmms6 or pQEmmsF. In order to remove any magnetite from the culture that was not directly interacting with cells, an equal volume of 0.3 M oxalic acid was applied, which dissolves magnetite²⁴³. After incubation the sample was centrifuged at which point a dark black pellet could be seen in cells producing Mms6, while those containing the empty vector produced pale yellow-brown pellets (Figure 3.4). MmsF producing cells also had visibly darker pellets (Figure 3.4). The pellets were suspended in PBS and the solution poured in to a petri dish atop a magnet. Suspensions produced from pQEmms6 containing cells were attracted to the magnet, visible in Figure 3.4, indicative of MNP uptake or attachment. MmsF producing cells were more difficult to suspend and became clumpy, however some of the debris could be described as being attracted to the magnet.

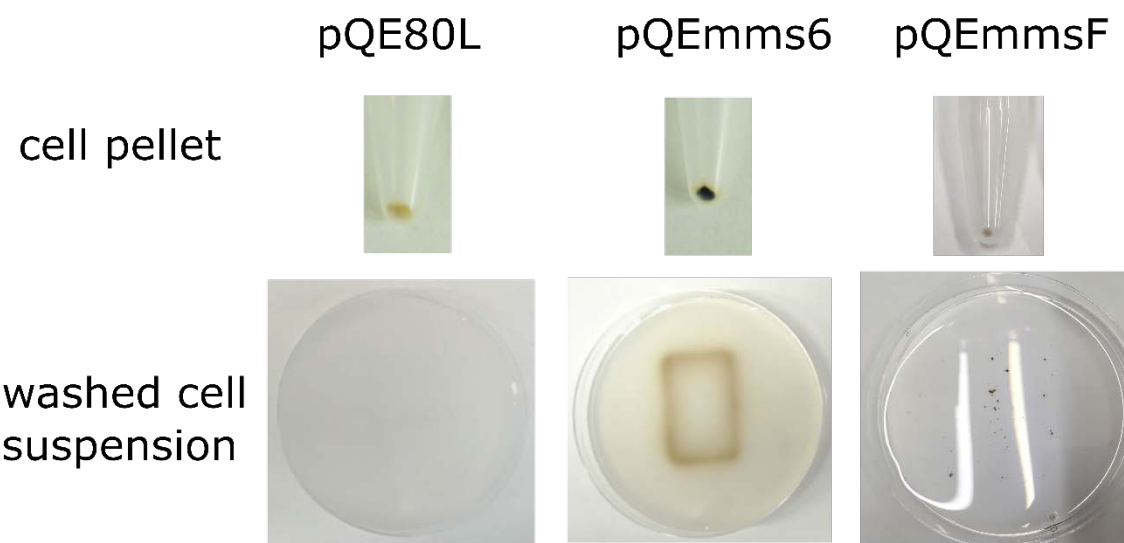


Figure 3.4 Cells containing pQEmms6 interact with magnetite

E. coli MG1655 cells were transformed with pQE80L, pQEmms6 or pQEmmsF and fresh single colonies were grown in 5 mL cultures at 37 °C, which were then subcultured at a 1:100 ratio by volume in 250 mL LB with 1 mM IPTG and 2 mM magnetite (synthesised by RTCP) at 37 °C for approximately 16 hours. The culture was then diluted with an equal volume of 0.3 M oxalic acid and incubated at room temperature for around thirty minutes with shaking and centrifuged to pellet cells, shown in top row of images. The pellets were suspended in PBS and 20 mL added to a petri dish over a 32 kg pull neodymium magnet before being photographed.

3.2.3. Development of a Magnetic Retention Assay

In order to produce a quantitative measurement of magnetic properties of cells producing Mms6 or MmsF, a magnetic retention assay (MRA) was developed, based on work from Pamela Silver's group^{239,240}. Figure 3.5 describes the workflow of this experiment, where magnetic cell separation columns (MACS®) produced by Miltenyi Biotec are used to separate magnetic from non-magnetic cells in a suspension. LD MACS columns were used in the original experiments where a magnetic *ftnA* allele was developed by directed evolution and random mutagenesis²³⁹.

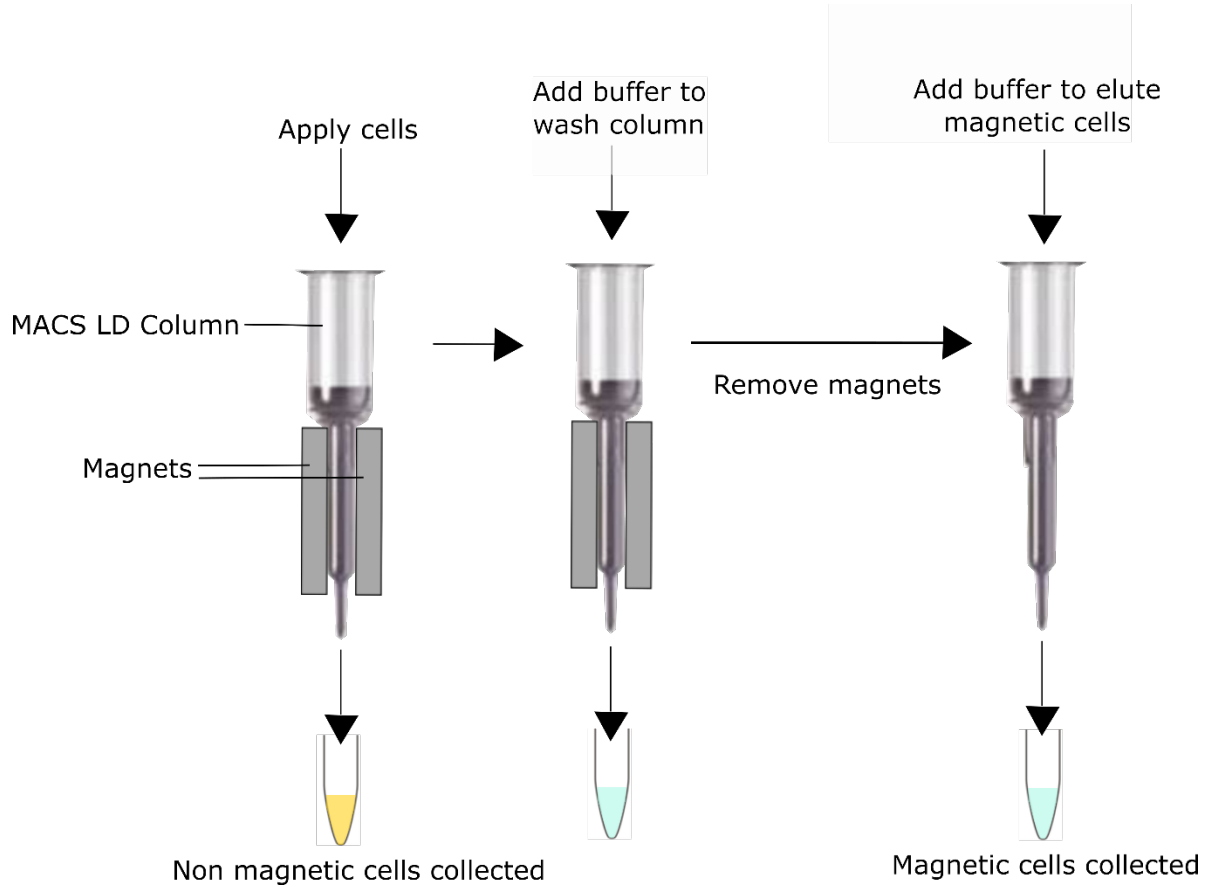


Figure 3.5 Magnetic Retention Assay (MRA)

Roughly 10^8 cells were added to a Miltenyi MACS LD column with a 22 kg pull neodymium magnet (first4magnets) attached to either side of the column where noted. The column was held using a clamp stand and with a 15 mL Corning tube below the outlet of the column to collect the flow through. Flow through was continually collected while 3 mL PBS was allowed to travel through the column as a non-magnetic fraction. The magnets were then removed and 3 mL of PBS was forced through the column using the provided plunger and the eluted fraction was deemed to contain only the magnetic cells as in previous work²³⁹. The cells were then counted using images collected with a light microscope at 60× magnification and particle analysis tools in imageJ.

In initial experiments, a culture was grown overnight with MG1655 cells containing pQE80L or pQEmms6 with 1 mM IPTG for induction. The overnight cultures were normalised to produce cell suspensions at 10^8 cells per mL in PBS, by estimation from the OD₆₀₀. Next, 1.5 mL of the resultant suspension was applied to an LD column straight out of the box, aligned by two 22 kg pull neodymium magnets, followed by washing with two column volumes of PBS. The flow through was collected throughout this time period. The magnets were then removed and 1.5 mL PBS was added and the supplied plunger was used to push this buffer through to elute any cells that had been magnetically retained. Cell suspensions in the flow through and eluted suspensions were normalised by centrifugation and resuspension, before cells were counted by taking images using a light microscope at 60 × magnification and analysed using imageJ to estimate cells per mL. Columns were retained after washing with PBS and stored in 96% EtOH.

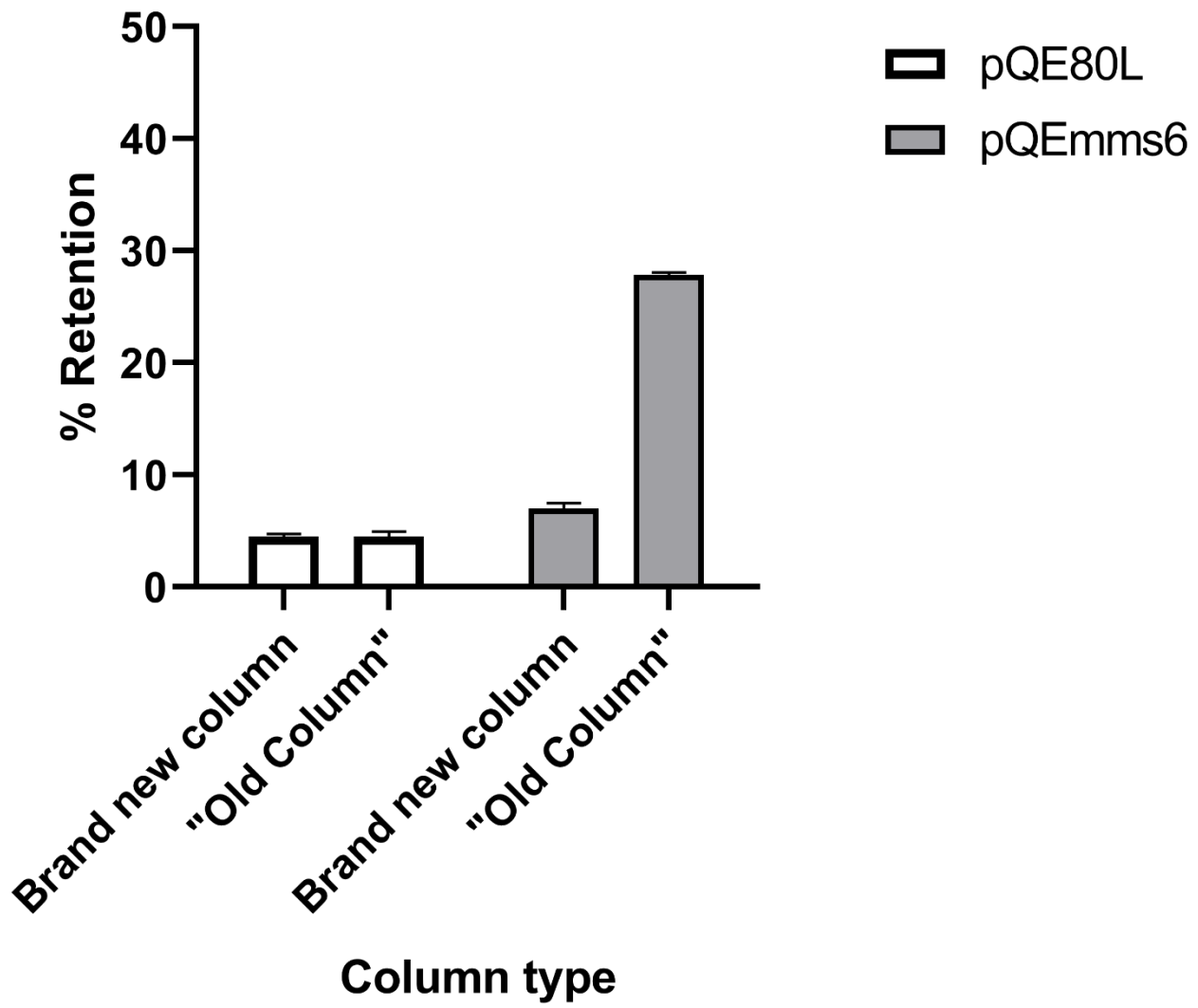
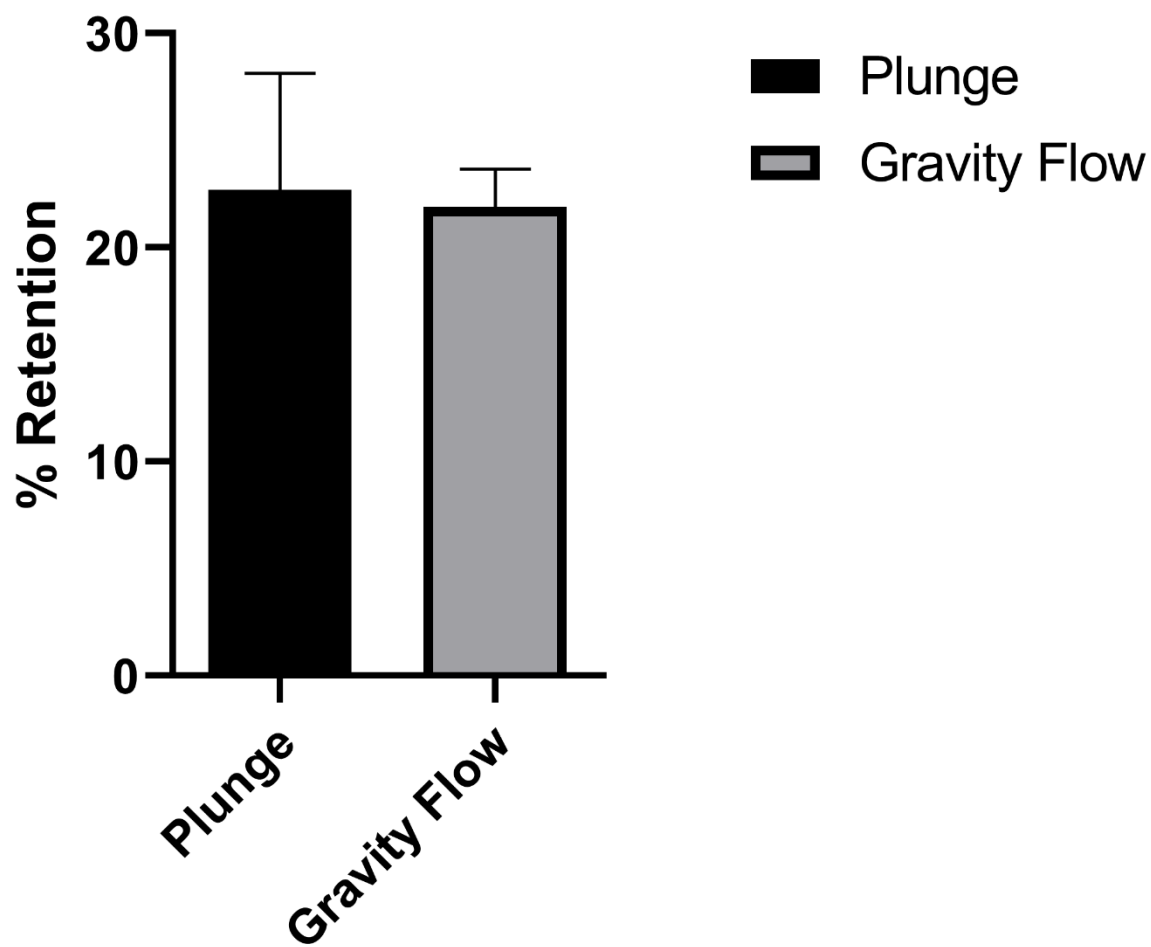


Figure 3.6 Initial Magnetic Retention Assays

E. coli MG1655 cells transformed with either pQE80L or pQEmms6 were grown overnight in LB cultures with 1 mM IPTG for induction and then cells per mL estimated from OD₆₀₀ measurements and adjusted to 2 × 10⁸ cells per mL. In the case of brand new columns, a MACS LD column was removed straight from its packaging and 0.5 mL added straight to the column upon to application of two 32 kg pull magnets to the sides of the LD column. “Old Columns” were columns that had been used up to three times previously and had been stored in 96 % EtOH during interim periods. Error bars are representative of the standard deviation of three biological replicates.

It can be seen in Figure 3.6 that using brand new columns did not permit cells containing pQEmms6 to be retained at any greater level on the magnetic column than the control pQE80L. However, columns that had been used around four times prior did produce retention in accordance with previously published work with magnetically enhanced cells^{239,240}. It was surmised that either equilibration of the column with buffer, or the act of plunging the columns in wash steps and elution steps, was somehow ‘maturing’ the columns in such a way that magnetic cells could be retained. In order to produce a reliable assay, it was necessary to investigate further. Thus, the equivalent volume of PBS to four experiments was allowed to either flow through the column under gravity, or was forced through using the plunger. Figure 3.8 shows that either of these pre-treatments was sufficient to allow pQEmms6 expressing cells to be retained on the column.



Column treatment

Figure 3.7 Comparison of MRA column pre-treatments on pQEmms6 containing cells

One MACS LD column was washed with 60 mL sterile PBS by gravity flow (marked here as “Gravity Flow”) and another was washed with 60 mL passed through using the supplied plunger (marked here as “Plunge”). Cells containing pQEmms6 were grown in 5 mL LB with 120 µg/mL ampicillin and 1 mM IPTG. The OD₆₀₀ of the culture was measured and then washed and suspended at an estimated cells per mL of 2×10^8 per mL in PBS. Next, 0.5 mL of the suspension was applied to each MACS LD column followed by 3 mL sterile PBS. Magnets were then removed and cells eluted by plunging of 3 mL sterile PBS through the column. Cells were then counted using light microscopy images and the particle analysis tool in ImageJ. Error bars are representative of two biological replicates.

As each of the pre-treatments gave a magnetic retention of around 20 % with pQEmms6 containing cells, it was concluded that equilibration of the column with buffer was the important factor in preparing the column. In experiments that followed the gravity flow method was used to equilibrate the column as this produced a smaller standard deviation between samples.

To validate and vindicate the new protocol truly, the *mftN* gene was cloned according to the point mutations in *ftnA* identified by Liu *et al*²³⁹. The *ftnA* allele bore non-synonymous SNPs producing amino acid substitutions at H34L and T64I. By including the mutated nucleotides in the overlapping regions of the primers used for Gibson assembly, three PCR fragments were generated which were assembled to produce the plasmid named pQEmftN, where MftN denotes Magnetic Ferritin. Next, an MRA was performed where MG1655 cells were freshly transformed with either pQE80L or pQEmftN and single colonies grown in 5 mL LB cultures with 120 µg/mL ampicillin and 1 mM IPTG overnight. The culture was washed in PBS and adjusted to an estimated cells per mL concentration of 2×10^8 in PBS, using calculations obtained by estimating an OD₆₀₀ of 1.0 relates to 10⁹ cells per mL. Finally, 0.5 mL was added to a MACS LD column and the protocol delineated in Figure 3.5 was followed.

Figure 3.9 shows that when *E. coli* MG1655 cells are transformed with pQEmftN around 40% of the cells are retained on the magnetic column, which is significantly more ($p=0.015$) than that of control cells containing only pQE80L, which are retained at around 15%.

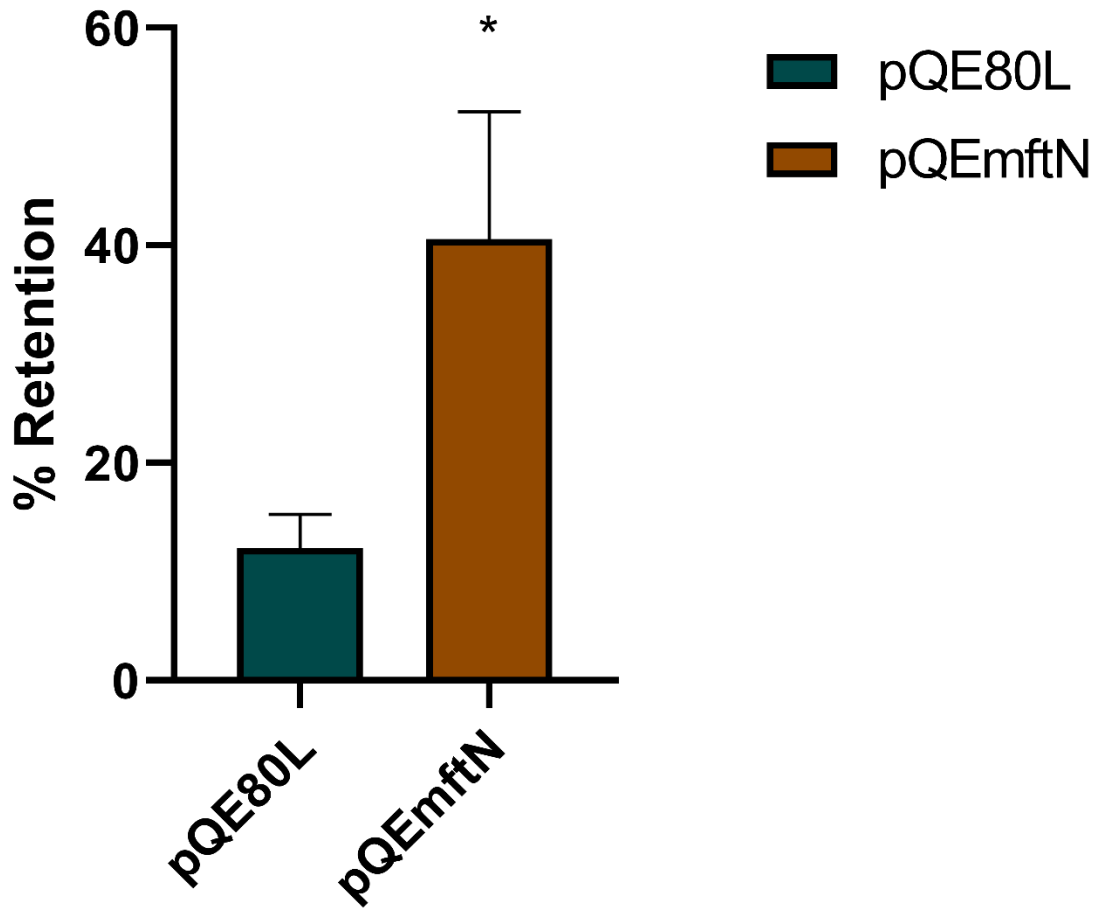


Figure 3.8 Validation and vindication of the MRA protocol using MftN

E. coli MG1655 cells were transformed with either pQE80L or pQEmftN and grown in 5 mL LB cultures with 120 µg/mL ampicillin and 1 mM IPTG. The cultures were washed in PBS and adjusted to an estimated concentration of 2×10^8 cells per mL and 0.5 mL of this suspension added to a MACS LD column and an MRA performed according to Figure 3.5. Cells were counted using images from light microscopy and the particle analysis tool in imageJ ($p=0.015$, non-parametric t-test, $n=3$, error bars representative of three biological replicates).

Given the vindication of the magnetic retention assay, the protocol was used to examine the effect on magnetic retention of *E. coli* MG1655 cells upon transformation with the pQEmms6 and pQEmmsF plasmids. In these assays fresh transformations of *E. coli* MG1655 cells were performed with pQE80L, pQEmms6 and pQEmmsF of which single colonies were grown in 5 mL LB cultures with 120 µg/ml ampicillin and 1 mM IPTG, alongside 1 mM magnetite where designated. The cultures were then washed in PBS and diluted to an estimated cell concentration of 2×10^8 cells per mL in PBS then applied to a MACS LD column in a 0.5 mL volume. The scheme in Figure 3.4 was then followed and cells counted using light microscopy images and the particle analysis tool in imageJ.

Figure 3.9 indicates a significant increase in retention upon expression of the pQEmms6 plasmid, which is not enhanced upon addition of exogenous magnetite. Expression of pQEmmsF in these conditions did not significantly enhance magnetic retention compared to pQE80L, whether magnetite was added or not (in LB alone, $p=0.071$, with magnetite $p=0.081$).

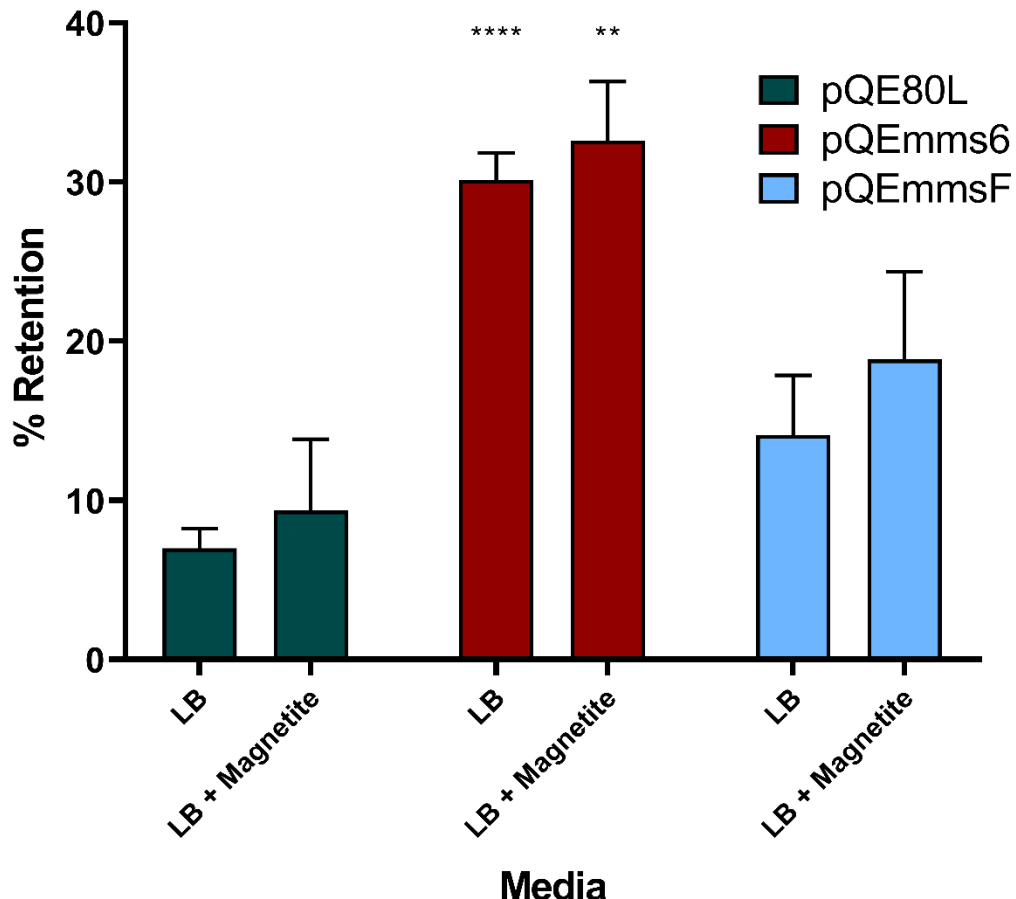


Figure 3.9 *E. coli* producing Mms6 is retained on a magnetic column.

MG1655 *E. coli* cells were transformed with pQE80L, pQEmmsF, or pQEmms6. Single colonies were grown in three individual replicates in 5 mL LB cultures in the presence of 120 µg/mL ampicillin, 1 mM IPTG and where indicated 2 mM magnetite. The cultures were washed in PBS and diluted to an estimated concentration of 2×10^8 cells per mL and 0.5 mL of this suspension added to a MACS LD column and the scheme followed in Figure 3.5. Cells in each fraction were counted to calculate percentage retention using light microscopy images and the particle analysis tool in imageJ. Unpaired t-tests were performed to calculate significant differences between pQEmms6 and pQEmmsF measurements and the relevant treatment of pQE80L producing no significant differences in the case of pQEmmsF (LB alone, $p=0.071$, with magnetite $p=0.081$, Holm Sidak T-test) and significant differences in expression of pQEmms6 (in LB alone $p<0.00001$, with magnetite $p=0.002$, Holm Sidak T-test, error bars representative of three biological replicates).

To test the hypothesis that the increase in magnetic retention seen by introduction of the *mms6* gene (Figure 3.9) was caused by a transformation of Fe in the growth medium into a magnetic form, the experiment was repeated using Chelex-treated LB medium. Chelex is a commercial reagent that is used to remove transition metal ions from a solution. As for previous experiments, *E. coli* MG1655 cells were transformed freshly with pQE80L or pQEmms6 and single colonies were cultured in three independent replicates in 5 mL of Chelex treated LB medium with 1 mM IPTG and 120 µg/mL ampicillin. It was observed that these cultures did not grow nearly as well as was normally expected in LB medium, with pQE80L expressing cells not reaching above an OD₆₀₀ of 0.3 and pQEmms6 containing cells not above 0.18. Cells were then washed in PBS and diluted to the appropriate cell concentration in PBS and MRAs performed as in Figure 3.5.

Figure 3.10 shows that there is no significant difference between pQE80L containing cells and pQEmms6 in terms of magnetic retention when these cells are cultured in Chelex-treated media.

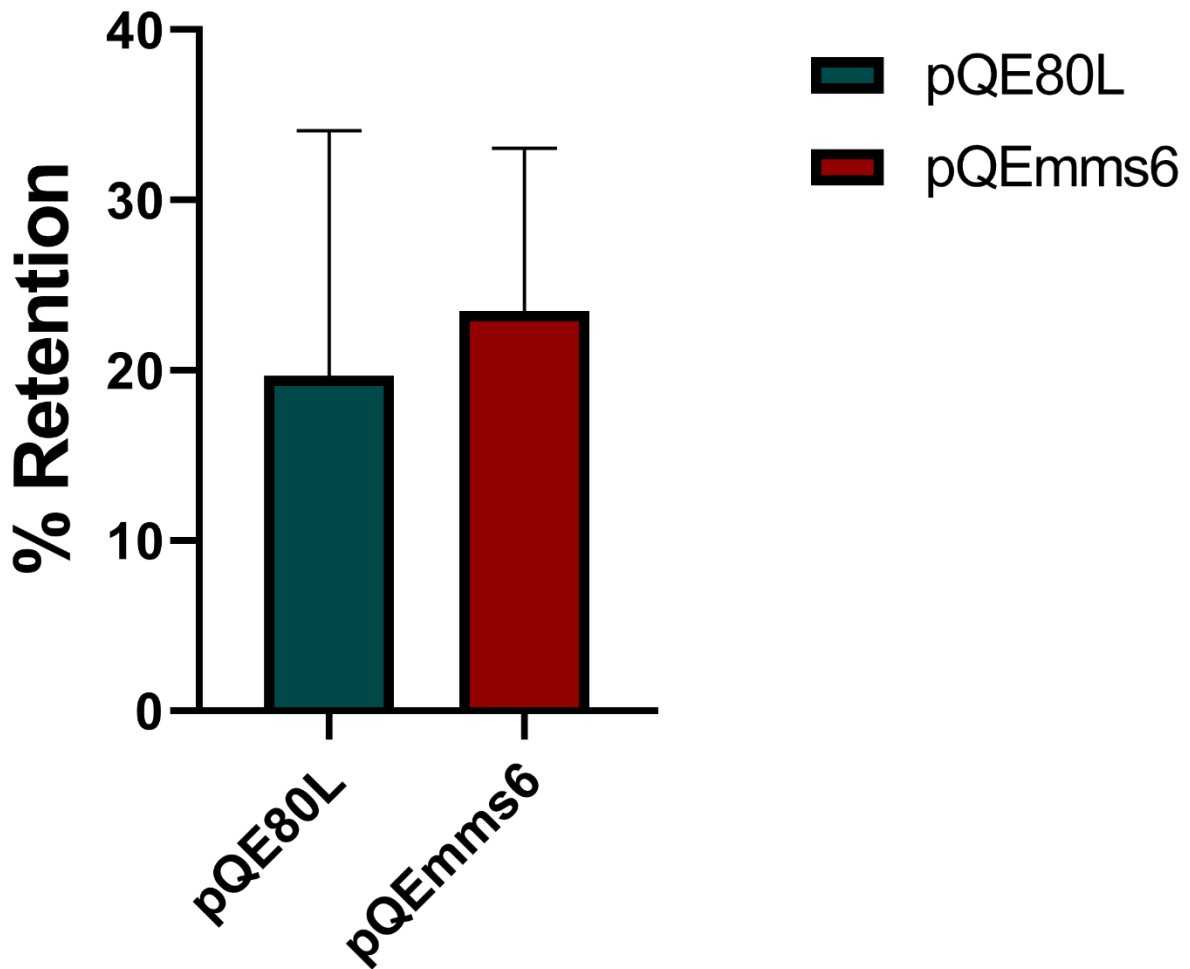


Figure 3.10 Growth in Chelex-treated LB medium affects retention of cells on the magnetic column

E. coli MG1655 cells were transformed with pQE80L or pQEmms6. Single colonies were grown in three individual 5 mL cultures overnight using LB treated with Chelex and 120 µg/mL ampicillin and 1 mM IPTG. Chelex treatment involved the addition of 5 g Chelex resin to 100 mL of LB, incubation for thirty minutes at ambient temperature and then centrifugation to remove the Chelex resin. Following this cells were washed in PBS and diluted to an estimated concentration of 2×10^8 cells per mL and 0.5 mL of this suspension added to a MACS LD column and the scheme followed in Figure 3.5. Cells in each fraction were counted to calculate percentage retention using light microscopy images and the particle analysis tool in imageJ. Error bars representative of three biological replicates.

3.2.4. Developing a Magnetite Pull Down Assay

In order to directly probe the MNP interacting properties of Mms6 and MmsF, a pull down strategy was deployed. Briefly, this involved growth of *E. coli* MG1655 cells with an induction period to produce the proteins, followed by lysis to generate a clarified suspension. The suspension was then incubated overnight with rotary shaking at 4 °C with concentrations of magnetite ranging from 0 to 100 mM, prepared as in Section 3.2.1. Samples were then magnetically separated in to wash and magnetite associated samples using a Magnarack and analaysed by SDS-PAGE, as described in Figure 3.11.

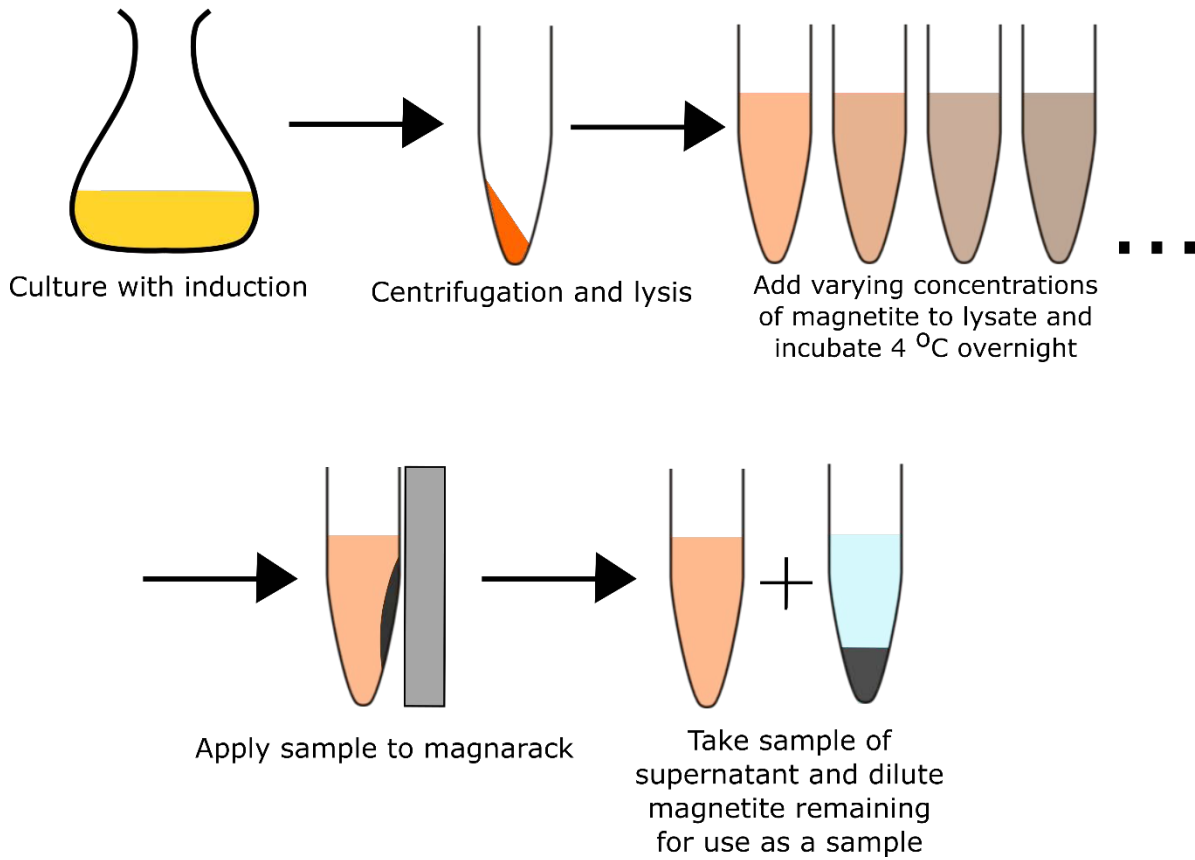


Figure 3.11 The MNP pull down experiment.

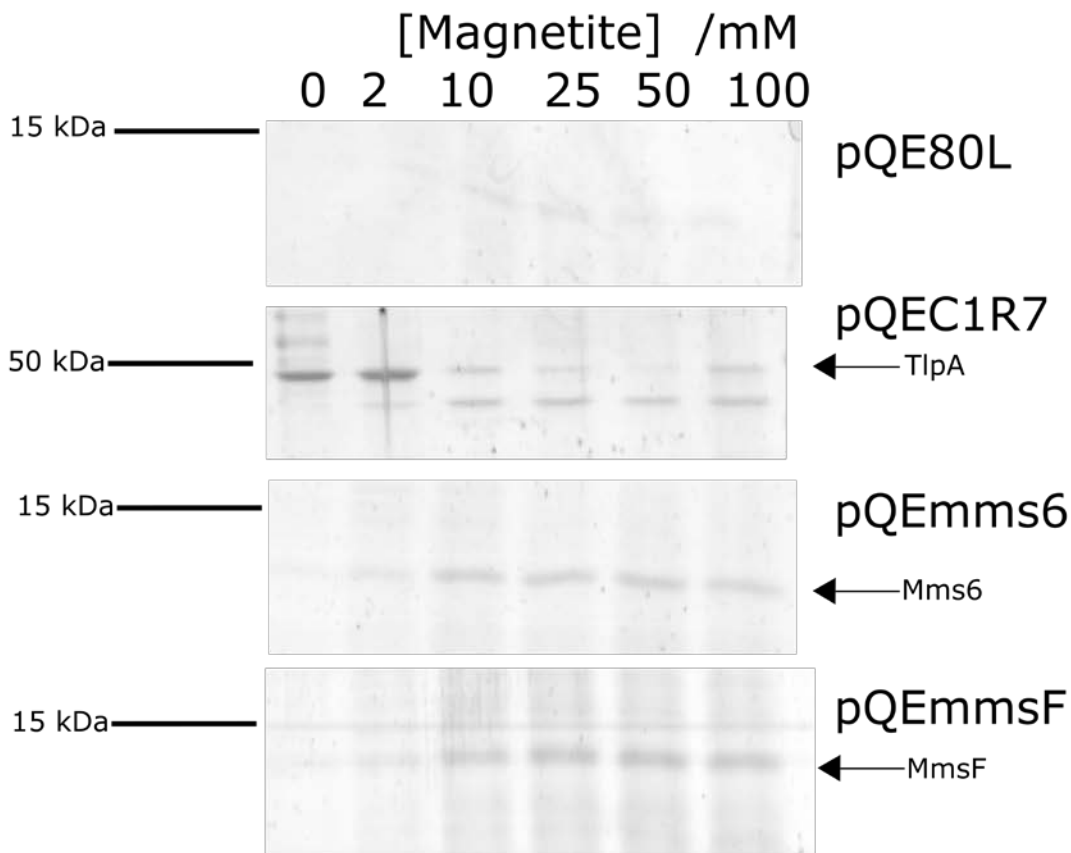
Initially, 50 mL cultures containing 1 mM IPTG were grown using a 5 mL starter culture using a single colony from a fresh transformation. This was then centrifuged and suspended in lysis buffer and sonicated, followed by centrifugation to remove unbroken cells and insoluble debris. Magnetite prepared by the RTCP method was added to 1 mL of the lysate at final concentrations of 0, 2, 10, 25, 50 and 100 mM and the tubes then incubated with rotary shaking at 4 °C for 16 hours. The tubes were then applied to a Magnarack to separate the magnetite from the lysate and the supernatant taken as a wash sample and lysate replaced with Tris.HCl buffer (50 mM, pH 8) to normalise the concentration of the magnetite-associated fraction. The samples were then analysed by SDS-PAGE.

In this experiment, negative controls were deployed using empty pQE80L containing cells, as well as a plasmid encoding the DNA binding protein TlpA²⁴⁴ (plasmid pC1R7), which was used as it has no characterised metal interacting properties^{244–247}. Additionally, cells containing the plasmids pQEmms6 and pQEmmsF were examined.

In these experiments, when pQE80L was used the native *E. coli* protein IscR was isolated in the magnetite associated fraction, (Figure 3.12) as observed by mass spectrometry, however no additional proteins were observed and none at the same size as Mms6 or MmsF. The band in accordance with TlpA where pC1R7 was used apparently diminished with increasing magnetite concentration, however additional bands in these controls confound this result.

Where Mms6 and MmsF were used a protein-staining band was seen to increase in intensity under SDS-PAGE as magnetite concentration in the sample was increased. In the samples with the most intense protein-staining SDS-PAGE bands, the section of gel at this size was excised and submitted for analysis by tryptic peptide mass spectrometry. This established the presence of Mms6 and MmsF in these pull down experiments (Figure 3.12B).

A



B

Plasmid	Protein Identified	MASCOT ID	Peptides
pQE80L	IscR	P0AGK8	GPGGGYLLGK
pQEmms6	Mms6	V6F5K9	AGAAPAAAQGAGTK
pQEmmsF	MmsF	A4U547	LPVVSWVADR, LPVVSWVADRI, DDEFVYFHAK

Figure 3.12 Both Mms6 and MmsF can be isolated in a magnetite pull down assay

A, Magnetite-associated fractions from magnetite pull down assays, obtained from lysates of MG1655 cultures containing the empty vector pQE80L, pQEC1R7, which over produces the *Salmonella typhimurium* protein TlpA, pQEmms6 or pQEmmsF. These lysates were subjected to the method delineated in Figure 3.11 and then analysed by SDS-PAGE on 18% (w/v) polyacrylamide gels stained using Instant blue (Expedeon).

B, Bands from experiments using plasmids, pQE80L, pQEmmsF and pQEmms6 were excised and analysed by tryptic peptide mass spectrometry by the Fingerprints Proteomics facility at University of Dundee. The proteins identified in each case are shown along with the database identifiers for the protein and the specific peptide hit.

3.2.5.Examination of Mms6 producing cells by TEM

Since Mms6 producing cells had increased retention in the magnetite retention assay where no exogenous magnetic material was supplied (Figure 3.9), it was hypothesised that they may be producing some magnetic material *de novo*. Given the propensity for Mms6 to produce MNPs as shown many times *in vitro*^{181,192,234,248,249}, TEM was performed on MG1655 cells containing pQEmms6 induced with 1 mM IPTG. Figure 3.13 shows the resultant micrographs and, under these conditions, no recognisable nanoparticles or any extra electron dense regions could be observed. Note however, that the electron microscopy did show that cells became coccoid in shape and displayed unusual ‘bubbles’, which could be invaginations of the inner membrane.

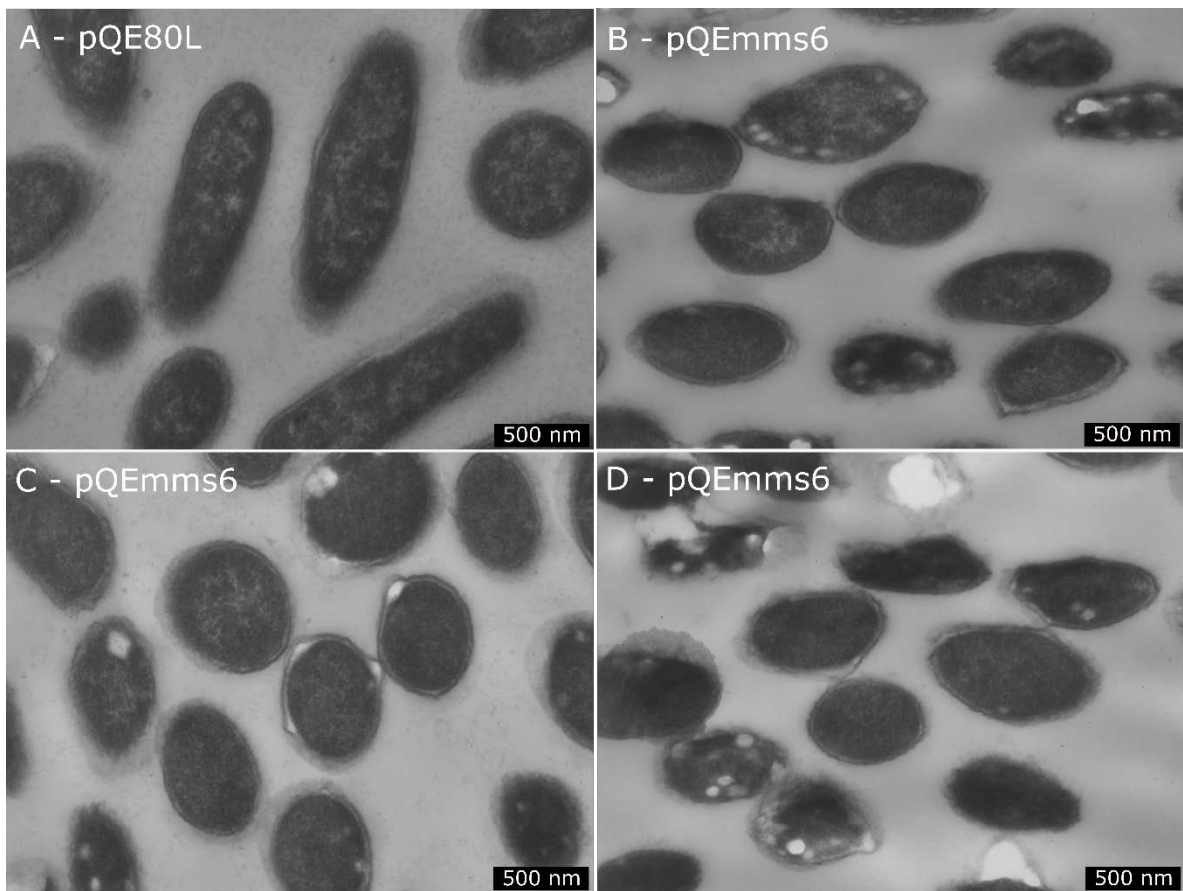


Figure 3.13 Cells producing Mms6 change shape and exhibit unusual intracellular structures.

E. coli MG1655 cells were transformed with the plasmids pQE80L (A) or pQEmms6 (B, C, D) and single colonies cultivated overnight in 5 mL LB medium with 120 µg/mL ampicillin and 1 mM IPTG overnight at 37 °C. Cells were then washed in PBS and fixed using glutaraldehyde buffer. Staining and sectioning of these was then carried out by Dr Alan Prescott at School of Life Sciences, Dundee University, and imaged on a JEOL JEM-2200FS transmission electron microscope.

The micrographs of Figure 3.13 were analysed using imageJ, which allowed the measurement of the lengths of every individual cell. Since orientation of cells cannot be accurately determined from a transmission electron micrograph (*i.e.* whether the section crosses a cell along the polar axis or across the mid-cell or somewhere in between these), the longest straight line of every cell in the field of view was measured in each image and plotted as a box plot. This showed a significant decrease in the average cell length upon production of Mms6 (Figure 3.14). Additionally, the diameters of all of the bubble-like structures were measured and found to be between 22 and 117 nm with the median value being around 61 nm (Figure 3.14).

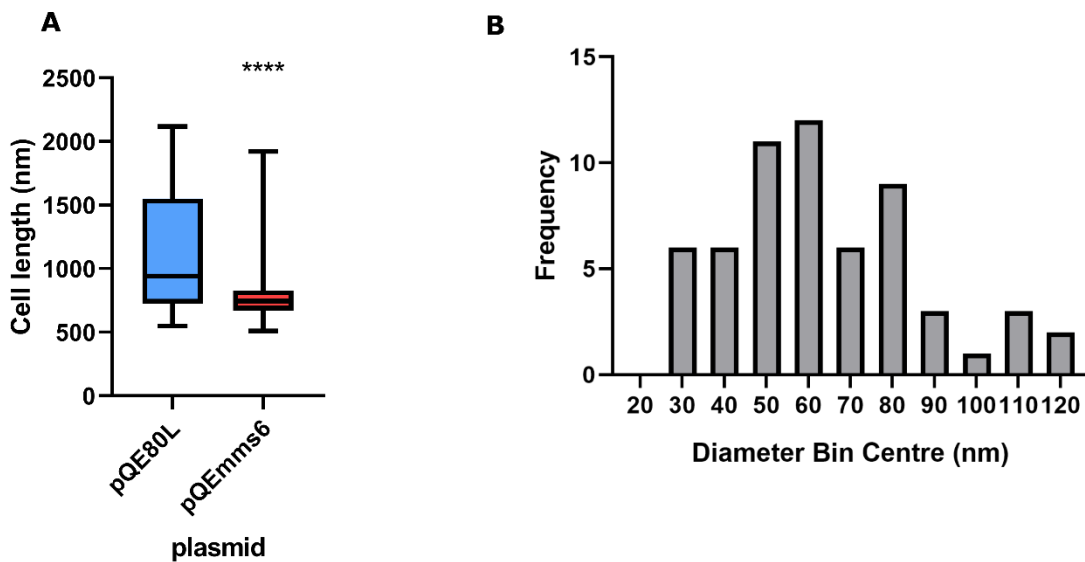


Figure 3.14 Cells shape changes significantly upon production of Mms6

A) Using images obtained by TEM as represented in Figure 3.13, the longest length of each cell that was entirely visible in the frame of the image was measured using the “Measure” tool in imageJ, n = 51 for pQE80L containing cells and n = 69 for pQEmms6 containing cells. The data were then plotted in boxplots and Mann-Whitney T-test performed indicating $p < 0.0001$. Cells containing pQE80L (control) shown in blue and pQEmms6 in red. **B)** Diameter of bubble/vesicle-like structures seen by TEM in Figure 3.3 were measured using the imageJ “Measure” tool and plotted in a histogram, n = 59.

3.2.6.Design and Characterisation of Magnetite Importers

The experimental work carried out in this thesis (Figures, 3.9, 3.10, and 3.12), and elsewhere^{181,192,248,249}, suggest Mms6 appears to be capable of producing magnetic material, however the nature of this material is as yet undescribed. TEM analyses have not indicated the presence of any MNPs in cells producing this protein (Figure 13). Additionally, Mms6 and MmsF appear to have MNP interacting properties (Figure 3.4, 3.12), however the cellular location of this activity is likely localised to the inner membrane and/or the periplasm. In the design set forth in Section 1.5.3, cytoplasmic thermosensitive proteins are anticipated to respond to a magnetically-stimulated hyperthermic signal. Producing or localising MNPs at the periplasmic or membrane-anchored level may not be useful for precisely activating proteins that are located in the cytoplasm. To overcome this, the magnetite interacting properties of Mms6 seen in Figure 3.12, and other proteins^{238,250}, could be exploited to engineer a synthetic magnetite importer protein.

In order to generate a synthetic MNP importer, the holin protein ChiW was chosen as a chassis membrane pore. As shown in Figure 3.16, the *Serratia marcescens* ChiW protein has a periplasmic and a cytoplasmic loop region, hereafter ‘p-loop’ and ‘c-motif’, respectively. These regions could be engineered to include motifs with demonstrated magnetite interacting properties, with the ultimate aim of driving the transport of magnetite through the inner membrane.

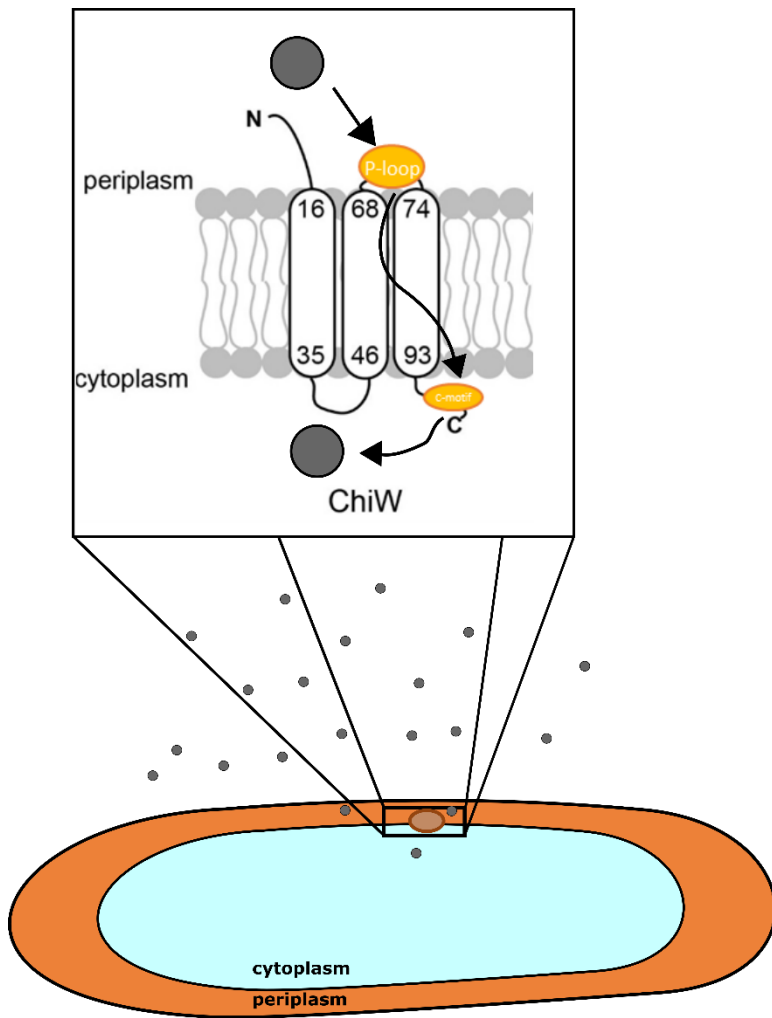


Figure 3.15 Designing a putative magnetite importer using the holin protein ChiW.

S. marcescens ChiW is an inner membrane protein that is predicted to form a homomultimeric pore. It has three transmembrane helices (amino acids 16-36, 46-68 and 74-93) producing a periplasmic loop region ('p-loop') and a cytoplasmic C-terminus ('c-motif'). By introducing magnetite interacting amino acid sequences to the native ChiW protein at the p-loop and c-motif regions it is hypothesised that MNPs may be driven across the inner membrane from the periplasm to the cytoplasm.

Three amino acid sequences have been reported to be involved in magnetite interactions (Table 3.1). One of these sequences is from Mms6, which has been indicated in a number of studies to be capable of *in vitro* MNP synthesis and interaction²³⁴. Another of these sequences was from the magnetosome membrane protein MamI, which was previously used to decorate *E. coli* flagella with MNPs²³⁸. The third of these sequences comes from a magnetite interacting adhiron²⁵⁰. Adhirs are proteins from bacteriophages that contribute to surface adhesion and host cell recognition. They have a well-defined region that is frequently modified to produce proteins and phages that recognise novel substrates or molecules. Rawlings *et al*²⁵⁰ used phage display to evolve a novel adhiron with this region iteratively modified to produce a novel protein that interacts with magnetite. These three amino acid sequences were codified here with the identifiers ‘6’, ‘M’ and ‘I’, as detailed in Table 3.1.

Table 3.1 Amino acid sequences implicated in protein interactions with magnetite

Protein origin	of Sequence	Code	Reference
Mms6	SDEEVE	6	181,234
MamI	WWWSVTEFLRG	M	238
MIA	QKFVPKSTN	I	250

A library of 15 variants of ChiW was produced by inverse PCR. In this method, 5' phosphorylated primers are designed which amplify an entire plasmid using a blunt ended polymerase. In this case Q5 DNA polymerase was used as it has reduced error rate²⁵¹. Two sets of primers were used, one which contained 3' targeting sequences for the ChiW p-loop and one with 3' targeting sequences for the c-motif. Therein, primer pairs contained 5' regions that incorporated the DNA sequences encoding the amino acid sequences delineated in Table 3.1.

First, it was necessary to quantify the magnetic retention of native ChiW producing cells under increasing magnetite concentrations to ensure that any increases in magnetite retention was ascribed solely to the insertion modifications made. The results of this experiment are seen in Figure 3.16.

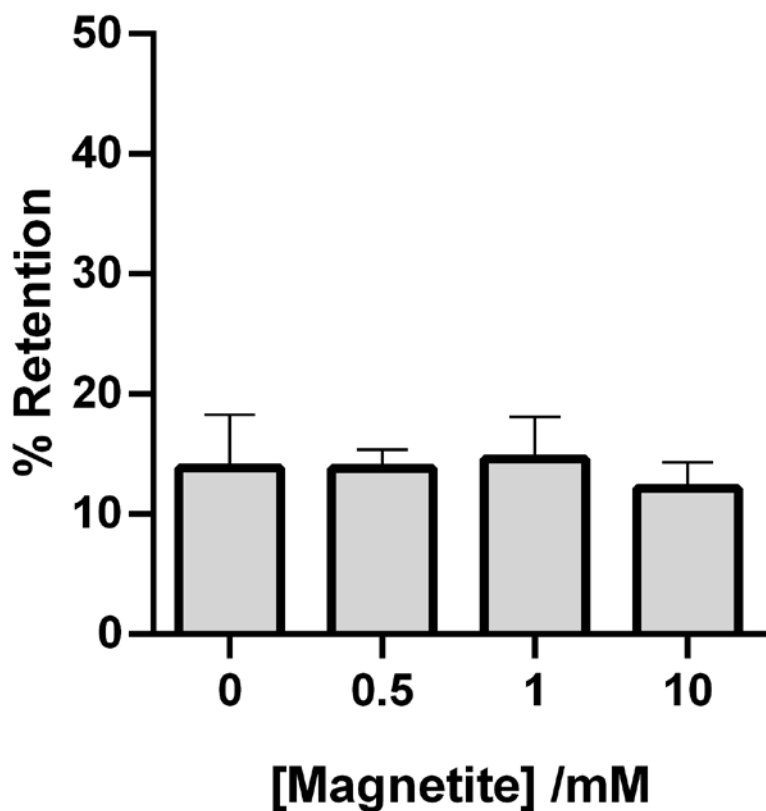


Figure 3.16 Cells producing native ChiW are poorly retained on a magnetic column

E. coli strain C43 was transformed with the plasmid pBAD18ChiWhis and single colonies were cultured overnight at 37 °C in 5 mL LB with 0.2 % (w/v) glucose, followed by culturing in 25 mL LB with 0.05 % (w/v) arabinose for induction to an OD₆₀₀ of 0.3 with magnetite added at concentrations of 0, 0.5, 1 and 10 mM. Cells were then washed in PBS and adjusted to an estimated cell concentration of 2×10^8 cells per mL and applied to an LD column as in the method set forth in figure 3.5. Cells in each fraction were counted using images obtained with a light microscope at 60 × magnification and particle analysis tools in imageJ. Error bars represent the standard deviation of three biological replicates.

The magnetite concentration to be used in library characterisation was set at 1 mM as this was judged to produce no effect on the cells magnetic retention phenotype when producing ChiW. Next, the library of 15 engineered ChiW variants was then characterised with the magnetic retention assay upon 0.05 % (w/v) arabinose induction and 1 mM magnetite, grown to an OD₆₀₀ of 0.3 in LB medium, with controls performed in the absence of magnetite, shown in Figure 3.17. A cut-off value of 15 % retention was set as the lower threshold for a positive interaction as this was the maximum value seen in negative controls using native ChiW production (Figure 3.17).

ChiW library MRAs

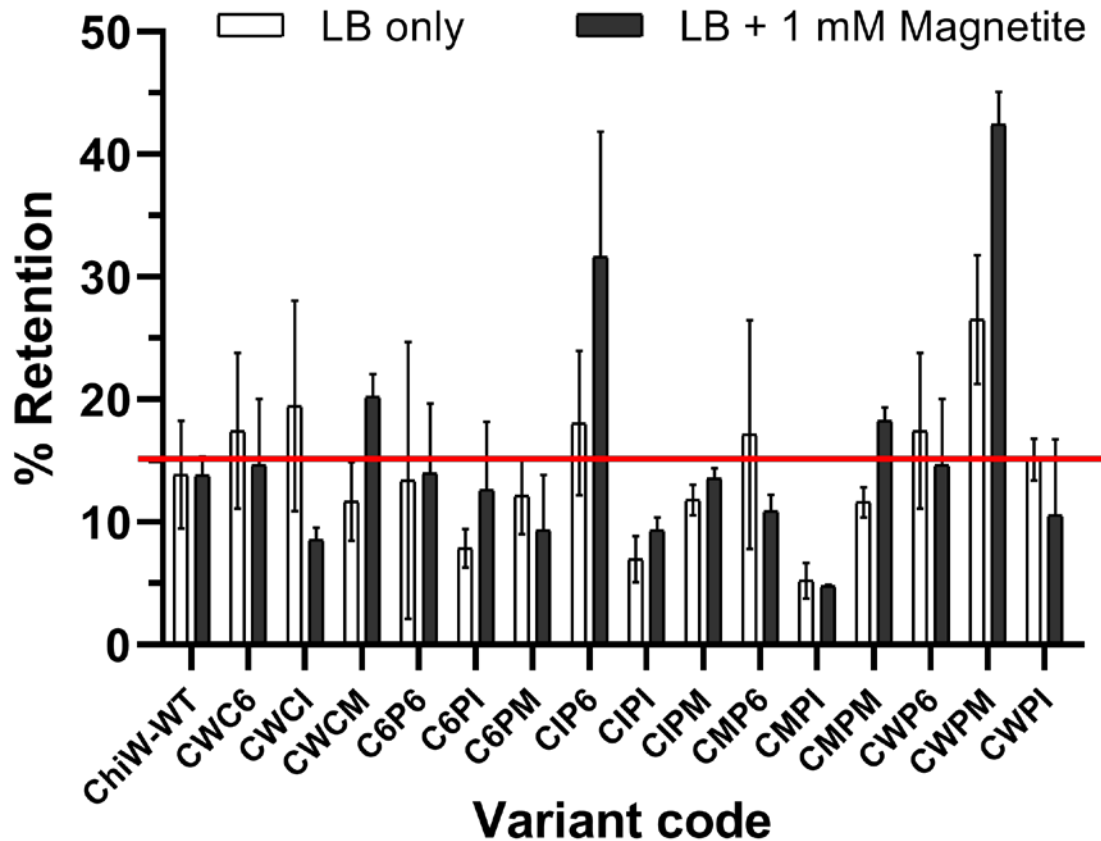


Figure 3.17 Identification of engineered ChiW variant proteins with increased magnetic retention behaviour

C43 *E. coli* cells were transformed with plasmids belonging to the library of *chiW* mutants. Single colonies were cultured in 5 mL LB cultures with 0.2 % (w/v) glucose for repression then subsequently subcultured in 25 mL LB with 0.05 % (w/v) arabinose to an OD₆₀₀ of 0.3 then washed in PBS and adjusted to an estimated cell concentration of 2 × 10⁸ cells per mL in PBS before being applied to an LD column and treated according to the method set forth in Figure 3.5. Cells in each fraction were counted using images obtained with a light microscope at 60 × magnification and particle analysis tools in imageJ. A threshold of 15 % retention marked with a red line was set as the minimum for forward consideration with this being greater upon addition of magnetite. Variants are designated here by the amino acid sequence code added, where C6- indicates the Mms6 sequence (as in table 3.1) was added as the c-motif and nothing at the p-loop, and C6P6 indicates that this sequence was added at both locations. Error bars represent the standard deviation of three biological replicates.

The ChiW variants bearing the code CWPM, CWCM, CMPM and CIP6 were all deemed to be “hits” in this screen given they exceeded the 15 % retention threshold (Figure 3.17). CWPM encodes a ChiW variant with the MamI sequence from Table 3.1 at the p-loop, CWCM encodes a ChiW variant with the same motif at the c-motif, and CMPM encodes a ChiW with this sequence at both the p-loop and the c-motif. CIP6 is a ChiW variant with the MIA motif at the c-motif and the Mms6 sequence at the p-loop.

Variants CWPM and CIP6 were examined by transmission electron microscopy as these had the greatest percentage retention of all variants tested. To do this, cells producing CWPM and CIP6 were grown identically as for the MRA; from 5 mL pre-cultures in LB with 0.3 % (w/v) glucose and then cultured in 25 mL LB and grown at 37 °C with orbital shaking at 200 rpm alongside 1 mM magnetite and 0.05 % (w/v) arabinose to an OD₆₀₀ of 0.3. Finally, 200 µL cells were added to 800 µL of glutaraldehyde fixing buffer and incubated at room temperature until sectioning. In this case, sectioning and staining was carried out by Dr Kathryn White at Electron Microscopy Research Services, Newcastle University. Sections were imaged on a Hitachi HT7800 TEM at 100 kV, shown in Figure 3.18.

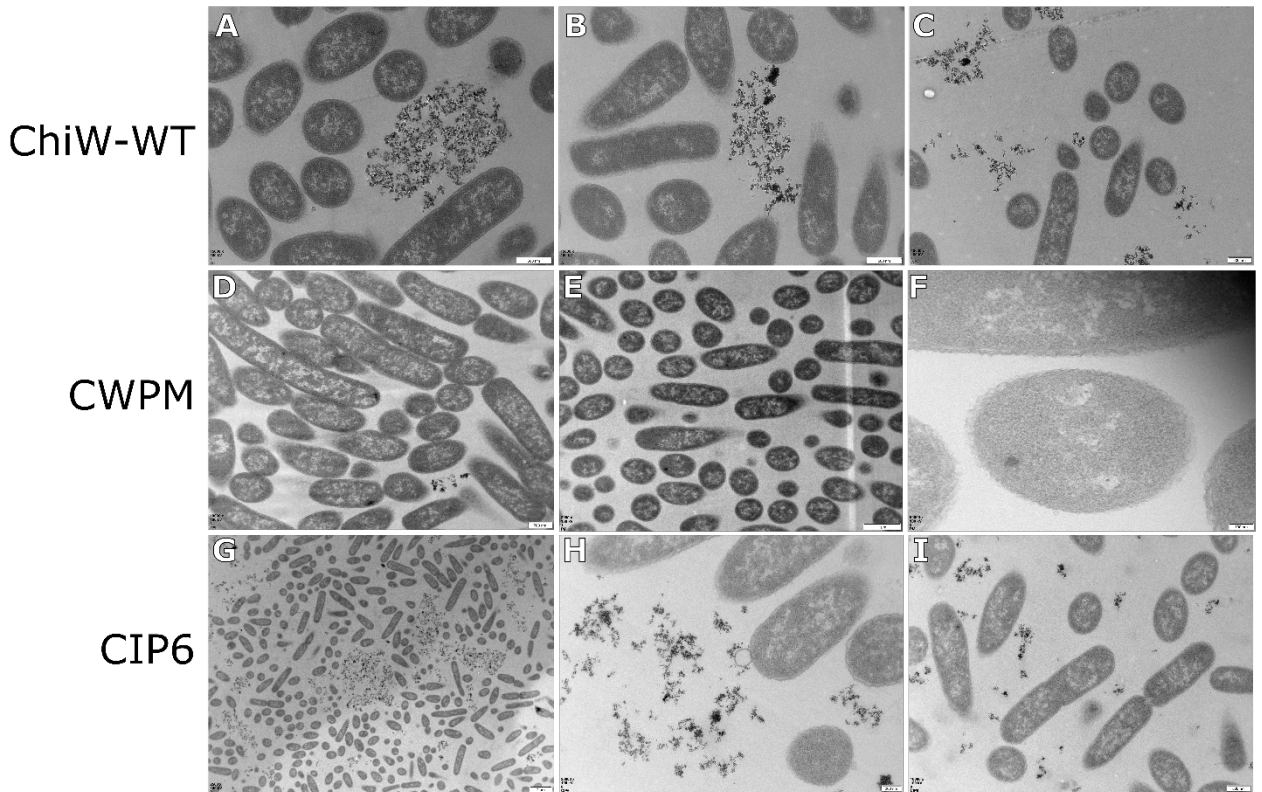


Figure 3.18 Extracellular magnetite nanoparticles are sparse in CWPM expressing cells

E. coli C43 cells that had been transformed with plasmids pBAD18knChiWhis, pCWPM or pCIP6 were grown with 0.05% (w/v) arabinose and 1 mM magnetite and fixed in glutaraldehyde fixing buffer. The sections produced were imaged using a Hitachi HT7800 TEM at 100 kV. A-C represent ChiW-WT, where scale bars indicate 500 nm, D-F represent the CWPM ChiW variant bearing the MamI amino acid sequence in the p-loop with scale bars indicative of 500 nm (D), 1 µm (E), and 100 nm (F), and G-I represent the CIP6 ChiW variant with the magnetite interacting adhiron amino acid sequence in the c-motif and the Mms6 region in the p-loop with scale bars representing 2 µm (G), 200 nm (H), and 500 nm (I).

3.3.Discussion

3.3.1.Mms6 production can produce magnetic phenotypes in *E. coli*

Heterologous production of Mms6 leads to an increase in magnetic retention of *E. coli* MG1655 regardless of the presence of exogenous magnetite (Figure 3.9). This agrees with previous *in vitro* studies on Mms6 where the purified protein has shown to be able to promote the homogenisation of MNP morphology and size, and where its heterologous expression in mammalian systems has produced Fe deposits and areas that are more magnetically responsive in atomic force microscopy^{192,195,252}. No MNPs were evident however in TEM analysis of Mms6 producing cells (Figure 3.13).

Figure 3.4 indicates that Mms6 within the membrane is capable of interacting with magnetite that is initially added extracellularly. This indicates that the MNPs added are also then capable of crossing the outer membrane. There is no evidence to suggest that *E. coli* possesses any outer membrane transporters that can transport MNPs, however, given the size range of the MNPs used in these experiments expressed in Figure 3.3, it is not outrageous to suspect that they could enter the periplasm by passive mechanisms. The outer membrane is a dynamic structure that is composed of peptidoglycan, phospholipid and lipopolysaccharides that in actively growing cells is constantly under breakdown and remanufacture as cells grow and divide. This presents the potential for pores to form in the outer membrane as it is remodelled and cells are dividing. Additionally, work on sacci, preparations of intact peptidoglycan sheaths from bacteria, has demonstrated that proteins of up to 25 kDa in size are capable of crossing the peptidoglycan layer, with the authors going so far as to posit that this size range is likely to even go as far as 50 kDa²⁵³. This size range is compatible with the sizes of nanoparticle used in these experiments (Figure 3.3), so it may be possible for individual MNPs to cross the PG layer. Together it may be possible for these MNPs to enter the periplasm, however it does require coalescence of an array of divergent and rare events.

Other investigators have designed a synthetic enzyme called FLPM6A using a *Rhodospirulum rubrum* ferroxidase fused with the C-terminal proposed magnetite precipitating region from Mms6¹⁹⁷. This produced similar phenotypes in *E. coli* to what full length Mms6 expression did in this study. Cells were retained in a similar magnetic retention assay and were attracted to a magnet. Moreover, and importantly in the context of this project, they could also be heated using oscillating electromagnetic fields¹⁹⁷. However, superconducting quantum interferometry device (SQUID) interrogation of these cells did not indicate any ferrimagnetism as would be expected of MNPs, instead characterising the cells

as only paramagnetic. The strong magnetic phenotype of these cells was thus described as “ultraparamagnetic”, a term not used previously in any formal description of a magnetic property. “Ultraparamagnetism” was then explained as oxidation and chelation of Fe in the cell *en masse*¹⁹⁷. The authors of this work have not displayed any TEM characterisation of cells expressing FLP6A, so it is not possible to describe what physical nature the Fe took in this case, *i.e.* confirm it is not in the form of NPs. This could help to describe the phenotype produced by Mms6 expression. In this case, expressing full length Mms6 does not appear to be producing MNPs however produces significantly increased magnetic properties compared to empty vector expressing cells. It may also be true that the magnetic phenotype produced upon expression of full length Mms6 could be described as “ultraparamagnetism”, however this will need to be vindicated by SQUID or other magnetic analyses.

Mms6 may then be producing Fe in a similar form to that which FLP6A produces. The common factor here is the region at the C terminus of Mms6. This has a small region of acidic and negatively charged amino acids SDEEVE. This has been described several of studies now^{181,234,254,255} and used to describe the unusual Fe responsive phenotypes of Mms6²³⁵. This study does not produce any data that explains how this region can mechanistically produce MNPs however the development of the magnetic phenotype observed here does corroborate these findings.

Other experimentation here (Figure 3.10) indicate that the Mms6 phenotype is dependent on Fe, which also aligns with the “ultraparamagnetic” phenotype produced with FLP6A¹⁹⁷. Work should be done to more rigorously test this hypothesis, however, as it was observed that cells could not grow to a ‘normal’ OD₆₀₀ in the Chelex treated LB. This adds a confounding factor that may contribute to the lack of phenotype under these conditions. In future, this experiment should be performed in a defined media where Fe can be titrated in to avoid any toxicity caused by its absence.

Both Mms6 and MmsF have a capability to self-assemble in to proteinosomes^{185,256,257}. This may help to describe the size control of MNP precipitation seen in *in vitro* experiments, where the proteins may homo-oligomerise around nascent MNPs. The homo-oligomerisation of Mms6 may go some way to explaining the ‘bubbles’ seen in TEM of Mms6 producing cells. These may be caused by oligo- or multimerisation of Mms6 at the membrane surface. This has not been observed in mammalian expression of Mms6 where TEM was performed, however the cellular environment presented by *E. coli* expression is more like that of the native environment experienced by Mms6 in MTB. Confocal laser scanning microscopy or total internal reflection microscopy may be useful tools to examine this property of Mms6. A GFP tagged version of the protein could be examined during heterologous

expression. This has indeed been performed previously in a native organism²⁵⁸. In *Magnetospirulum magneticum*, GFP tagged Mms6 was shown to change from diffuse localisation throughout the cell to foci along the central polar axis likely correlating to magnetosomes when conditions were changed from aerobic to microaerobic²⁵⁹. This was not observed dynamically in single cells however so it is not possible to conclude that individual proteins can move in this way or it is caused by a change in trafficking contributed to by other proteins upon Mms6 translation.

3.3.2. MmsF may interact with MNPs but does not produce magnetic material de novo

MmsF has previously been demonstrated to have similar properties to Mms6 in MNP morphology homogenisation, however phenotypes in heterologous expression studies have not been published. Interestingly, affinity of MmsF for magnetite was indicated in pull down experiments, however it did not produce any phenotype upon heterologous expression alone in magnetic retention assays. This disparity indicates a capability in this expression system for Mms6 to produce magnetic material *de novo* but not MmsF.

Mms6 has a single transmembrane region with its C terminus oriented towards the periplasm. MmsF, through different predictions, has either one or two transmembrane helices, with the C terminus either in the cytoplasm or periplasm. Alignment of Mms6 and MmsF indicate that MmsF bears a similar sequence to the SDEEVE region of Mms6, Figure 3.19. Indeed, if all 15 of the proteins indicated by the most recent reviews of magnetosome biogenesis to be direct contributors to MNP nucleation and growth are aligned, a small region containing aspartate and glutamate residues is found at the C terminus of seven of these, Figure 3.19. This presents an avenue of investigation to explain the contribution of each of these proteins to the chemical pathway of MNP formation in magnetosomes.

MamM	REIGDTTKPSFSDQPLSFDEVMLSKVDN-	318
MamR	RILGSNLVE-YMNR-	79
MamO	IA--NSSVLVFWASVAGSVVAFIHGGSTGLIHWEAPVTALVMIPGAYVG-GILGARLMR	606
MamI	-	69
MamE	RL--DAA---IKAATAAGQQILLKVHRNGQEFWI-----VL	772
MamN	-----PE-----LASAAAAGLOFTH-----REYVRWGLPLMGIFLVLSVTYIA-VLAG-----	437
MamC	LR--HGK-----SAEAT-----SDEDILR-----EELA-----	125
MamD	-----GA-----PD-----SDDALLA-----AVGEE-----	314
Mms6	-----IE-----AAASDEEVEL-----RDALS-----	144
Mms5	-----AE-----PA-----AEAV-----	215
MamS	-----NAE-----LYAKSVLIGGRTCKL-----DDEGLALWMTVQ-----	180
MmsF	-----LLVD-----DDEFVYF-----IAKQGLVIWMWGVLAFLFALHVPVLGKWIFGFSSMG-----	77
MamF	-----LLMS-----DDEVVYF-----IAKQGLVLWMMWSILAMFALHLPGIGKWLFGFSSMG	81

MamM	-	318
MamR	-	79
MamO	VLPVRVULKGIYAAATMAAIAIKMLTTV-	632
MamI	-	69
MamE	-	772
MamN	-	437
MamC	-	125
MamD	-	314
Mms6	-	144
Mms5	-	215
MamS	-	180
MmsF	VLVF\$LLGLVS\$WFQRAWKLPVVS\$WADRI	107
MamF	VLMLS\$WGLVSVALRRTWRLPLISHWALI	111

Figure 3.19 Proteins predicted to be direct contributors to MNP precipitation.

Amino acid sequences corresponding to Mms6, MmsF, Mms5, MamC, MamD, MamE, MamM, MamO, MamS, MamR, MmN, MamF and MamI from *Magnetospirulum gryphiswaldense* MSR-1 were downloaded from KEGG²⁴² and added to a new fasta file. The sequences were then aligned using the ClustalOMEGA server. Results shown indicate the region at the C terminus of the alignment, with a red box around the aligned region of acidic residues.

In other studies MmsF has been demonstrated to be capable of homogenising the geometry and size of MNPs produced in *in vitro* experiments with similar effects to Mms6 has¹⁸⁵. It is possible that the acidic and negatively charged amino acids are partly responsible for this in each protein, and possibly explains the *de novo* magnetic material synthesis indicated by Mms6. However, this was not reflected in MmsF, despite the presence of this similar region. There are two possible explanations for this.

The RDDEFV sequence in MmsF may well be responsible for the observed MNP interactions seen in *in vitro* experiments. *In vivo* studies however do not seem to reflect this. The difference may be the localisation of the motif. Some structural predictions of MmsF²⁵⁵ and other *in silico* work conflict about the membrane topology of MmsF. Using the amino acid sequence for MmsF from *M. gryphiswaldense* provided by KEGG²⁴², *in silico* membrane topology prediction was performed using the OCTOPUS²⁶⁰ and TMHMM²⁶¹ algorithms. This predicted that the RDDEFV motif of MmsF should lie in the cytoplasm, where other published work has predicted that this should lie in the periplasmic region²³⁶. Should the cytoplasmic hypothesis be correct, this may inhibit its interaction properly with Fe since cytoplasmic Fe is rapidly stored in ferritins upon uptake. The cytoplasm is also an oxidising environment, which does not reflect the reducing environment in the periplasm where the Mms6 motif would lie, and also that which is the site of MNP precipitation in MTBs.

The MNP precipitating properties of MmsF and the RDDEFV sequence should be probed. This could be investigated by replacing the SDEEVE region of Mms6 with the RDDEFV region of MmsF and comparing this to an AAAAA substitution in the same location and full length Mms6 in magnetic retention assays. This would also allow interrogation of the SDEEVE region of Mms6 and its contribution to the magnetic phenotype produced upon Mms6 expression.

Alternatively, both Mms6 and MmsF in these experiments (Figure 3.12) were N terminally His-tagged. This may also confound the observation the Mms6 and MmsF interact with magnetite, where the interaction may be determined only by the His-tag. These experiments should be repeated with protein which lacks a His-tag in order to determine if this is true.

3.3.3.CWPM may import MNPs

In characterisation of the library of ChiW variants by MRA, the only common feature among magnetic hits was the presence of the magnetite interaction sequence from MamI. This sequence did not have an aligned acidic or negatively charged region in alignments in Figure 3.20, however it has the strongest track record for magnetite interaction in protein engineering approaches seen as yet. The Mms6 derived sequence and the magnetite interacting adhiron derived sequence only contributed to an increase in

retention in the MRA when they were each included together in the CIP6 configuration, and only this one. This may be due to limitations in the properties of the adhiron sequence (coded I) at periplasmic locations and the preferred location of the Mms6 sequence (coded 6) at the periplasmic location. Additionally, there is a very large standard deviation in these experiments using the CIP6 allele demonstrating a large degree of variation in the data.

CWPM was the best in initial characterisation, and in TEM there were few extracellular MNPs observed. It was possible, in some cases, to identify what might be intracellular MNPs. This needs better characterisation, including controls with no MNPs, and attempts to observe MNP uptake in sphaeroplasts or synthetic vesicles.

The CWPM fusion produced cells that were the most retained upon magnetite addition in MRAs for the initial screen of the ChiW library (Figure 3.18). Upon further characterisation by TEM (Figure 3.19), cells expressing this fusion were incubated with arabinose induction and 1 mM magnetite, fewer MNPs were seen in the extracellular milieu around cells (Figure 3.19D, E, F) and in some cases, what might be described as MNPs were visible inside cells (Figure 3.19, D, F). Techniques such as XRD or SAED could be applied in imaging of these grids to examine the putative MNPs with greater resolution. These would be able to indicate if these bodies are crystalline (using XRD) and what atoms make them up (using SAED).

Alternatively, if CWPM could be purified and examined in synthetic vesicles or sphaeroplasts, MNP uptake may be possible to observe. These experiments would reduce some of the electronic background produced by cell cytoplasmic material in images to make imported MNPs easier to discern.

3.3.4..... but MNP import defeats the purpose of this project

Holins are widely considered to be toxic proteins since they have evolved to form pores in the inner membrane of bacterial cells to facilitate lysis for bacteriophage proliferation²⁶². While the conditions used in these experiments are based on previous work that allowed stable expression of ChiW, that being in the absence of its substrate ChiX^{263,264}, the possibility cannot be ignored that the modifications introduced have potentiated the ability of ChiW to form multimeric pores. The addition of acidic residues may have contributed to an increase in hydrophilic properties of specific regions of the protein. It is these hydrophilic regions which face the interior of the pore formed by holin multimers and increasing hydrophilicity may contribute to the threshold for pore formation from these variants²⁶².

The model for holin pore formation is based on multimerisation of the protein in the inner membrane in to “rafts” up to a critical point at which point the rafts produce a hole in the lipid bilayer^{262,265}. This presents the complication of how perhaps this strategy may not even be tenable. Stable expression of ChiW relies upon it causing minimal toxicity, and thus minimal pore formation, *i.e.* the protein is expressed in the inner membrane but very few or zero pores are formed. In the case of ChiW, ring-like structures may be produced by its multimerisation in the inner membrane, but open pores are only likely produced in the presence of its substrate, the endopeptidase ChiZ^{263,264}. In this case, the potential for MNPs to cross the inner membrane *via* a ChiW produced pore is reduced. For this reason, ChiW engineering may not be an effective strategy for producing novel substrate importers.

The field of biomineratisation has a number of theories that describe the interface between biomineralling proteins and the crystal structures that they interact with. One significant school of thought posits that the structure of peptide must cradle the crystal structure it interacts with in order to facilitate that interaction, however more recently contrasting hypotheses have been brought forward from observations of inherently disordered proteins and peptides in interactions with their partner minerals. By studying hydroxyapatite mineralising proteins *in vitro* the flexible polyelectrolyte model has been produced²⁶⁶. This states that electrostatic bonds and interactions between amino acids in protein primary structures and the protein’s partner biominerals are what govern their interaction moreso than other effects that are brought about by secondary or tertiary protein structures.

Recently, proteins from MTBs that contribute to MNP crystallisation have been shown to bear this disordered property in certain regions, including Mms6.²⁵⁵ It is possible that the expression of the MNP interacting region exogenously within the ChiW structure “forced” a kind of order in to the structure formed by the region and prevented it from working. Holins like ChiW do not have a disordered structure like that seen in Mms6 and the disordered nature of this protein might not be effectively carried forward when it is incorporated in to another more highly ordered structure. Additionally, the data in this study involving Mms6 and other published studies on Mms6 have facilitated the cooperative action of many Mms6 proteins. This may also contribute to the properties of this protein, especially given its propensity to form micelles or proteinosomes²⁵⁷. This should be the subject of future investigation in to Mms6 and other magnetite crystallising proteins.

Initially, one aim of this Chapter was to develop a strategy to import MNPs in to the cell. A better way to do this might be by using cell penetrating peptides conjugated to magnetite. These have been developed for drug delivery in mammalian systems, and as antimicrobials in bacterial contexts. There

are examples of cell penetrating peptides that are capable of entering the cytoplasm from outside the cell without affecting membrane stability, but interfering with DNA and RNA at a cytoplasmic level^{267,268}. Cell penetrating peptides with these properties could be conjugated to MNPs and used as a mechanism to force MNPs in to the cytoplasm of bacteria. This strategy overall however does not allow MNPs to be utilised at a level that is genetically encoded, maintaining the necessity for continual repurchase of additional materials in the form of MNPs.

3.3.5. Identification of Genes for Magnetic “Aerial” Production

The production of MNPs *de novo* by Mms6 or MmsF has not been demonstrated, however Mms6 can produce magnetic properties at least at the level of entire cells, and each of these proteins appears to have some affinity for exogenously produced MNPs. In relation to the greater aims of this project, this may be of some use. Upon closer interrogation of the SDEEVE and RDDEFV regions of Mms6 and MmsF, it may be possible to attach these to target proteins and allow specific MNP – protein conjugation, provided adequate mechanisms for getting MNPs inside the cell.

The work that produced the *mftN* allele also demonstrated that expression of this allele produced electron dense nanoparticles visible by TEM. Experimentation here has replicated the magnetic retention phenotype produced in the original work, the observation of NPs should also be probed. Purification of NPs using strong magnetic forces would be a novel way to characterise their production and their magnetic properties. Should these prove to be magnetic, the MftN protein would prove invaluable for aerial formation.

Meister¹⁰⁴ has commented on the physical limits of magnetism that could occur within ferritins and how this is likely minimal, so the structure and characteristics of these MNPs would also be interesting from this perspective. The susceptibility of Mms6 expressing cells to magnetic hyperthermia should be investigated. By encoding a reporter that responds to temperature in to cells also expressing Mms6 this could be performed. Investigations in instigating synthetic magnetoreception in mammalian systems have employed either exogenous magnetite or ferritins that are stimulated by oscillating magnetic fields. A genetically encoded magnetic aerial producer has not yet been properly investigated¹⁰⁴.

In the present study, Mms6 expression has been identified as a source of *de novo* bio-magnetism. This should be investigated for its suitability as a genetically encoded “aerial”. It remains to be explained

however what the physical source of this magnetism is, *i.e.* is it formed from a magnetic nanoparticle, as seen in mammalian expression systems^{192,249} or an “ultraparamagnetic” phenomenon?¹⁹⁷

Nonetheless this phenotype would be useful for inducing magnetic hyperthermia. The next natural step is to produce a synthetic temperature sensitive transcriptional program in *E. coli* that might be controlled using magnetic hyperthermia made possible by harnessed Mms6.

Chapter 4:
Development of Temperature Responsive Synthetic Gene Circuits

4.1. Introduction

Synthetic gene circuits have been developed in efforts to recreate electronic-type phenomena in biological systems. The best known of these, and original, is the Repressilator.⁴² The Repressilator (described in Section 1.3.2) uses three transcriptional repressors that repress each other's transcription, giving rise to a transcriptional program with oscillatory properties. The Repressilator and its contemporaries^{72,269–271} were made possible by the standardisation and characterisation of transcriptional tools that have been used widely in recombinant DNA technologies in the past. The Repressilator, for example, uses the transcriptional repressors LacI, cI and TetR alongside their respective promoters.

It could be argued that the Repressilator was not perfect, and fine-tuning of its DNA design (including adding additional redundant promoter sequences, and adding protein degradation tags) was necessary to improve it⁶³. Even after these improvements, Repressilator-type gene circuits have recently been observed to have limitations where they appear to lose their oscillations with extended experimental runs⁶³.

Characterisation and standardisation of individual genetic elements is essential to the development of synthetic biology as a field and as a technology. Widening the range of these parts with good characterisation data and standards should increase the potential for synthetic genetic circuitry. There are few examples of synthetic gene circuits with temperature responsive properties and so this ability should be explored further from this perspective.

The central aim of this project is to develop a novel regulatory system controlled by nanoparticles that can be heated by a magnetic hysteresis loop. Previous Chapters have dealt with engineering metal nanoparticles, and next we will focus on harnessing temperature-dependent transcriptional systems. Proteinaceous elements were considered primarily as it was proposed that their conjugation with magnetic nanoparticles would be easier to engineer using the amino acid sequences detailed in table 3.1, and the wider field in general would benefit from the characterisation of more temperature influenced transcriptional regulators. Heat shock elements have been effectively characterised however utilising these genetic elements may foment off-target effects leading to unpredictable and undesired metabolic burden.

4.1.1.The *Salmonella typhimurium* protein TlpA

The literature contains limited examples of transcriptional regulators that are responsive to temperature. *S. typhimurium* (a Gram-negative murine pathogen that is closely related to *E. coli*) has a protein called TlpA, which exhibits coiled coil structures that facilitate homodimer formation²⁷². TlpA also contains a DNA-binding domain that is used to repress transcription of its own promoter²⁴⁴. There is apparently no associated phenotype that results from a *tlpA* deletion in *S. typhimurium*²⁴⁵, however the biophysical properties of the protein and its interactions with itself and DNA have been well studied^{244,246,272}.

Investigators were originally interested in the protein as it had similar properties to mammalian muscle myosin protein when observed with techniques such as circular dichroism²⁷². Biochemical characterisation of the protein showed that this protein had a coiled-coil region that served as an interaction interface allowing the formation of homodimers or even multimers, where “intermediate filament-like” structures were observed by TEM²⁷³.

TlpA was described to have DNA binding properties with its own promoter region and was found to repress transcription from its own promoter^{244,245}. Later, it was discovered that this repressive property was dependent on temperature where at elevated temperatures (43-45 °C) TlpA protein accumulates in the cell, whereas a mutant with disrupted DNA binding ability accumulated to similar levels under all temperatures tested (30-45 °C). Transcriptional analysis of *tlpA* vindicated the hypothesis that this was a function of decreased transcription at lower temperatures. TlpA is therefore a transcriptional repressor at low temperatures (30 °C), but lacks this function at higher temperatures (43-45 °C)²⁴⁷. CD spectroscopy also indicated that increasing temperature causes conformational changes in TlpA²⁴⁷. In combination with DNase footprinting and EMSA experiments²⁴⁴, it was concluded that TlpA is a temperature sensitive transcriptional regulator.

The model for transcriptional repression through TlpA, is described in Figure 4.1, where dimeric TlpA protein represses transcription from the *tlpA* promoter mediated through direct interaction with this DNA region. Elevated temperature causes a change in conformation that prevents homodimer formation and thus permission of transcription of the *tlpA* promoter.

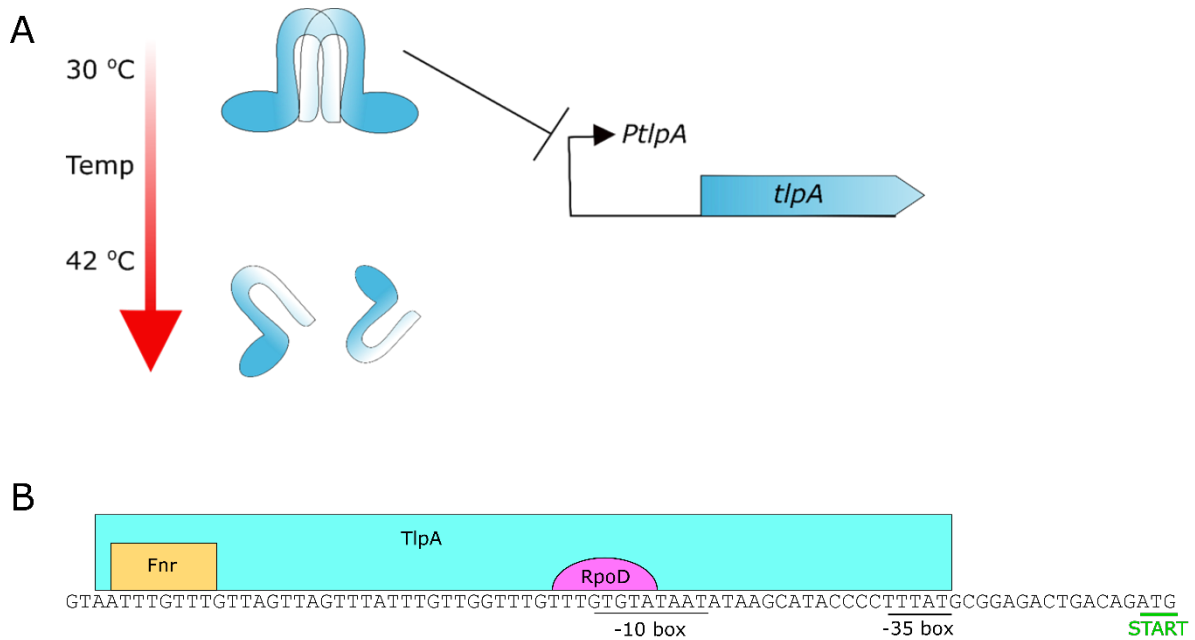


Figure 4.1 TlpA is a transcriptional repressor influenced by temperature

A, At 30 °C TlpA forms homodimers with its coiled coil regions. These then act as transcriptional repressors, repressing the *tlpA* promoter, the only identified TlpA sensitive region. At temperatures of 42 °C and above, the TlpA homodimer breaks down and the monomeric proteins are unable to repress transcription of the *tlpA* promoter. Thus the promoter is activated.

B, The *PtlpA* promoter of *S. typhimurium* contains a TlpA binding site which overlaps with binding sites for RpoD and the anaerobiosis/aerobiosis regulator protein Fnr, predicted by the BPROM algorithm²⁷⁴.

There has also been interest in the temperature influence of the TlpA coiled coils and their interactions for biotechnological applications. It has been demonstrated through these investigations that the TlpA coiled coil structure is reversibly denatured through temperature changes between 10 °C and 65 °C.²⁴⁶ By combining this property with GFP fusion to TlpA, investigators have made TlpA mediated temperature reporters that rely solely on protein structural changes with no dependence on downstream events²⁴⁶. In these experiments, the DNA binding domain of TlpA was replaced with GFP. GFP shows enhanced fluorescence as a dimer, as such temperature influenced melting of the TlpA homodimer produced relatable changes in GFP fluorescence²⁴⁶.

4.1.2.The Transcriptional Repressor MogR and its Antirepressor GmaR

Listeria monocytogenes is a Gram-positive intracellular food-borne pathogen found in cheeses and cured meats. When it enters a host cell *L. monocytogenes* engages in a transcriptional program that causes a transition from its motile state to a non-motile state¹¹⁸. This process involves repression of specific promoters controlling transcription of genes required for flagellar assembly, and it is temperature-dependent.

A protein titled Motility Gene Repressor (MogR) was identified as the first protein directly regulating the motile-to-non-motile switch in *L. monocytogenes*¹¹⁸. The *flaA* promoter of *L. monocytogenes* was shown in *lacZ* transcriptional fusion assays to be inactive at 37 °C and active at 30 °C. By deploying a pull down experiment using DNA with the sequence of the *flaA* promoter region, MogR was discovered and implicated in regulating a number of genes required for motility^{118,275}. As such, deletion of the *mogR* gene conferred a reduction in virulence in an *in vitro* murine model which was decided to be caused by over accumulation of FlaA protein in this strain¹¹⁸.

Further analysis by microarray, DNase I footprinting of the *flaA* promoter region and EMSA identified a TTTT-N₅-AAAA motif in the putative MogR binding regions that occurs twice separated by eight nucleotides. The identified motif was found to be essential for the MogR:DNA interaction²⁷⁵, however the dependence on temperature for complex formation remained elusive until the discovery of the glycosyl-transferase protein GmaR²⁷⁶.

The *gmaR* gene was discovered as a gene regulated by the response regulator DegU^{120,276}. DegU promotes *gmaR* transcription, while MogR represses it. GmaR is a glycosyl-transferase protein that

glycosylates the FlaA protein to stabilise it. EMSAs using purified MogR and GmaR indicated that GmaR was able to inhibit MogR interaction with the *flaA* promoter at 30 °C but not at 37 °C²⁷⁷. This was further examined by bacterial two hybrid experiments that revealed the influence of temperature increases on MogR:GmaR interaction. By using truncations of the protein it was established that regions between amino acids 1 – 140 of MogR and 350 – 637 of GmaR were necessary for this interaction²⁷⁷. This work has posited that GmaR is intrinsically unstable and is degraded quickly at 37 °C, while at 30 °C it is stabilised through interaction with MogR. Since DNA binding to MogR was seen to occur independently of temperature *in vitro*²⁷⁷, it remains to be seen if there is a conformational change in either of these proteins that governs the removal of GmaR from MogR or if degradation is the sole factor determining the switch, from *flaA* repression to derepression.

A model can be drawn for MogR:GmaR influenced gene expression in *L. monocytogenes* (Figure 4.2). At 30 °C, the transcriptional repressor MogR is sequestered by its antirepressor GmaR whose transcription is promoted by DegU, allowing transcriptional units whose promoters bear the MogR binding sequence TTTT-N₅-AAAA to be transcribed. At 37 °C GmaR is not present, governed either by a temperature influenced conformational change, degradation of GmaR or both, which is perpetuated by MogR dependent repression of GmaR transcription. This is described by the cartoon in Figure 4.2.

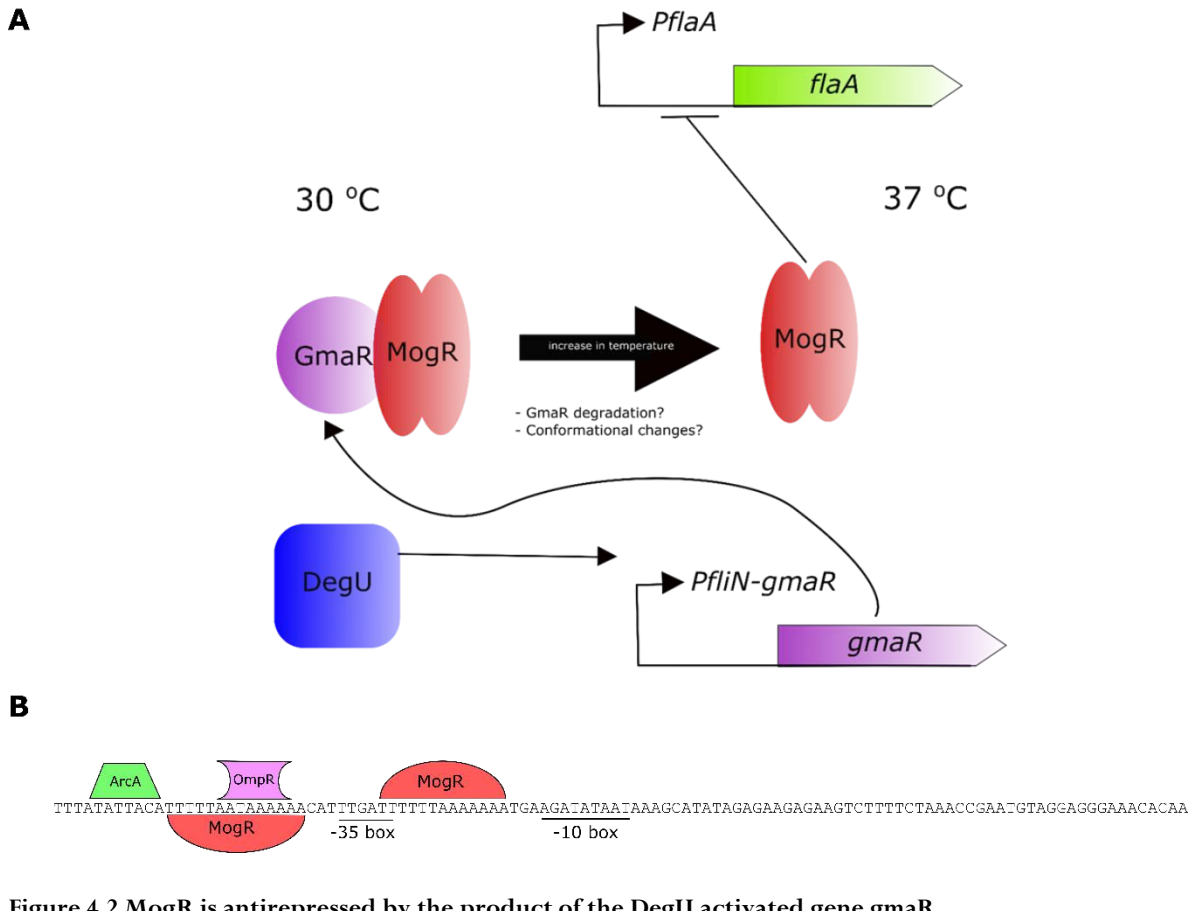


Figure 4.2 MogR is antirepressed by the product of the DegU activated gene gmaR

A, At 30 °C, the response regulator DegU activates transcription of the *gmaR* encoding locus *PflinN-gmaR*. GmaR at this temperature interacts with the transcriptional repressor, sequestering it away from DNA and the promoters it specifically repressed. At 37 °C, representing the environment inside the host, GmaR is no longer present, influenced by either GmaR degradation, conformational changes in GmaR or both. MogR is then free to repress promoters such as the *flaA* promoter or the *PflinN-gmaR* promoter. This leads to repression of genes encoding flagellar assembly and ensures GmaR is not expressed to retain the non-motile state.

B, the *PflaA* promoter has ArcA and OmpR binding sites predicted by BPROM²⁷⁴. The binding site identified for MogR overlaps with and surrounds the -35 region.

4.1.3.Aims

The aims of this Chapter were to use the TlpA and MogR:GmaR systems to produce temperature responsive transcriptional programs in *E. coli*. These will be central to the design of the magnetically stimulated genetic induction platform set out in this thesis.

4.2. Results

4.2.1. Construction of a Synthetic Gene Circuit Using TlpA

The *tlpA* gene from *Salmonella typhimurium str. ST47* was cloned using Gibson assembly in to the pQE80L background vector under the control of the T5lac promoter 5' of its multiple cloning site alongside the strong double terminator BioBrick BBa_B0015, the *tlpA* promoter region (-125-1 nt upstream of the *tlpA* start codon) from the same strain and wild type *gfpmut3b* in the architecture expressed in Figure 4.3.

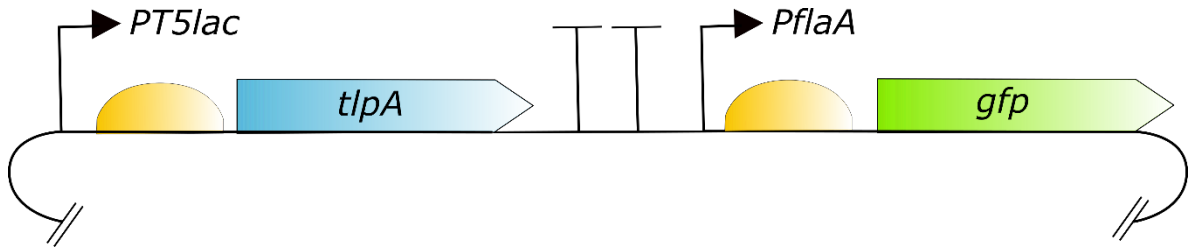


Figure 4.3 The pC1R7 plasmid encodes *tlpA*, and *gfpmut3b* under the control of the *PtlpA* promoter

The pQE80L plasmid backbone was linearised by BamHI and HindIII digestion and PCR primers designed to amplify DNA fragments encoding *tlpA*, BBa_B0015, *PtlpA* and *gfp* to sufficiently overlap for Gibson Assembly in the order displayed above. The resulting plasmid was named pC1R7 for the first circuit, and seventh replicate of colonies picked for screening.

By cloning TlpA 3' to the pQE80L BamHI site it was placed in-frame for insertion of an N-terminal hexahistidine tag. To verify that TlpA could be produced by *E. coli* alongside GFP, *E. coli* strain MG1655 cells was transformed with pC1R7 and single colonies grown overnight in 5 mL LB with 1 mM IPTG and 120 µg/mL ampicillin at 30 °C, 37 °C and 42 °C in Infors shakers with 250 rpm orbital shaking. Next, OD₆₀₀ cell density measurements were taken and suspensions were prepared with normalised amounts of cells before Western immunoblots were performed using α -His and α -GFP, presented in Figure 4.4.

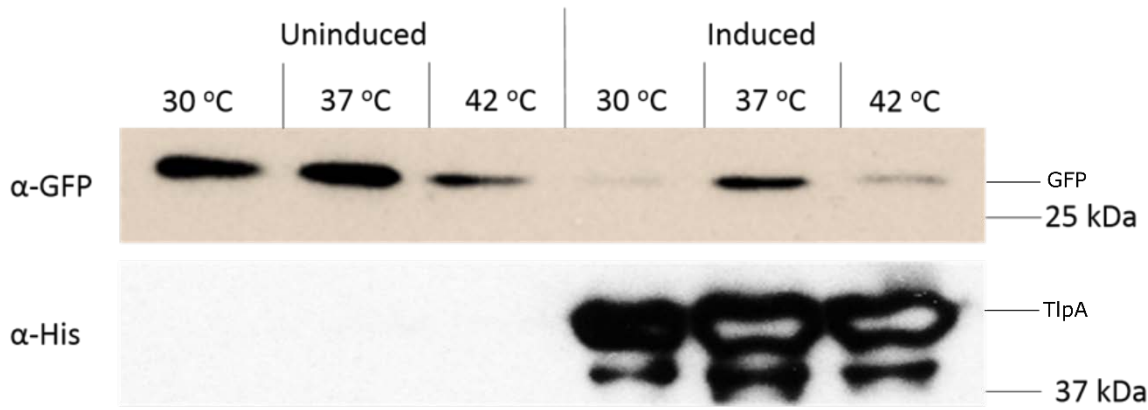


Figure 4.4 GFP and TlpA proteins are produced by pC1R7

E. coli MG1655 cells were transformed with pC1R7 and single colonies grown overnight in 5 mL LB with μ g/mL ampicillin and either zero (uninduced) or 1 mM (induced) IPTG and separate cultures incubated overnight at 30 °C, 37 °C and 42 °C. 0.5 mL cells were then removed and diluted to a final OD₆₀₀ of 0.3. Cells were then pelleted by centrifugation and resuspended in 50 μ L Laemmli sample buffer and boiled for five minutes. Next, 5 μ L of each of these samples were then subjected to Western immunoblot analysis where proteins were separated on 18 % (w/v) polyacrylamide gels, of which the protein was then transferred to a nitrocellulose membrane by semi-dry transfer with carbonate buffer. Membranes were blocked in 5 % (w/v) fat-free milk powder then probed with either α -GFP antibody (Roche) or α -His antibody (Abcam), followed by a secondary α -mouse antibody (Biorad) conjugated to HRP allowing development with ECL and imaged using exposure in a dark room to Medical X-Ray film (Konica).

In order to test the hypothesis that pC1R7 should upregulate GFP expression in accordance with increasing temperature, *E. coli* MG1655 cells were transformed with pC1R7 and single colonies grown at 25 °C, 30 °C, 34 °C and 37 °C in LB with a range of IPTG concentrations. At time points representing 4 hours and 8 hours post inoculation, an aliquot of cells was removed and GFP fluorescence measured using a Biotek HTX platereader (Figure 4.5).

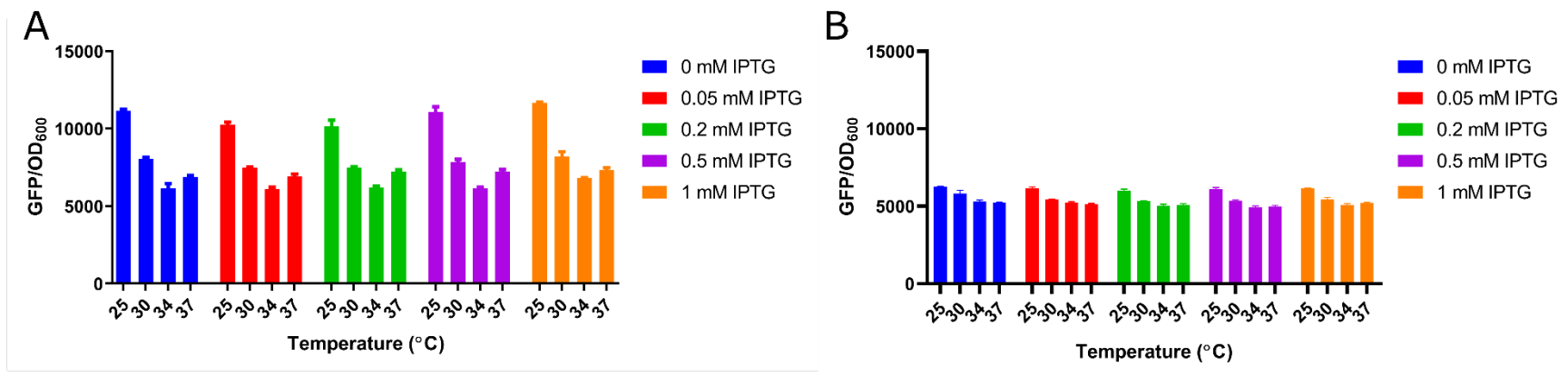


Figure 4.5 TlpA does not activate transcription with increasing temperature in small cultures

E. coli MG1655 cells were transformed with pC1R7 and grown overnight in 5 mL LB cultures at 25 °C, 30 °C, 34 °C and 37 °C with 250 rpm orbital shaking, with either 0, 0.05, 0.2, 0.5 or 1 mM IPTG. **(A)** 4 hours and **(B)** 8 hours post inoculation 200 µL was removed from the culture in to a 96 well plate and the OD₆₀₀ and GFP fluorescence was measured using a microplate reader. GFP fluorescence was normalised to the measured OD₆₀₀. Error bars are standard deviations representative of three biological replicates.

Other investigations into synthetic gene circuits have noted that culture conditions, such as growth medium, culture volume, and aeration among others, can affect circuit behaviour^{278,279}. As a result, in the next experiments the temperature range analysed was also extended up to 44 °C (Figure 4.6) to test the hypothesis that greater temperatures are required to relieve inhibition of GFP expression, since Western blot analysis can be considered as not an effective quantitative tool. In these experiments (Figure 4.6), *E. coli* MG1655 cells were transformed with pC1R7 and grown in overnight LB starter cultures before being used to inoculate 25 mL LB cultures in 250 mL conical flasks. These were incubated at 30 °C, 37 °C and 44 °C with 250 rpm orbital shaking and 1 mM IPTG in three biological replicates. Following 6 hours and 24 hours growth, 200 µL aliquots were removed and analysed using a microplate reader (Figure 4.6).

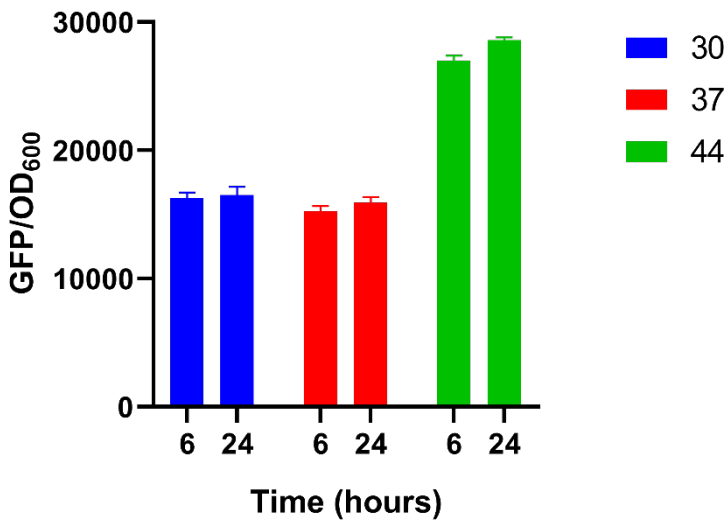


Figure 4.6 When cultured in 250 mL conical flasks at 44 °C, GFP expression is increased in pC1R7 containing cells

E. coli MG1655 cells were transformed with pC1R7 and cultured overnight in LB cultures then inoculated 1:100 in to 25 mL LB in 250 mL conical flasks with 1 mM IPTG and 120 µg/mL ampicillin. Six hours and 24 hours post inoculation, 200 µL aliquots were removed to a 96 well microplate and the OD₆₀₀ and GFP fluorescence was measured with a Biotek HTX platereader. The GFP fluorescence was normalised to the relevant OD₆₀₀ reading. Error bars are representative of three biological replicates.

4.2.2. Construction of a Synthetic Gene Circuit using MogR and GmaR

The genes *mogR* and *gmaR* were amplified by PCR from using gDNA extracted from the *L. monocytogenes str.* EGD-E as template. Next, a reporter construct was built using Gibson assembly in to the pQE80L background vector (Figure 4.7). The system is under the control of the T5lac promoter 5' of its multiple cloning site alongside the strong double terminator BioBrick BBa_B0015, the *flaA* promoter region (*PflaA*, -135-1 nt upstream of the *tlpA* start codon) from *L. monocytogenes str.* EGD-E ,and *gfpmut3b* in the architecture expressed in Figure 4.7.

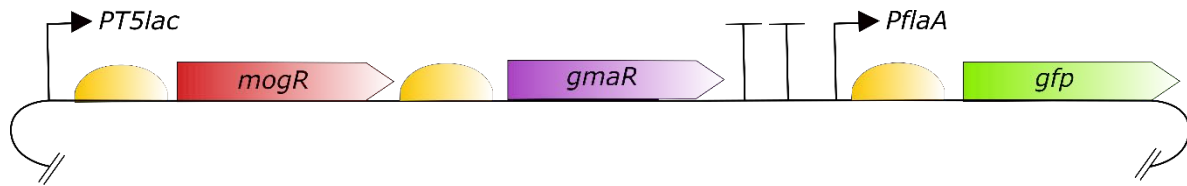


Figure 4.7 The pMOGMAR plasmid encodes a synthetic operon with *mogR* and *gmaR*, in parallel with a *gfpmut3b* MogR sensitive reporter

The pQE80L plasmid backbone was linearised by BamHI and HinDIII digestion and PCR primers designed to amplify DNA fragments encoding *mogR*, *gmaR*, BBa_B0015, *PflaA* and *gfpmut3b* to sufficiently overlap for Gibson Assembly in the order displayed above. The resulting plasmid was named pMOGMAR, as a portmanteau of MogR and GmaR.

4.2.3.pMOGMAR responds to temperature and IPTG

To test the hypothesis that the temperature dependence on transcription from *PflaA* can be reproduced in *E. coli*, pMOGMAR was subject to a range of experiments. First, to qualitatively characterise pMOGMAR, *E. coli* MG1655 cells were transformed with the plasmid and then patched on to LB agar plates containing 120 µg/mL ampicillin with either zero or 1 mM IPTG. Photographs taken of these patches using a Leica DMS1000 digital microscope with blue light attachment are shown in Figure 4.8.

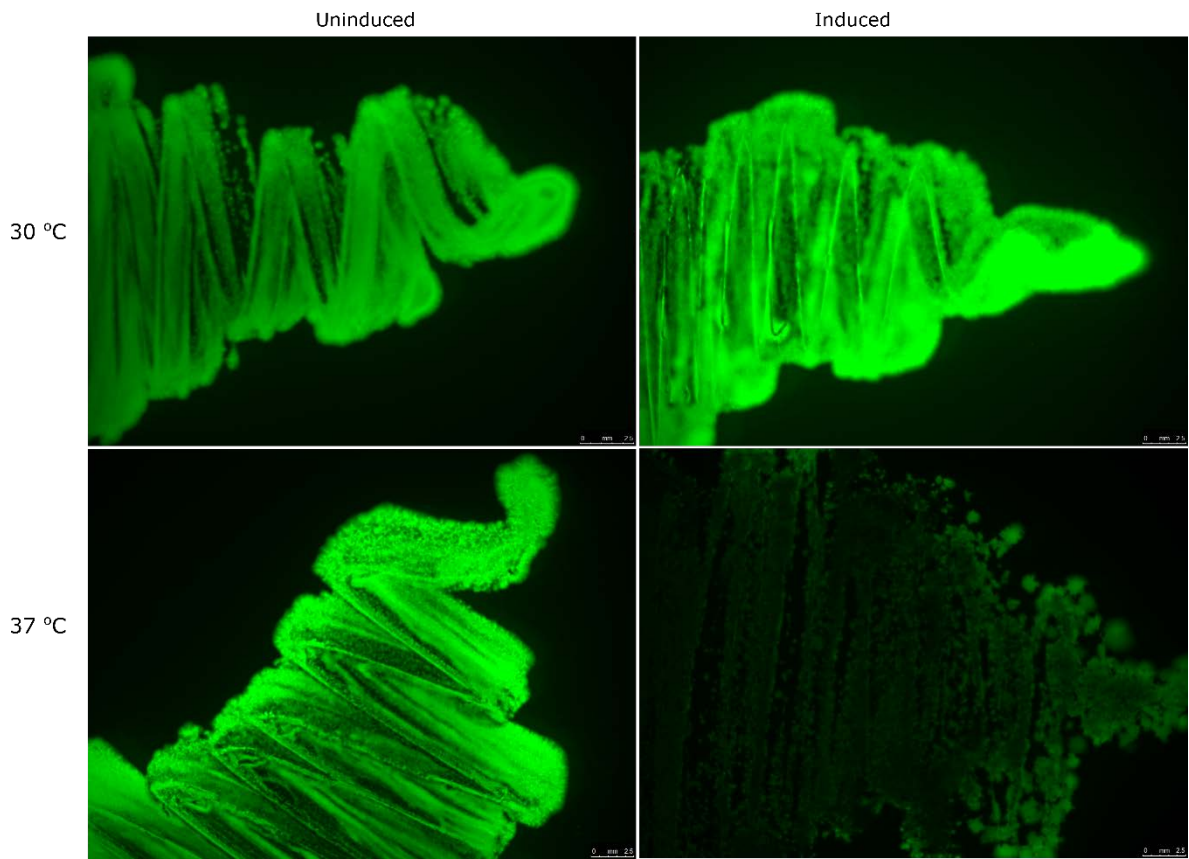


Figure 4.8 Evidence for temperature-dependent GFP production in *E. coli* using pMOGMAR.

The pMOGMAR plasmid was transformed into *E. coli* MG1655 cells and then single colonies patched onto LB agar plates with 120 µg/mL ampicillin and 1 mM IPTG. Separate plates were then incubated overnight at either 30 °C or 37 °C then imaged using a Leica DSM1000 digital microscope.

To make quantitative measurements of GFP production over a range of temperatures by pMOGMAR, its behaviour in 5 mL cultures over a range of IPTG concentrations was analysed. A broader range of temperatures was included in an effort to find a temperature critical for repression. In this experiment, *E. coli* MG1655 cells were transformed with pMOGMAR and single colonies were inoculated in 5 mL LB starter cultures. These were then inoculated to a final OD₆₀₀ of 0.01 in to 5 mL cultures and grown at 24 °C, 30 °C, 33.5 °C and 37 °C with 250 rpm orbital shaking for four hours. Following this, 200 µL aliquots were removed from each culture and analysed for GFP fluorescence using a Biotek HTX platereader (Figure 4.9).

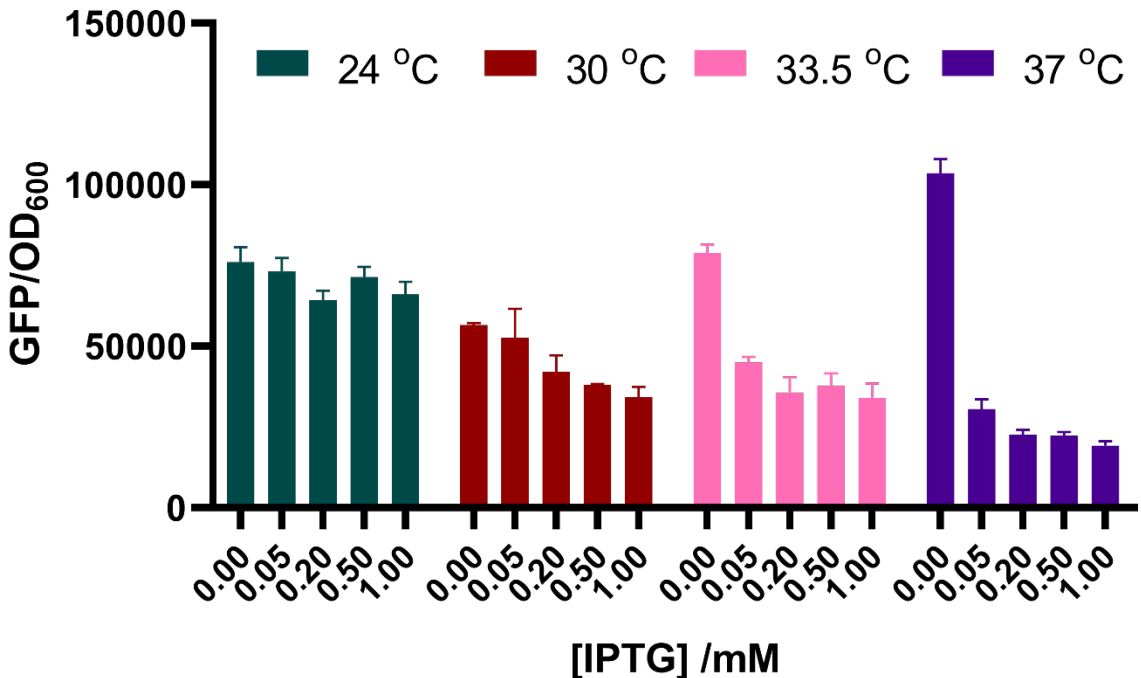


Figure 4.9 In pMOGMAR containing cells, GFP expression is inhibited as IPTG concentration increases

E. coli MG1655 cells were transformed with pMOGMAR and single colonies were inoculated in to 5 mL LB cultures and grown at 37 °C overnight with rotary shaking. These were then diluted to an OD₆₀₀ of 0.01 in to fresh 5 mL LB cultures with 120 µg/mL ampicillin and either zero, 0.05, 0.2, 0.5 or 1 mM IPTG and incubated with 250 rpm orbital shaking with three biological replicates each at 24 °C, 30 °C, 33.5 °C and 37 °C. After four hours, 200 µL samples were removed from each culture and placed in a 96 well microplate and the OD₆₀₀ and GFP fluorescence was measured using a Biotek HTX plate reader. GFP fluorescence was normalised to the relevant OD₆₀₀. Error bars represent standard deviation of three biological replicates.

Next, to probe the findings of Figure 4.9 with greater resolution, efforts were made to determine the optimal IPTG concentration that could repress the production of GFP. These experiments were conducted over 16 hour time courses in 96 well microplates to facilitate measurement of a number of conditions (Figure 4.10). Taken together, the information arising from Figures 4.9 and 4.10 suggest that a final concentration of 0.12 mM IPTG or less would be sufficient to saturate transcription from the *P_{T5}lac* promoter in pMOGMAR.

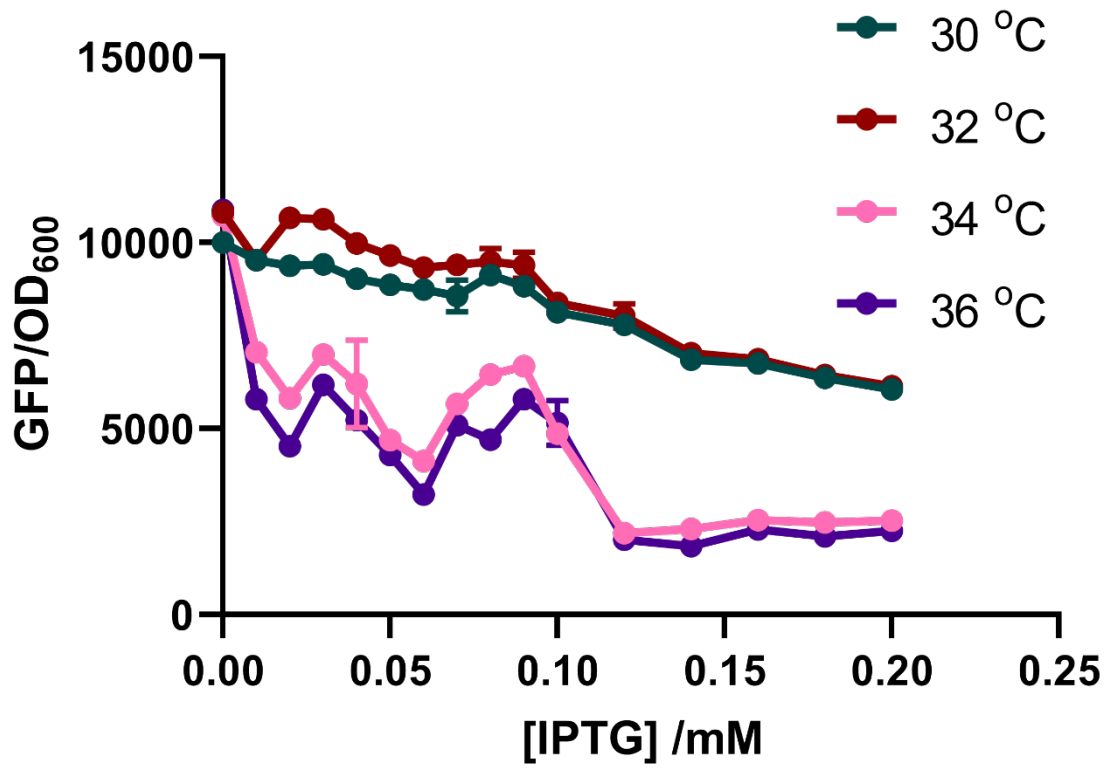


Figure 4.10 IPTG concentration and temperature influence GFP production by pMOGMAR

E. coli MG1655 cells were transformed with pMOGMAR and single colonies were inoculated in to 5 mL LB cultures with 120 µg/mL ampicillin and grown with rotary shaking overnight. These cultures were then inoculated in 96 well microplates in 200 µL LB at a final OD₆₀₀ of 0.01. IPTG was added in advance to these wells at concentrations of 0, 0.01, 0.02, 0.03, 0.04, 0.05, 0.06, 0.07, 0.08, 0.09, 0.1, 0.12, 0.14, 0.16, 0.18, and 0.2 mM to produce three biologically independent cultures with each. This was performed in parallel runs in a Biotek HTX platereader at with orbital shaking at 200 rpm and incubation at either 30 °C, 32 °C, 34 °C or 36 °C. Error bars represent standard deviation of three biological replicates.

4.2.4. Improving pMOGMAR characterisation

The data shown in Figures 4.9 and 4.10 indicate that pMOGMAR was downregulating GFP expression in response to increased IPTG concentrations, even at cooler temperatures, with this effect apparently saturating at around 0.12 mM IPTG. There were a few observations made that may explain this. First, there is no characterisation of the *PflaA* promoter alone in these experiments. It is therefore possible that the repression of GFP production at these temperatures was due to innate properties of the promoter or interactions of the promoter with divergent elements in *E. coli*. There is also the possibility that biophysical properties of the GFP protein could produce different levels of fluorescence at different temperatures. For example, GFP is most fluorescent when it forms homodimers. The GFPmut3b protein is described as weakly dimeric, however temperature could influence the stability of these dimers, or even stability of monomeric GFP such that fluorescence is abrogated in individual proteins. Additionally, LB medium has a small degree of fluorescence which might confound GFP fluorescence measurements taken also. Last, it is possible that repression of GFP production at temperatures of 30 °C and below observed with the addition of IPTG is caused by an imbalance of MogR and GmaR protein in the cell. An excess of MogR could lead to repression under most conditions where there is insufficient antirepressor GmaR to relieve this.

To address these issues, a plasmid was constructed in the same background as pMOGMAR by deleting the region from the start codon of *mogR* to the 3' end of the BBa_B0015 double terminator biobrick. This produced pFLA-gfp, which includes the *PflaA* promoter controlling the transcription of *gfpmut3b*. All experiments were henceforth performed in the rich defined medium EZ Glc, which has no background fluorescence²⁸⁰.

First of all, the pFLA-gfp promoter was examined for its behaviour at different temperatures. In these experiments, *E. coli* MG1655 cells were transformed with pFLA-gfp and single colonies grown in overnight cultures at 37 °C with rotary shaking. Cultures were then inoculated in to 96 well plates in EZ Glc medium with either zero or 0.12 mM IPTG and incubated for 18 hours in a microplate reader at 24 °C, 30 °C, 36 °C and 42 °C in parallel while OD₆₀₀ and GFP fluorescence were measured every ten minutes, shown in Figure 4.11.

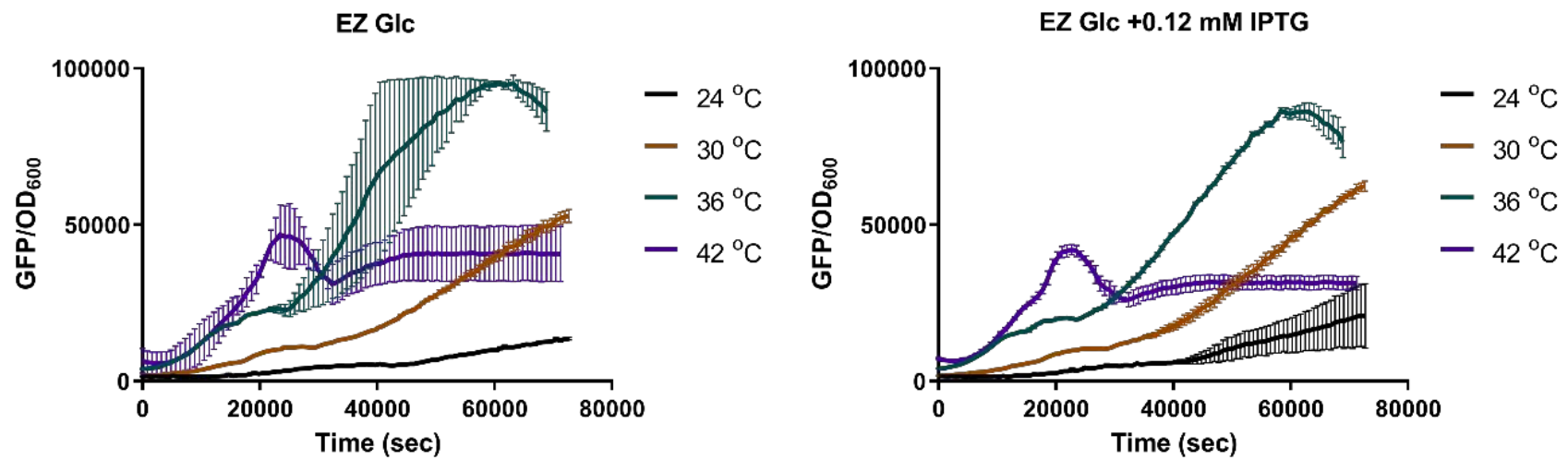


Figure 4.11 PflaA shows divergent activities at different temperatures

MG1655 cells were transformed with pFLA-gfp and single colonies grown overnight in EZ Glc medium at 37 °C with rotary shaking. Cultures were then inoculated into 150 µL EZ Glc cultures with the addition of 120 µg/mL ampicillin and either zero or 0.12 mM IPTG in round bottomed 96 well microplates at a final OD₆₀₀ of 0.01. Microplates were then incubated with linear shaking in a Tecan Infnite MNano+ platereader for 18 hours with GFP fluorescence measured with excitation and emission wavelengths 523 and 488 nm, respectively, every ten minutes. Error bars represent standard deviation of four biological replicates.

Examining this data, it is possible to see at 36 °C and 42 °C there is multi-phasic expression rates of GFP, compared to almost linear production rates at other temperatures. The drop in GFP fluorescence that occurs at 42 °C is especially concerning. This could be explained by changes in carbon source or carbon preference during prolonged culture that influences catabolite repression regulons. The hypothesis that *PflaA* is catabolite repressed then needed to be tested. Catabolite repression of PflaA could affect circuit behaviour in different culture conditions, or even in different phases of growth in the same culture conditions which would limit its usefulness across different settings.

To test the hypothesis that *PflaA* is catabolite repressed, MG1655 cells were transformed with pFLA-gfp and grown in overnight starter cultures in EZ Glc medium at 37 °C. These were then inoculated into 150 µL EZ cultures in 96 well plates with the addition of either 0.2 % (w/v) glucose or 0.4 % (v/v) glycerol. Plates were incubated in a platereader at 42 °C for 18 hours and OD₆₀₀ and GFP fluorescence measured every ten minutes, displayed in Figure 4.12.

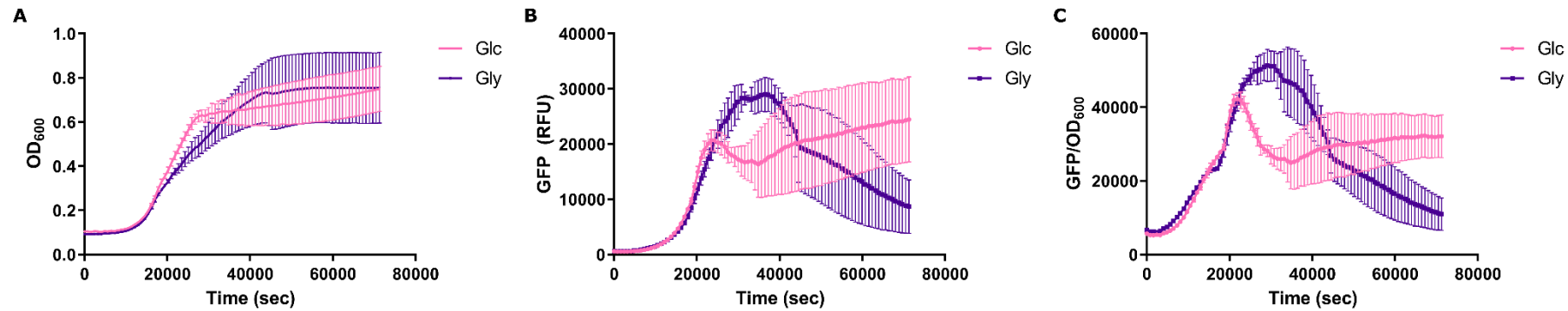


Figure 4.12 PflaA shows similar behaviours in exponential phase when grown using glucose or glycerol as a carbon source.

MG1655 cells were transformed with pFLA-gfp and grown for approximately four hours in 5 mL LB cultures at 37 °C in EZG Glc media overnight. Cultures were then inoculated at a final OD₆₀₀ of 0.01 in to 150 µL cultures using EZ media with the addition of 0.4 % glycerol or 0.2 % glucose in round bottomed 96 well plates. Plates were then incubated with linear shaking at 42 °C for 18 hours with GFP fluorescence and OD₆₀₀ measured every ten minutes. A, showing the change in OD₆₀₀ over this period, B, the raw GFP fluorescence data obtained over this period, and C , the GFP fluorescence from B normalised to the OD₆₀₀ in A. Error bars represent standard deviation of four biological replicates.

It was decided that, since in these experiments *PflaA* has variable activities at different temperatures, it should be used as a standard in all experiments during the characterisation of pMOGMAR going forward, as has been performed by previous investigators of synthetic gene circuits^{279,281}. Additionally, the similar behaviours in GFP production during exponential phase of growth led to the decision to focus future work on cells in the exponential growth phase.

It was also not out of the question that biophysical factors influence GFP fluorescence at different temperatures, which could confound analysis of temperature sensitive circuits like pMOGMAR. Thus the hypothesis that GFP fluorescence fluctuates with temperature needed to be tested.

In an effort to understand the specific differences in GFP fluorescence at different temperatures a plasmid was constructed in the pQE80L vector by linearising with BamHI and HinDIII before cloning in the *gfpmut3b* gene by Gibson assembly. This produced the plasmid pQEgfp. To generate a large volume of cells producing GFP, MG1655 cells transformed with pQEgfp were cultured in 500 mL LB and centrifuged to produce ~0.3 g cell pellets. These pellets were suspended in lysis buffer (50 mM Tris pH 8, 50 mM NaCl, DnaseI, 0.1 µg/mL lysozyme) and then sonicated for five minutes. The suspension was then clarified by centrifugation and 150 µL of the resultant crude extract transferred to a 96 well plate which was incubated at 30 °C, 36 °C and 42 °C, for 18 hours with GFP fluorescence measured every ten minutes. At each temperature a different cell pellet was used, and so to ensure any differences between temperatures were not explained by pellet-to-pellet variation, a single lysate was incubated at 30 °C, 36 °C and 42 °C progressively and its GFP fluorescence measured at each temperature independently, and shown in Figure 4.13

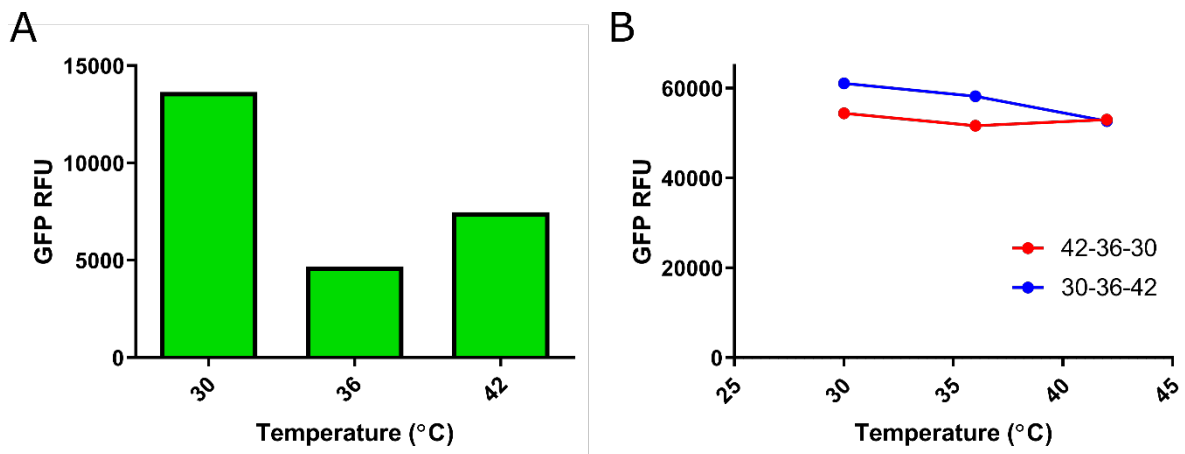


Figure 4.13 GFP is most fluoresescent at 30 °C

Lysates were prepared by five minute sonication treatments of cell pellets at roughly 0.3 g (wet weight) of MG1655 *E. coli* cultures expressing pQEgfp with 1 mM IPTG in 500 mL LB in baffled 2 L conical flasks at 37 °C with linear shaking overnight. A, 150 µL lysate was incubated at 30 °C, 36 °C and 42 °C in a Tecan Infinite MNano+ platereader and GFP fluorescence measured using excitation and emission at 528 and 488 nm using lysates prepared on parallel experiments for each temperature. B, a single lysate preparation as in A was incubated in a Tecan Infinite MNano+ platereader for 30 minutes at 30 °C and GFP fluorescence measured as in A, followed by 30 minutes at 36 °C and 30 minutes at 42 °C with GFP fluorescence measured identically in each case (blue line). In red is shown results for an identical experiment using the same lysate sample but temperature incubations performed in reverse. A single experiment was performed in each case.

4.2.5. Translation of *gmaR* may be a limiting factor

In Figures 4.9 and 4.10, it was seen that some repression of GFP expression was observed at lower temperatures, especially at higher IPTG concentrations. Based on the model of how MogR and GmaR influence transcription from the *flaA* promoter (Figure 4.2), there should be no inhibition of transcription at these temperatures (24–30 °C). It was hypothesised that cellular GmaR protein may be limiting under these conditions to antirepress MogR.

To test the hypothesis that GmaR levels within the cell are limiting, it was decided that RBS strengths should be measured for *mogR* and *gmaR*. The DeNovoDNA RBS calculator and design tool was used, which is an algorithm that scans a given sequence for translational start codons and then makes structural prediction of the mRNA that might surround the putative start codon around the 16 nt upstream and downstream of this site to determine its accessibility to ribosomes. An arbitrary score is calculated based on the predicted free energy of binding between the putative mRNA and the ribosome, and the putative mRNA and other regions of itself. This score is called the translational initiation rate, TIR.

First, the TIR of native *mogR* and the *gmaR* were predicted using the reverse engineering algorithm in the RBS calculator, shown in Table 4.1. These were found to be at around 700 units and 300 units, respectively.

To test the hypothesis that increasing the TIR of *gmaR* would improve circuit behaviour and GFP expression at 24 – 30 °C, three synthetic RBSs were produced using the DeNovoDNA RBS Calculator. The “weakest” of these had a TIR that was designed to match the *mogR* RBS and two more were designed to exceed this, at TIRs 10,000 and 20,000 units, respectively. These are also displayed in Table 4.1.

Table 4.1 Predicted TIRs of designated RBSs in pMOGMAR and its variants

RBS sequence is shown in purple capitals, and start codon of each ORF in green.

Plasmid	3' ORF	RBS sequence	No. nt.	Predicted Translation Initiation Rate
pMOGMAR	<i>mogR</i>	...att AAAGAGGAGAAA AUG	12	690
pMOGMAR	<i>gmaR</i>	...tataaacaaatgtaa AUG	Not defined	285.0
pMOGMAR-700	<i>gmaR</i>	...tataaacaaatgtaa AGATCCCGGTAG ATATAAAGAGACGCCA AUG	28	700.16
pMOGMAR-10K	<i>gmaR</i>	...tataaacaaatgtaa TGCTCATCCCGT AACGGAGGGCTCAAAAAACATCAAGGT CAT TTAUG	32	10004.96
pMOGMAR-20K	<i>gmaR</i>	...tataaacaaatgtaa AAAGAGGAGAAA TACTAG AUG	18	20683.37

The RBSs were inserted into pMOGMAR by inverse PCR, where primers are designed to include an insertion and amplify the entire length of a plasmid producing a linear copy of the plasmid with the insertion sequence at either the 5' or 3' end or both. By using a blunt ended polymerase in this reaction and the NEB produced “KLD” kit with the produced DNA fragment, 5' phosphate groups can be added to the PCR product, the original (methylated) template DNA removed with DpnI digestion and plasmid circularised by using T4 ligase in a single reaction. Primers were designed which included the synthetic RBS sequences seen in Table 4.1 to be inserted using this method. The resulting plasmids were named pMOGMAR-700, pMOGMAR-10K and pMOGMAR-20K after the strengths of the RBSs inserted.

To characterise how these new pMOGMAR variants behaved at different temperatures, MG1655 was transformed and the cells cultured in EZ Glc media at 24 °C, 30 °C, 36 °C and 42 °C with and without the addition of 0.12 mM IPTG and GFP fluorescence and OD₆₀₀ measurements taken across a time-course of 18 hours (Figure 4.14). The pFLA-gfp plasmid was included in parallel in these experiments as an internal standard to which all measurements from pMOGMAR, pMOGMAR-700, pMOGMAR-10K and pMOGMAR-20K were normalised giving a final value termed “promoter activity”. Promoter activity is given by division of a sample measurement of OD₆₀₀ normalised GFP fluorescence to that of pFLA-gfp under the same conditions. Figure 4.14 shows the behaviour of each of these plasmids in exponential phase of growth, and Figure 4.15 shows behaviour at stationary phase.

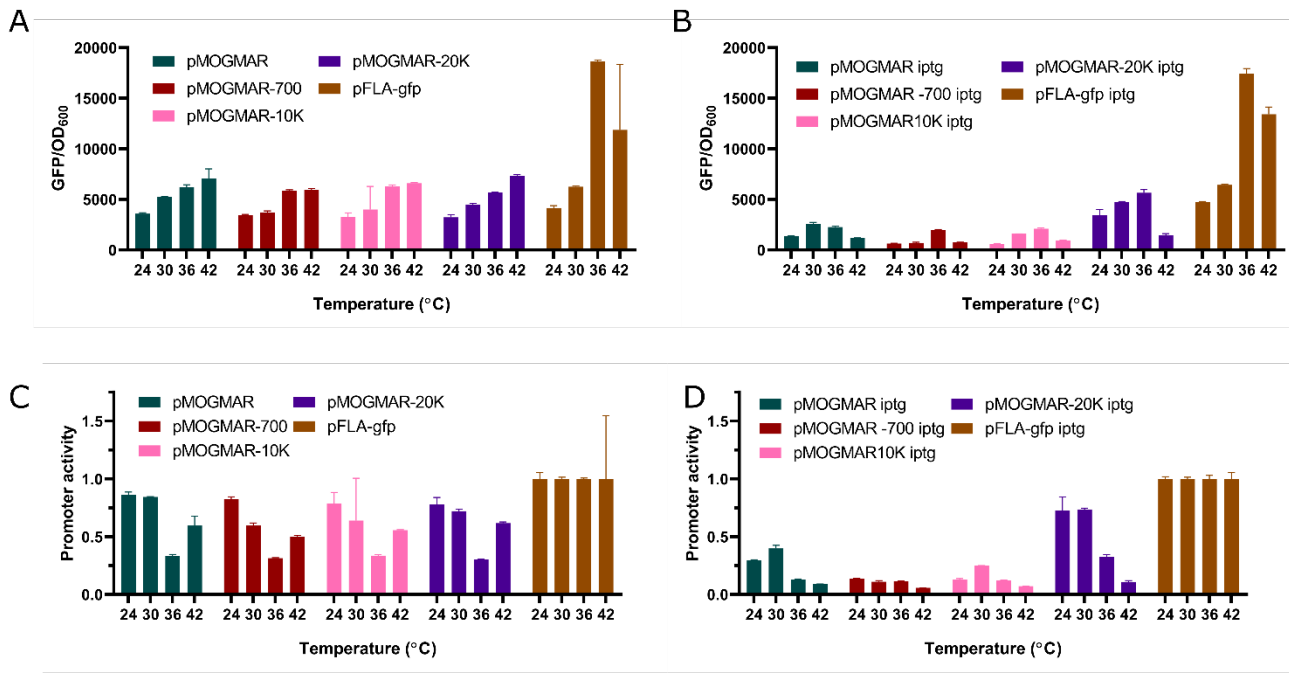


Figure 4.14 pMOGMAR-20K shows enhanced promoter activity at 24–30 °C compared to pMOGMAR, pMOGMAR-700 and pMOGMAR-10K during exponential phase

E. coli MG1655 cells were transformed with pMOGMAR, pMOGMAR-700, pMOGMAR-10K, pMOGMAR-20K and pFLA-gfp. Single colonies of each were incubated for approximately four hours at 37 °C with rotary shaking in LB. These cultures were then inoculated in to 150 µL EZ Glc medium with either zero (A, C) or 0.12 mM IPTG (B, D) in 96 well plates at a final OD₆₀₀ of 0.01. The plate was then incubated at 24 °C, 30 °C, 36 °C and 42 °C in a Tecan Infinite MNano+ plate reader with OD₆₀₀ and GFP fluorescence measured every ten minutes. Using OD₆₀₀ traces, an exponential phase time point was marked as the timepoint in the middle of the exponential phase of the curve. A, B, GFP fluorescence data was normalised to OD₆₀₀ measurements (GFP/OD₆₀₀) and bar charts plotted of this data at this timepoint in exponential phase. C, D, this data was normalised to the appropriate measurements from pFLA-gfp to produce promoter activity estimations. Error bars represent standard deviations of four biological replicates.

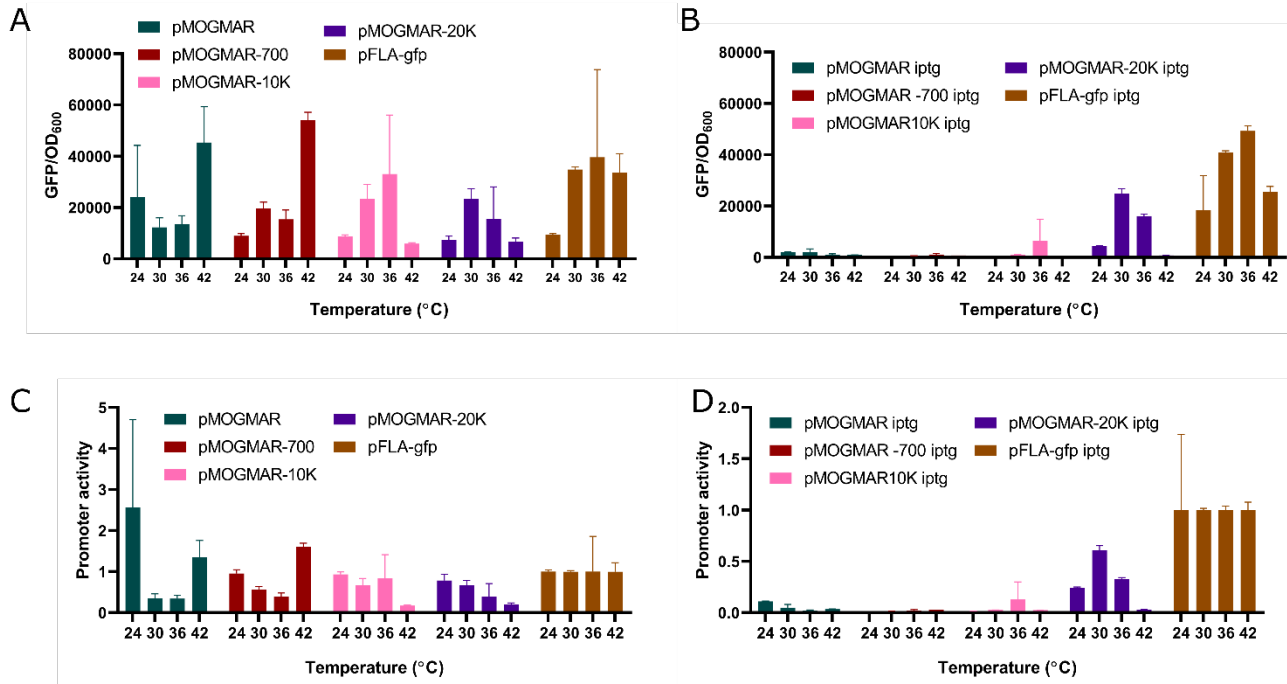


Figure 4.15 pMOGMAR activity is noisy at stationary phase, and promoter activity is minimal in most variants

E. coli MG1655 cells were transformed with pMOGMAR, pMOGMAR-700, pMOGMAR-10K, pMOGMAR-20K and pFLA-gfp. Single colonies of each were incubated overnight at 37 °C. These cultures were then inoculated in to 150 µL EZ Glc medium with either zero (A,C) or 0.12 mM IPTG (B,D) in 96 well plates. The plate was then incubated at 24 °C, 30 °C, 36 °C and 42 °C in a Tecan Infinite MNano+ plate reader with OD₆₀₀ and GFP fluorescence measured every ten minutes. Data from the final timepoint for each sample was taken as a stationary phase timepoint. A,B, GFP fluorescence data was normalised to OD₆₀₀ measurements (GFP/OD₆₀₀) and bar charts plotted of this data at this timepoint in exponential phase. C,D, this data was normalised to the appropriate measurements from pFLA-gfp to produce promoter activity estimations. Error bars represent standard deviations of four biological replicates.

4.2.6.The pMOGMAR-20K plasmid outperforms pMOGMAR as a sensor

Thus far, analysis of pMOGMAR and its variants has relied on spectrophotometric characterisation of cultures of cells *en masse*. Flow cytometry is a technology that permits quantification of GFP or other fluorophores in individual cells. Flow cytometry was next utilised to compare the differences between the behaviours of cells containing pMOGMAR with its optimised sister plasmid pMOGMAR-20K and the positive control pFLA-gfp. pMOGMAR-20K was utilised in these experiments over pMOGMAR-700 and pMOGMAR-10K as it showed the best correlated promoter activity with temperature.

E. coli MG1655 cells were separately transformed with pMOGMAR, pMOGMAR-20K, pFLA-gfp and pQE80L and single colonies were cultured overnight in EZ Glc media. Cultures were then diluted to a final OD₆₀₀ of 0.01 in EZ Glc medium supplemented with 120 µg/mL ampicillin and either zero or 0.12 mM IPTG. Cultures were grown in parallel at 30 °C and 42 °C with 300 rpm orbital shaking to exponential phase. Exponential phase was defined by taking 150 µL samples from a culture every 30 minutes and measuring the OD₆₀₀ to produce a growth curve, presented in Figure 4.16.

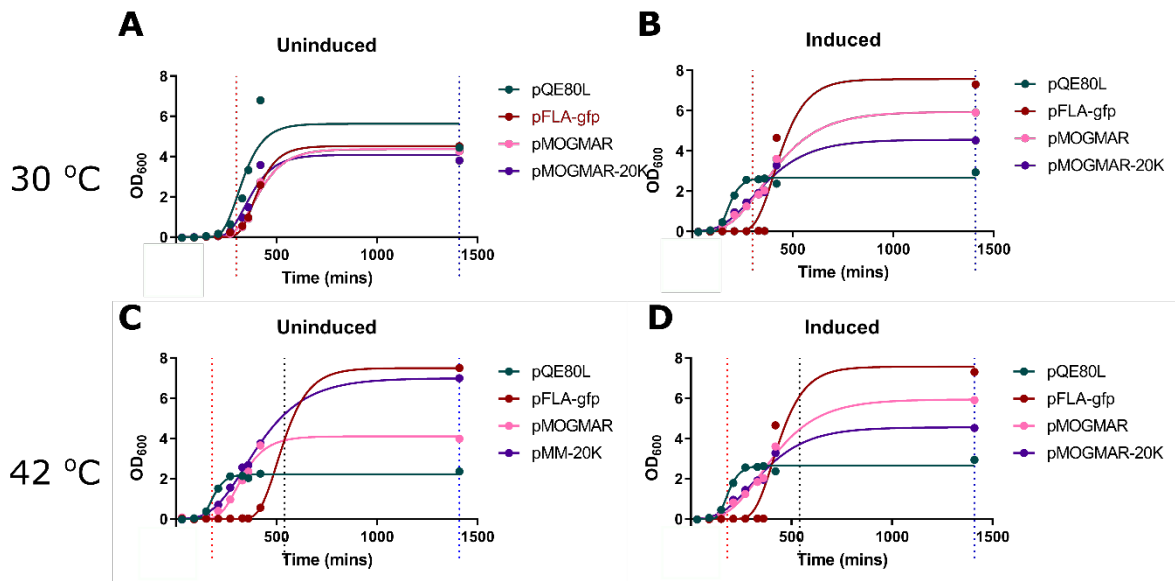


Figure 4.16 pFLA-gfp containing cells have a growth defect, while pMOGMAR and pMOGMAR-20K containing cells have similar growth profiles to each other

MG1655 cells were transformed with pQE80L, pMOGMAR, pMOGMAR-20K and pFLA-gfp. Single colonies were then cultured overnight in EZ Glc media with 120 µg/mL ampicillin then subcultured in 3 mL EZ Glc with or without 0.12 mM IPTG in 14 mL round bottomed tubes. These 3 mL cultures were incubated at 30 °C (A,B) or 42 °C (C, D) standing upright in Infors shaking incubators with orbital shaking at 300 rpm. Every 30 minutes, 100 µL of culture was removed and OD₆₀₀ was measured using a Tecan Infinite MNano+ platereader. The Gompertz curve fitting equation was applied using Graphpad Prism 8 to this data. The exponential phase time point where samples were taken in future experiments are marked on these graphs with a red dotted line, and the stationary phase sampling time point in blue. An additional black line indicates the time point where exponential phase samples were taken from pFLA-gfp cultures at 42 °C, which differed due to their extended lag phase.

In order to measure GFP levels in individual cells, a 0.5 mL aliquot was removed from cultures grown as in Figure 4.16 at the exponential phase time point marked in red and washed twice in an equal volume of PBS. The washed suspension was then diluted 1/100 in to sterile PBS and analysed by flow cytometry. Samples were also obtained identically after overnight cultivation to obtain samples representative of the late stationary phase as used in Figure 4.16. First, histograms were plotted showing the number of cells with different levels of GFP fluorescence (Figure 4.17).

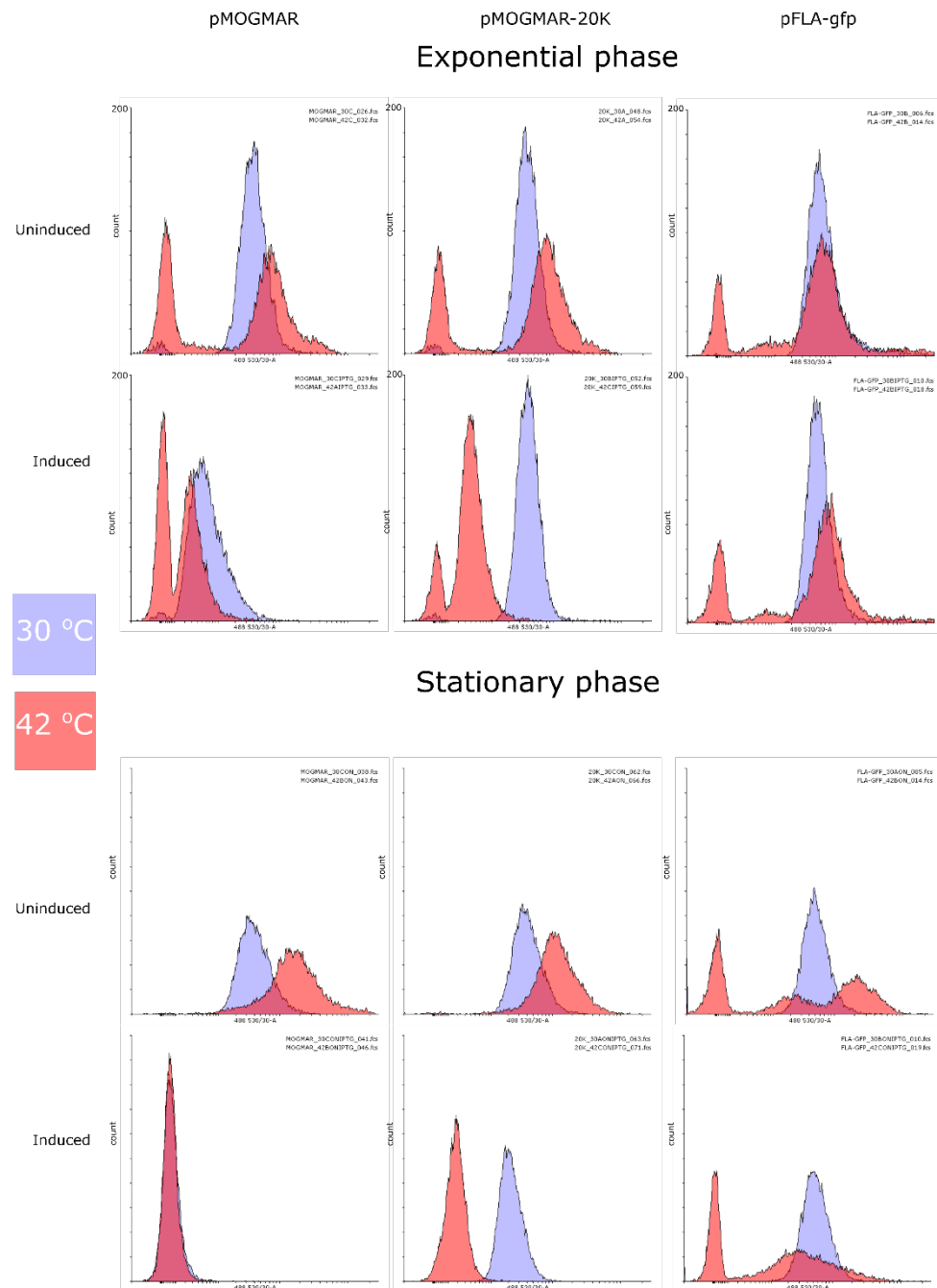


Figure 4.17 GFP production by pMOGMAR-20K is repressed at 42 °C

E. coli MG1655 cells were transformed with pMOGMAR, pMOGMAR-20K or pFLA-gfp and cultured overnight in EZ Glc media. Cells were then washed in sterile media and diluted to a final OD₆₀₀ of 0.01 in 3 mL cultures with 120 µg/mL ampicillin and either zero or 0.12 mM IPTG in 14 mL volume Nunc tubes. Three independent cultures were grown in replicate using each plasmid at temperatures of 30 °C and 42 °C with 300 rpm orbital shaking. At an exponential growth point determined in figure 4.16, a sample of cells was taken and washed in PBS twice, before being diluted 1/100 in sterile PBS and analysed by flow cytometry using a BD Fortessa X20 flow cytometer where a total of 10,000 events were recorded for each individual sample with voltages of 632 for FSC, 286 for SSC and 458 for GFP. Gates were drawn using FSC and SSC data using Flowing software²⁸² to eliminate debris and other contaminants from the data and then 488/530 datapoints plotted in histograms shown here.

Using the data in Figure 4.17, geometric means of fluorescence were calculated using Flowing software²⁸². Geometric means were utilised to then calculate “promoter activity”, which again was defined by normalising the measurements from one pMOGMAR-20K sample to the average of measurements of the appropriate data relating to pFLA-gfp (Figure 4.18).

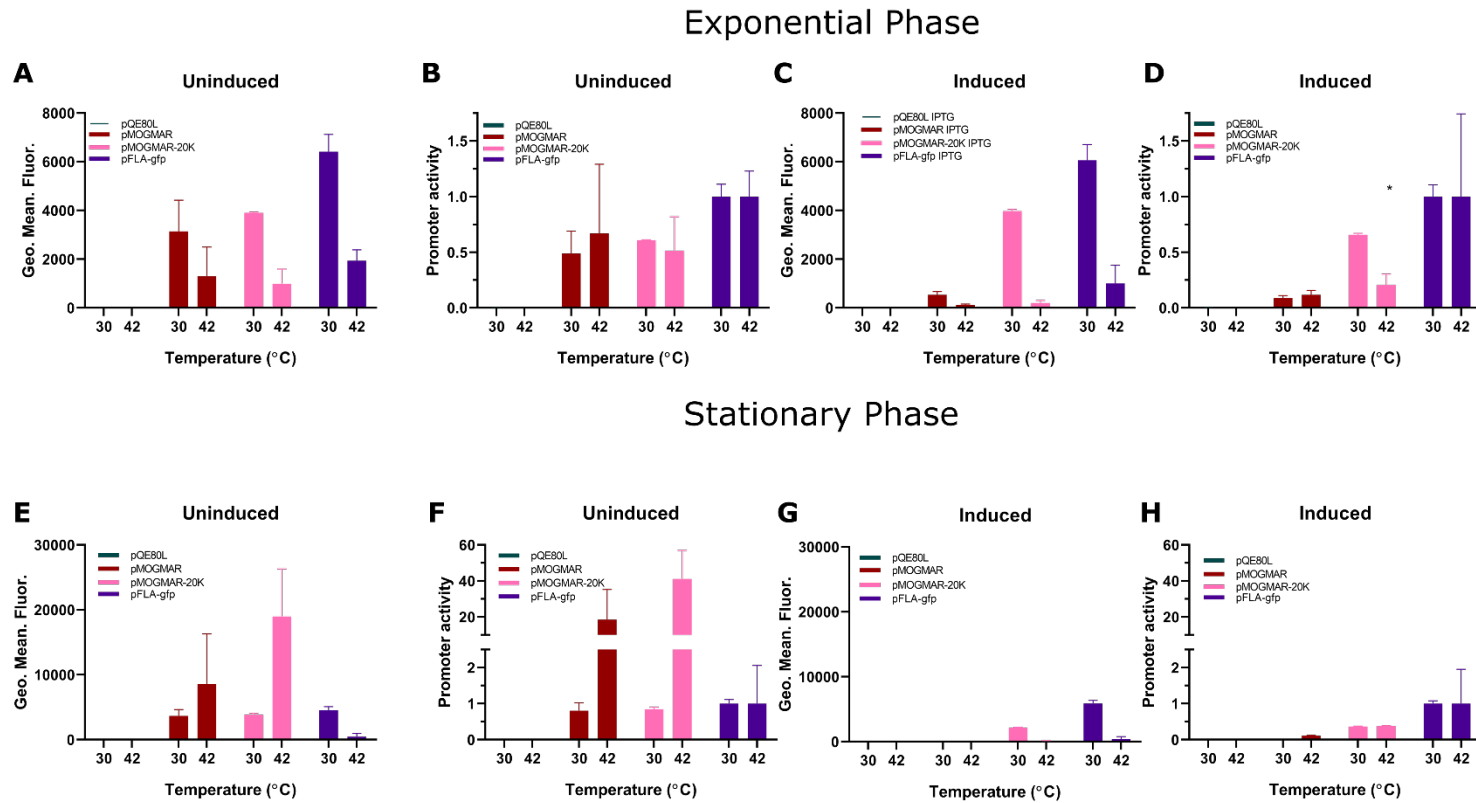


Figure 4.18 Temperature influenced behaviours of pMOGMAR plasmids break down at stationary phase

Using data generated in Figure 4.17, A,C,E,F, geometric means of fluorescence of each sample were calculated using Flowing software and plotted accordingly. B, D, G, H. These measurements were used to calculate promoter activity by normalising the geometric mean of fluorescence to the average of appropriate pFLA-gfp measurements. Error bars represent standard deviation of four biological replicates.

Using data in Figure 4.18 it is difficult to make judgements on whether individual cells are responding to temperature in a manner dependent on MogR and GmaR. Moreover, this analysis does not take advantage of the nature of data produced by flow cytometry. For this reason the data produced in Figure 4.17 was utilised to calculate the proportion of cells in an “ON” state. As seen in Figure 4.19, the ON state was defined using data produced for pFLA-gfp at 30 °C. A gate was drawn around cells falling around the peak produced in histograms for this data as in Figure 4.19A. This was applied to all other samples and the percentage of the total number of cells falling in this range was calculated and plotted in Figure 4.19B-D.

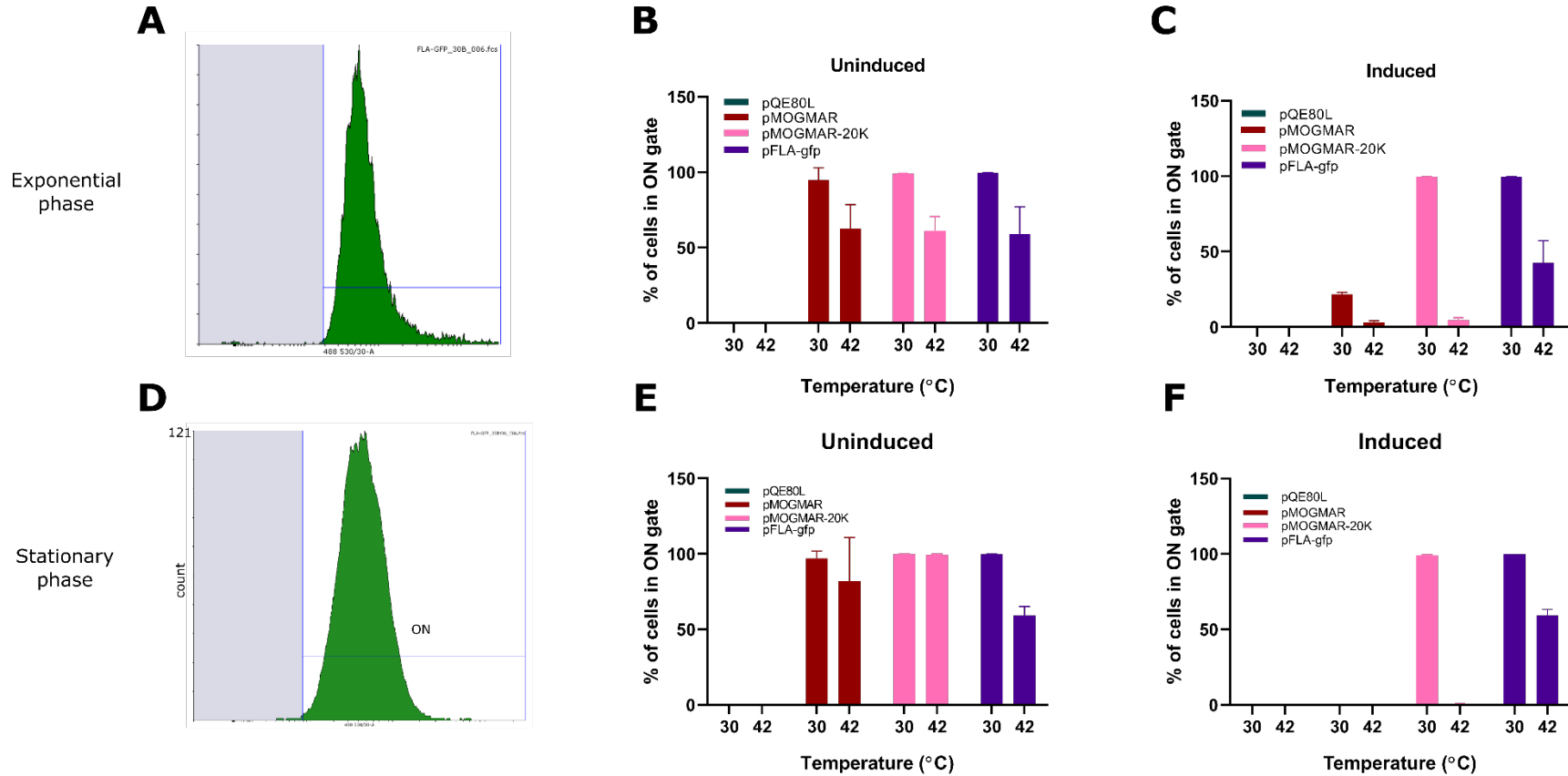


Figure 4.19 At both exponential phase and stationary phase, pMOGMAR-20K cells are turned off at 42 °C.

A, Using data collected in figure 4.17, a gate was determined using samples representing cells expressing pFLA-gfp at 30 °C that was named “ON”, shown in the unshaded area. This represents the level of GFP expression at the maximum range of promoter activity in these conditions. This gate was applied to all samples collected and the percentage of cells of the total that fall in to this range were calculated and plotted. B,C, exponential phase samples with (C) and without (B) 0.12 mM IPTG. D,E, stationary phase samples with (E) and without (D) 0.12 mM IPTG. Error bars represent standard deviations of four biological replicates.

4.2.7.The biochemical influence of temperature on MogR : GmaR interaction is still unclear

In order to make pMOGMAR-20K and the proteins it encodes useful for the broader synthetic biology community, the nature of the interaction between these two proteins should be better understood to make them easier to engineer and utilise in more complex programs. To begin, it was first necessary to interrogate the nucleotide and amino acid sequences of *gmaR* and *mogR* encoding genes for factors that could influence their activity *in vivo*. First, the presence of rare codons that could affect the translation rate of *mogR* or *gmaR* was probed. To do this, the nucleotide sequences for *mogR* and *gmaR* were obtained from KEGG and then submitted to the Rare Codon Caltor, which identifies rare codons based on data from NCBI GenBank, shown in Figure 4.21.

A

MogR

The Number of Bases in the above Sequence = 921

The Number of Codons in the above Sequence = 307

B

GmaR

The Number of Bases in the above Sequence = 1914

The Number of Codons in the above Sequence = 638

C

Amino Acid	Rare Codon	Frequency of Occurrence
Arginine	CGA	0
	CGG	1
	AGG	0
	AGA	3
Glycine	GGA	1
	GGG	2
Isoleucine	AUA	1
Leucine	CUA	5
Proline	CCC	0
Threonine	ACG	0

Repeated and/or Consecutive Rare Codons

AUA AGA = 1

GGG AGA = 1

Amino Acid	Rare Codon	Frequency of Occurrence
Arginine	CGA	6
	CGG	3
	AGG	0
	AGA	4
Glycine	GGA	6
	GGC	2
Isoleucine	AUA	1
Leucine	CUA	10
Proline	CCC	1
Threonine	ACG	6

Repeated and/or Consecutive Rare Codons

ACG GGA = 1

GGA CGA = 1

CUA GGA = 1

Figure 4.20 There are numerous rare codons in *mogR* and *gmaR*.

The nucleotide sequences for (A) *mogR* and (B) *gmaR* were analysed using the RBS Caltor tool, which then shows the entire nucleotide sequence with rare codons highlighted. Tables showing rare codons present in (C) *mogR* and (D) *gmaR* and the amino acids they encode.

The occurrence of rare codons in both MogR and GmaR made it necessary to study the expression of these proteins. The initial cloning design facilitated the inclusion of a hexahistidine tag at the N-terminus of MogR. To this end, MG1655 cells were transformed with pMOGMAR and single colonies inoculated in to LB and incubated at 30 °C, 37 °C or 42 °C overnight. Samples were then taken and normalised to an OD₆₀₀ of 0.3 and probed by Western blot using α -His antibody, Figure 4.21.

In order to probe the expression of GmaR, a new version of pMOGMAR-20K was generated by KLD reaction. Primers were designed to amplify the entirety of pMOGMAR-20K from the beginning of the *gmaR* CDS in the forward direction and the 3' end of the synthetic RBS with insertions at 5' and 3' ends of the primer such as to add a HA tag to the N-terminus of GmaR. This produced pMOGMAR-20KNHA.

pMOGMAR-20KNHA was used to transform *E. coli* MG1655 cells and single colonies were inoculated in to LB and cultivated at 30 °C, 37 °C and 42 °C overnight. Samples were taken four hours post inoculation and overnight and normalised to an OD₆₀₀ of 0.3. These samples were then used in Western blots and probed with an α -HA antibody, Figure 4.21.

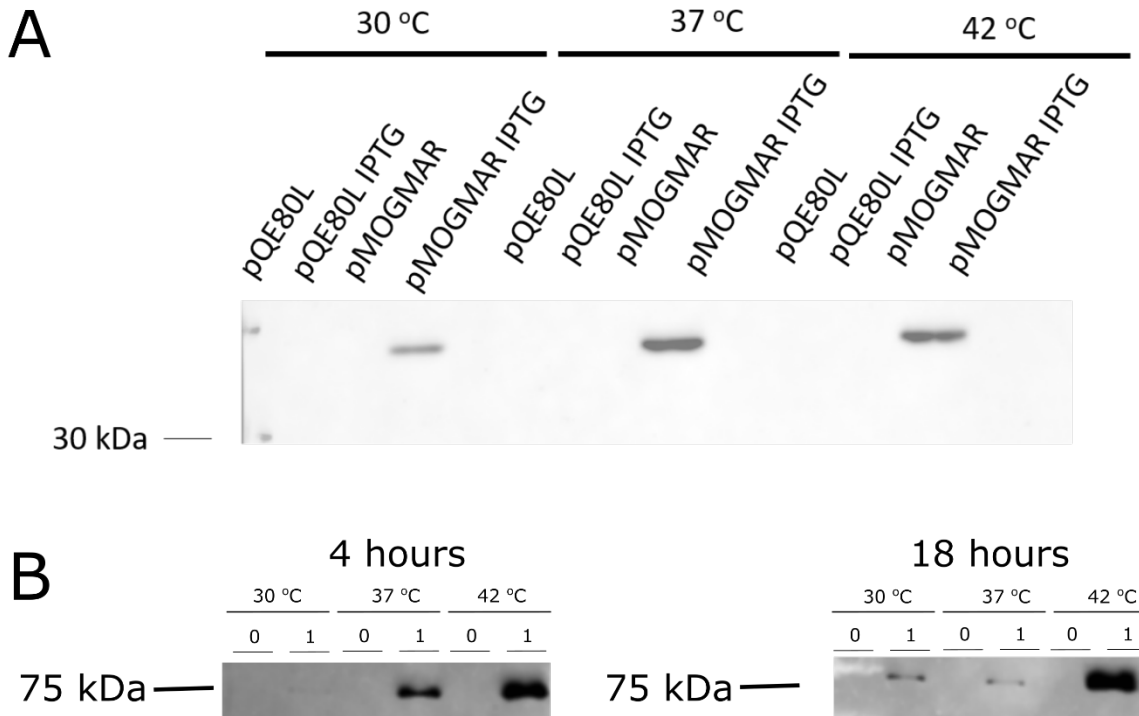


Figure 4.21 Both MogR and GmaR can be detectably produced in *E. coli*

A, MG1655 cells were transformed with pMOGMAR and pQE80L as a negative control. Single colonies were inoculated in to LB and cultured at 30 °C, 37 °C and 42 °C with separate cultures at each temperature containing either zero or 0.12 mM IPTG. After overnight incubation, samples were taken from the cultures, washed and diluted to a final OD₆₀₀ of 0.3. These were then mixed with 2x Laemmli sample buffer and run on 12 % polyacrylamide gels before being transferred to a nitrocellulose membrane which was blocked with 5 % m/v milk powder then probed with α -His antibody (Alpha Diagnostics HISP11-M) and developed using ECL (Biorad). B, pMOGMAR-20KNHA was transformed in to MG1655 *E. coli* cells and single colonies were cultured in LB at 30 °C, 37 °C and 42 °C with independent cultures grown with the addition of either zero (0) 0.12 mM IPTG (1). Samples were obtained four hours post inoculation and 18 hours post inoculation. These samples were washed and diluted to a final OD₆₀₀ of 0.3 and then added to 2x Laemmli sample buffer and electrophoresed on a 12 % polyacrylamide gel. Protein contents of the gel were transferred using Towbin buffer and wet transfer apparatus to a nitrocellulose membrane and probed with a α -HA antibody (Sigma, H3663).

Having demonstrated that both MogR and GmaR are detectably expressed by Western blot in this experimental system, it was then necessary to study the interaction between the two proteins and what amino acid features could contribute to this.

First, the amino acid sequences for MogR and GmaR (*L. monocytogenes* str. EGD-e) were obtained from KEGG and domain architectures predicted from these sequences using the Simple Modular Architecture Research Tool (SMART) algorithm, shown in Figure 4.20AB. The sequence for GmaR was used to predict its tertiary structure using the Phyre2 algorithm. This was able to predict the structure of amino acids 177-633 in GmaR, shown in Figure 4.20D. A structure of the DNA binding domain from MogR (amino acids 1-162) was obtained previously and it shown in Figure 4.20C.

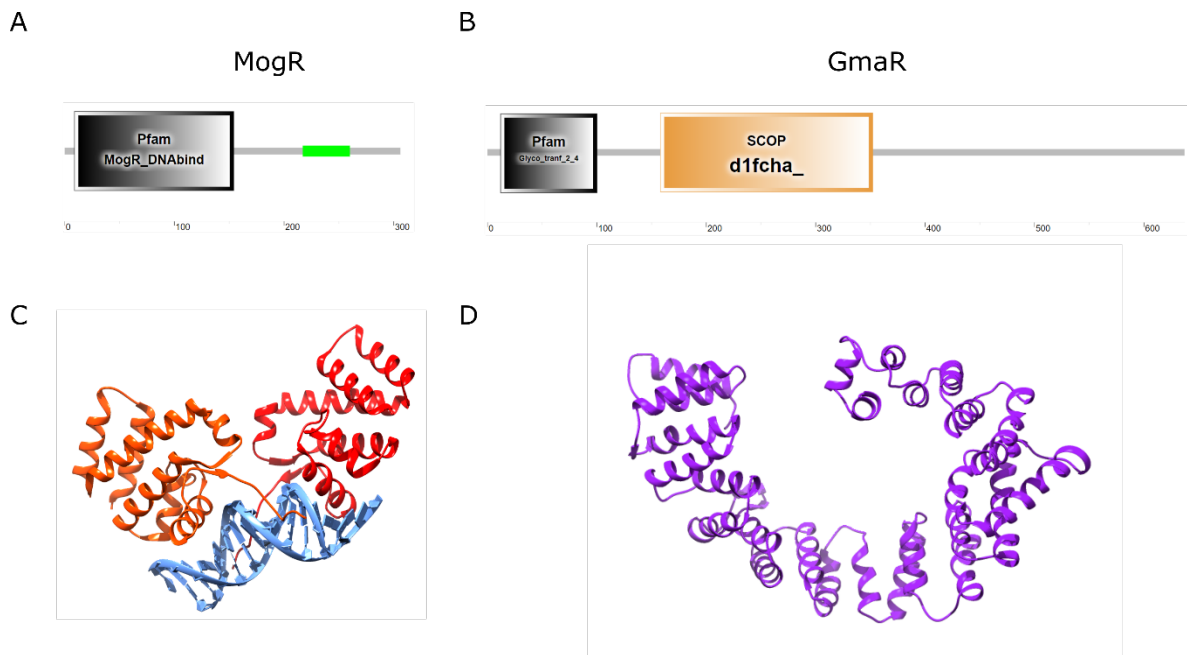


Figure 4.22 MogR and GmaR each contain putative domains for protein:protein interactions

The amino acid sequences for *L. monocytogenes* strain EGD-e orthologues of (A,C) *mogR* and (B,D) *gmaR* were obtained from KEGG and the SMART domain architecture prediction tool was used to produce images of the putative domains present. A,C The Pfam MogR_DNA binding domain is a domain defined by MogR crystallographic data (PDB: 3FDQ, shown in C), and shown in green is a coiled coil region. B The Pfam Glyco_transf_2_4 is a glycosyl transferase domain, in agreement with the function identified in previous work, and the d1fcha_ SCOP predicted domain is a tetracopeptide repeat domain, and D the amino acid sequence for GmaR was obtained from KEGG and entered in to the Phyre2²⁸³ server which predicts this structure at the C terminal region of GmaR (amino acids 177-633) based on homology to the human nata-amino acetyltransferase complex 2.

The putative df1cha Pfam domain in GmaR and the coiled coil region in MogR present the propensity for protein:protein interactions in each of these proteins individually, so it was natural to then study the interaction between them. Work published previously has indicated that MogR and GmaR interact with each other using bacterial two-hybrid experiments²⁷⁷. To challenge this hypothesis, a pull-down method was attempted using an FPLC platform.

In this experiment, MG1655 *E. coli* cells were transformed with pMOGMAR-20K and cultured in 500 mL LB medium with the addition of 120 µg/mL ampicillin and 0.12 mM IPTG at 37 °C overnight. Cells were harvested by centrifugation and then lysed using a cell disruptor, before the removal of debris and unbroken cells by centrifugation. This lysate was then added to a HisTrapFF 5 mL column (GE Healthcare) using an AKTA Pure system to bind the His-tagged MogR and any other proteins that it may be interacting with. Bound protein was eluted from the column using a linear gradient elution to a final concentration of 500 mM imidazole. Samples were collected in 0.5 mL fractions and analysed by SDS-PAGE displayed in Figure 4.22A.

Seen in Figure 4.22A, an extra band at around 75 kDa corresponding to GmaR was observed. This band was excised and analysed by mass spectrometry (Figure 4.22B), which established that the most abundant protein in this sample was GmaR. Western immunoblots were also performed using these samples to verify the presence of His-tagged MogR, Figure 4.22C.

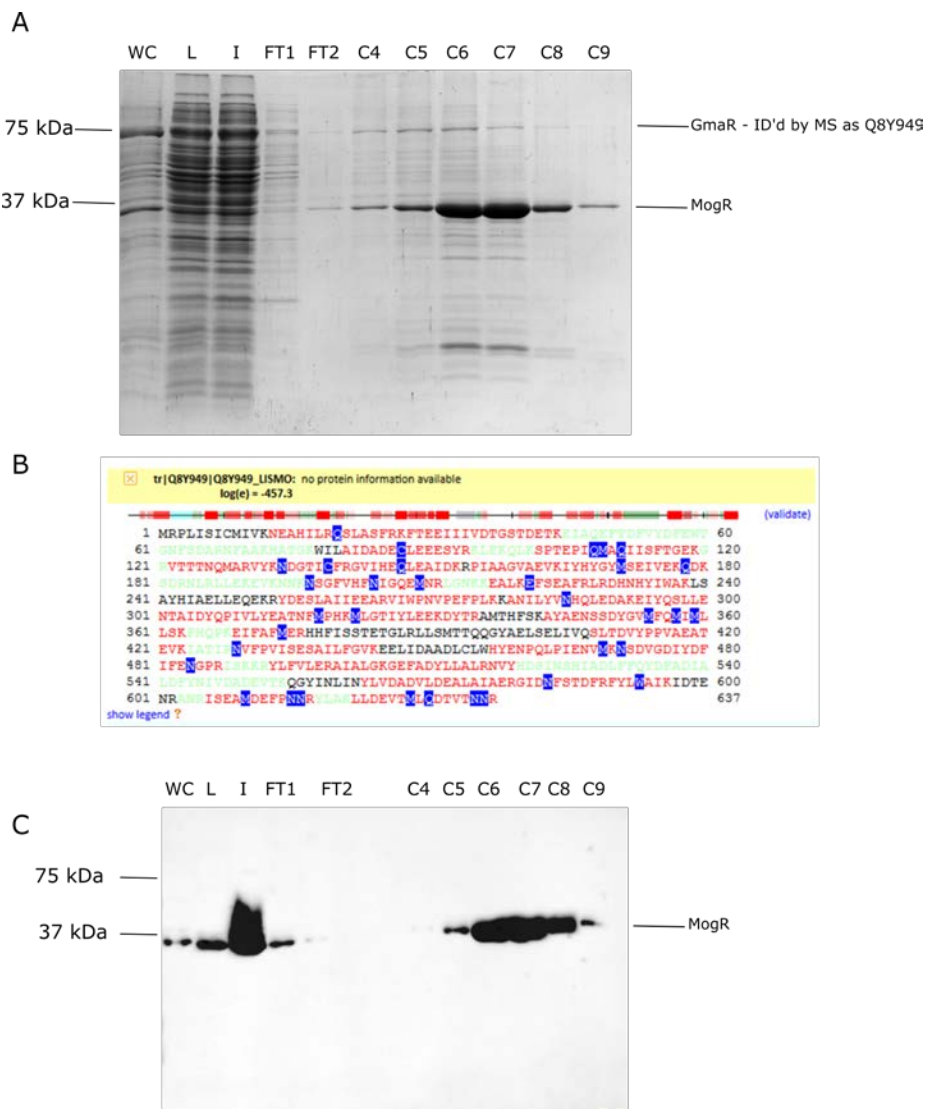


Figure 4.23 GmaR can be co-purified with MogR

A. coli MG1655 cells were transformed pMOGMAR-20K and single colony starter cultures were cultured overnight in LB at 37 °C. These were then used to inoculate a 500 mL culture in LB in a 2 L conical flask which was incubated overnight at 37 °C with 120 µg/mL ampicillin and 0.12 mM IPTG. A 0.5 mL sample was retained for future analysis (WC) then the culture was then centrifuged at 15,000 rpm in (what kind of centrifuge?) and suspended in lysis buffer (50 mM Tris, pH 7.4, 150 mM NaCl, 0.1 mg/mL lysozyme, 0.1 mg/mL DnaseI) before being lysed using a cell disruptor. Unbroken cells and other debris were removed by centrifugation and the supernatant retained for use as lysate. The lysate (L) was added to a HisTrapFF 5 mL column (GE Healthcare) using an AKTA Pure system. Flow through (FT1 and FT2) was collected throughout this process. Protein was eluted using a buffer containing 500 mM which was added over a gradient elution step from 0 - 100 % over 50 mL. A Peak was observed in the region concerning fractions C4 - C9. Samples were then analysed by SDS-PAGE on a 12 % acrylamide gel which was stained using Instant Blue (Expedeon).

B, The bands highlighted in A were excised and analysed by mass spectrometry by Newcastle University Protein and Proteome Analysis (NUPPA), with all identified peptides aligned with the Global Proteome Machine (GPM) database²⁸⁴ to Uniprot²⁸⁵ entries, with hits on the GmaR protein (Uniprot: Q8Y949). Image shows screenshot from GPM results, with predicted peptides in red and green, with those detected in green. 82 % of peptides hit matched this Uniprot entry with contaminant removal.

C, Using the samples under analysis in A, Western analysis was performed. Samples were electrophoresed by SDS-PAGE on 12 % polyacrylamide gels and the protein then transferred using wet transfer apparatus and Towbin buffer to a nitrocellulose membrane. This was then blocked with 5 % w/v milk powder then probed with α -His antibody (Alpha Diagnostics) and developed with ECL, imaged with a Syngene GBox Chemi XX6.

Data in Figure 4.22 is a good indication that MogR and GmaR interact with each other. There is still some ambiguity however about how and why the interaction between MogR and GmaR breaks down at higher temperatures. There are indications in the literature that degradation of GmaR is the factor that liberates MogR at higher temperatures, however there has been no *in vitro* investigation of the interaction between the two proteins at different temperatures. Thus a hypothesis that a temperature dependent conformational change in either MogR or GmaR alters the interaction between the two proteins is yet to be adequately challenged.

To test the hypothesis that MogR and GmaR remain intact but do not interact at 42 °C compared to lower temperatures, a pull down approach was deployed. MG1655 cells were transformed with pMOGMAR-20KNHA and single colonies were pre-cultured overnight in LB at 37 °C. These were then inoculated into a 500 mL culture in LB in a 2 L conical flask. Cells were harvested by centrifugation and then lysed using a cell disruptor. Pull down buffers (50 mM Tris HCl pH8, 50 mM NaCl, 0-500 mM imidazole) were pre-incubated at room temperature, 30 °C and 42 °C. 100 µL of 50 % magnetic α -His resin beads slurry (Amintra Nickel Magnetic Affinity Resin, Expedeon) was applied to 1 mL of lysate which was then incubated for 90 minutes at room temperature, 30 °C or 42 °C. The tube was then added to a MagnaRack and once beads had migrated an “unbound” sample was taken, followed by two washes of the beads with pre-incubated buffer. Protein was then eluted from the beads with three elution steps using pre-warmed buffer at 500 mM imidazole. Samples were then subjected to Western analysis using α -His and α -HA antibodies to probe for the presence of His-tagged MogR and HA-tagged GmaR.

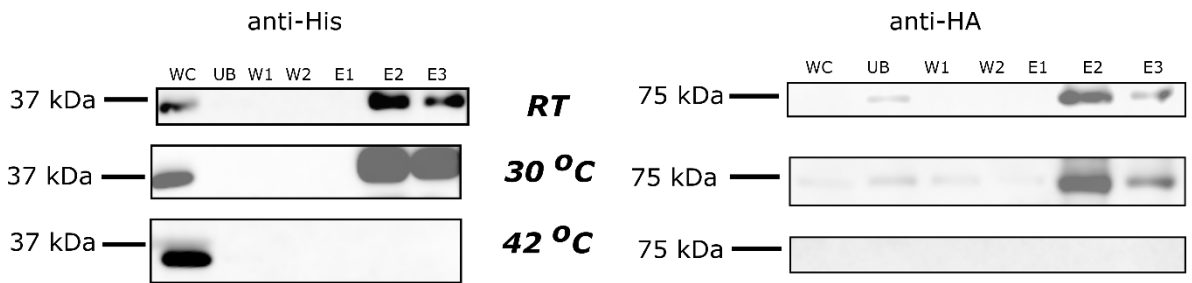


Figure 4.24 MogR interacts with GmaR at room temperature and 30 °C but not at 42 °C

MG1655 *E. coli* cells were transformed with the plasmid pMOGMAR-20KNHA and single colonies precultured at 37 °C overnight. This was used to inoculate a 500 mL LB culture in a 2 L conical with 0.12 mM IPTG and µg/mL ampicillin which was incubated overnight at 30 °C with linear shaking. Cells were harvested by centrifugation then lysed using a cell disruptor. Debris and unbroken cells were removed from the suspension by centrifugation and the supernatant used as lysate (L). The lysate was incubated with Amintra Ni charged magnetic beads at room temperature, 30 °C and 42 °C, after the beads were equilibrated in PD buffer at the same temperature using pre-warmed buffer. Using a magnarack the beads and any associated protein were separated from the lysate and the lysate removed and kept as the unbound fraction (UB). Beads were washed twice in PD buffer (W1, W2) and then three elution steps were performed with PD buffer containing 500 mM imidazole (E1, E2, E3). All of these samples were then subjected to parallel Western analyses using α-His antibody to probe for the presence of MogR and α-HA antibody to probe for GmaR.

Since GmaR was undetectable in each sample collected from experiments at 42 °C in Figure 4.23, this failed to support the hypothesis that both MogR and GmaR remain intact as temperature increases and the change in interaction is driven by conformational changes. The hypothesis was then considered that GmaR is inherently unstable and is degraded more rapidly at 42 °C than lower temperatures.

To investigate this, MG1655 cells were transformed with pMOGMAR-20KNHA and inoculated in to 5 mL LB pre-cultures which were incubated overnight at 37 °C then inoculated in to a 500 mL LB culture with 0.12 mM IPTG which was incubated overnight with linear shaking in a 2 L conical flask at 30 °C. Cells were harvested by centrifugation in four separate volumes and then suspended independently at approximately 0.1 g cells per mL buffer in four different buffers. PDL1 contained 50 mM Tris HCl, pH 8 and 50 mM NaCl alone. PDL2 was the same with addition of protease inhibitor tablets (Roche EDTA free Protease inhibitor), PDL3 identical to PDL1 save for the addition of 5 mM EDTA, while PDL4 contained both 5 mM EDTA and protease inhibitor. By combining these arrangements of protease inhibitors, degradation of GmaR may be analysed and some insight into the class of protease degrading it may be obtained. Cell suspensions were lysed by sonication and the debris and unbroken cells removed by centrifugation. 1 mL of each lysate was incubated at 30 °C and 42 °C for 90 minutes with samples taken throughout the timecourse. These samples were then analysed by Western blots using α -HA antibody.

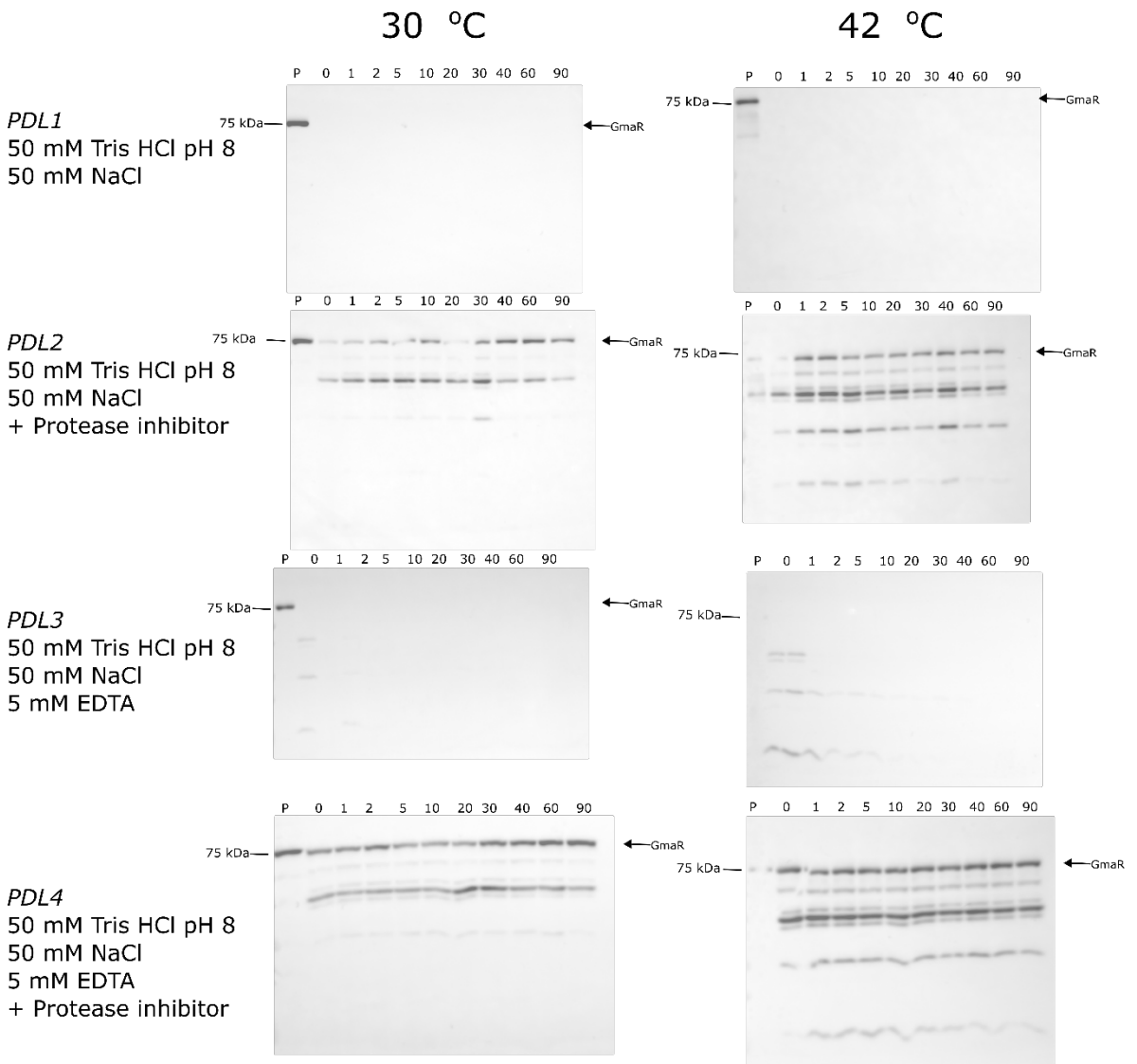


Figure 4.25 GmaR is degraded by proteases

E. coli MG1655 cells were transformed with pMOGMAR-20KNHA and single colonies precultured in 5 mL LB at 37 °C overnight. These were used to inoculate a 500 mL LB culture in a 2 L conical flask with 120 µg/mL ampicillin and 0.12 mM IPTG. The culture was incubated overnight at 30 °C with a 0.5 mL sample taken as the whole cell pellet (P), then cells were harvested by centrifugation in four separate volumes of 50 mL. Each pellet was weighed and suspended in parallel at 0.1 mg cells per mL in a different buffer. PDL1 contained 50 mM Tris HCl, pH 8 and 50 mM NaCl alone. PDL2 was the same with addition of protease inhibitor tablets (Roche EDTA free Protease inhibitor), PDL3 identical to PDL1 save for the addition of 5 mM EDTA, while PDL4 contained both 5 mM EDTA and protease inhibitor. Cells were lysed by sonication and then clarified by centrifugation. The lysate of each of the four suspensions was incubated for 90 minutes at 30 °C and 42 °C with samples taken at 0, 1, 2, 5, 10, 20, 30, 40, 60 and 90 minutes. Each sample was then mixed with 2× Laemmli sample buffer and run on 12 % (w/v) polyacrylamide gels, with the protein in the gel then transferred to a nitrocellulose membrane with wet transfer apparatus and Towbin buffer. The membrane was blocked with 5 % (w/v) fat-free milk powder then incubated with α-HA antibody (Sigma) followed by a secondary α-mouse antibody. The bands were then developed using ECL and the membrane imaged using a Syngene GBox Chemi XX6.

4.3.Discussion

4.3.1.The pC1R7 system needs improved characterisation and optimisation

Results presented in Figure 4.6 indicate that pC1R7 can activate GFP expression at 44 °C when cells are cultured in conical flasks, but not in universal tubes. There are differences between these two culture conditions in aeration and how well shaken the culture will be. Both aeration and shaking should be better in conical flasks in these conditions which may explain this effect. Aeration may influence GFP fluorescence intensity as oxygen is required for maturation of the fluorophore. In this case, gene circuit behaviour may be similar in each culture condition but poorer aeration in universal tubes may be limiting the magnitude of fluorescence.

Beyond this however it is difficult to draw proper conclusions about whether this circuit is effectively activating GFP expression as temperature increases using this data. There was no characterisation of the *PtlpA* promoter in a *tlpA* context. This raises the possibility that the promoter alone is regulated differently at different temperatures regardless of TlpA activity. In future, the *PflaA* promoter should be characterised independently by constructing a plasmid in the same background as pC1R7 which encodes only the *PtlpA* promoter in the absence of any CDS in the region which may be controlled by the T5lac promoter on this plasmid.

Characterisation in defined rich EZ media would also remove background fluorescence from LB cultures and improve repeatability between experiments. Flow cytometry should also be deployed to characterise pC1R7 and any derivatives in these conditions to improve the resolution of our understanding of its behaviour.

In parallel, a synthetic gene circuit using TlpA was produced by the Shapiro group²⁸⁶. This showed effective activation of expression of the relevant promoter at around 44 °C also, but only after around 20 hours of culture. Their plasmid was engineered to respond to ranges of different temperatures and encoded in more complex thermal logic circuits. The rich non-defined media 2YT was used in these studies also which indicated that rich defined media may not be entirely necessary for circuit characterisation, but absolutely favourable to control or understand certain unpredictable factors. There was also some characterisation of the *PtlpA* promoter in this work which vindicated TlpA binding to the *tlpA* promoter with EMSA experiments and found the interesting property of the *PtlpA* promoter to act bidirectionally. There was however no characterisation of the promoter at different temperatures, which is a shortcoming of their study.

4.3.2.The pMOGMAR-20K system is an improved version of pMOGMAR but requires additional optimisation

It was observed that GmaR translation rate may have been lacking in experiments presented in Figures 4.8, 4.9 and 4.10. RBS engineering to improve GmaR translation rates using synthetic RBS design using algorithms made publicly available at DeNovoDNA improved the antirepressive effects observed as seen in Figures 4.14, 4.15, 4.17 and 4.19 in the production of pMOGMAR-20K. This study was partially analogous to some of the biological experiments performed to test the DeNovoDNA RBS design algorithm²⁸⁷.

In an elegant set of experiments, sadly relegated to supplemental material²⁸⁸, synthetic RBSs were designed to control translation of a range of fluorescence proteins. Regimes were set forth where RBS sequence was unaltered but CDS context was changed, and RBS sequence changed but CDS context maintained. In experiments where CDS context remained unchanged, analogous to this work where synthetic RBS were applied to the same *gmaR* coding region, the effect of RBS strength appeared to plateau at a predicted dG_{Tot} (which describes the combined free energy of interaction between mRNA and ribosomes, mRNA and itself) that is far below that of pMOGMAR-20K. Interestingly, pMOGMAR-20K was the best performer. There are a few possible explanations for this. There was actually no quantification of GmaR expression under divergent RBSs in this work, only inferences made from anti-repressive phenotypes associated with GmaR protein production. It is possible that in pMOGMAR-20K plasmids, the *gmaR* RBS may have an excessive strength in a monocistronic context, however mRNA structure or stability may be affected by the presence of the upstream *mogR* CDS.

The DeNovoDNA RBS calculator only considers 16 nt upstream and downstream of a designated start codon. Structural prediction of the MogR and GmaR encoding mRNAs in pMOGMAR variants may reveal regions of *mogR* that affect the ability of the *gmaR* RBS to bind ribosomes in pMOGMAR-10K but not pMOGMAR-20K. To our knowledge, there has not been any characterisation of the efficacy of the DeNovoDNA RBS calculator in polycistronic contexts and this work may have revealed this shortcoming.

4.3.3.Flow Cytometry is an insightful tool for genetic circuit characterisation

The use of flow cytometry compared to platereader quantification of GFP expression in pMOGMAR expressing cells provided unparalleled insight into the circuit behaviour compared to other work presented here. This technology allowed examination of individual cells to produce great

insight to circuit behaviour. Figure 4.18 shows geometric mean of fluorescence measured in samples *en masse*. This is analogous to a platereader measurement and showed similar results, where only upon normalising these measurements to the internal standard pFLA-gfp data did appear to show the desired repression upon temperature increases. This does not unlock, however, the entirety of the potential of this data.

By examining histograms of proportions of cells it is clear that pMOGMAR-20K at exponential phase with IPTG at 30 °C forms populations of cells that are phenotypically distinct with respect to GFP expression to those grown at 42 °C. It was possible to quantify this by using data from pFLA-gfp expressing cells to produce an “ON” gate which defined the “on” state for the circuit. This showed that under these conditions almost all cells (>99%) were in the “on” state at 30 °C while at 42 °C almost no cells (<5%) were. This was demonstrably dependent on IPTG application where uninduced pMOGMAR-20K expressing cells showed similar proportions in the “on” state at 30 °C and 42 °C compared to pFLA-gfp expressing cells. Interestingly, using this metric, the decreased proportion of “on” pMOGMAR-20K expressing cells at 42 °C seemed to hold fairly well up until stationary phase. Using this metric, this might indicate that pMOGMAR-20K is a robust circuit that can maintain its state over long periods. This requires more investigation however. By using a turbidostat like platform, cultures may be maintained and monitored over long periods. Despite this however, looking at histograms in Figure 4.17, there are obvious differences between populations of cells expressing pMOGMAR-20K at 30 °C and 42 °C at stationary phase compared to exponential phase. Peaks in these figures are broader compared to those observed in exponential, indicating a larger degree of heterogeneity in GFP expression at this growth phase. This might be explained by stresses exerted upon cells by high cell densities at stationary phase that promote divergence of physiology away from non-essential programs such as that encoded by pMOGMAR and its variants. Indeed, it is possible that there are sub-populations of cells that have completely obviated attention to pMOGMAR expression or regulation and any GFP measured at this point is what is left over in cells. There is a significant area in these histograms of cells which contain reduced GFP, these cells may be those which have disposed of or mutated the plasmid such that GFP is no longer expressed at all and all that is left is GFP which is reduced in cellular concentration only by cell division due to its remarkable stability. If the plasmid has been mutated however it may be expected that a population of cells arises with enormously increased GFP expression, however this is unlikely as mutations like this are unlikely to be selected for.

Where pMOGMAR-20K seemed to show maintenance of “on” state from exponential phase through to stationary phase, pMOGMAR showed around 22 % of cells in the “on” state at 30 °C with IPTG, which was reduced at 42 °C under the same conditions, which was lost almost entirely

by stationary phase. The lack of properly defined RBS controlling GmaR translation in this circuit may lead to a greater likelihood of mutations to occur that would prevent its expression. Put simply, there are few defined factors controlling its translation in the first place, so any change at the nucleotide level could abolish *gmaR* translation entirely. Again, it is also just as likely that any one mutation could occur that would promote GmaR expression, however by stationary phase, this is unlikely to confer any selective advantage and thus these cells would be removed from the population.

Examination of histograms also gives invaluable insight to the *PflaA* promoter. At 42 °C, flow cytometry data revealed that expression from this promoter appears somewhat noisy at both exponential phase and stationary phase. When cultured at 30 °C, a single peak is seen in these histograms, however at 42 °C an additional peak is observed at the bottom end of the GFP fluorescence scale. This peak at the low end of the scale is maintained also under all conditions where pMOGMAR variants were cultured at 42 °C. In pFLA-gfp expressing cells under these conditions, additional cells were observed at virtually every spot on the GFP fluorescence scale at 42 °C. This is an indication that *PflaA* is very strong promoter that at the somewhat stressful temperature of 42 °C is subject to downregulation or mutation that produces this degree of heterogeneity observed in figure 4.17.

It is also interesting that the best level of repression seen using pMOGMAR plasmids was at 42 °C. The native system was studied in *L. monocytogenes* with “on” and “off” states at 30 °C and 37 °C respectively²⁷⁷. It is possible that in *L. monocytogenes* extra endogenous genetic factors, which are not encoded by the *E. coli* genome in models used here, contribute to inhibiting *PflaA* and related promoters in a temperature sensitive manner. For example, the master regulator DegU, which is absent in *E. coli*, has been demonstrated to have a role in this regulon too¹²⁰. Alternatively it may be possible that this is a new discovery about how the MogR:GmaR system coordinates temperature based stimuli, with it having one switch sensitive to host body temperature, and another sensitivity to fever conditions. This hypothesis of course would require further investigation in *L. monocytogenes*.

4.3.4. Improving the pMOGMAR-20K reporter

Despite promising results seen in flow cytometry experiments discussed above, it is clear that *PflaA* promoter activity still needs improvement at 30 °C. This is made clear by the reduced level of GFP fluorescence seen in flow cytometry and plate reader experiments displayed in Figures 4.14 and 4.19.

The use of an IPTG sensitive promoter may not be the best approach in synthetic gene circuits. This has facilitated comparison between induced and uninduced states, but control of the T5lac promoter by IPTG occurs in a saturating exponential fashion. Additionally, it is clear in this work that the T5lac promoter is at least slightly leaky. For this reason pMOGMAR variants should be produced that make use of constitutive promoters of varying strength, with *mogR* and *gmaR* expressed as discrete transcriptional units. The Andersen library of promoters is a commonly deployed library of promoters like this with good characterisation data and is readily available as part of the iGEM distribution kit and registry of standard parts²⁸⁹. Additionally, there are a range of RBSs that are available as part of other genetic part kits such as the CIDAR MoClo kit²⁹⁰ that these promoters may be combined with alongside *mogR* and *gmaR* in a combinatorial design producing a library of many hundreds that could be screened using FACS for desired properties or selection using the *PflaA* promoter controlling expression of an antibiotic resistance, or auxotrophy complementing gene.

The pQE80L plasmid was used as the backbone in pMOGMAR plasmids. This is a high copy vector and may cause increased burden on cells. This at first thought may be a good reason to change to a single or lower copy vector, or encode the circuit on the chromosome. However, modelling work has indicated that the genomic and molecular geography inside the cell can influence the efficacy of transcription factors and synthetic gene circuits^{291–293}.

Reviews by field leaders^{271,294} have resolved that low copy number of genetic elements (CDS, promoters, etc), proteins, or other small molecules contributes to high levels of noise in both synthetic gene circuits and naturally occurring programs too. Experimental data has demonstrated that these levels of noise can cause circuit instability, and even mutation in the plasmid towards the circuit state which confers a selective advantage²⁹⁵.

High copy vectors provide a high copy number of each gene encoded and thus better expression of them, along with greater physical number of the promoters they control, giving better chances that they will find each other. However stochastic transcription from promoters unoccupied by MogR in pMOGMAR contexts cannot be avoided in this case.

Moving the pMOGMAR circuit in to a different plasmid context with a reduced copy number could reduce this effect. It may be assumed that expression of GmaR and MogR as well as GFP reporter expression would be affected in a linear fashion in this regard, however some studies have observed that copy number fluctuation can cause unpredictable changes in gene expression or activity of the genes encoded²⁹⁶.

Additionally, other modelling work indicates that genetic locality defined by nucleotide distance (rather than nm distance) also influences the efficacy of transcription factors on their respective promoters. The closer a promoter is to the genomic location in nucleotides of the CDS of a transcription factor controlling it, the more effective that transcription factor becomes. The advantage of this effect is calculated to deteriorate beyond around two kilobases²⁹². By placing the *PflaA* reporter module in between transcriptional units controlling *mogR* and *gmaR* it may be possible to enclose the *PflaA* promoter within this two kilobase region that would increase efficacy regardless of copy number.

4.3.5.A model of the circuit encoded by pMOGMAR-20K

Data presented in Figures 4.20-24 have attempted to define effectively the factor that increased transcriptional repression by MogR at increased temperatures. This ultimately sought to define the factor that causes the breakdown in interaction between MogR and GmaR. When lysates were incubated at 42 °C, it was not possible to purify MogR, let alone GmaR along with it. This could indicate that each of these proteins are unstable at this temperature. Repeating this experiment using lysate incubated at 37 °C, as the system was originally studied in *L. monocytogenes* may produce different results. Another interpretation of this is that both proteins are unstable at this temperature and each require an interacting partner to stabilise at this temperature. MogR crystal structures in association with DNA indicate that it is a functional repressor as a dimer, so MogR homodimerisation at elevated temperatures may stabilise it. This hypothesis favours a conformational change in either MogR or GmaR that would promote GmaR dissociation from MogR and turnover, leading to MogR homodimerisation under these conditions. Identifying the stoichiometry of the MogR:GmaR interaction would aid investigation of this hypothesis.

Nonetheless, MogR mediated repression was evident at 42 °C in Figures 4.14, 4.17 and 4.19. This may be explained by *in vitro* factors destabilising the MogR protein. For example, the destruction of its interacting partner GmaR, if this is occurring in these conditions, or the lack of stabilising DNA produced by DnaseI addition in lysis buffers.

Using data in Figure 4.24 that investigates GmaR stability in the presence of different protease inhibitors at different temperatures it was possible to conclude that GmaR is degraded readily by cellular proteases, with cytoplasmic, non-metal binding proteases being the most effective at this. Another control indicating degradation rate of a relatively stable protein under the same conditions would be helpful to deduce if GmaR is inherently unstable. It is not possible to conclude beyond any doubt however that GmaR is any more degraded at 42 °C than at 30 °C. In fact, degradation appears to have occurred already at the zero timepoint, which indicates that at the instant of lysis, degradation by these proteases has begun.

If GmaR is intrinsically unstable, its interaction with MogR at cooler temperatures could stabilise it, in alignment with work in *L. monocytogenes* *in vivo*. A conformational change in either MogR or GmaR could still be occurring that causes the interaction to break down, followed by GmaR degradation.

There have been studies of GmaR by circular dichroism (CD) over a range of temperatures that permit the theory that temperature influences GmaR structure *in vitro*. Mutants of GmaR should be produced by random mutagenesis and selected to find a variant that interacts with MogR independent of temperature. Structural analysis of the protein produced by this allele by CD over a range of temperatures would reveal whether a structural change is involved in the breakdown of this interaction.

Because Figure 4.24 supports the hypothesis that GmaR is degraded similarly *in vitro* at either 30 °C or 42 °C, it was possible to conclude that a conformational change in GmaR is the most relevant factor mediating the change in interaction between MogR and GmaR. *In vivo* detection of GmaR seen in figure 4.21 was demonstrated at 30 °C and 42 °C, while under similar conditions (Figures 4.14, 4.15, 4.17 and 4.19), phenotypes indicative of MogR dependent transcriptional repression were observed. This would indicate that either MogR is far in excess of GmaR under these conditions, or that GmaR is present but not in a conformational state coherent with an interaction with MogR.

It is possible then to build a speculative model as a synthesis of data produced in the work presented here and work performed studying the *L. monocytogenes* system. MogR is a transcriptional repressor that represses transcription of specific genes bearing the TTTT-N₅-AAAA motif such as *PflaA*. GmaR interacts with MogR at 30 °C but not at 42 °C, causing derepression of these promoters at 30 °C. This breakdown in interaction is governed by changes in conformation in GmaR.

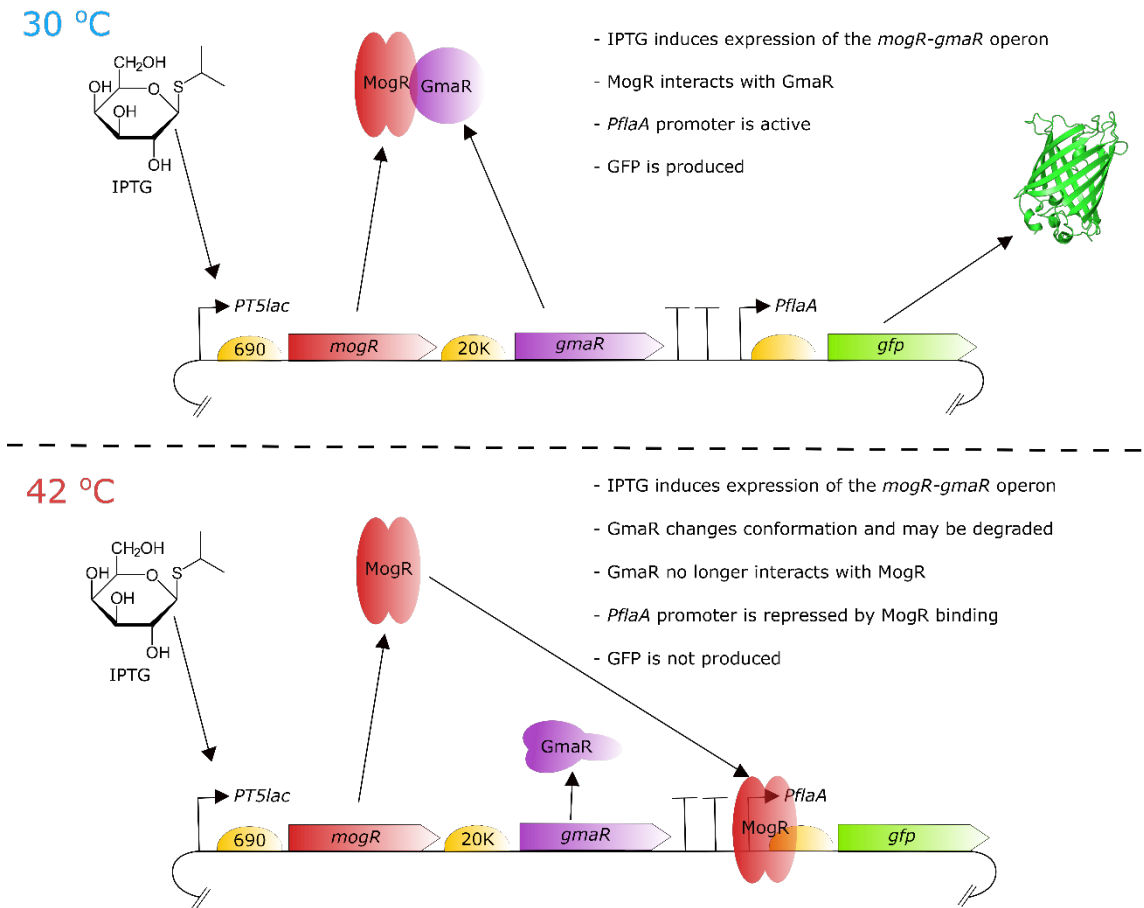


Figure 4.26 pMOGMAR-20K produces GFP at 30 °C and does not at 42 °C

At 30 °C, IPTG induces transcription from the T5lac promoter, leading to expression of MogR and GmaR, with translation governed by RBSs with TIRs of 690 with respect to *mogR* and 20,000 with respect to *gmaR*. GmaR and MogR proteins interact with each other. The *P_{flaA}* promoter is free for transcription by RNA Pol and GFP is expressed. At 42 °C, IPTG induces expression of MogR and GmaR proteins, but interaction between the two is broken down, caused by possible conformational changes in GmaR and also potential degradation of GmaR. This leaves MogR free to interact with the *P_{flaA}* promoter and repress transcription from it, inhibiting GFP expression.

Chapter 5:
Future Work

5.1.The Future of Remote Control of Gene Circuits (RC/GC)

5.1.1.A Prototype RC/GC model using pMOGMAR-20K and Mms6

The over-arching aim of this thesis was to design and characterise tools that would allow magnetically stimulated remote control of genetic circuits (RC/GC). By pulling together work from Chapters 3 and 4 it may now be possible to produce a prototype platform for this based on bacterial transcription. Chapter 3 demonstrated that production of Mms6 in *E. coli* cells can induce *de novo* magnetism, so by combining this with the temperature-dependent transcriptional responses attributed to the pMOGMAR-20K system we may now be close to having the initial tools to examine the effect of magnetic hyperthermia on bacterial transcription.

The remaining question that surrounds the pMOGMAR-20K reporter system relates to how dynamic it can be. In this work, the pMOGMAR-20K system has only been studied as a comparison of cultures grown in parallel at different temperatures. In order to study the capability of a single growing culture to switch between expression ‘ON’ and ‘OFF’ states (such as the states quantified by flow cytometry in Figures 4.17 and 4.19) upon temperature changes a turbidostat experimental set up should be produced. The most reliable and robust characterisations of all pMOGMAR plasmids have considered cells which are at exponential phase. By deploying a turbidostat, the idea is that pMOGMAR-20K containing cells could be maintained in an exponential phase-like state indefinitely. Approaches like this have been used by other investigators in synthetic biology^{297,298} and is favoured by mathematical modellers for its supposed maintenance of a steady state (i.e. constant growth rate, constant concentrations of proteins and their activities *etc.*). Turbidostat devices have been invented for exactly this purpose and many of their designs are open source^{297–300}. Otherwise, exponential phase may be maintained manually by continual dilution of a culture once a pre-determined OD₆₀₀ has been reached or simply at intelligently informed time points.

Specifically, for a pMOGMAR-20K experiment, cells would be maintained at exponential phase at 42 °C, until a constant level of GFP fluorescence has been reached. GFP levels could be determined either by calculations of promoter activity using plate reader measurements as in Figure 4.14, or by flow cytometry as in Figures 4.17, 4.18 and 4.19. Based on the present evidence, a promoter activity of around 0.1 (or around 7 % of cells in an “ON” state) would be the aim to be maintained over a period of many dilutions. Once this has been established, the temperature would be changed to 30 °C, which, based on the evidence described here, would be expected to produce around 99 % of cells in an “ON” state (e.g. Figure 4.19) and a promoter activity of around 0.75. The time taken to reach these benchmarked values in the turbidostat will indicate how dynamic the circuit is.

The dynamic capabilities of the pMOGMAR-20K system would also be greatly aided by the addition of degradation tags on the proteins GmaR, MogR and GFP. This may optimise response time to temperature changes where proteins are more rapidly turned over and would aid the study of system dynamics. This approach would be most useful in the case of the GFP reporter, which has been described as having a high level of stability in cells and is proposed only really to reduce in cellular concentration through cell division induced dilution of the protein³⁰¹. Degradation tags have been deployed in synthetic gene circuits previously^{42,63,64}, where the *ssrA* tag sequence is frequently used. The SsrA tag is a motif added by the ssRA RNA that rescues stalled ribosomes and facilitates interaction with the chaperone SspB. The SspB protein then introduces SsrA-tagged proteins into the ClpXP proteolytic apparatus. A range of synthetic versions of the *ssrA* tag have developed , which alter the affinity of the interaction with SsrB, that have allowed tunable protein turnover rates to be engineered^{36,301}.

Another improvable aspect of pMOGMAR-20K is the *PflaA* promoter. The activity of the *PflaA* promoter was seen to produce heterogeneous populations of cells with respect to GFP production (Figure 4.17). Indeed, in all plasmids tested, at 42 °C, an additional population of cells was observed that exhibited little to no GFP expression. When taken together with analysis of the growth rate of pFLA-gfp containing cells, it is hypothesised that there is perhaps a metabolic burden effect induced by the strength of this promoter. Analysis of the *PflaA* promoter's strength in parallel with the Andersen library of promoters²⁸⁹ by qPCR methods would aid investigation of this hypothesis. Should *PflaA* prove to be causing a metabolic burden effect, promoter engineering could be performed. Work by Mannan *et al*⁴³ has combined strong promoter elements with mutagenized binding sites for LacI to produce libraries of promoters with differing sensitivities and dynamic ranges in response to IPTG. MogR has a well-defined DNA recognition sequence²⁷⁵ (as LacI does) thus raising the opportunity to combine engineering binding affinities with other diverse promoter elements to produce synthetic MogR-sensitive promoters with reduced burden effects. Alternatively, recent work has used a burden-responsive transcriptional regulon to activate a dCas9 transcriptional repressor system³⁰². This study examined transcriptomic data and discovered that the *htpG1* promoter of *E. coli* is highly active under conditions where heterologous pathways cause growth or metabolic defects. The *htpG1* promoter was then placed in control of a guide RNA that directed dCas9 to occupy the promoters of the heterologous elements suspected of causing the metabolic burden. This approach could be modified to produce a *PflaA* targeting guide RNA to dynamically regulate any burden caused by this promoter.

5.1.2.RC/GC Applicable Apparatus from the Broader Field

In the course of preparing this thesis two independent papers from the Shapiro group have produced tools analogous to those delineated in Chapters 3 and 4^{197,286}. First, the synthetic enzyme FLPM6A was designed and characterised. When expressed in *E. coli* this synthetic enzyme produced cells with increased magnetic properties that were described as “ultraparamagnetic”¹⁹⁷, a definition that might also cover the phenotype seen upon Mms6 production in Figure 3.9. Cells expressing Mms6 or FLPM6A should be placed in oscillating magnetic fields to test if they are susceptible to magnetic hyperthermia. A set up could be prepared using an infra-red thermometer and an oscillating field coil which encases a reaction tube. By pointing the thermometer’s beam at the centre of the coil, the temperature in the centre could be measured *in situ* in real time.

Second, synthetic temperature responsive circuits were reported using the TlpA protein and its native promoter, as in Figures 4.5 and 4.6. This circuit was developed further by mutation of the *tlpA* promoter region and artificial selection to alter the temperatures to which the circuit was responsive, providing a range of temperature-activated circuits²⁸⁶. By combining “ultraparamagnetic” cells with the new TlpA-containing circuits and pMOGMAR-20K, an apparatus for testing a magnetically stimulated genetic circuit is plainly now available.

5.1.3.The Glass Catfish and its Genetically-Encoded Electromagnetic Perception

Recently, a gene conferring sensation of magnetic fields to the glass catfish *Kryptopterus bicirrhosus* was discovered¹¹⁰. Glass catfish were demonstrated to be capable of sensing and responding to magnetic fields, both static and oscillating, when they were observed to physically avoid magnets placed in or near their aquarium¹¹⁰. By cloning cDNA from mRNA isolated from the electrosensitive anal fin, it was possible to alter current responses to magnetic stimulation by expression of a specific subset of the cDNA clones in a *Xenopus laevis* oocyte model¹¹⁶. Analysis of this set of cDNA clones identified a small gene product of 15 kDa that was proposed to be responsible for the electromagnetic perception phenotype and thus named Electromagnetic Perception Gene (EPG).

Purification of the EPG protein product from *E. coli* cells and biophysical analysis of the protein did not reveal any structural changes in response to static magnetic fields in circular dichroism experiments¹¹⁰. The presence of Fe in the protein was also not supported by any experiments, nor did bioinformatic predictions of the protein's structure predict the presence of any Fe-S clusters¹¹⁰. Nonetheless, expression of EPG in human embryonic kidney cells reproduced a form of magnetic sensitivity. By using the Ca²⁺ reporter fura-2/AM, EPG-expressing cells were seen to alter their intracellular Ca²⁺ levels in response to magnetic fields. The Ca²⁺ was proposed to originate from both an extracellular location and from the Ca²⁺ storing endoplasmic reticulum, substantiated through the employment of specific transporter inhibitors. EPG could also elicit magnetically influenced changes in neuronal signalling in a tissue culture model and an *in vivo* rat brain study¹¹⁰. These results propose the hypothesis that the EPG product interacts with Ca²⁺ channels in a manner that is influenced by magnetic fields. Mechanistic detail of this however is, as yet, elusive.

The study by Krishnan *et al*¹¹⁰ had clinical aspirations, however reconstitution of the EPG protein's activity in a microbial context would be useful two-fold. First, microbial expression could provide an excellent model for studying the EPG mechanism, where there are few homologs of mammalian neuronal specific genes, and a minimal set of genetic elements required for the phenotype could be assembled. This minimal set could then inform the application of EPG in a clinical context, either for use in medicinal backgrounds or as a laboratory tool. In parallel, however, the assembly of a minimal set of genes required for the EPG phenotype in microbial contexts would provide an excellent launch pad for developing a magnetically stimulated genetic circuit for use in biotechnology. If microbial Ca²⁺ import can be controlled using magnetic stimuli, a Ca²⁺ responsive transcriptional program could be initiated downstream. Furthermore, study of the biochemical interaction between EPG and these putative Ca²⁺ transporters could allow engineering of other proteins to respond to EPG too.

5.2.New Projects Inspired by This Research

5.2.1.Development of a Pd-based reporter for H₂ production

In Chapter 2, Pd(II) reduction by *E. coli* strains was studied. During the course of these experiments, it was observed that two different colour changes happened during the reaction. First, a bacterial suspension containing Pd(II) changed colour from pale yellow to colourless during Pd-NP formation (after the nanoparticles were removed). And second, the suspended Pd-NPs were black. Thus a yellow colour was lost, and a black colour was gained. It is possible that these colour changes could be of use in the discovery of novel hydrogen or hydrogenase-producing clones or organisms. In particular, a high-throughput colourimetric assay would be very useful in selecting hydrogenase-positive clones from either laboratory-based engineering efforts, or from unknown isolates from environmental samples, or from genes identified from meta-genomic explorations.

To characterise the colour changes further, Hungate tubes were filled with 5 mL MOPS buffer, formate and Pd(II). They were then incubated overnight with various bacterial strains before 200 uL samples of the suspensions were analysed by spectroscopy (Figure 5.1). The results show that sterile (no cells) controls produced an absorbance peak at 340 nm, which was also present in samples containing non Pd-NP forming FTD150 cells (no FHL enzyme) and FTD89 samples where formate was not included (limited FHL activity). The absorbance peak at 340 nm was quenched in conditions where Pd-NPs were formed (Figure 5.1). Thus, a peak at 340 nm could only be produced in conditions studied that include Pd(II) salts, but not where H₂ could be produced. In conditions where Pd(II) salts are present and H₂ can be produced (*i.e.* in Figure 5.1AB), the absorbance at 340 nm is reduced compared to when formate is not added, and H₂ evolution is not possible. In these samples Pd-NPs are also visibly present in the sample as a black precipitate.

In this system, it has been demonstrated that Pd(II) precipitation to Pd-NPs produces a colour change from pale yellow soluble Pd(II) to black precipitated Pd-NPs in a colourless suspension. This could be followed by loss of absorbance at 340 nm upon H₂ production in these experiments (Figure 5.1). It is possible that this property of the reaction could be exploited to develop a new protocol for screening for Hyd-3 active phenotypes. This would be useful as a counter screen when engineering metabolic pathways for H₂ production, samples with broken H₂ producing activity would be easily distinguishable either by eye or machine in a high throughput way. Alternatively, it might be used to screen for H₂ producing phenotypes in varying cultivation conditions in model organisms, or for identifying previously uncultured organisms with H₂ producing properties.

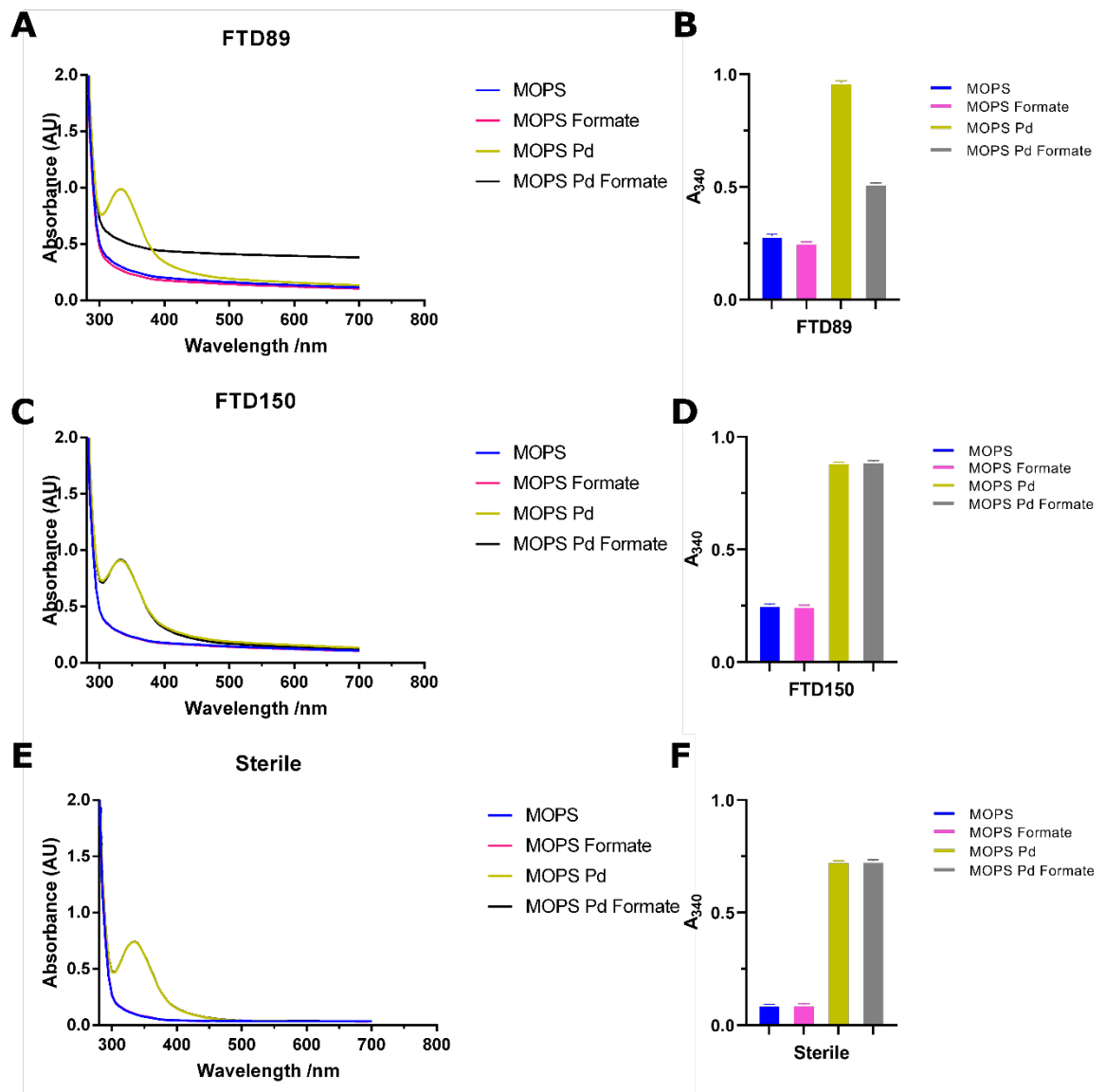


Figure 5.1 An absorbance peak at 340 nm is diminished upon Pd-NP formation

(A, B) Cells of *E. coli* strains FTD89 (FHL⁺) (and (C, D) FTD150 (FHL⁻), and (E, F) sterile controls, were suspended in MOPS buffer containing 0.2% (w/v) formate, 0.75 mM Pd(II) or both and incubated overnight at 37 °C. Samples from each treatment were then analysed by measuring absorbance over spectra from 280 – 700 nm.

5.3. Concluding Remarks

While there has been work presented in this thesis, and by other investigators, in to the development of temperature sensing transcriptional programs using proteins²⁸⁶, other mechanisms could be used. RNA-based thermometers that have structural elements which occlude a RBS until resolution by the appropriate temperature have been investigated extensively^{304,305}, with effective *in silico* prediction of melting temperatures³⁰⁵. These could also be deployed in magnetically-stimulated transcriptional program.

Beyond transcription however, specific proteins may be inactivated or activated by temperature changes. For example, a change in temperature could activate an enzyme, or change a protein:protein interaction influencing a pathway. Classical Michaelis-Menten enzyme kinetic models suppose that each enzyme has an optimum temperature for activity. By maintaining cells at temperatures below this (for example using mesophilic *E. coli* harbouring an enzyme from a thermophile), magnetic hyperthermia could be used to transiently increase local intracellular temperature leading to a spike of specific enzymatic activity.

Recently, a genetically encoded mechanism for producing gas vesicles originally identified in photosynthetic aquatic bacteria was reconstituted in *E. coli*³⁰⁶. These have been demonstrated to be useful as ultrasound contrast agents *in vivo*^{306,307}. Reviews on the topic of biological responses to ultrasound have proposed a “sonogenetic” mechanism, which could act analogously to magnetogenetics³⁰⁸. By sonogenetic mechanisms, millimetre scale areas can be heated by ultrasound with genetically encoded downstream functional effects²⁸⁶.

A synthetic pathway that produced 2,3,-butanediol in an enantiomerically pure (R,R) composition was recently found to be limited by conventional IPTG controlled mechanisms³⁰⁹. (R,R)-2,3-butanediol is a useful fuel precursor and industrial solvent precursor. This pathway combined enzymes from *Bacillus subtilis* and *Klebsiella pneumoniae* to divert pyruvate towards (R,R)-2,3,-butanediol production through acetolactate synthase and acetolactate decarboxylase from *B. subtilis* and a butanediol oxidase from *K. pneumoniae*. This was a useful development where in the native organisms, these substrates are involved in the pentose phosphate pathway and the enzymes are reversible, making it difficult to build up the product. When these enzymes were placed under the control of a IPTG sensitive *trc* promoter, IPTG addition was seen to reduce (R,R)-2,3-butanediol production by about three quarters compared to its absence. Enzyme activities were measured from crude lysates of cells expressing the pathway and found that there was no general defect in enzyme activities when cells were grown in IPTG and all enzymes were expressed. A burden effect was the proposed cause of this where IPTG caused over expression of the enzymes, causing detrimental

carbon flux away from central metabolism³⁰⁹. By implementing a RC/GC mechanism to control this pathway, subtler and more sophisticated control may be achieved. Cells could be stimulated at precise time intervals to produce an iterative biodynamic program of building biomass, pathway activation and performance, followed by biomass recovery. RC/GC mechanisms could also provide dramatically subtler induction of this pathway such that it is more effective than it is with IPTG activation, or without.

Besides high value metabolic products, magnetogenetic pathways could be utilised in bio-integrated electronic platforms or materials. Biological systems can coordinate far more chemical stimuli than electronic analogues can. Using magnetogenetic pathways, an electronic device could influence the behaviour of a biological component, making biological elements part of the array of components that can be compiled in to microelectronic devices.

Engineered microbes that live inside futuristic building materials have already been shown to be able to contribute to dynamic changes in the material^{310,311}, however by integrating a magnetogenetic component, they could respond dynamically in synchronicity with, and informed by, developing “smart home” devices.

Chapter 6:
Materials and Methods

6.1. Microbiological Methods

6.1.1. Bacterial Culture Methods

Routinely, *E. coli* strains were cultured on solid LB media with the recipe 10 gL⁻¹ NaCl, 10 gL⁻¹ tryptone and 5 gL⁻¹ Yeast Extract and 1 % (m/v) agar. Liquid LB cultures were grown in LB to this recipe with the exception of agar. A single colony was removed from an agar plate and added to 5 mL LB for starter cultures or minipreps. All medias were autoclaved and cooled prior to culturing. Cultures were then incubated overnight at 37 °C with rolling agitation.

When required, 125 mg/mL ampicillin dissolved in water added to a final concentration of 125 ug/ml to cooled media, or 50 mg/mL kanamycin diluted to a concentration of 50 ug/mL where appropriate.

Larger LB cultures used in certain experiments were diluted 1 in 100 unless stated otherwise, in to the appropriate volume of LB in a conical flask with 200 rpm orbital shaking.

Table 6.1 Media Recipes used for bacterial cultivation in this thesis

Medium	Components	Final Concentration	Sterilisation
Lysogeny Broth (LB)	NaCl Tryptone Yeast Extract	10 g/L 10 g/L 5 g/L	Autoclave
LB agar	NaCl Tryptone Yeast Extract Agar	10 g/L 10 g/L 5 g/L 1.5 % (w/v)	Autoclave
M9 media	CaCl ₂ MgSO ₄ Cas-amino acids Andreasson's Trace Elements solution	0.1 mM 2 mM 0.4 % (w/v) 0.1 % (v/v)	Filtered Filtered Autoclave Filtered
EZ Media	Tricine (MW 179.2) Iron Sulfate Ammonium Chloride Potassium Sulfate Calcium Chloride Magnesium Chloride Sodium Chloride Ammonium Molybdate Boric Acid Cobalt Chloride Cupric Sulfate Manganese Chloride Zinc Sulfate Potassium Phosphate Dibasic, Anhydrous Potassium Hydroxide Adenine Cytosine Uracil Guanine L-Alanine L-Arginine HCl L-Asparagine L-Aspartic Acid, Potassium Salt L-Glutamic Acid, Potassium Salt L-Glutamine L-Glycine L-Histidine HCl H ₂ O L-Isoleucine L-Proline L-Serine L-Threonine L-Tryptophan L-Valine L-Leucine	4.0 mM 0.01 mM 9.5 mM 0.276 mM 0.5 µm 0.525 mM 50 mM 2.92×10^{-7} mM 4.00×10^{-5} mM 3.02×10^{-6} mM 9.62×10^{-7} mM 8.08×10^{-6} mM 9.74×10^{-7} mM 1.32 mM 1.5 mM 0.199 mM 0.199 mM 0.199 mM 0.8 mM 5.2 mM 0.4 mM 0.4 mM 0.6 mM 0.6 mM 0.8 mM 0.2 mM 0.4 mM 0.4 mM 10 mM 0.4 mM 0.1 mM 0.6 mM 0.8 mM 0.4 mM 0.2 mM 0.4 mM	

L-Lysine HCl	0.1 mM	
L-Methionine	0.2 mM	
L-Phenylalanine	0.01 mM	
L-Cysteine HCl	0.01 mM	
L-Tyrosine	0.01 mM	
Thiamine HCl	0.01 mM	
Calcium Pantothenate	0.01 mM	
para-Amino Acid	Benzoic	0.01 mM
para-Hydroxy Acid	Benzoic	
2,3-diHydroxy Acid	Benzoic	

Sterile on provision,
Combined with filter
sterilised MiliQ H₂O

All were made up using autoclaved deionised water with the exception of EZ media. This was made using the addition of filter sterilised MiliQ water.

Table 6.2 List of bacterial strains utilised in this thesis

Strain name	Species	Genotype	Reference
MC4100	<i>E. coli</i>	F- [araD139]B/r Δ(araF-lac)169 &lambda- flhD5301 Δ(fruK-yeiR)725 (fruA25) relA1 rpsL150(strR) rbsR22 Δ(fimB-fimE)632(:IS1) deoC1	³¹²
FTD150	<i>E. coli</i>	As MC4100, ΔhyaB, ΔhybC, ΔhycE, ΔhyfB-R (specR)	³¹³
FTD89	<i>E. coli</i>	As MC4100, ΔhyaB, hybC	³¹⁴
IC010	<i>E. coli</i>	As MC4100, ΔhyaB, hycE	¹⁴¹
IC009	<i>E. coli</i>	As MC4100, ΔhybC, hycE	¹⁴¹
MG1655	<i>E. coli</i>	F-, λ-, rph-1 , Wild type <i>E. coli</i> , K-12 derivative,	³¹⁵
DH5α	<i>E. coli</i>	F-, φ80dlacZΔM15, Δ(lacZYAargF)U169, deoR, recA1, endA1, hsdR17(rK-, mK+), phoA, supE44, λ- , thi-1, gyrA96, relA1	³¹⁶
C43	<i>E. coli</i>	F- ompT gal dcm hsdSB(rB- mB-) (DE3)	³¹⁷
MC1061	<i>E. coli</i>	araD139 Δ(araA-leu)7697 ΔlacX74 galK16 galE15(GalS) lambda- e14- mcrA0 relA1 rpsL150(strR) spoT1 mcrB1 hsdR2	³¹⁸

6.1.2. Plasmid Extraction

Bacteria bearing the plasmid desired were cultured as stated in 6.1 in 5 mL cultures and were then centrifuged to harvest cells. The pellet was resuspended in 200 uL of the NEB Monarch Miniprep kit resuspension buffer and removed to a clean Eppendorf tube. 200 uL of the lysis buffer from this kit was then added followed by inversion of the tube to mix. Next 400 uL of the neutralisation buffer was added and the tube inverted until the colour was uniformly yellow. The tube was then centrifuged in an Eppendorf Epmotion benchtop centrifuge at 13300 rpm for 5 minutes. The supernatant that developed was added to a supplied NEB Monarch Miniprep column and centrifuged under the same conditions for one minute. The flow through was discarded and 200 uL “Wash 1” buffer was added to the membrane followed by another minute of centrifugation, then the addition of 400 uL of the “Wash 2” buffer and another minute of centrifugation. 30 uL of the provided Elution Buffer was then added directly to the surface of the membrane and incubated at room temperature for approximately five minutes. The column was then added to a clean Eppendorf tube and centrifuged for one minute to elute the plasmid in to the clean tube. The DNA concentration of the resultant elution was measured using a Nanodrop ND1000 (Thermo).

6.1.3. Preparation of Competent *E. coli* cells and their Transformation

A starter culture of the appropriate strain of *E. coli* was prepared and inoculated in to a 25 mL LB culture. This was grown to an OD₆₀₀ of between 0.3 and 0.6 and centrifuged in at 4 °C for ten minutes. The pellet was then resuspended in ice cold Transformation Buffer (TSB) and allowed to

rest on ice for approximately 30 minutes. Cells were either transformed immediately or flash frozen in liquid N₂ and stored at -80 °C until required.

50 uL of competent cells were thawed on ice and the desired volume of plasmid was added and incubated on ice for up to 30 minutes. The entire tube was then placed in a water bath at 42 °C for no longer than 90 seconds, then transferred immediately back to ice and incubated for up to five minutes. 750 uL LB was then added to the competent cells and they were incubated at 37 °C for one hour before plating on selective media.

6.1.4. Reduction of Pd(II) to Pd(0)

MC4100, FTD150, FTD89, IC009 or IC010 were grown in 5 mL LB starter cultures before being inoculated in to M9 media and grown statically in absolutely full 35 mL universal tubes to instigate anaerobic growth with glucose as the sole carbon source, for approximately 16 hours at 37 °C.

Cultures were washed in MOPS buffer and adjusted to an OD₆₀₀ of 0.3. in MOPS buffer. Samples were prepared with either 0.2 % (w/v) Na formate, 0.75 mM Na₂PdCl₄ or both in 5 mL in Hungate tubes. These tubes were then incubated at 37 °C overnight.

6.1.5. Gas Chromatography

Cell suspensions were prepared in MOPS buffer as in section 6.6. After overnight incubation, 1.5 mL gas was removed from the tube headspace and applied to a Shimadzu GC-2014 gas chromatographer. The size of the H₂ peak was deemed to be that that appeared at around 90 seconds of chromatography, this was analysed to measure the concentration of H₂ in the tube as a function of the area under the curve of the peak. This was related to pre-programmed standards and normalised to the OD₆₀₀ of the sample to calculated μM H₂ per unit OD₆₀₀ of cells in each tube.

6.1.6. Characterisation of Pd(II) reduction by OD₆₀₀

E. coli cells of the strains MC4100, FTD150, FTD89, IC009 or IC010 were grown in 5 mL LB starter cultures which were substituted in to 35 mL static anaerobic cultures in LB. These were then diluted to an OD₆₀₀ of 0.3 in MOPS buffer after washing twice in MOPS buffer. Three biological replicate reactions were prepared with each strain in 96 well plates in 250 uL volumes containing the OD₆₀₀ adjusted suspension and either 0.2 % (v/v) sodium formate, 0.75 mM Na₂PdCl₄, or both.

The 96 well plate was then placed in a Bioteck Synergy HT platereader and incubated at 37 °C for 16 hours with no shaking, measuring OD₆₀₀ of each well every 20 minutes. OD₆₀₀ increases were used a proxy measurement for PdNP formation.

6.1.7.Spectral Scanning of PdNP production reactions

Hungate tubes containing cultures of MC4100, FTD150 and FTD89 were prepared as in section 6.1.4 in three biological replicates. After overnight incubation a 200 uL of buffer from each tube was removed and added to a 96 well plate. The plate was then placed in a Biotek Synergy H1 plate reader with monochromator attachment and absorbance of each sample measured at wavelengths between 280 and 700 nm in 5 nm increments

6.1.8.Magnetic Retention Assay

5 mL cultures were grown from a fresh transformation of MG1655 *E. coli* cells containing pQE80L, pQEmms6, pQEmmsF or pQEmftN were grown overnight with 1 mM IPTG. The OD₆₀₀ was measured and cells per mL estimated from the proposition that an OD₆₀₀ of 1.0 relates to concentration of 10⁹ cells per mL. The culture was washed in PBS and adjusted to a cell concentration of 2 x 10⁸ cell's per mL in PBS. An Miltenyi Biotec MACS LD column was prepared by allowing 60 mL of PBS to pass through the column by gravity flow, then a 32 kg pull neodymium magnet (first4magnets) was applied to each side of the column. 0.5 mL of the cell suspension was added to the column with a falcon tube placed below the tube to catch flow through. 3 mL of PBS, corresponding to two column volumes, was allowed to flow through and collected in the same tube. The magnets were then removed and 1.5 mL PBS was added to the column and the provided plunger used to elute the retained cells and repeated once more. The flow through and elution tubes were then centrifuged to pellet cells resuspended in 0.5 mL PBS. 20 uL of the resultant suspension was then added to a microscope slide and viewed with a Leica light microscope. Using imageJ, contrast was enhanced and the thresholding tool was applied such that the cells were visible only as dark bodies in the image. Watershedding tool was applied to insert a one pixel line between cells that were close together to remove the possibility that two cells might be counted as one. Particle analysis was then performed to count the dark bodies in the image with circularity threshold of 0.5. Three slides from each replicate with three images from each were prepared. This data was then used to calculate the cells per mL in the suspension. The percentage of cells in the eluted fraction from the sum of each was then calculated as the percentage retention.

6.1.9.Platereader Characterisation of pMOGMAR and associated variants

E. coli MG1655 cells were transformed with the appropriate plasmids and cultured in 5 mL of the relevant media (LB, M9 or EZ media) overnight with selection. OD₆₀₀ was then measured and the culture was diluted to an OD₆₀₀ of 0.01 in sterile media containing ampicillin at 120 µg/mL and IPTG at the relevant concentration (0 – 2 mM). 150 µL of the suspension was transferred to a single

well of a 96 well plate in three replicates per IPTG concentration tested, with three biological replicates of each plasmid characterised. For characterisation of the original pMOGMAR plasmid as in figure 4.7, flat bottomed plates were used, and characterisation of subsequent variants in EZ Glc media was conducted in round bottomed 96 well plates.

The 96 well plate was then placed in a BioTek Synergy HT platereader, for the original characterisation of pMOGMAR in LB media, or a Tecan Infinite MNano+ in other experiments and incubated at the designated temperature with shaking (orbital where flat bottomed plates were used, and linear shaking for round bottomed plates). OD₆₀₀ and GFP fluorescence was measured using excitation at 488 and emission at 528 at 15 minute intervals.

6.1.10. Initial Characterisation of pMOGMAR and pC1R7

Overnight cultures were grown in LB from fresh transformation of MG1655 *E. coli* cells with the appropriate plasmids. These were diluted to an OD₆₀₀ of 0.1 in LB media and incubated in Infors shakers with 250 rpm orbital shaking at the designated temperatures. 200 µL samples were taken at the given timepoints and OD₆₀₀ and GFP fluorescence measured on a Biotek Synergy HT platereader.

For conical flask experiments, fresh MG1655 *E. coli* transformations were grown in overnight cultures and inoculated at a final OD₆₀₀ of 0.1 in 25 mL of M9 or LB media and separate flasks incubated in Infors shakers at 250 rpm at the designated temperatures. Hourly, 200 µL samples were taken at the given timepoints and OD₆₀₀ and GFP fluorescence measured on a Biotek Synergy HT platereader.

6.1.11. Flow Cytometry

E. coli MG1655 cells were transformed as indicated in the text and then three independent single colonies were cultivated in starter cultures overnight in EZ Glc media at 37 °C with µg/mL ampicillin. Cultures were then diluted and inoculated at a final OD₆₀₀ of 0.01 in fresh sterile EZ Glc media with the addition of µg/mL ampicillin and either zero or 0.12 mM IPTG and incubated in Infors shakers in racks holding the tubes vertically and shaken orbitally at 300 rpm, with replicates performed at either 30 °C or 42 °C. Cultures were incubated until they had reached exponential phase then washed in sterile PBS and diluted 100 x in to sterile PBS and measured using a BD Fortessa X20 flow cytometer using FSC (632 V), SSC (286 V) and 488/530 (458 V) channels. Data was then analysed using Flowing software.

6.2.Molecular Biology and Biochemistry Methods

6.2.1.Polymerase Chain Reaction

Primers from primer table were selected as appropriate. For plasmid assembly purposes, Q5 2x PCR Master Mix (NEB) was used with the addition of 0.1 uM of each forward and reverse primer. Typical PCR program conditions are delineated in Table 6.4.

Table 6.3 showing standard PCR program conditions

Temperature (°C)	Time (seconds)
95	30
Begin Cycle	
95	30
50-69	30
72	60 s per kilobase in amplicon
End Cycle, repeat 28 times	
72	At least 5 minutes

Primer name	SEQUENCE 5' – 3'	Info
MF-1-FOR	ATGCTGAAACCAGAAAT GATT	Used in Gibson assembly reaction to produce pQEmftN. Amplifies up the 5' fragment of <i>ftnA</i> in the forward direction
MF-1-REV	TAAGATAGCTGCACCAG G	Used in Gibson assembly reaction to produce pQEmftN. Amplifies up the 5' fragment of <i>ftnA</i> in the reverse direction, introducing a mutation at nt 101 of C-T
MF-2-FOR	CTTACCTTCGAAGGTGC TGC	Used in Gibson assembly reaction to produce pQEmftN. Amplifies up the 5' fragment of <i>ftnA</i> in the forward direction, introducing a mutation at nt 101 of C-T
MF-2-REV	GCATCAGTCAGGTAATC AAAC	Used in Gibson assembly reaction to produce pQEmftN. Amplifies up the 5' fragment of <i>ftnA</i> in the reverse direction, introducing a mutation at nt 189 of G-C
MF-3-FOR	TGCCGGCAATTACCGC GTATTA	Used in Gibson assembly reaction to produce pQEmftN. Amplifies up the 5' fragment of <i>ftnA</i> in the forward direction, introducing a mutation at nt 189 of G-C
MF-3-REV	GTTTGTTGTGTCGAGGG T	Used in Gibson assembly reaction to produce pQEmftN. Amplifies the 5' fragment of <i>ftnA</i> in the reverse direction, introducing a mutation at nt 189 of G-C
Mms6- ploop- FOR	AAGTGGAGCAGGAATT AAGTGGGCGAATT	Used to generate ChiW variants with the Mms6 sequence (Table 3.1) in the ChiW p-loop. A 5' phosphate was added to these.
Mms6- ploop- REV	CCTCGTCAGACAGGCC ATCAACGCCAGCG	Used to generate ChiW variants with the Mms6 sequence (Table 3.1) in the ChiW p-loop. A 5' phosphate was added to these.

MamI-ploop-FOR	CTGAGTTCTTACGCGGG GAATTAAGTGGGCGAA TTT	Used to generate ChiW variants with the MamI sequence (Table 3.1) in the ChiW p-loop. A 5' phosphate was added to these.
MamI-ploop-REV	TAACCGACCACCACAC AGGCCCATCAACGCCAG CG	Used to generate ChiW variants with the MamI sequence (Table 3.1) in the ChiW p-loop. A 5' phosphate was added to these.
MIA-ploop-FOR	CAAGAGCACGAACGAATTA AAGTGGGCGAATT	Used to generate ChiW variants with the MIA sequence (Table 3.1) in the ChiW p-loop. A 5' phosphate was added to these.
MIA-ploop-REV	GGCACAAATTTTGCGAG GCCCATCAACGCCAGCG	Used to generate ChiW variants with the MIA sequence (Table 3.1) in the ChiW p-loop. A 5' phosphate was added to these.
Mms6-cter-FOR	AAGTGGAGCAG CATCATCATCACCACCA CCA	Used to generate ChiW variants with the Mms6 sequence (Table 3.1) in the ChiW c-motif location. A 5' phosphate was added to these.
Mms6-cter-REV	CCTCGTCAGAGGCCGCA AGCTTTTACCCCT	Used to generate ChiW variants with the Mms6 sequence (Table 3.1) in the ChiW c-motif location. A 5' phosphate was added to these.
MamI-cter-FOR	CTGAGTTCTTACGCGGG CATCATCATCACCACCA CCA	Used to generate ChiW variants with the MamI sequence (Table 3.1) in the ChiW c-motif location. A 5' phosphate was added to these.
MamI-cter-REV	TAACCGACCACCACAG GCCGCAAGCTTTTACCC CT	Used to generate ChiW variants with the MamI sequence (Table 3.1) in the ChiW c-motif location. A 5' phosphate was added to these.
MIA-cter-FOR	C AAG AGC ACG AAC CATCATCATCACCACCA CCA	Used to generate ChiW variants with the MIA sequence (Table 3.1) in the ChiW c-motif location. A 5' phosphate was added to these.
MIA-cter-REV	GGCACAAATTTGGGC CGCAAGCTTTTACCCCT	Used to generate ChiW variants with the MIA sequence (Table 3.1) in the ChiW c-motif location. A 5' phosphate was added to these.

PMM10K-F	TAACAAAGAGGTCTTATGCG GCCGTTAATTCGAT	Used in a KLD reaction to add a synthetic RBS to pMOGMAR mediating <i>gmaR</i> translation producing the plasmid pMOGMAR-10K
PMM10K-R	AGATCTACCGGGATCTT TACATTGTTATAATT TT	Used in a KLD reaction to add a synthetic RBS to pMOGMAR mediating <i>gmaR</i> translation producing the plasmid pMOGMAR-10K
PMM20K-F	AAACACAAATGCGTAAA GGAGAAAGAACCTTTCA	Used in the generation of pMOGMAR-20K, adds a synthetic RBS mediating <i>gmaR</i> translation using pMOGMAR as a template
PMM20K-R	CCCTCCTACATTTGTG TTCCCTCCTACATT	Used in the generation of pMOGMAR-20K, adds a synthetic RBS mediating <i>gmaR</i> translation using pMOGMAR as a template
PMM700-F	TATAAAGAGACGCCA A TGCGGCCGTTAATTTCG AT	Used in the generation of pMOGMAR-700, adds a synthetic RBS mediating <i>gmaR</i> translation using pMOGMAR as a template
PMM700-R	TGTCTGCTACTACCATTACAT TTGTTTATAATTTCG	Used in the generation of pMOGMAR-700, adds a synthetic RBS mediating <i>gmaR</i> translation using pMOGMAR as a template
PMMRBS-SEQ-F	TAG-CCA-GCA-GCT- CGT-TGT	Sequencing primer used to sequence synthetic RBS insertions in pMOGMAR variants
QEFOR	CCC GAA AAG TGC CAC CTG	Primer used to sequence inserted DNA in the multiple cloning site of pQE80L plasmids
QEREV	GTT CTG AGG TCA TTA CTG GAT	Primer used to sequence inserted DNA in the multiple cloning site of pQE80L plasmids
BADFOR	ATGCCATAGCATTTC TCC	Primer used to sequence plasmids constructed in the pBAD18 background
TLPA-FOR	GCATCACCATCACCATC ACGATGCGTCCGGCGAC ATAC	Used to amplify <i>tlpA</i> CDS from <i>S. typhimurium</i> used in pC1R7 Gibson assembly reaction
TLPAREV	TGATGCCTGGTTATCAC GCATTCTGGCCAC	Used to amplify <i>tlpA</i> CDS from <i>S. typhimurium</i> and used in pC1R7 Gibson assembly reaction
TB0015FO-R	TGCGTGATAACCAGGCA TCAAATAAAAC	Used to amplify the BBa_B0015 double terminator biobrick used in pC1R7 Gibson assembly reaction

TB0015RE	GCACAGCATGTATAAAC GCAGAAAGGCC	Used to amplify the BBa_B0015 double terminator biobrick used in pC1R7 Gibson assembly reaction
PTLPAFO	TGCGTTTATACATGCTG TGCCAGCAATTTC	Used to amplify the promoter controlling <i>tlpA</i> transcription in <i>S. typhimurium</i> used in pC1R7 Gibson assembly reaction
PTLPARE	CTTTACGCATCTGTCAG TCTCCGCATAAAAG	Used to amplify the promoter controlling <i>tlpA</i> transcription in <i>S. typhimurium</i> used in pC1R7 Gibson assembly reaction
TGFPFOR	AGACTGACAGATGCGTA AAGGAGAAGAAC	Used to amplify <i>gfpmut3b</i> used in pC1R7 Gibson assembly reaction
TGFPREV	AGTCCAAGCTCAGCTAA TTATTATTATTTGTATA GTTCATCCATG	Used to amplify <i>gfpmut3b</i> used in pC1R7 Gibson assembly reaction
QEGFPFO	GCATCACCATCACCATC ACGGATCCATGCGTAAA GGAGAAGAAC	Used to amplify <i>gfpmut3b</i> used in pQEgfp Gibson assembly reaction
QEGFPRE	AGTCCAAGCTCAGCTAA TTAAGCTTTATTATT GTATAGTTCATCCATG	Used to amplify <i>gfpmut3b</i> used in pQEgfp Gibson assembly reaction
MM- mogR-F	GCATCACCATCACCATC ACGGATCCATGCCTAAA TCAGAAATAAGAAAATT AC	Used to amplify <i>mogR</i> from <i>L. monocytogenes</i> str. EGD-e in the contrusction of pMOGMAR
MM- mogR-R	ACGGCCGCATTTACATT TGTTTATAATTTCTTT GAATAC	Used to amplify <i>mogR</i> from <i>L. monocytogenes</i> str. EGD-e in the contrusction of pMOGMAR
MM- gmaR-F	ACAAATGTAAATGCGGC CGTTAATTCG	Used to amplify <i>gmaR</i> from <i>L. monocytogenes</i> str. EGD-e in the contrusction of pMOGMAR
MM- gmaR-R	TGATGCCTGGCTATCGA TTGTTTGTAAACAGTGTC	Used to amplify <i>gmaR</i> from <i>L. monocytogenes</i> str. EGD-e in the contrusction of pMOGMAR
MM- B0015-F	CAATCGATAGCCAGGCA TCAAATAAAAC	Used to amplify Biobrick BBa_B0015 in the construction of pMOGMAR

MM-B0015-R	ATTAaaaATGTAATATA AACGCAGAAAGGCC	Used to amplify Biobrick BBa_B0015 in the construction of pMOGMAR
MM-pfla-F	TGCGTTATATTACATT TTTTAATAAAAAACATT TAGATTTGATTTTTAA AAAAATG	Used to amplify the <i>PflaA</i> promoter from <i>L. monocytogenes</i> str. EGD-e in the construction of pMOGMAR
MM-pfla-R	CTTTACGCATTTGTGTT TCCCTCCTACATTC	Used to amplify the <i>PflaA</i> promoter from <i>L. monocytogenes</i> str. EGD-e in the construction of pMOGMAR
MM-gfp-F	GGAAACACAAATGCGTA AAGGAGAAGAAC	Used to amplify <i>gfpmut3b</i> in the construction of pMOGMAR
MM-gfp-R	AGTCCAAGCTCAGCTCA GCTAATTAAGCTTTAT TATTGTATAGTCATC CATG	Used to amplify <i>gfpmut3b</i> in the construction of pMOGMAR
MMS6-F	GCATCACCATCACCATC ACGATGCCAGCCAAAT CGCC	Used to amplify a codon optimized version of <i>mms6</i> from <i>M. gryphiswaldense</i> in the construction of pQEmms6
MMS6-R	AGTCCAAGCTCAGCTAA TTATCAGCTCAAAGCGT CACG	Used to amplify a codon optimized version of <i>mmsF</i> from <i>M. gryphiswaldense</i> in the construction of pQEmms6
MMSF-F	GCATCACCATCACCATC ACGATGGTAGAGGCTAT CTTGC	Used to amplify a codon optimized version of <i>mmsF</i> from <i>M. gryphiswaldense</i> in the construction of pQEmmsF
MMSF-R	AGTCCAAGCTCAGCTAA TTATCAAATGCGATCCG CAAC	Used to amplify a codon optimized version of <i>mms6</i> from <i>M. gryphiswaldense</i> in the construction of pQEmmsF

6.2.2. Colony PCR

For screening positive colonies during the cloning workflow, bacterial colonies were used directly as PCR template. 12 uL of sterile distilled water was placed on a sterile petri dish lid and a single bacterial colony was picked from the transformation plate. This was resuspended in the water droplet, with 3 uL of the resultant suspension added to a PCR reaction mixture, and another 3 uL was placed on a dried agar plate with the appropriate selective antibiotic.

PCRs were performed as in table 6.2 with an extended 15 minute initial step at 95 degrees. PCR used 2x G2 Green PCR Master Mix (Promega).

6.2.3.Gibson Assembly

PCR fragments were generated using the appropriate primers from Table X.Y and Q5 2x Master Mix (NEB). These were either gel purified or PCR purified where necessary. When assembling one DNA fragment in to a vector, a mixture with a molar ratio of 2:1 insert to vector was prepared in a PCR tube along with 10 uL NEBuilder HiFi DNA Assembly Master Mix and sterile MiliQ water added to a final volume of 20 uL. This was then incubated at 50 °C in an Eppendorf PCR machine for one hour before transforming 2 uL of the reaction mixture.

6.2.4.Site Directed Mutagenesis of Plasmids

Primers were designed to amplify the entire length of the plasmid with the desired nucleotide insertion, deletion or substitution at the extreme 5' or 3' end of either the forward or reverse primer respectively. PCR was then performed using Q5 PCR 2x Master Mix. This produces a linear DNA fragment representing the plasmid with the desired mutation at the 5' and/or 3' ends that can be ligated back to a circular piece of DNA. In cases where more than one nucleotide were inserted to plasmid, the sequence was inserted roughly in halves to the extreme 5' or 3' end of the primer. The fragment was PCR purified and was added in to KLD reaction as per the manufacturer's instructions. This contains a 5' DNA kinase to phosphorylate the 5' ends of the blunt ended DNA fragments, T4 DNA ligase to ligate the blunt strands producing circular DNA with the desired mutation, and Dpn1 which selectively degrades methylated DNA at GATC sites. The reaction mixture was then incubated for up to 30 minutes at room temperature before the total volume being added to 50 uL of competent cells for transformation.

6.2.5.Buffer Recipes and Solutions

Table 6.4 List of buffers used in this thesis and their recipes

Buffer	Ingredients
MOPS	40 mM MOPS (3-(N-morpholino)propanesulfonic acid 10 mM NaAc 1 mM EDTA
PBS	137 mM NaCl, 2.7 mM KCl and 75.4 mM Na ₂ PO ₄ 24.6 mM NaPO ₄
Pull down buffers	50 mM Tris HCl pH 8 50 mM NaCl 0-500 mM Imidazole
Purification buffers	50 mM Tris HCl pH 7.5 150 mM NaCl 50 - 500 mM Imidazole
Lysis buffer	As purification buffer 1 protease inhibitor tablet / 100 mL buffer 0.1 mg/mL DnaseI 0.1 mg/mL Chicken egg lysozyme
Transfer buffer	5 mM Tris HCl pH 8.3 38.4 mM Glycine 20 % (v/v) Methanol
SDS-PAGE Running Buffer	5 mM Tris-HCl pH 8.3 38.4 mM Glycine 0.1 % (w/v) SDS
Tris Buffered Saline (TBS)	20 mM Tris HCl pH 7.6 137 mM NaCl
TBS-T	As TBS above 0.1 % (v/v) Tween20
Tris-Acetate-EDTA (TAE)	40 mM Tris HCl pH 8.0 1.142 % (v/v) acetic acid 1 mM EDTA
Laemmli buffer (2x concentrated)	950 uL Laemmli 50 uL β-mercaptoethanol
Transformation buffer	20 ml LB 1 ml 1 M MgSO ₄ 1 ml DMSO 2 g PEG 6000
Fractionation buffer	30 mM Tris HCl, pH8 20 % (w/v) Sucrose 1 mM EDTA

6.2.6. Room Temperature Co-Precipitation of Magnetite

0.01 mol of Fe(ii)SO₄ was added to 100 mL of sterile deionised water with three drops of HCl with stirring with a magnetic stirrer. Once this was in suspension, 0.02 mols Fe(III) citrate was added and allowed to suspend. Following this 0.09 mols powdered NaOH was added and magnetite precipitation was evident from the colour change from brown to black. This was allowed to continue to stir for no more than one hour, the beaker was then sat atop two 32 kg pull neodymium magnets (first4magnets) for at least an hour to allow magnetic material to settle at the bottom. With the magnets held in place, liquid was poured off and replaced with 100 mL of fresh deionised water. This was then repeated at least three times. Upon the final decantation, the entire suspension was resuspended in 20 mL sterile deionised water. One mL of the suspension was centrifuged to produce a dry pellet that could be weighed to estimate concentration assuming purity of the suspension. Before each application of the suspension in an experiment, it was sonicated for 30 seconds using a Branson digital sonifier to ensure homogeneity of NPs and minimise clumping.

6.2.7. Magnetite washing experiment

E. coli cells of the strain MG1655 transformed with the plasmids pQE80L, pQEmms6, or pQEmmsF were grown in 5 mL precultures that were subcultured in to 100 mL volume cultures in 500 mL conical flasks in LB media with the addition of ampicillin and 1 mM IPTG, and 1 mM magnetite. This was incubated at 37 °C for approximately 16 hours with 200 rpm orbital shaking. An equal volume then of 0.3 M oxalic acid (Sigma) was added to the culture and incubated for approximately thirty minutes before then being centrifuged and resuspended in a further 100 mL 0.3 M oxalic acid and centrifuged again. Small volumes were removed and centrifuged independently for photographs. The final pellets were resuspended in 50 mL PBS and poured in to a Petri dish sat atop a 32 kg pull neodymium magnet and imaged.

6.2.8. Magnetite Pull Downs

50 mL cultures of MG1655 *E. coli* were grown from substitution of a 5 mL starter culture with 1 mM IPTG induction. Cell pellets were harvested and lysed in lysis buffer with 5 minutes of sonication (30 s on, 10 s off, 10 % amplitude, Branson digital sonifier), the resultant suspension then lysed to remove intact cells and insoluble material. The lysate was adjusted to 0.2 mg /mL total protein concentration and magnetite added at concentrations 0, 2, 10, 25, 50, 100 mM in separate Eppendorf tubes containing one mL of the adjusted lysate. The suspensions were then incubated overnight with rotary agitation at 4 °C. Following this, the tubes were applied to a magnarack for 30 minutes and the supernatant removed and kept as a n unbound fraction leaving the magnetite attracted to the side of the tube. The supernatant was replaced with buffer to normalise the concentration to the unbound fraction, and taken as a magnetite associated fraction.

This was then subjected to analysis by SDS-PAGE and Coomassie staining with Instant Blue (Expedeon).

6.2.9.GmaR degradation experiment

E. coli MG1655 cells were transformed with pMOGMAR-20KNHA and single colonies inoculated in to starter cultures in 5 mL LB medium with 120 µg/mL ampicillin and incubated overnight at 37 °C with linear shaking. This was then inoculated 1/100 in to a 500 mL LB culture with 120 µg/mL ampicillin and 0.12 mM IPTG and incubated overnight at 30 °C. A sample of 0.5 mL of this culture was retained and used as a “whole cell” pellet control for protein production in subsequent Western blots. Cells from the culture were harvested by centrifugation and approximately 0.3 g was resuspended in lysis buffer at a cell concentration of 0.1 g cells per mL buffer and lysed by sonication. Debris and unbroken cells were removed by centrifugation and the supernatant stored on ice and utilised as lysate. Ten individual samples of 0.5 mL lysate were stored in 1.5 mL Eppendorf tubes and incubated in heat block set to 30 °C at a separate time each, these being 0, 1, 2, 5, 10, 20, 30, 40, 60 and 90 minutes. This was repeated at 42 °C also and each sample was then diluted in 2 x Leammlie buffer and analysed by Western blot using α -HA antibody to probe for GmaR production.

6.2.10.Co-purification of His-tagged MogR with GmaR

pMOGMAR-20K plasmid was transformed in to *E. coli* MG1655 cells, of which single colonies were then cultured overnight in 5 mL starter cultures with 120 ug/mL ampicillin in LB medium. These were then inoculated in to a 500 mL LB culture with the addition of 0.12 mM IPTG and 120 ug/mL ampicillin and incubated with linear shaking at 30 °C overnight. Cells from the culture were harvested by centrifugation then resuspended in lysis buffer (see table 6.4) at a final cell weight concentration of approximately 0.1 g cells per mL buffer. The suspension was then lysed using two passes in a cell disruptor (make/model?). The lysate was cleared of debris and unbroken cells by centrifugation then applied to a 5 mL HisTrapFF column (GE) using an AKTA Pure FPLC system. The HisTrapFF column was first equilibrated using Purification Buffer A (see Table 6.1) at 2 mL/minute flow rate until three column volumes had been applied. Lysate was added to the column using a super loop at 1 mL/min, followed by washing of the column with purification buffer A at 2 mL/min until the UV trace stabilised, while flow through was collected throughout. The UV detector was then blanked and the elution phase was initiated. To elute protein bound to the column, a gradient wash was used with mixing of purification buffers A and B using the discrete pumps in the FPLC hardware. An elution gradient was utilised from 0-50 % buffer B over ten column volumes, then over another ten column volumes, from 50-100 % buffer B. A peak in the

UV trace was seen during the elution, and samples collected during this period were analysed by SDS-PAGE and Western blot.

6.2.11. Fractionation of *E. coli* Cells

A culture was grown as necessary and centrifuged to harvest a cell pellet from 30 mL of culture. This pellet was resuspended in 7.5 mL fractionation buffer (Table 6.4) and incubated at room temperature for at least 10 minutes. Cells were again harvested by centrifugation before being resuspended in 1 mL ice cold 5 mM MgSO₄ and incubated on ice for at least 10 minutes. Cells were once again harvested by centrifugation and the supernatant in this instance retained as a periplasmic fraction. The pellet was retained as sphaeroplasts which were resuspended in 2 mL 50 mM Tris HCl (pH 8) and sonicated twice for 30 seconds. The broken sphaeroplasts were then centrifuged and the supernatant retained as a membrane and cytoplasmic fraction, with the pellet retained as an insoluble fraction. Membranes were then separated from soluble cytoplasmic components by ultracentrifugation at 80,000 rpm for 45 minutes. The pellet was retained as a membrane fraction which was resuspended in 50 mM Tris HCl (pH 8) and the supernatant retained as a cytoplasmic fraction. Samples were mixed with Laemmli sample buffer prior to SDS-PAGE analysis.

Chapter 7:Bibliography

1. McGovern, P. E. *et al.* Fermented beverages of pre- and proto-historic China. *Proc. Natl. Acad. Sci. U. S. A.* **101**, 17593–8 (2004).
2. de la Fuente-Salcido, N. M. *et al.* Isolation and characterization of bacteriocinogenic lactic bacteria from M-Tuba and Tepache, two traditional fermented beverages in México. *Food Sci. Nutr.* **3**, 434–442 (2015).
3. Redzepi, R., Zilber, D. (Chef), Sung, E. & Troxler, P. *The Noma guide to fermentation : foundations of flavor.* (Artisan, 2018).
4. Barbra Streisand. Barbra Streisand Explains: Why I Cloned My Dog - The New York Times. *New York Times* (2018). Available at: <https://www.nytimes.com/2018/03/02/style/barbra-streisand-cloned-her-dog.html>. (Accessed: 6th July 2018)
5. Charles Weizmann. Improvements in the Bacterial Fermentation of Carbohydrates and in Bacterial Cultures for the same. (1919). doi:GBD191504845 19150329
6. Jones, D. T. & Woods, D. R. Acetone-butanol fermentation revisited. *Microbiol. Rev.* **50**, 484–524 (1986).
7. Atsumi, S., Hanai, T. & Liao, J. C. Non-fermentative pathways for synthesis of branched-chain higher alcohols as biofuels. *Nature* **451**, 86–89 (2008).
8. Check Hayden, E. *Renewable rubber hits the road.* *Nature* (Nature Publishing Group, 2011). doi:10.1038/news.2011.568
9. Platt, J. A. U. M. Genetically modified microbes producing isoprenoids. (2010).
10. Galanie, S., Thodey, K., Trenchard, I. J., Filsinger Interrante, M. & Smolke, C. D. Complete biosynthesis of opioids in yeast. *Science* **349**, 1095–100 (2015).
11. Hawkins, K. M. & Smolke, C. D. Production of benzylisoquinoline alkaloids in *Saccharomyces cerevisiae*. *Nat. Chem. Biol.* **4**, 564–573 (2008).
12. Win, M. N., Klein, J. S. & Smolke, C. D. Codeine-binding RNA aptamers and rapid determination of their binding constants using a direct coupling surface plasmon resonance assay. *Nucleic Acids Res.* **34**, 5670–5682 (2006).
13. Thodey, K., Galanie, S. & Smolke, C. D. A microbial biomanufacturing platform for natural and semisynthetic opioids. *Nat. Chem. Biol.* **10**, 837–844 (2014).
14. Trenchard, I. J., Siddiqui, M. S., Thodey, K. & Smolke, C. D. De novo production of the

- key branch point benzylisoquinoline alkaloid reticuline in yeast. *Metab. Eng.* **31**, 74–83 (2015).
15. Jacob, F., Ullmann, A. & Monod, J. Délétions fusionnant l'opéron lactose et un opéron purine chez Escherichia coli. *J. Mol. Biol.* **13**, 704–719 (1965).
 16. Jacob, F. ; O., Perrin, D., Sanchez, C. & Monod, J. The Operon: A Group of Genes Whose Expression is Coordinated by an Operator.
 17. Jacob, F., Lwoff, A. & Monod, J. The Nobel Prize in Physiology or Medicine 1965. Available at: https://www.nobelprize.org/nobel_prizes/medicine/laureates/1965/. (Accessed: 4th July 2018)
 18. De Boer, H. A., Comstock, L. J. & Vassert, M. The tac promoter: A functional hybrid derived from the trp and lac promoters (hybrid promoters/controlled gene expression/promoter efficiency/synthetic DNA/portable Shine-Dalgarno region). *Biochemistry* **80**, 21–25 (1983).
 19. Donovan, R. S., Robinson, C. W. & Glick, B. R. Review: Optimizing inducer and culture conditions for expression of foreign proteins under the control of the lac promoter. *J. Ind. Microbiol.* **16**, 145–154 (1996).
 20. Chalmers, J. J. *et al.* Effects of temperature on Escherichia coli overproducing beta-lactamase or human epidermal growth factor. *Appl. Environ. Microbiol.* **56**, 104–11 (1990).
 21. Harcum, S. W. & Bentley, W. E. Response dynamics of 26-, 34-, 39-, 54-, and 80-kDa proteases in induced cultures of recombinant Escherichia coli. *Biotechnol. Bioeng.* **42**, 675–685 (1993).
 22. Pack, P. *et al.* Improved Bivalent Miniantibodies, with Identical Avidity as Whole Antibodies, Produced by High Cell Density Fermentation of Escherichia coli. *Nat. Biotechnol.* **11**, 1271–1277 (1993).
 23. Takagi, H., Morinaga, Y., Tsuchiya, M., Ikemura, H. & Inouye, M. Control of Folding of Proteins Secreted by a High Expression Secretion Vector, pIN-III-ompA: 16-Fold Increase in Production of Active Subtilisin E in Escherichia Coli. *Nat. Biotechnol.* **6**, 948–950 (1988).
 24. Schein, C. H. Production of Soluble Recombinant Proteins in Bacteria. *Nat. Biotechnol.* **7**, 1141–1149 (1989).
 25. Shin, C. S., Hong, M. S., Bae, C. & Lee, J. Enhanced Production of Human Mini-Proinsulin

- in Fed-Batch Cultures at High Cell Density of Escherichia coli BL21(DE3)[pET-3aT2M2]. *Biotechnol. Prog.* **13**, 249–257 (1997).
26. Chen, W. B., Nie, Y., Xu, Y. & Xiao, R. Enhancement of extracellular pullulanase production from recombinant Escherichia coli by combined strategy involving auto-induction and temperature control. *Bioprocess Biosyst. Eng.* **37**, 601–608 (2014).
27. Glick, B. R. Metabolic Load and Heterologous Gene Expression. *Biotocmology Adwn~s* **13**, 247–261 (1995).
28. Studier, F. W. Protein production by auto-induction in high-density shaking cultures. (2005). doi:10.1016/j.pep.2005.01.016
29. Yang, P. *et al.* A New Strategy for Production of 5-Aminolevulinic Acid in Recombinant Corynebacterium glutamicum with High Yield. *Appl. Environ. Microbiol.* **82**, 2709–2717 (2016).
30. Williams, T. C., Peng, B., Vickers, C. E. & Nielsen, L. K. The *Saccharomyces cerevisiae* pheromone-response is a metabolically active stationary phase for bio-production. *Metab. Eng. Commun.* **3**, 142–152 (2016).
31. Burg, J. M. *et al.* Large-scale bioprocess competitiveness: the potential of dynamic metabolic control in two-stage fermentations. *Curr. Opin. Chem. Eng.* **14**, 121–136 (2016).
32. Na, D. *et al.* Metabolic engineering of Escherichia coli using synthetic small regulatory RNAs. *Nat. Biotechnol.* **31**, 170–174 (2013).
33. Brophy, J. A. & Voigt, C. A. Antisense transcription as a tool to tune gene expression. *Mol Syst Biol* **12**, (2016).
34. Nakashima, N., Ohno, S., Yoshikawa, K., Shimizu, H. & Tamura, T. A vector library for silencing central carbon metabolism genes with antisense RNAs in Escherichia coli. *Appl. Environ. Microbiol.* **80**, 564–73 (2014).
35. Williams, T. C. *et al.* Quorum-sensing linked RNA interference for dynamic metabolic pathway control in *Saccharomyces cerevisiae*. *Metab. Eng.* **29**, 124–134 (2015).
36. McGinness, K. E., Baker, T. A. & Sauer, R. T. Engineering Controllable Protein Degradation. *Mol. Cell* **22**, 701–707 (2006).
37. Tu, G. F., Reid, G. E., Zhang, J. G., Moritz, R. L. & Simpson, R. J. C-terminal extension of truncated recombinant proteins in Escherichia coli with a 10Sa RNA decapeptide. *J. Biol.*

- Chem.* **270**, 9322–6 (1995).
38. Wah, D. A. *et al.* Flexible Linkers Leash the Substrate Binding Domain of SspB to a Peptide Module that Stabilizes Delivery Complexes with the AAA+ ClpXP Protease. *Mol. Cell* **12**, 355–363 (2003).
 39. Sauer, R. T. *et al.* Sculpting the Proteome with AAA+ Proteases and Disassembly Machines. *Cell* **119**, 9–18 (2004).
 40. Brockman, I. M. & Prather, K. L. J. Dynamic knockdown of *E. coli* central metabolism for redirecting fluxes of primary metabolites. *Metab. Eng.* **28**, 104–113 (2015).
 41. Torella, J. P. *et al.* Tailored fatty acid synthesis via dynamic control of fatty acid elongation. *Proc. Natl. Acad. Sci. U. S. A.* **110**, 11290–5 (2013).
 42. Elowitz, M. B. & Leibler, S. A synthetic oscillatory network of transcriptional regulators. *Nature* **403**, 335–338 (2000).
 43. Mannan, A. A., Liu, D., Zhang, F. & Oyarzún, D. A. Fundamental Design Principles for Transcription-Factor-Based Metabolite Biosensors. *ACS Synth. Biol.* **6**, 1851–1859 (2017).
 44. Rosano, G. L. & Ceccarelli, E. A. Recombinant protein expression in *Escherichia coli*: advances and challenges. *Front. Microbiol.* **5**, (2014).
 45. Guzman, L. M., Belin, D., Carson, M. J. & Beckwith, J. Tight regulation, modulation, and high-level expression by vectors containing the arabinose PBAD promoter. *J. Bacteriol.* **177**, 4121–30 (1995).
 46. Kelly, C. L. *et al.* Synthetic Chemical Inducers and Genetic Decoupling Enable Orthogonal Control of the *rhaBAD* Promoter. *ACS Synth. Biol.* **5**, 1136–1145 (2016).
 47. Kelly, C. L., Taylor, G. M., Hitchcock, A., Torres-Méndez, A. & Heap, J. T. A Rhamnose-Inducible System for Precise and Temporal Control of Gene Expression in Cyanobacteria. *ACS Synth. Biol.* **7**, 1056–1066 (2018).
 48. Ramos, J. L. *et al.* The TetR family of transcriptional repressors. *Microbiol. Mol. Biol. Rev.* **69**, 326–56 (2005).
 49. Skerra, A. Use of the tetracycline promoter for the tightly regulated production of a murine antibody fragment in *Escherichia coli*. *Gene* **151**, 131–5 (1994).
 50. Papenfort, K. & Bassler, B. L. Quorum sensing signal–response systems in Gram-negative bacteria. *Nat. Rev. Microbiol.* **14**, 576–588 (2016).

51. Egland, K. A. & Greenberg, E. P. Quorum sensing in *Vibrio fischeri*: elements of the luxI promoter. *Mol. Microbiol.* **31**, 1197–1204 (1999).
52. Fuqua, W. C., Winans, S. C. & Peter Greenberg², E. MINIREVIEW Quorum Sensing in Bacteria: the LuxR-LuxI Family of Cell Density-Responsive Transcriptional Regulatorst. *J. Bacteriol.* **176**, 269–275 (1994).
53. Shong, J. & Collins, C. H. Engineering the *esaR* Promoter for Tunable Quorum Sensing-Dependent Gene Expression. *ACS Synth. Biol.* **2**, 568–575 (2013).
54. Shong, J., Huang, Y.-M., Bystroff, C. & Collins, C. H. Directed Evolution of the Quorum-Sensing Regulator EsaR for Increased Signal Sensitivity. *ACS Chem. Biol.* **8**, 789–795 (2013).
55. Isaacs, F. J. *et al.* Engineered riboregulators enable post-transcriptional control of gene expression. *Nat. Biotechnol.* **22**, 841–847 (2004).
56. Adhya, S. & Gottesman, M. Control of Transcription Termination. *Annu. Rev. Biochem.* **47**, 967–996 (1978).
57. Roberts, J. W. Mechanisms of Bacterial Transcription Termination. *Journal of Molecular Biology* (2019). doi:10.1016/j.jmb.2019.04.003
58. Lucks, J. B., Qi, L., Mutualik, V. K., Wang, D. & Arkin, A. P. Versatile RNA-sensing transcriptional regulators for engineering genetic networks. *Proc. Natl. Acad. Sci. U. S. A.* **108**, 8617–22 (2011).
59. Roßmanith, J. & Narberhaus, F. Exploring the modular nature of riboswitches and RNA thermometers. *Nucleic Acids Res.* **44**, 5410–23 (2016).
60. Ellington, A. D. & Szostak, J. W. In vitro selection of RNA molecules that bind specific ligands. *Nature* **346**, 818–822 (1990).
61. Lynch, S. A. & Gallivan, J. P. A flow cytometry-based screen for synthetic riboswitches. *Nucleic Acids Res.* **37**, 184–92 (2009).
62. Borujeni, A. E., Mishler, D. M., Wang, J., Huso, W. & Salis, H. M. NAR Breakthrough Article Automated physics-based design of synthetic riboswitches from diverse RNA aptamers. *Nucleic Acids Res.* **44**, 1–13 (2015).
63. Potvin-Trottier, L., Lord, N. D., Vinnicombe, G. & Paulsson, J. Synchronous long-term oscillations in a synthetic gene circuit. *Nature* **538**, 514–517 (2016).
64. Prindle, A. *et al.* Rapid and tunable post-translational coupling of genetic circuits. *Nature*

- 508**, 387–91 (2014).
65. McMillen, D., Kopell, N., Hasty, J. & Collins, J. J. Synchronizing genetic relaxation oscillators by intercell signaling. *Proc. Natl. Acad. Sci. U. S. A.* **99**, 679–84 (2002).
 66. Hasty, J., Isaacs, F., Dolnik, M., McMillen, D. & Collins, J. J. Designer gene networks: Towards fundamental cellular control. *Chaos An Interdiscip. J. Nonlinear Sci.* **11**, 207 (2001).
 67. Ruben Perez-Carrasco, A., Barnes, C. P., Schaerli, Y., Isalan, M. & Briscoe, J. Combining a Toggle Switch and a Repressilator within the AC-DC Circuit Generates Distinct Dynamical Behaviors. (2018). doi:10.1016/j.cels.2018.02.008
 68. Garcia-Ojalvo, J., Elowitz, M. B. & Strogatz, S. H. Modeling a synthetic multicellular clock: repressilators coupled by quorum sensing. *Proc. Natl. Acad. Sci. U. S. A.* **101**, 10955–60 (2004).
 69. Chen, Y., Kim, J. K., Hirning, A. J., Josi , K. & Bennett, M. R. Emergent genetic oscillations in a synthetic microbial consortium. *Science (80-.).* **349**, 986–989 (2015).
 70. Swinburne, I. A., Miguez, D. G., Landgraf, D. & Silver, P. A. Intron length increases oscillatory periods of gene expression in animal cells. *Genes Dev.* **22**, 2342–6 (2008).
 71. Fung, E. *et al.* A synthetic gene-metabolic oscillator. *Nature* **435**, 118–122 (2005).
 72. Gardner, T. S., Cantor, C. R. & Collins, J. J. Construction of a genetic toggle switch in *Escherichia coli*. *Nature* (2000). doi:10.1038/35002131
 73. Wu, M. *et al.* Engineering of regulated stochastic cell fate determination. doi:10.1073/pnas.1305423110
 74. Lou, C. *et al.* Synthesizing a novel genetic sequential logic circuit: A push-on push-off switch. *Mol. Syst. Biol.* **6**, 350 (2010).
 75. Ellis, T., Wang, X. & Collins, J. J. Diversity-based, model-guided construction of synthetic gene networks with predicted functions. *Nat. Biotechnol.* (2009). doi:10.1038/nbt.1536
 76. Sohka, T. *et al.* An externally tunable bacterial band-pass filter. *Proc. Natl. Acad. Sci.* **106**, 10135–10140 (2009).
 77. Sohka, T., Heins, R. A. & Ostermeier, M. Morphogen-defined patterning of *Escherichia coli* enabled by an externally tunable band-pass filter. *J. Biol. Eng.* **3**, 10 (2009).
 78. Kong, W., Blanchard, A. E., Liao, C. & Lu, T. Engineering robust and tunable spatial

- structures with synthetic gene circuits. *Nucleic Acids Res.* **45**, 1005–1014 (2017).
79. Rubens, J. R., Selvaggio, G. & Lu, T. K. Synthetic mixed-signal computation in living cells. *Nat. Commun.* **7**, 11658 (2016).
80. Lillacci, G., Aoki, S. K., Schweingruber, D. & Khammash, M. A synthetic integral feedback controller for robust tunable regulation in bacteria. *bioRxiv* 170951 (2017). doi:10.1101/170951
81. Young, D. D. & Deiters, A. Photochemical Activation of Protein Expression in Bacterial Cells. *Angew. Chemie Int. Ed.* **46**, 4290–4292 (2007).
82. Binder, D. *et al.* Light-responsive control of bacterial gene expression: precise triggering of the lac promoter activity using photocaged IPTG. *Integr. Biol.* **6**, 755–765 (2014).
83. Masuda, S. & Bauer, C. E. AppA is a blue light photoreceptor that antirepresses photosynthesis gene expression in Rhodobacter sphaeroides. *Cell* **110**, 613–623 (2002).
84. Tabor, J. J. *et al.* A synthetic genetic edge detection program. *Cell* **137**, 1272–81 (2009).
85. Sean Crosson, ‡, Sudarshan Rajagopal, ‡ and & Keith Moffat*, ‡,§. The LOV Domain Family: Photoresponsive Signaling Modules Coupled to Diverse Output Domains†. (2002). doi:10.1021/BI026978L
86. Möglich, A., Ayers, R. A. & Moffat, K. Design and signaling mechanism of light-regulated histidine kinases. *J. Mol. Biol.* **385**, 1433–44 (2009).
87. Gong, W. *et al.* Structure of a biological oxygen sensor: a new mechanism for heme-driven signal transduction. *Proc. Natl. Acad. Sci. U. S. A.* **95**, 15177–82 (1998).
88. Tabor, J. J., Levskaya, A. & Voigt, C. A. Multichromatic control of gene expression in *Escherichia coli*. *J. Mol. Biol.* **405**, 315–24 (2011).
89. Fernandez-Rodriguez, J., Moser, F., Song, M. & Voigt, C. A. *Engineering RGB color vision into Escherichia coli*. *Nature Chemical Biology* **13**, 706–708 (Nature Publishing Group, 2017).
90. Mouritsen, H. & Ritz, T. Magnetoreception and its use in bird navigation. *Current Opinion in Neurobiology* (2005). doi:10.1016/j.conb.2005.06.003
91. Wajnberg, E., Cernicchiaro, G., Acosta-Avalos, D., El-Jaick, L. J. & Esquivel, D. M. S. Induced remanent magnetization of social insects. *J. Magn. Magn. Mater.* (2001). doi:10.1016/S0304-8853(00)00832-5

92. Ferreira, J. *et al.* Comparative magnetic measurements on social insects. in *Journal of Magnetism and Magnetic Materials* (2005). doi:10.1016/j.jmmm.2004.11.124
93. Blakemore, R. Magnetotactic bacteria. *Science* (80-.). **190**, 377–379 (1975).
94. Uebe, R. & Schüler, D. Magnetosome biogenesis in magnetotactic bacteria. *Nat. Rev. Microbiol.* **14**, 621–637 (2016).
95. Abraçado, L. G., Esquivel, D. M. S., Alves, O. C. & Wajnberg, E. Magnetic material in head, thorax, and abdomen of *Solenopsis substituta* ants: A ferromagnetic resonance study. *J. Magn. Reson.* (2005). doi:10.1016/j.jmr.2005.05.006
96. Hiscock, H. G. *et al.* The quantum needle of the avian magnetic compass. *Proc. Natl. Acad. Sci. U. S. A.* **113**, 4634–4639 (2016).
97. Maeda, K. *et al.* Magnetically sensitive light-induced reactions in cryptochrome are consistent with its proposed role as a magnetoreceptor. *Proc. Natl. Acad. Sci. U. S. A.* **109**, 4774–4779 (2012).
98. Coey, J. M. D. Introduction - A Brief History of Magnetism. in *Magnetism and Magnetic Materials* (2009).
99. Coey, J. M. D. Magnetism of Electrons. in *Magnetism and Magnetic Materials*
100. Cao, E., Cordero-Morales, J. F., Liu, B., Qin, F. & Julius, D. TRPV1 Channels Are Intrinsically Heat Sensitive and Negatively Regulated by Phosphoinositide Lipids. *Neuron* **77**, 667–679 (2013).
101. Stanley, S. A. *et al.* Radio-wave heating of iron oxide nanoparticles can regulate plasma glucose in mice. *Science* **336**, 604–8 (2012).
102. Stanley, S. A., Sauer, J., Kane, R. S., Dordick, J. S. & Friedman, J. M. Remote regulation of glucose homeostasis in mice using genetically encoded nanoparticles. *Nat. Med.* **21**, 92–8 (2015).
103. Uebe, R., Schüler, D., Jogler, C. & Wiegand, S. Reevaluation of the complete genome sequence of *Magnetospirillum gryphiswaldense* MSR-1 with single-molecule real-time sequencing data. *Genome Announc.* **6**, (2018).
104. Meister, M. Physical limits to magnetogenetics. *Elife* **5**, (2016).
105. Wheeler, M. A. *et al.* Genetically targeted magnetic control of the nervous system. *Nat. Neurosci.* **19**, 756–761 (2016).

106. Papaefthymiou, G. C. The Mössbauer and magnetic properties of ferritin cores. *Biochim. Biophys. Acta - Gen. Subj.* **1800**, 886–897 (2010).
107. Fantechi, E. *et al.* A Smart Platform for Hyperthermia Application in Cancer Treatment: Cobalt-Doped Ferrite Nanoparticles Mineralized in Human Ferritin Cages. *ACS Nano* **8**, 4705–4719 (2014).
108. Howard, J. & Hudspeth, A. J. Compliance of the hair bundle associated with gating of mechanoelectrical transduction channels in the bullfrog's saccular hair cell. *Neuron* **1**, 189–99 (1988).
109. Chen, R., Romero, G., Christiansen, M. G., Mohr, A. & Anikeeva, P. Wireless magnetothermal deep brain stimulation. *Science (80-.).* **347**, 1477–1480 (2015).
110. Krishnan, V. *et al.* Wireless control of cellular function by activation of a novel protein responsive to electromagnetic fields. doi:10.1038/s41598-018-27087-9
111. Slonczewski, J.L., Foster, J. W. Table 5.1 Basic Environmental Classification of Microorganisms. in *Microbiology an Evolving Science, 4th Edition* 159–159 (2009).
112. Falconi, M. *et al.* Thermoregulation of Shigella and Escherichia coli EIEC pathogenicity. A temperature-dependent structural transition of DNA modulates accessibility of virF promoter to transcriptional repressor H-NS. *EMBO J.* **17**, 7033–7043 (1998).
113. Di Martino, M. L., Falconi, M., Micheli, G., Colonna, B. & Prosseda, G. The Multifaceted Activity of the VirF Regulatory Protein in the Shigella Lifestyle. *Front. Mol. Biosci.* **3**, 61 (2016).
114. Maurelli, A. T. & Sansonetti, P. J. Identification of a chromosomal gene controlling temperature-regulated expression of Shigella virulence. *Proc. Natl. Acad. Sci. U. S. A.* **85**, 2820–4 (1988).
115. Tran, C. N. *et al.* A multifactor regulatory circuit involving H-NS, VirF and an antisense RNA modulates transcription of the virulence gene icsA of Shigella flexneri. *Nucleic Acids Res.* **39**, 8122–8134 (2011).
116. Prosseda, G. *et al.* The virF promoter in Shigella: more than just a curved DNA stretch. *Mol. Microbiol.* **51**, 523–537 (2004).
117. Kamp, H. D. & Higgins, D. E. Transcriptional and post-transcriptional regulation of the GmaR antirepressor governs temperature-dependent control of flagellar motility in *Listeria monocytogenes*. *Mol. Microbiol.* **74**, 421–435 (2009).

118. Gründling, A., Burrack, L. S., Bouwer, H. G. A. & Higgins, D. E. Listeria monocytogenes regulates flagellar motility gene expression through MogR, a transcriptional repressor required for virulence. *Proc. Natl. Acad. Sci. U. S. A.* **101**, 12318–23 (2004).
119. Kamp, H. D. & Higgins, D. E. A protein thermometer controls temperature-dependent transcription of flagellar motility genes in listeria monocytogenes. *PLoS Pathog.* (2011). doi:10.1371/journal.ppat.1002153
120. Shen, A., Kamp, H. D., Gründling, A. & Higgins, D. E. A bifunctional O-GlcNAc transferase governs flagellar motility through anti-repression. *Genes Dev.* **20**, 3283–95 (2006).
121. Taran, M., Rad, M. & Alavi, M. Biosynthesis of TiO₂ and ZnO nanoparticles by Halomonas elongata IBRC-M 10214 in different conditions of medium. *Bioimpacts* **8**, 81–89 (2018).
122. Vijayakumar, P. S., Selvakumar, S., Gholap, R. S., Singh, A. P. & Prasad, B. L. V. Vice to Virtue: Intracellular Biogenic Nanoparticles for the Generation of Carbon Supported Catalysts. *J. Nanosci. Nanotechnol.* **10**, 905–911 (2010).
123. Johnston, C. W. *et al.* Gold biomineratization by a metallophore from a gold-associated microbe. *Nat. Chem. Biol.* (2013).
124. Reith, F. *et al.* Biogeochemical cycling of gold: Transforming gold particles from arctic Finland. *Chem. Geol.* **483**, 511–529 (2018).
125. Kunoh, T. *et al.* Biosorption of metal elements by exopolymer nanofibrils excreted from Leptothrix cells. *Water Res.* **122**, 139–147 (2017).
126. Kunoh, T. *et al.* Green Synthesis of Gold Nanoparticles Coupled with Nucleic Acid Oxidation. (2017). doi:10.1021/acssuschemeng.7b02610
127. Shakibaie, M. *et al.* Cytotoxic and antioxidant activity of the biogenic bismuth nanoparticles produced by Delftia sp. SFG. *Mater. Res. Bull.* **104**, 155–163 (2018).
128. Kamaraj, S. K., Venkatachalam, G., Arumugam, P. & Berchmans, S. Bio-assisted synthesis and characterization of nanostructured bismuth (III) sulphide using Clostridium acetobutylicum. *Mater. Chem. Phys.* **143**, 1325–1330 (2014).
129. Parikh, R. Y., Ramanathan, R., Coloe, P. J., Bhargava, S. K. & Patole, M. S. Genus-Wide Physicochemical Evidence of Extracellular Crystalline Silver Nanoparticles Biosynthesis by Morganella spp. *PLoS One* **6**, 21401 (2011).

130. Parikh, R. Y. *et al.* Extracellular Synthesis of Crystalline Silver Nanoparticles and Molecular Evidence of Silver Resistance from *Morganella* sp.: Towards Understanding Biochemical Synthesis Mechanism. doi:10.1002/cbic.200700592
131. Pantidos, N., Edmundson, M. C. & Horsfall, L. Room temperature bioproduction, isolation and anti-microbial properties of stable elemental copper nanoparticles. (2017). doi:10.1016/j.nbt.2017.10.002
132. Anil Kumar, S. *et al.* Nitrate reductase-mediated synthesis of silver nanoparticles from AgNO₃. *Biotechnol. Lett.* **29**, 439–445 (2007).
133. Jain, N., Bhargava, A., Majumdar, S., Tarafdar, J. C. & Panwar, J. Extracellular biosynthesis and characterization of silver nanoparticles using *Aspergillus flavus* NJP08: A mechanism perspective. doi:10.1039/c0nr00656d
134. Kumar Barik, S. *et al.* Synthesis of silver nanoparticles from *Bacillus brevis* (NCIM 2533) and their antibacterial activity against pathogenic bacteria Synthesis of silver nanoparticles from *Bacillus brevis* (NCIM 2533) and their antibacterial activity against pathogenic bacteria. (2018). doi:10.1016/j.micpath.2018.01.038
135. Klaus, T., Joerger, R., Olsson, E. & Granqvist, C. G. Silver-based crystalline nanoparticles, microbially fabricated. *Proc. Natl. Acad. Sci. U. S. A.* **96**, 13611–4 (1999).
136. Wang, P., Song, Y., Fan, H. & Yu, L. Bioreduction of azo dyes was enhanced by in-situ biogenic palladium nanoparticles. *Bioresour. Technol.* **266**, 176–180 (2018).
137. Windt, W. De, Aelterman, P. & Verstraete, W. Bioreductive deposition of palladium (0) nanoparticles on *Shewanella oneidensis* with catalytic activity towards reductive dechlorination of polychlorinated biphenyls. *Environ. Microbiol.* **7**, 314–325 (2005).
138. Omajali, J. B., Mikheenko, I. P., Merroun, M. L., Wood, J. & Macaskie, L. E. Characterization of intracellular palladium nanoparticles synthesized by *Desulfovibrio desulfuricans* and *Bacillus benzeovorans*. *J. Nanopart. Res.* **17**, 264 (2015).
139. Yong, P., Rowson, N. A., Farr, J. P. G., Harris, I. R. & Macaskie, L. E. Bioreduction and biocrystallization of palladium by *Desulfovibrio desulfuricans* NCIMB 8307. *Biotechnol. Bioeng.* **80**, 369–379 (2002).
140. Yong, P., Paterson-Beedle, M., Mikheenko, I. P. & Macaskie, L. E. From bio-mineralisation to fuel cells: biomanufacture of Pt and Pd nanocrystals for fuel cell electrode catalyst. *Biotechnol. Lett.* **29**, 539–544 (2007).

141. Deplanche, K., Caldelari, I., Mikheenko, I. P., Sargent, F. & Macaskie, L. E. Involvement of hydrogenases in the formation of highly catalytic Pd(0) nanoparticles by bioreduction of Pd(II) using *Escherichia coli* mutant strains. *Microbiology* **156**, 2630–2640 (2010).
142. Orozco, R. L. *et al.* Towards an integrated system for bio-energy: hydrogen production by *Escherichia coli* and use of palladium-coated waste cells for electricity generation in a fuel cell. *Biotechnol. Lett.* **32**, 1837–1845 (2010).
143. Bunge, M. *et al.* Formation of palladium(0) nanoparticles at microbial surfaces. *Biotechnol. Bioeng.* **107**, 206–215 (2010).
144. Elias, D. A., Suflita, J. M., McInerney, M. J. & Krumholz, L. R. Periplasmic cytochrome c₃ of *Desulfovibrio vulgaris* is directly involved in H₂-mediated metal but not sulfate reduction. *Appl. Environ. Microbiol.* **70**, 413–20 (2004).
145. Ramanathan, R. *et al.* Aqueous phase synthesis of copper nanoparticles: a link between heavy metal resistance and nanoparticle synthesis ability in bacterial systems. *Nanoscale* **5**, 2300–2306 (2013).
146. Hasan, S. S. *et al.* Bacterial Synthesis of Copper/Copper Oxide Nanoparticles Molecular analyses of microbial diversity associated with the Lonar soda lake in India View project Filaria repository project View project Bacterial Synthesis of Copper/Copper Oxide Nanoparticles. *Artic. J. Nanosci. Nanotechnol.* **8**, 1–6 (2008).
147. Seema Raja Balwant Singh College, B., Varshney, R., Bhaduria, S., Gaur, M. & Pasricha, R. Characterization of copper nanoparticles synthesized by a novel microbiological method. (2010). doi:10.1007/s11837-010-0171-y
148. Biomed Eng, N., Varshney etal, R., Varshney, R., Bhaduria, S. & Pasricha, R. OPEN ACCESS Copper Nanoparticles Synthesis from Elec-troplating Industry Effluent Citation: Ratnika Varshney, et al. Copper nanoparticles synthesis from electroplating industry effluent. *Nano Biomed. Eng. Nano Biomed. Eng* **3**, 115–119 (2011).
149. Yong, P., Rowson, N. A., Farr, J. P. G., Harris, I. R. & Macaskie, L. E. Bioaccumulation of palladium by *Desulfovibrio desulfuricans*. *J. Chem. Technol. Biotechnol.* **77**, 593–601 (2002).
150. Haefeli, C., Franklin, C. & Hardy, K. Plasmid-determined silver resistance in *Pseudomonas stutzeri* isolated from a silver mine. *J. Bacteriol.* **158**, 389–92 (1984).
151. Peiris, M. M. K., Fernando, • S S N, Jayaweera, • P M, Arachchi, • N D H & Guansekara, • T D C P. Comparison of Antimicrobial Properties of Silver Nanoparticles Synthesized

- from Selected Bacteria. (2088). doi:10.1007/s12088-018-0723-3
152. Gupta, A., Matsui, K., Lo, J.-F. & Silver, S. Molecular basis for resistance to silver cations in *Salmonella*. *Nat. Med.* **5**, 183–188 (1999).
 153. Giessen, T. W. & Silver, P. A. Converting a Natural Protein Compartment into a Nanofactory for the Size-Constrained Synthesis of Antimicrobial Silver Nanoparticles. (2016). doi:10.1021/acssynbio.6b00117
 154. Naik, R. R., Stringer, S. J., Agarwal, G., Jones, S. E. & Stone, M. O. Biomimetic synthesis and patterning of silver nanoparticles. *Nat. Mater.* **1**, 169–172 (2002).
 155. Capeness, M. J., Edmundson, M. C. & Horsfall, L. E. Nickel and platinum group metal nanoparticle production by *Desulfovibrio alaskensis* G20. *N. Biotechnol.* **32**, 727–731 (2015).
 156. Orozco, R. L. *et al.* Towards an integrated system for bio-energy: hydrogen production by *Escherichia coli* and use of palladium-coated waste cells for electricity generation in a fuel cell. *Biotechnol. Lett.* **32**, 1837–1845 (2010).
 157. Reith, F. *et al.* Mechanisms of gold biominerization in the bacterium *Cupriavidus metallidurans*. *Proc. Natl. Acad. Sci. U. S. A.* **106**, 17757–62 (2009).
 158. Shakibaie, M. *et al.* Cytotoxic and antioxidant activity of the biogenic bismuth nanoparticles produced by *Delftia* sp. SFG. *Mater. Res. Bull.* **104**, 155–163 (2018).
 159. Blakemore, R. P., Maratea, D. & Wolfe2, R. S. Isolation and Pure Culture of a Freshwater Magnetic *Spirillum* in Chemically Defined Medium. *J. Bacteriol.* **140**, 720–729 (1979).
 160. Frankel RB, Blakemore RP, W. R. Magnetite in freshwater magnetotactic bacteria. *Science* (80-.). **203**, 1355–6 (1979).
 161. Balkwill, D. L., Maratea, D. & Blakemore, R. P. Ultrastructure of a Magnetotactic *Spirillum*. *J. Bacteriol.* **141**, 1399–1408 (1980).
 162. Gorby, Y. A., Beveridge, T. J. & Blakemore1, R. P. Characterization of the Bacterial Magnetosome Membrane. *J. Bacteriol.* **170**, 834–841 (1988).
 163. Uebe, R. & Schüller, D. Magnetosome biogenesis in magnetotactic bacteria. *Nat. Publ. Gr.* **14**, (2016).
 164. Arakaki, A., Webb, J. & Matsunaga, T. A novel protein tightly bound to bacterial magnetic particles in *Magnetospirillum magneticum* strain AMB-1. *J. Biol. Chem.* (2003).

165. Blakemore, R. P., Frankel, R. B. & Kalmijn, A. J. South-seeking magnetotactic bacteria in the Southern Hemisphere. *Nature* **286**, 384–385 (1980).
166. Spormann, A. M. & Wolfe, R. S. Chemotactic, magnetotactic and tactile behaviour in a magnetic spirillum. *FEMS Microbiol. Lett.* **22**, 171–177 (1984).
167. Zhulin, I. B., Bespalov, V. A., Johnson, M. S. & Taylor, B. L. Oxygen taxis and proton motive force in Azospirillum brasilense. *J. Bacteriol.* **178**, 5199–204 (1996).
168. Lefèvre, C. T., Frankel, R. B., Pósfai, M., Prozorov, T. & Bazylinski, D. A. Isolation of obligately alkaliphilic magnetotactic bacteria from extremely alkaline environments. *Environ. Microbiol.* (2011). doi:10.1111/j.1462-2920.2011.02505.x
169. Keim, C. N. *et al.* Multicellular life cycle of magnetotactic prokaryotes. *FEMS Microbiol. Lett.* (2004). doi:10.1016/j.femsle.2004.09.035
170. Lefèvre, C. T., Abreu, F., Lins, U. & Bazylinski, D. A. Nonmagnetotactic multicellular prokaryotes from low-saline, nonmarine aquatic environments and their unusual negative phototactic behavior. *Appl. Environ. Microbiol.* (2010). doi:10.1128/AEM.00408-10
171. Grünberg, K., Wawer, C., Tebo, B. M. & Schüler, D. A Large Gene Cluster Encoding Several Magnetosome Proteins Is Conserved in Different Species of Magnetotactic Bacteria. *Appl. Environ. Microbiol.* **67**, 4573–4582 (2001).
172. Lin, W. *et al.* Origin of microbial biomineralization and magnetotaxis during the Archean. *Proc. Natl. Acad. Sci.* (2017). doi:10.1073/pnas.1614654114
173. Murat, D., Quinlan, A., Vali, H. & Komeili, A. Comprehensive genetic dissection of the magnetosome gene island reveals the step-wise assembly of a prokaryotic organelle. *Proc. Natl. Acad. Sci.* **107**, 5593–5598 (2010).
174. Yamamoto, D. *et al.* Visualization and structural analysis of the bacterial magnetic organelle magnetosome using atomic force microscopy. **107**, (2010).
175. Zeytuni, N. *et al.* Self-recognition mechanism of MamA, a magnetosome-associated TPR-containing protein, promotes complex assembly. *Proc. Natl. Acad. Sci. U. S. A.* **108**, E480-7 (2011).
176. Faivre, D., Böttger, L. H., Matzanke, B. F. & Schüler, D. Intracellular magnetite biomineralization in bacteria proceeds by a distinct pathway involving membrane-bound

- ferritin and an iron(II) species. *Angew. Chemie - Int. Ed.* **46**, 8495–8499 (2007).
177. Nakamura, C., Burgess, J. G., Sode, K. & Matsunaga, T. An iron-regulated gene, magA, encoding an iron transport protein of Magnetospirillum sp. strain AMB-1. *J. Biol. Chem.* **270**, 28392–6 (1995).
178. Schüler, D. Genetics and cell biology of magnetosome formation in magnetotactic bacteria. *FEMS Microbiol. Rev.* **32**, 654–672 (2008).
179. Hershey, D. M. *et al.* MamO Is a Repurposed Serine Protease that Promotes Magnetite Biominerization through Direct Transition Metal Binding in Magnetotactic Bacteria. *PLoS Biol* **14**, (2016).
180. Hershey, D. M. *et al.* Magnetite Biominerization in Magnetospirillum magneticum Is Regulated by a Switch-like Behavior in the HtrA Protease MamE *. (2016). doi:10.1074/jbc.M116.731000
181. Bird, S. M., Rawlings, A. E., Galloway, J. M. & Staniland, S. S. Using a biomimetic membrane surface experiment to investigate the activity of the magnetite biominerisation protein Mms6. *RSC Adv.* (2016). doi:10.1039/c5ra16469a
182. Tanaka, M., Mazuyama, E., Arakaki, A. & Matsunaga, T. MMS6 protein regulates crystal morphology during nano-sized magnetite biominerization in vivo. *J. Biol. Chem.* **286**, 6386–92 (2011).
183. Prozorov, T. *et al.* Protein-Mediated Synthesis of Uniform Superparamagnetic Magnetite Nanocrystals. *Adv. Funct. Mater.* **17**, 951–957 (2007).
184. Murat, D. *et al.* The magnetosome membrane protein, MmsF, is a major regulator of magnetite biominerization in Magnetospirillum magneticum AMB-1. doi:10.1111/j.1365-2958.2012.08132.x
185. Rawlings, A. E. *et al.* Self-assembled MmsF proteinosomes control magnetite nanoparticle formation in vitro. *Proc. Natl. Acad. Sci. U. S. A.* **111**, 16094–9 (2014).
186. Scheffel, A. *et al.* An acidic protein aligns magnetosomes along a filamentous structure in magnetotactic bacteria. *Nature* **440**, 110–114 (2006).
187. Pradel, N., Santini, C.-L., Bernadac, A., Fukumori, Y. & Wu, L.-F. Biogenesis of actin-like bacterial cytoskeletal filaments destined for positioning prokaryotic magnetic organelles. (2006).

188. Taoka, A., Asada, R., Wu, L.-F. & Fukumori, Y. Polymerization of the actin-like protein MamK, which is associated with magnetosomes. *J. Bacteriol.* **189**, 8737–40 (2007).
189. Katzmann, E., Scheffel, A., Gruska, M., Plitzko, J. M. & Schüler, D. Loss of the actin-like protein MamK has pleiotropic effects on magnetosome formation and chain assembly in *Magnetospirillum gryphiswaldense*. *Mol. Microbiol.* **77**, 208–224 (2010).
190. Carillo, M. A., Bennet, M. & Faivre, D. Interaction of Proteins Associated with the Magnetosome Assembly in Magnetotactic Bacteria As Revealed by Two-Hybrid Two-Photon Excitation Fluorescence Lifetime Imaging Microscopy Förster Resonance Energy Transfer. *J. Phys. Chem. B* (2013). doi:10.1021/jp4086987
191. Hartung, A. *et al.* Labeling of macrophages using bacterial magnetosomes and their characterization by magnetic resonance imaging. *J. Magn. Magn. Mater.* **311**, 454–459 (2007).
192. Goldhawk, D. E., Rohani, R., Sengupta, A., Gelman, N. & Prato, F. S. Using the magnetosome to model effective gene-based contrast for magnetic resonance imaging. *Wiley Interdisciplinary Reviews: Nanomedicine and Nanobiotechnology* (2012). doi:10.1002/wnan.1165
193. Felfoul, O., Mokrani, N., Mohammadi, M. & Martel, S. Effect of the chain of magnetosomes embedded in magnetotactic bacteria and their motility on Magnetic Resonance imaging. in *2010 Annual International Conference of the IEEE Engineering in Medicine and Biology* 4367–4370 (IEEE, 2010). doi:10.1109/IEMBS.2010.5627106
194. Goldhawk, D. E. *et al.* Magnetic Resonance Imaging of Cells Overexpressing MagA, an Endogenous Contrast Agent for Live Cell Imaging. *Mol. Imaging* **8**, 7290.2009.00006 (2009).
195. Elfick, A. *et al.* Biosynthesis of magnetic nanoparticles by human mesenchymal stem cells following transfection with the magnetotactic bacterial gene mms6. *Sci. Rep.* (2017). doi:10.1038/srep39755
196. Shipunova, V. O. *et al.* Data on characterization of magnetic nanoparticles stabilized with fusion protein of Barstar and C-term part of Mms6. *Data Br.* **21**, 1659–1663 (2018).
197. Ramesh, P. *et al.* Ultraparamagnetic Cells Formed through Intracellular Oxidation and Chelation of Paramagnetic Iron. *Angew. Chemie Int. Ed.* (2018). doi:10.1002/anie.201805042

198. Nima, Z. A. *et al.* Bioinspired magnetic nanoparticles as multimodal photoacoustic, photothermal and photomechanical contrast agents. *Sci. Rep.* **9**, 887 (2019).
199. Chen, C. *et al.* Killing of *Staphylococcus aureus* via Magnetic Hyperthermia Mediated by Magnetotactic Bacteria. *Appl. Environ. Microbiol.* **82**, 2219–2226 (2016).
200. Pat-Espadas, A. M., Razo-Flores, E., Rangel-Mendez, J. R. & Cervantes, F. J. Direct and Quinone-Mediated Palladium Reduction by *Geobacter sulfurreducens*: Mechanisms and Modeling. *Environ. Sci. Technol.* **48**, 2910–2919 (2014).
201. Azizi, S. *et al.* Green synthesis palladium nanoparticles mediated by white tea (Camellia sinensis) extract with antioxidant, antibacterial, and antiproliferative activities toward the human leukemia (MOLT-4) cell line. *Int. J. Nanomedicine* **Volume 12**, 8841–8853 (2017).
202. Rotaru, A.-E., Jiang, W., Finster, K., Skrydstrup, T. & Meyer, R. L. Non-enzymatic palladium recovery on microbial and synthetic surfaces. *Biotechnol. Bioeng.* **109**, 1889–1897 (2012).
203. Yong, P., Paterson-Beedle, M., Mikheenko, I. P. & Macaskie, L. E. From bio-mineralisation to fuel cells: biomanufacture of Pt and Pd nanocrystals for fuel cell electrode catalyst. *Biotechnol. Lett.* **29**, 539–544 (2007).
204. Mikheenko, I. P., Rousset, M., Dementin, S. & Macaskie, L. E. Bioaccumulation of palladium by Desulfovibrio fructosivorans wild-type and hydrogenase-deficient strains. *Appl. Environ. Microbiol.* **74**, 6144–6 (2008).
205. Sargent, F. The Model [NiFe]-Hydrogenases of *Escherichia coli*. *Adv. Microb. Physiol.* **68**, 433–507 (2016).
206. Lukey, M. J. *et al.* How *Escherichia coli* is equipped to oxidize hydrogen under different redox conditions. *J. Biol. Chem.* **285**, 3928–38 (2010).
207. Ballantine, S. P. & Boxer, D. H. Nickel-containing hydrogenase isoenzymes from anaerobically grown *Escherichia coli* K-12. *J. Bacteriol.* **163**, 454–9 (1985).
208. Ballantine, S. P. & Boxer, D. H. Isolation and characterisation of a soluble active fragment of hydrogenase isoenzyme 2 from the membranes of anaerobically grown *Escherichia coli*. *Eur. J. Biochem.* **156**, 277–84 (1986).
209. Lü, W. *et al.* pH-dependent gating in a FocA formate channel. *Science* **332**, 352–4 (2011).

210. Sawers, G. *The hydrogenases and formate dehydrogenases of Escherichia coli*. *Antonie van Leeuwenhoek* **66**, (1994).
211. Stephenson, M. & Stickland, L. H. Hydrogenlyases: Bacterial enzymes liberating molecular hydrogen. *Biochem. J.* **26**, 712–24 (1932).
212. Pakes, W. C. C. & Jollyman, W. H. XXXIII.—The collection and examination of the gases produced by bacteria from certain media. *J. Chem. Soc., Trans.* **79**, 322–329 (1901).
213. Abràmoff, M. D. Image Processing with ImageJ. *Imaging Softw.* (2004).
214. Rasbans, W. . ImageJ. *ImageJ, National Institutes of Health, Bethesda, MD, USA* Available at: <https://imagej.nih.gov/ij/>.
215. Sun, X., Ariza, M. P., Ortiz, M. & Wang, K. G. Atomistic modeling and analysis of hydride phase transformation in palladium nanoparticles. *J. Mech. Phys. Solids* **125**, 360–383 (2019).
216. Boudellal, M. 5. Power-to-gas strategies. in *Power-to-Gas* 99–137 (De Gruyter, 2018). doi:10.1515/9783110559811-006
217. Maeland, A. J. Hydrides for Hydrogen Storage. in *Recent Advances in Hydride Chemistry* 531–556 (Elsevier, 2001). doi:10.1016/B978-044450733-4/50018-8
218. and, T. T. & Miyake*, M. Size Control of Palladium Nanoparticles and Their Crystal Structures. (1998). doi:10.1021/CM9705808
219. Yamauchi, M. & Kitagawa, H. Hydrogen absorption of the polymer-coated Pd nanoparticle. *Synth. Met.* **153**, 353–356 (2005).
220. Lovley, D. R. Syntrophy Goes Electric: Direct Interspecies Electron Transfer. *Annu. Rev. Microbiol.* **71**, 643–664 (2017).
221. Canavese, G. *et al.* Nanoparticle-assisted ultrasound: A special focus on sonodynamic therapy against cancer. *Chem. Eng. J.* **340**, 155–172 (2018).
222. Osminkina, L. A. *et al.* Porous silicon nanoparticles as efficient sensitizers for sonodynamic therapy of cancer. *Microporous Mesoporous Mater.* **210**, 169–175 (2015).
223. Coey, J. M. D. *Magnetism and magnetic materials*. (Cambridge University Press, 2009).
224. Wiltschko, R. & Wiltschko, W. Magnetoreception. *BioEssays* **28**, 157–168 (2006).
225. Lambinet, V., Hayden, M. E., Reigl, K., Gomis, S. & Gries, G. Linking magnetite in the abdomen of honey bees to a magnetoreceptive function. *Proc. R. Soc. B Biol. Sci.* **284**,

20162873 (2017).

226. Lambinet, V., Hayden, M. E., Reid, C. & Gries, G. Honey bees possess a polarity-sensitive magnetoreceptor. *J. Comp. Physiol. A* **203**, 1029–1036 (2017).
227. Rickli, M. & Leuthold, R. H. Homing in Harvester Termites: Evidence of Magnetic Orientation. *Ethology* **77**, 209–216 (2010).
228. Maher, B. A. Magnetite biomineralization in termites. *Proc. R. Soc. B Biol. Sci.* (1998). doi:10.1098/rspb.1998.0354
229. Wiltschko, W. & Wiltschko, R. Magnetic orientation and magnetoreception in birds and other animals. *Journal of Comparative Physiology A: Neuroethology, Sensory, Neural, and Behavioral Physiology* (2005). doi:10.1007/s00359-005-0627-7
230. Lefèvre, C. T. *et al.* Comparative genomic analysis of magnetotactic bacteria from the Deltaproteobacteria provides new insights into magnetite and greigite magnetosome genes required for magnetotaxis. *Environ. Microbiol.* (2013). doi:10.1111/1462-2920.12128
231. Schübbe, S. *et al.* Characterization of a spontaneous nonmagnetic mutant of *Magnetospirillum gryphiswaldense* reveals a large deletion comprising a putative magnetosome island. *J. Bacteriol.* **185**, 5779–5790 (2003).
232. Jogler, C. *et al.* Comparative analysis of magnetosome gene clusters in magnetotactic bacteria provides further evidence for horizontal gene transfer. *Environ. Microbiol.* (2009). doi:10.1111/j.1462-2920.2009.01854.x
233. Lohße, A. *et al.* Genetic dissection of the mamAB and mms6 operons reveals a gene set essential for magnetosome biogenesis in *magnetospirillum gryphiswaldense*. *J. Bacteriol.* (2014). doi:10.1128/JB.01716-14
234. Staniland, S. S. & Rawlings, A. E. Crystallizing the function of the magnetosome membrane mineralization protein Mms6. *Biochem. Soc. Trans.* **44**, 883–90 (2016).
235. Rawlings, A. E. *et al.* Ferrous Iron Binding Key to Mms6 Magnetite Biominerallisation: A Mechanistic Study to Understand Magnetite Formation Using pH Titration and NMR Spectroscopy. *Chem. - A Eur. J.* **22**, 7885–7894 (2016).
236. Nudelman, H. & Zarivach, R. Structure prediction of magnetosome-associated proteins. *Front. Microbiol.* (2014). doi:10.3389/fmicb.2014.00009
237. Raschdorf, O. *et al.* Genetic and Ultrastructural Analysis Reveals the Key Players and Initial

- Steps of Bacterial Magnetosome Membrane Biogenesis. *PLoS Genet.* **12**, (2016).
238. Bereczk-Tompa, É., Pósfai, M., Tóth, B. & Vonderviszt, F. Magnetite-Binding Flagellar Filaments Displaying the MamI Loop Motif. *ChemBioChem* **17**, 2075–2082 (2016).
239. Liu, X. *et al.* Engineering Genetically-Encoded Mineralization and Magnetism via Directed Evolution. *Sci. Rep.* **6**, 38019 (2016).
240. Nishida, K. & Silver, P. A. Induction of Biogenic Magnetization and Redox Control by a Component of the Target of Rapamycin Complex 1 Signaling Pathway. *PLoS Biol.* **10**, e1001269 (2012).
241. Kolinko, I. *et al.* Biosynthesis of magnetic nanostructures in a foreign organism by transfer of bacterial magnetosome gene clusters. *Nat. Nanotechnol.* **9**, 193–7 (2014).
242. Kanehisa, M. & Goto, S. KEGG: Kyoto Encyclopedia of Genes and Genomes. *Nucleic Acids Res.* **28**, 27–30 (2000).
243. Blesa, M. A. *et al.* Decontamination and Decommissioning of Nuclear Facilities. *J. Chem. Soc., Faraday Trans. 1* **26**, 1489 (1987).
244. Hurme, R., Berndt, K. D., Namork, E. & Rhen, M. DNA binding exerted by a bacterial gene regulator with an extensive coiled-coil domain. *J. Biol. Chem.* **271**, 12626–31 (1996).
245. Gal-Mor, O., Valdez, Y. & Finlay, B. B. The temperature-sensing protein TlpA is repressed by PhoP and dispensable for virulence of *Salmonella enterica* serovar Typhimurium in mice. *Microbes Infect.* **8**, 2154–2162 (2006).
246. Naik, R. R., Kirkpatrick, S. M. & Stone, M. O. The thermostability of an α -helical coiled-coil protein and its potential use in sensor applications. *Biosens. Bioelectron.* **16**, 1051–1057 (2001).
247. Hurme, R., Berndt, K. D., Normark, S. J. & Rhen, M. A Proteinaceous Gene Regulatory Thermometer in *Salmonella*. *Cell* **90**, 55–64 (1997).
248. Galloway, J. M. *et al.* Biotemplated magnetic nanoparticle arrays. *Small* (2012). doi:10.1002/smll.201101627
249. Elfick, A. *et al.* Biosynthesis of magnetic nanoparticles by human mesenchymal stem cells following transfection with the magnetotactic bacterial gene mms6. *Sci. Rep.* **7**, 39755 (2017).
250. Rawlings, A. E. *et al.* Phage display selected magnetite interacting Adhirons for shape

- controlled nanoparticle synthesis. *Chem. Sci.* **6**, 5586–5594 (2015).
251. Potapov, V. & Ong, J. L. Examining Sources of Error in PCR by Single-Molecule Sequencing. *PLoS One* **12**, e0169774 (2017).
252. Kerans, F. *et al.* The Potential of Intrinsically Magnetic Mesenchymal Stem Cells for Tissue Engineering. *Int. J. Mol. Sci.* **19**, 3159 (2018).
253. Demchick, P. & Koch, A. L. The permeability of the wall fabric of Escherichia coli and Bacillus subtilis. *J. Bacteriol.* **178**, 768–73 (1996).
254. Feng, S. *et al.* Integrated self-assembly of the Mms6 magnetosome protein to form an Iron-responsive structure. *Int. J. Mol. Sci.* (2013). doi:10.3390/ijms140714594
255. Nudelman, H. & Zarivach, R. Structure prediction of magnetosome-associated proteins. *Front. Microbiol.* **5**, 9 (2014).
256. Bird, S. M., El-Zubir, O., Rawlings, A. E., Leggett, G. J. & Staniland, S. S. Materials Chemistry C Materials for optical, magnetic and electronic devices A novel design strategy for nanoparticles on nanopatterns: interferometric lithographic patterning of Mms6 biotemplated magnetic nanoparticles Emerging Investigators 2016: Novel design strategies for new functional materials A novel design strategy for nanoparticles on nanopatterns: interferometric lithographic patterning of Mms6 biotemplated magnetic nanoparticles. *J. Mater. Chem. C* **4**, 3875–4080 (2016).
257. Wang, L. *et al.* Self-Assembly and Biphasic Iron-Binding Characteristics of Mms6, A Bacterial Protein That Promotes the Formation of Superparamagnetic Magnetite Nanoparticles of Uniform Size and Shape. *Biomacromolecules* **13**, 98–105 (2012).
258. Arakaki, A. *et al.* Comparative subcellular localization analysis of magnetosome proteins reveals a unique localization behavior of Mms6 protein onto magnetite crystals. *J. Bacteriol.* (2016). doi:10.1128/JB.00280-16
259. Arakaki, A. *et al.* Comparative Subcellular Localization Analysis of Magnetosome Proteins Reveals a Unique Localization Behavior of Mms6 Protein onto Magnetite Crystals. *J. Bacteriol.* **198**, 2794–802 (2016).
260. Viklund, H. & Elofsson, A. OCTOPUS: improving topology prediction by two-track ANN-based preference scores and an extended topological grammar. *Bioinformatics* **24**, 1662–1668 (2008).
261. Krogh, A., Larsson, B., von Heijne, G. & Sonnhammer, E. L. . Predicting transmembrane

- protein topology with a hidden markov model: application to complete genomes. *J. Mol. Biol.* **305**, 567–580 (2001).
262. Young, R. Phage Lysis: Three Steps, Three Choices, One Outcome. *J. Microbiol.* **52**, 243–258 (2014).
263. Owen, R. A. *et al.* Structure and activity of ChiX: a peptidoglycan hydrolase required for chitinase secretion by *Serratia marcescens*. *Biochem. J.* **475**, 415–428 (2018).
264. Hamilton, J. J. *et al.* A holin and an endopeptidase are essential for chitinolytic protein secretion in *Serratia marcescens*. *J. Cell Biol.* **207**, 615–26 (2014).
265. Cahill, J. & Young, R. Phage Lysis: Multiple Genes for Multiple Barriers. *Adv. Virus Res.* **103**, 33–70 (2019).
266. Hunter, G. K., O'young, J., Grohe, B., Karttunen, M. & Goldberg, H. A. The Flexible Polyelectrolyte Hypothesis of Protein-Biomineral Interaction. *Langmuir* **26**, 18639–18646 (2010).
267. Oikawa, K., Islam, M. M., Horii, Y., Yoshizumi, T. & Numata, K. Screening of a Cell-Penetrating Peptide Library in *Escherichia coli*: Relationship between Cell Penetration Efficiency and Cytotoxicity. *ACS Omega* **3**, 16489–16499 (2018).
268. Moniruzzaman, M., Islam, M. Z., Sharmin, S., Dohra, H. & Yamazaki, M. Entry of a Six-Residue Antimicrobial Peptide Derived from Lactoferricin B into Single Vesicles and *Escherichia coli* Cells without Damaging their Membranes. *Biochemistry* **56**, 4419–4431 (2017).
269. Sohka, T. *et al.* An externally tunable bacterial band-pass filter.
270. Jusiak, B. *et al.* Synthetic Gene Circuits.
271. Collins, J. J., Endy, D., Hutchison Iii, C. A. & Roberts, R. J. EDITORIAL—SYNTHETIC BIOLOGY. *Nucleic Acids Res.* **38**, 2513–2513 (2010).
272. Koskis, P. *et al.* A New a-Helical Coiled Coil Protein Encoded by the *Salmonella typhimurium* Virulence Plasmid*. *J. Biol. Chem.* **267**, 12258–12265 (1992).
273. Hurmesg, R., Namorkfl, E., Nurmiah-Lassilall, E.-L. & Rhens, M. Intermediate Filament-like Network Formed in Vitro by a Bacterial Coiled Coil Protein*. *J. Biol. Chem.* **269**, 10675–10682 (1994).
274. Solovyev, V. & Salamov, A. AUTOMATIC ANNOTATION OF MICROBIAL GENOMES AND

275. Shen, A., Higgins, D. E. & Panne, D. Recognition of AT-Rich DNA Binding Sites by the MogR Repressor. *Structure* **17**, 769–777 (2009).
276. Gueriri, I. *et al.* The DegU orphan response regulator of Listeria monocytogenes autorepresses its own synthesis and is required for bacterial motility, virulence and biofilm formation. doi:10.1099/mic.0.2008/017590-0
277. Kamp, H. D. & Higgins, D. E. A Protein Thermometer Controls Temperature-Dependent Transcription of Flagellar Motility Genes in Listeria monocytogenes. *PLoS Pathog.* **7**, e1002153 (2011).
278. Moser, F. *et al.* Genetic Circuit Performance under Conditions Relevant for Industrial Bioreactors. *ACS Synth. Biol.* **1**, 555–564 (2012).
279. Brophy, J. A. N. & Voigt, C. A. Principles of genetic circuit design. *Nat. Methods* **11**, 508–520 (2014).
280. Neidhardt, F. C., Bloch, P. L. & Smith, D. F. Culture medium for enterobacteria. *J. Bacteriol.* **119**, 736–47 (1974).
281. Kelly, J. R. *et al.* Measuring the activity of BioBrick promoters using an in vivo reference standard. *J. Biol. Eng.* **3**, 4 (2009).
282. Perttu Terho. Flowing Software v2.5.1. Available at: <http://flowingsoftware.btk.fi/>. (Accessed: 19th June 2019)
283. Kelley, L. A., Mezulis, S., Yates, C. M., Wass, M. N. & Sternberg, M. J. E. The Phyre2 web portal for protein modeling, prediction and analysis. *Nat. Protoc.* **10**, 845–858 (2015).
284. Robertson Craig, †, John P. Cortens, ‡ and & Ronald C. Beavis*, †,‡. Open Source System for Analyzing, Validating, and Storing Protein Identification Data. (2004). doi:10.1021/PR049882H
285. UniProt: a worldwide hub of protein knowledge. *Nucleic Acids Res.* **47**, D506–D515 (2019).
286. Piraner, D. I., Abedi, M. H., Moser, B. A., Lee-Gosselin, A. & Shapiro, M. G. Tunable thermal bioswitches for in vivo control of microbial therapeutics. *Nat. Chem. Biol.* **13**, 75–80 (2017).
287. Salis, H. M. The ribosome binding site calculator. *Methods Enzymol.* **498**, 19–42 (2011).

288. Salis, H. M., Mirsky, E. A. & Voigt, C. A. Automated design of synthetic ribosome binding sites to control protein expression. *Nat. Biotechnol.* **27**, 946–950 (2009).
289. Chris Anderson. Promoters/Catalog/Anderson - parts.igem.org. *Registry of Standard Parts* (2006). Available at: <http://parts.igem.org/Promoters/Catalog/Anderson>. (Accessed: 25th June 2019)
290. Iverson, S. V., Haddock, T. L., Beal, J. & Densmore, D. M. CIDAR MoClo: Improved MoClo Assembly Standard and New *E. coli* Part Library Enable Rapid Combinatorial Design for Synthetic and Traditional Biology. *ACS Synth. Biol.* **5**, 99–103 (2016).
291. Kim, J., Goñi-Moreno, A., Calles, B. & de Lorenzo, V. Spatial organization of the gene expression hardware in *Pseudomonas putida*. *Environ. Microbiol.* **21**, 1645–1658 (2019).
292. Stoof, R., Wood, A. & Goñi-Moreno, Á. A model for the spatio-temporal design of gene regulatory circuits. *bioRxiv* 522946 (2019). doi:10.1101/522946
293. Goñi-Moreno, Á., Benedetti, I., Kim, J. & de Lorenzo, V. Deconvolution of Gene Expression Noise into Spatial Dynamics of Transcription Factor–Promoter Interplay. *ACS Synth. Biol.* **6**, 1359–1369 (2017).
294. Sprinzak, D. & Elowitz, M. B. Reconstruction of genetic circuits. *Nature* **438**, 443–448 (2005).
295. Kashiwagi, A., Urabe, I., Kaneko, K. & Yomo, T. Adaptive Response of a Gene Network to Environmental Changes by Fitness-Induced Attractor Selection. *PLoS One* **1**, e49 (2006).
296. Aw, R. & Polizzi, K. M. Can too many copies spoil the broth? *Microb. Cell Fact.* **12**, 128 (2013).
297. McGeachy, A. M., Meacham, Z. A. & Ingolia, N. T. An Accessible Continuous-Culture Turbidostat for Pooled Analysis of Complex Libraries. *ACS Synth. Biol.* **8**, 844–856 (2019).
298. Guarino, A. *et al.* A low cost, open source Turbidostat design for in-vivo control experiments in Synthetic Biology. *bioRxiv* 617423 (2019). doi:10.1101/617423
299. J. T. Sauls, T. K. Evolvinator - OpenWetWare. *OpenWetware* Available at: <https://openwetware.org/wiki/Evolvinator>. (Accessed: 8th July 2019)
300. Theodosiou, P. *et al.* EvoBot: Towards a Robot-Chemostat for Culturing and Maintaining Microbial Fuel Cells (MFCs). in 453–464 (Springer, Cham, 2017). doi:10.1007/978-3-319-63537-8_38

301. Andersen, J. B. *et al.* New unstable variants of green fluorescent protein for studies of transient gene expression in bacteria. *Appl. Environ. Microbiol.* **64**, 2240–6 (1998).
302. Ceroni, F. *et al.* Burden-driven feedback control of gene expression. *Nat. Methods* (2018). doi:10.1038/nmeth.4635
303. Schroeder, B. C., Cheng, T., Jan, Y. N. & Jan, L. Y. Expression Cloning of TMEM16A as a Calcium-Activated Chloride Channel Subunit. *Cell* **134**, 1019–1029 (2008).
304. Neupert, J. & Bock, R. Designing and using synthetic RNA thermometers for temperature-controlled gene expression in bacteria. *Nat. Protoc.* **4**, 1262–1273 (2009).
305. Sen, S., Apurva, D., Satija, R., Siegal, D. & Murray, R. M. Design of a Toolbox of RNA Thermometers. *ACS Synth. Biol.* **6**, 1461–1470 (2017).
306. Farhadi, A. *et al.* Recombinantly expressed gas vesicles as nanoscale contrast agents for ultrasound and hyperpolarized MRI. *AIChE J.* **64**, 2927–2933 (2018).
307. Shapiro, M. G. *et al.* Biogenic gas nanostructures as ultrasonic molecular reporters. *Nat. Nanotechnol.* **9**, 311–316 (2014).
308. Maresca, D. *et al.* Biomolecular Ultrasound and Sonogenetics. *Annu. Rev. Chem. Biomol. Eng.* **9**, 229–252 (2018).
309. Ji, X.-J. *et al.* Constructing a synthetic metabolic pathway in *Escherichia coli* to produce the enantiomerically pure (R, R)-2,3-butanediol. *Biotechnol. Bioeng.* **112**, 1056–1059 (2015).
310. Noshi, C. I. & Schubert, J. J. Self-Healing Biocement and Its Potential Applications in Cementing and Sand-Consolidation Jobs: A Review Targeted at the Oil and Gas Industry. in *SPE Liquids-Rich Basins Conference - North America* (Society of Petroleum Engineers, 2018). doi:10.2118/191778-MS
311. Ariyanti, D., H, N. A., ayani & Hadiyanto. Feasibility of Using Microalgae for Biocement Production through Biocementation. *J. Bioprocess. Biotech.* **02**, 1–4 (2012).
312. Casadaban, M. J. Transposition and fusion of the lac genes to selected promoters in *Escherichia coli* using bacteriophage lambda and Mu. *J. Mol. Biol.* **104**, 541–555 (1976).
313. Redwood, M. D., Mikheenko, I. P., Sargent, F. & Macaskie, L. E. Dissecting the roles of *Escherichia coli* hydrogenases in biohydrogen production. *FEMS Microbiol. Lett.* **278**, 48–55 (2008).
314. Sargent, F., Stanley, N. R., Berks, B. C. & Palmer, T. Sec-independent Protein

- Translocation in *Escherichia coli*. *J. Biol. Chem.* **274**, 36073–36082 (1999).
315. Blattner, F. R. *et al.* The complete genome sequence of *Escherichia coli* K-12. *Science* **277**, 1453–62 (1997).
 316. Grant, S. G., Jessee, J., Bloom, F. R. & Hanahan, D. Differential plasmid rescue from transgenic mouse DNAs into *Escherichia coli* methylation-restriction mutants. *Proc. Natl. Acad. Sci. U. S. A.* **87**, 4645–9 (1990).
 317. Miroux, B. & Walker, J. E. Over-production of Proteins in *Escherichia coli*: Mutant Hosts that Allow Synthesis of some Membrane Proteins and Globular Proteins at High Levels. *J. Mol. Biol.* **260**, 289–298 (1996).
 318. Casadaban, M. J. & Cohen, S. N. Analysis of gene control signals by DNA fusion and cloning in *Escherichia coli*. *J. Mol. Biol.* **138**, 179–207 (1980).